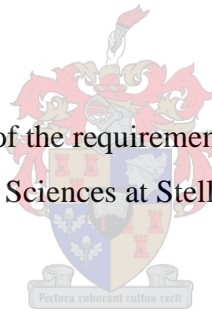


STELLENBOSCH UNIVERSITY

An investigation of the petrogenesis of the Buddusò I-type granites and its mafic enclaves in Sardinia, Italy.

Roxanne Soorajlal

“Thesis presented in partial fulfilment of the requirements for the degree of Master of Science in
the Faculty of Earth Sciences at Stellenbosch University”.



Supervisor: Professor Gary Stevens, University of Stellenbosch, SA

Co-Supervisor: Federico Farina, University of Geneva, Switzerland

Date: December 2017

Declaration

By submitting this thesis electronically, I declare that the entirety of the work contained therein is my own, original work, that I am the sole author thereof (save to the extent explicitly otherwise stated), that reproduction and publication thereof by Stellenbosch University will not infringe any third party rights and that I have not previously in its entirety or in part submitted it for obtaining any qualification. The following sections of work were generated in laboratories where I did not work; Lu-Hf data was generated in Frankfurt by Axel Gerdes, U-Pb data was generated in Stellenbosch by Dirk Frei, the XRF data was generated in Stellenbosch by Rianna Rossouw.

Date: December 2017

Copyright © 2017 Stellenbosch University

All rights reserved

Abstract

There is still great debate surrounding the petrogenesis of I-type granites with mafic enclaves. The granite controversy indulges three prevalent processes/models surrounding the typical range in chemistry portrayed by common I-type granites; 1) magma mixing/mingling, 2) differential entrainment of material from the source and 3) fractional crystallisation from the source. There are three predominant theories which describe the petrogenesis of mafic enclaves: 1) they represent cumulate fragments, 2) blobs of hybrid magma representing a mixture of a mafic magma mixing with a felsic host magma and 3) fragments of recrystallized metamorphic rocks inherited from the source during partial melting from a parent magma. Mafic enclaves are widely considered to represent evidence for magma mixing/ mingling of a mafic magma and felsic host magma in I-type granites.

The Buddusò Pluton is a perfect example of a common I-type granitic body with mafic enclaves. This study aims to; 1) explain the origin of the compositional variation seen in the granitic units as well as the mafic enclaves, 2) constrain the most consistent model for the petrogenesis of the Buddusò pluton. This study will make use of a blend of geo-analytical techniques; field relations, whole rock geochemistry, petrography, mineral chemistry, zircon geochronology and Lu-Hf and U-Pb isotopic analysis of the zircons from both mafic enclaves and granites to aid in meeting the aims of the study.

The Buddusò pluton is comprised of three units; an inner unit comprised of leucogranites, a middle unit comprised of granite compositions and an outer unit comprised of granodiorites. Mafic enclaves exist throughout the pluton, increasing in abundance from the inner to outer units. Granites from all units show negative correlations for all major elements except K_2O with respect to SiO_2 . They show an increase in Al_2O_3 , CaO , FeO , MgO , TiO_2 and, P_2O_5 with decreasing SiO_2 from the inner unit through to the outer unit. Granites show tighter correlations with respect to the major and trace elements vs. SiO_2 with trends portrayed by the mafic enclaves. Mafic enclaves show a similar mineral assemblage to the granites (*sensu lato*) with a higher proportion of mafic minerals, both contain complexly zoned plagioclase crystals. U-Pb isotope data indicated a crystallisation age of $294 \pm 2 Ma$ for both granites and mafic enclaves and revealed that the age of the source was fairly close in age to that of the pluton ($292 \pm 5 Ma$ (Del Moro et al., 1975)). $\epsilon_{Hf(t)}$ values from Lu-Hf isotope analyses suggest that both the granites and mafic enclaves have crustally derived isotopic signatures and showed small scale isotopic

variation within individual samples. The small scale $\epsilon_{\text{Hf}(t)}$ range gets larger from the inner unit through to the middle unit.

Field and petrographical evidence; contact morphologies, presence of reaction minerals, crystal exchange, presence of acicular apatite, bladed biotite, and compositionally zoned plagioclase all suggest that the mafic enclave magma did see interaction with the granitic magma most probably prior to emplacement. Plagioclase, biotite and K-feldspar show similar mineral chemistries in both granites and mafic enclaves suggesting that, for element ratios important to these minerals, the mafic magma largely equilibrated with the chemistry of the host granite magma. Hornblende shows differing chemical compositions in mafic enclaves in comparison to the granites. A mixing model was designed which mixed each of the enclave compositions with the most leucocratic granite (sample BG32) in 5wt. % increments in order to investigate if the hypothetical mixed magmas would overlap in composition with the compositional range portrayed by the granites. The study concluded that the mafic enclaves saw varying degrees of hybridisation by the granite magma and the range seen in granite compositions were not produced by mixing with the mafic to intermediate magmas which formed the enclaves.

A fractionation model was run at 3Kbars using 3.4wt. % H₂O for three heating paths at 700, 800 and 900°C using two different starting compositions as a means of modelling crystal fractionation. Melt was then extracted sequentially in 5 wt. % increments until melt no longer existed in the system. The compositions of the crystal enriched magma and the melt separated from it were compared with the compositions of the granites and enclaves. The second model set up using B27, a granite from the middle unit, as a starting composition achieved a good linear fit with respect to major element chemistry. However, the model explained a probable emplacement mechanism as well as a process causing the mineral variation in the granite unit, it did not explain the enclave compositions.

The study concluded that the mafic enclave magma and granite magma are crustally derived and comagmatic based on their similar range in mineral compositions, similar magmatic age and Hf isotope signature. The magmas are proposed to be produced via partial melting of an andesitic source. The primary mechanism shaping the chemistry of the magmas is peritectic mineral entrainment and co-entrainment of accessory suite minerals when melting occurs. The magma is injected into the magma chamber in two pulses closely separated in time. The mafic enclave magma was injected first with a higher fraction of entrained ferromagnesian minerals and began to crystallise. This mafic enclave magma was considerably hotter and came from a deeper magma chamber. The granitic magma was then injected with a lower fraction of entrained

ferromagnesian minerals resulting in a composition close to that of the intermediate granites. The mafic enclave magma mush (crystals + magma) interacted with the granite magma via chemical exchange, diffusion and mechanical transfer during ascent prior to emplacement. The mafic enclave magma was consequently hybridised and the more viscous granite magma flowed over crystallised sheets of enclave magma consequently breaking it up into smaller pieces. Upon emplacement, the Buddusò Pluton saw a deformation event consequently disturbing the magma chamber. This deformation allowed for a low temperature filter pressing process to squeeze melt of the granite mush (enclave hybridised blobs of crystal and melt + less mafic granite magma) and mobilise it into the low-pressure zones. The crystal accumulation was representative of the granodiorites' compositions and the squeezed off melt was representative of the leucogranites' compositions. The entire pluton was not affected by the deformation therefore some parts of the pluton did not undergo melt:crystal separation and consequently retained their original magma compositions. This would result in the three granitic units; granodiorites with abundant mafic enclaves; granites with fewer mafic enclaves and leucogranites with no mafic enclaves.

Abstrak

Daar word steeds grootliks gedebateer rondom die petrogenese van I-tipe graniete met mafiese enklaves. Die graniet polemieë gee oor aan drie heersende prosesse/modelle rondom die tipiese chemiese reeks wat voorgestel word deur algemene I-tipe graniete; 1) magma menging/vermenging, 2) differensieële inlaaiing van materiaal vanaf die oorsprong, en 3) fraksionele kristallisatie van/vanaf die oorsprong. Daar is drie predominerende teorieë wat die petrogenese van mafiese enklaves beskryf: 1) voorstellende kumulitiewe fragmente, 2) blobbe hibriediese magma wat 'n mengsel van mafiese magma vermenging met 'n felsiese hostie voorstel, en 3) fragmente van gerikristalliseerde metamorfiese klip wat van die oorsprong ge-erf is gedurende gedeeltelike smagmaing daarvan (die oorsprong). Mafiese enklaves word wyd oorweeg om magma menging/vermenging van 'n mafiese magma en 'n felsiese hostie magma voor te stel in I-tipe graniete.

Die Buddusò Pluton is 'n perfekte voorbeeld van 'n algemene I-tipe granitiese liggaam met mafiese enklaves. Hierdie studie beoog om 1) die oorsprong van die komposisionele variasie wat gesien word in die granitiese eenhede sowel as die mafiese enklaves te verduidelik, 2) om die mees konsekwente model vir die petrogenese van die Buddusò pluton op te stel. Hierdie studies al gebruik maak van 'n mengsel geo-analitiese tegnieke, veld verhoudinge, geheel klip geochemie, petrografie, mineral chemie, zircon geochronologie en Lu-Hf U-Pb isotopiese analiese van die zircons vanaf beide die mafiese enklaves en die graniete om hulp te bied om die doel van die studie te bereik.

Die Buddusò pluton bestaan uit drie eenhede; 'n binneste eenheid wat uit leukograniete bestaan, 'n middelste eenheid met granitiese komposisies en 'n buitenste eenheid wat uit granodiorite bestaan. Mafiese enklaves kom voor reg deur die pluton en verhoog in voorkoms vanaf die binneste tot die buitenste eenhede. Graniete van alle eenhede wys negatiewe korrelasie met alle hoof elemente behalwe K_2O met betrekking tot SiO_2 . Hulle wys 'n verhoging in Al_2O_3 , CaO , FeO , MgO , TiO_2 en P_2O_5 met dalende SiO_2 vanaf die binneste eenheid deur tot die buitenste eenheid. Graniete wys 'n stywer korrelasie met betrekking tot die hoof- en spoorelemente teenoor SiO_2 in vergelyking met sy mafiese enklaves. Die mafiese enklaves wys 'n soortgelyke minerale versameling as die graniete (*sensu lato*) met 'n hoër verhouding van mafiese minerale, albei bevat kompleks gezoneerde plagioklaas kristalle. U-Pb isotope data dui 'n kristallisatie ouderdom van $294 \pm Mj$ vir beide graniete en mafiese enklaves en openbaar dat die ouderdom

van die oorsprong heelwat na aan die ouderdom van die pluton is. $\epsilon_{\text{Hf}(t)}$ waardes vanaf Lu-Hf isotope analise suggesteer dat beide die granietes en mafiese enklaves het isotopiese handtekening wat vanaf die kors afgelei is en het kleinskaal isotopiese variasie binne-in die monsters. Die kleinskaal $\epsilon_{\text{Hf}(t)}$ reeks word groter vanaf die binneste eenheid deur tot die middelste eenheid.

Veld en petrografiese bewyse, kontak morfologieë, die teenwoordigheid van reaksie minerale, kristal verruiling, die teenwoordigheid van ‘acicular’ apatiet, lemvormige biotiet en komposisioneel gezoneerde plagioklaas almal suggesteer dat die mafiese enklave magma die interaksie met die granitiese magma gesien het, mees waarskynlik voor inplasing. Plagioklaas, biotiet en K-feldspar wys soortgelyke mineraal chemies in beide graniete en mafiese enklaves wat suggesteer dat die minerale reeds ekwilibrium bereik het. Hornblende wys verskillende chemiese komposisies in mafiese enklaves in vergelying met die graniete. ‘n vermengings model was ontwerp wat elk van die enklaves komposisies gemeng het met die mees leukokratische graniet (monster BG32) in 5wt. % inkrement. Die natuurlike monsters van die graniete en enklaves het nie op die vermengings lyn vir al die hoof elemente gelê nie. Die studie sluit af dat die mafiese enklaves verskillende grade van hibridisasie gesien het by die graniet magma.

‘n Fraksionele model was gedoen by 3Kbars met 3.4wt. % H₂O vir drie verhitte paaie by 700, 800 en 900°C deur gebruik te maak van twee verskillende begin-komposisies om fraksionele kristallasie uit te beeld. Magma was dan opeenvolgend in 5 wt. % inkrement onttrek totdat die magma nie in die sisteem bestaan het nie. Die tweede model was opgestel deur gebruik te maak van B27, ‘n graniet van die middelste eenheid, as ‘n begin-komposisie het goed gepas. Hoewel die model ‘n waarskynlike inplasing-meganisme verduidelik sowel as ‘n proses wat die variasie in die granitiese eenheid veroorsaak, verduidelik dit nie die enclave komposisies nie.

Die studie sluit af dat die mafiese enclave magma en die granitiese magma deur van kors afgelei is en komagmatis gebaseer is op hul soortgelyke reeks in komposisie, soortgelyke magmatiese ouderdom en Hf isotopiese handtekening. Die magmas is voorgestel om deur parsieële smagmaing van ‘n andesitiese oorsprong geproduseer is. Die primêre meganisme wat die magmas vorm is die peritektiese mineral invoering en ko-invoering van bykomstige suite minerale wanneer smagmaing plaasvind. Die magma is ingespuut binne-in die magma kamer in twee pulse met ‘n klein tydgleuf tussen-in. Die mafiese enclave magma was eers ingespuut met ‘n hoër fraksie ingevoerde ferromagnesiese minerale en toe begin kristalliseer. Die granitiese magma was dan ingespuut met ‘n laer fraksie ingevoerde ferromagnesiese minerale wat ‘n

komposisie na aan die van die intermediêre graniete tot gevolg het. Die mafiese enklave magma mush (kristalle + magma) het met die graniet magma 'n interaksie ondergaan via chemiese verruiling, diffusie en meganiese oordrag gedurende daling voor inplasing plaasgevind het. Die mafiese enklave magma was gevolglik gehybridiseer en die meer viskeuse magma het oor gekristalliseerde velle van enklave magma gevloei en dit gevolglik in kleiner stukke gebreek het. Tydens inplasing het die Buddusò Pluton 'n vervormings gebeurtenis beleef en tot gevolg die magma kamer versteur. Die vervorming het 'n lae temperatuur filter druk proses toegelaat om die magma van die graniet mush te druk (enklave gehybridiseerde blabbe van kristal en magma + minder mafiese graniet magma) en dit te mobiliseer na die lae-druk zones wat deur die differensieële stres van die vervorming geskep is. Die kristal ophoping was verteenwoordigend van die granodiorites se komposisies en dit het die magma wat verteenwoordigend van die leukogranietes se komposisies is afgedruk. Die hele pluton was nie geraak deur die vervorming nie en het daartoe tot gevolg dat sommige dele van die pluton die graniet mush se komposisie behou. Dit sou die drie granitiese eenhede tot gevolg hê; granodiorites met vollop mafiese enklaves, granietes met minder mafiese enklaves en leukogranietes met geen mafiese enklaves nie.

Table of Contents

Declaration	i
Abstract	ii
Abstrak	v
Table of Contents	viii
Acknowledgements	xii
List of Figures	xiii
List of Tables.....	xvii
List of Abbreviations and Terms.....	xviii
Chapter 1: Introduction	1
1.1 Granites; the debate around I-types and their sources	1
1.2 Mafic Enclaves as a petrogenetic tool.....	2
1.3 The Buddusò Pluton; a perfect study area with common I-type granites hosting mafic enclaves	3
Chapter 2: Geological Setting and Past Work.....	4
2.1 Geological Setting	4
2.2 Past work.....	5
2.2.1 Sardinia-Corsica Batholith	5
2.2.2 The Buddusò Pluton.....	6
2.2.3 Using the Buddusò pluton; a case study to aid understanding the petrogenesis of the Sardinia-Corsica Batholith	11
2.3 Recent work published using mafic enclaves to understand petrogenetic processes of magmatic bodies.....	14
2.3.1 Magma mixing or mingling	14
2.3.2 Fractional Crystallisation	15
2.3.3 A combination of several processes, case study ; Central Victoria, Australia, Clemens et al. (2016a).....	15

Chapter 3: Analytical Techniques	18
3.1 Field work and sampling	18
3.2 Microscopic petrography	19
3.3 Mineral chemical analysis	19
3.4 Whole-rock geochemistry	20
3.4.1 Sample preparation.....	20
3.4.2 LA-ICPMS	20
3.5 Isotope analysis of zircons	21
3.5.1 Zircon sample preparation.....	21
3.5.2 U-Pb Isotope analysis.....	21
3.5.3 Lu-Hf-Yb Isotope analysis	22
Chapter 4: Results	23
4.1 Field Relations	23
4.2 Petrography	25
4.2.1. Granites	25
4.2.2 Enclaves	26
4.2.3 Plagioclase.....	27
4.3 Mineral Chemistry	29
4.3.1 Plagioclase.....	29
4.3.2 Potassium Feldspars	32
4.3.3 Biotite	34
4.3.4 Hornblende	36
4.4 Whole-rock Geochemistry	38
4.4.1 Major element geochemistry	41
4.4.2 Trace element geochemistry	45
Chapter 5: Using Zircon as a tool to understand the petrogenesis of the Buddusò Pluton	49
5.1 Zircon Crystals	49
5.2 U-Pb Isotope analysis.....	50

5.3 Lu-Hf Isotope analysis	53
Chapter 6: Discussion and Interpretations	58
6.1 Magma mixing as a mechanism for shaping the petrogenesis of the Buddusò Pluton	58
6.1.1 Evidence of mafic enclave magma and felsic granite magma interaction	58
6.1.2 Hybridisation.....	64
6.2 Phase Equilibrium modelling: Evaluating the role of Crystal Fractionation	66
6.2.1 Fractional crystallization vs. Crystal fractionation	66
6.2.2 Fractionation model set up	66
6.2.3 Fractionation modelling results and interpretation	70
6.2.4 Petrogenetic Model	74
6.3 Peritectic assemblage entrainment (PAE)	79
6.3.1 The source of the Buddusò Pluton	79
6.3.2 PAE Petrogenetic Model.....	80
Conclusions and Summaries	76
Future Research.....	78
References	79
Appendices	90
Appendix I: Geological Setting and Past Work	90
Appendix II: Whole-rock Geochemistry.....	91
Major element chemistry.....	91
Trace element chemistry	94
Appendix III: Mineral Chemistry.....	97
Plagioclase.....	97
Potassium Feldspar.....	106
Biotite.....	109
Hornblende	112
Appendix IV: Zircon	114
Appendix V: Discussion	119

Magma mixing	119
Crystal Fractionation.....	122

Acknowledgements

This research was funded by the South African National Research Foundation (NRF) in the form of grant funding to Professor Gary Stevens via the SARChI programme and an MSc bursary to Roxanne Soorajlal.

I would like to thank my supervisor Professor Gary Stevens for his guidance and continuous support throughout this project. Thank you for not giving up on me. Thank you to my co-supervisor Dr Federico Farina. I would like to thank Matt Mayne for helping me with the fractionation modelling. I would like to thank everyone at Stellenbosch's CAF facility for all the help and support. To Nishal Samayiyi, Dumi Makhaye, Lauren Hendricks and Alexander dos Ramos, thank you so much for all your unconditional support and help throughout the project. To my friends and family – I am grateful to each of you for always being there, your faith and belief in me has carried me through.

List of Figures

Figures	Pages
1. Geological map of the Buddusò pluton (redrawn from Barbey et al., 2008) showing sites B-D, F-I and L-N where samples were collected. Corresponding GPS locations can be found in Table 2.....	7
2. Graph showing Sr-Nd isotopic data for the Buddusò Pluton for granites and mafic enclaves. $^{87}\text{Sr}/^{86}\text{Sr}$ initial ratios and $\epsilon\text{Nd}(t)$ values were calculated for 286 Ma, values are from Barbey et al. (2008)	9
3. Plates A-H showing various granitic textures seen in the field. Plates E-H showing various enclave textures seen in the field. A) A contact close by the area of Santa Reparata can be seen, the contact shows a leucocratic granite (bottom left) and a more mafic granite (top right). B) Shows an undeformed igneous texture showing quartz, plagioclase and potassium feldspar crystals. C) shows the textural differences seen in the granites; the leucogranite (bottom left) has a finer grained texture compared to the more coarse grained mafic granite (top right). D) The finer grained enclave shows an elongated protuberance. E) Plate E shows an xenolith that has cusps and flames. F & G) the feldspar crystals in the enclaves are euhedral and are similar in size to the feldspar microphenocrysts seen in the granites. H) Coarser grained enclave.....	23
4. Thin section photographs of granites in XPL (a-c) showing similar coarse grained textures with varying mineral assemblages; a) granodiorites from the outer unit (BG48), b) granite from the middle unit (BG23) and c) leucogranite from the inner unit (BG25).Scale bar=100um. Ms;Muscovite, Bt;Biotite, Ep;Epidote, Ap;Apatite, Hbl;Hornblende, Sph; Sphene, Pl;Plagioclase, Qtz;Quartz and Kfs;K-feldspar.....	25
5. Thin section photographs of enclaves in PPL: A-B) contact between granite (left) and enclave (right) showing a high concentration of amphiboles and biotite, enclave shows a foliation which is absent in the granite, (BG44) C) enclave showing a higher ratio of felsic:mafic minerals(BG22), D) enclave showing a fine grained, homogenous intergranular texture. (BG12D) (A), (B), (C) are from the middle unit and (D) is from the the outer unit.....	26
6. Plagioclase crystals showing A) epidote core and rims with foliation bending around phenocryst in PPL) B) Carlsbad twinning with foliation uninterrupted by phenocrysts in XPL in enclave sample BG16 C&D) plagioclase crystals in PPL showing epidote core and rims in granite sample BG12C2. Scale bar= 100um*.....	28
7. Representative compositions of the plagioclase from enclaves (blue squares) and granites (black triangles). Formula based on 8 O atoms. A full set of all mineral compositions generated in the study can be found Appendix III. Diagram based on Irvine and Baragar, (1971). An=Anorthite, Ab = Albite, Or = Orthoclase.....	29
8. Plagioclase crystals showing epidote core and rims with foliation bending around phenocryst in PPL overlaid by a traverse showing anorthite (An%) content for plagioclase only. $\text{An}=\text{Ca}/(\text{Ca}+\text{Na}+\text{K})\times 100$ (BG44) An calculations can be found in Appendix III.....	30
9. Thin section photos in PPL (A&C) of plagioclase phenocrysts in granite sample BG12C2 with backscatter electron images of the same crystals in (B&D) overlaid by a traverse showing anorthite (An)% content for plagioclase only. $\text{An}=\text{Ca}/(\text{Ca}+\text{Na}+\text{K})\times 100$	

- numbers in black are spot no. analyses, Scale bar =200um (A&C). *An calculations can be found in Appendix III.....31
10. a) A) AFM diagram showing all samples from this study and samples from a study carried out by Barbey et al. (2008). $Alk=Na_2O+K_2O$, $FeO^*=Total\ Fe\ content\ (FeO_3+FeO)$. All samples from both studies plot in the calc-alkaline field with the exception of two granites from Barbey et al. (2008) study plot in the Tholeiitic field. B) Discrimination diagram of normative albite, anorthoclase and orthoclase plotted for samples of enclaves and granites from both studies. Granites from the inner and middle unit, from this study, plot in the granite field whilst granites from the outer unit plot in the granodiorite field. The enclave and mixed samples plot in the tonalite field with the exception of sample BG15mix and BG21. Both diagrams have been plotted using data weight normalized according to Irvine and Baragar (1971) overlaid with petrographic fields of Barker (1979).....41
 - b) Discrimination diagram showing $Al/(Na+K)$ vs $Al/(Ca+Na+K)$. All granite samples from this study plot in the peraluminous section and enclaves plot in the metaluminous field with exception of samples BG15mix and BG16mme plotting in the peraluminous field. Diagram uses Shand's Index (1943) superimposed by discrimination fields of Maniar and Piccoli 1989) using molar proportions.....42
 11. Harker plots comparing granite and enclave compositions from this study with those from the study conducted by Barbey et al. (2008). Pearson's coefficient (R) and Spearman's rank order coefficient (R') values are given for the data from Barbey et al. (2008) and Pearson's coefficient (r) and Spearman's rank order coefficient (r') values are given for the samples from this study. Refer to Appendix: II for full regression parameters and graphs.....44
 12. A) Harker plots comparing granite and enclave compositions from this study with those from the study conducted by Barbey et al. (2008). All trace elements plotted are measured in ppm. Refer to Appendix II for full data set.....45
 - B) Harker plots of granite and enclave compositions from this study with those from the study conducted by Barbey et al. (2008). All trace elements plotted are measured in ppm. Refer to Appendix: II for full dataset. $LREE=La+Ce+Pr+Nd+Sm+Eu+Gd$, $HREE= Tb+Dy+Ho+Er+Tm+Yb+Lu$46
 13. A-D) Chondrite- normalized REE patterns and E-H) Primitive mantle-normalized trace element diagrams. Primitive mantle-normalized trace element diagrams for enclave samples BG 8 and BG 9 (E1), BG21, BG22 and BG29 (E2), BG38 and BG15mme (E3) and BG16mme, BG15mix and BG16mix (E4). Normalization values are from McDonough and Sun (1995) for primitive mantle and from Sun and McDonough (1989) for Chondrite.....48
 14. Cathodoluminescence images of zircon crystals from granites. Sample names and magnification included on each image. Zircon crystals are subhedral to euhedral in shape and show strong oscillatory zoning. Apatite inclusions can be seen in figures E and C.....49
 15. Relative probability plot showing distribution of ages for the concordant magmatic zircons crystals from samples BG15, BG26 and BG35. n refers to the number of concordant crystals, with concordance measured between 95 – 105%. Uncertainty on individual age analyses can be found in Appendix 1V.....50
 16. Wetherill Concordia diagrams for magmatic zircon crystals of the three samples; A) BG15, B) BG26 and C) BG35. Error ellipses are plotted at 2σ52
 17. A): Lu-Hf and U-Pb zircon results for enclave sample BG15 from the middle unit, and granite samples BG26 (middle unit) and BG35 (outer unit) from the Buddusò pluton. Values for Depleted Mantle (DM) and Chondritic Uniform Reservoir (CHUR) shown

- on figure were according to Vervoort et al. (2000) and Blichert & Albarède (1997) respectively. Magmatic age refers to the age of proposed age of granite crystallisation. TDM is referred to as the crustal residence age which estimates the time elapsed since the crustal domain hosting the zircon was extracted from the depleted mantle Scherer (2007). B) Magnified image to show spread of zircon population represented in box B on Fig.17A..... 53
18. $\epsilon_{\text{Hf}}(t)$ vs. U-Pb zircon results for enclave sample BG15 from the middle unit and granite samples BG26 (middle unit) and BG35(outer unit) from the Buddusò pluton. Values for Depleted Mantle (DM) and Chondritic Uniform Reservoir (CHUR) shown on figure were according to Vervoort et al. (2000) and Blichert & Albarède (1997) respectively. Inset shows the composition of the majority zircon population of magmatic zircons analysed. The 2σ error on Hf isotope ± 0.00003 to ca.1 ϵ unit (Farina et al., 2014). Magmatic age refers to the age of proposed age of granite. TDM is referred to as the crustal residence age which estimates the time elapsed since the crustal domain hosting the zircon was extracted from the depleted mantle (Scherer,2007)54
19. $\epsilon_{\text{Hf}}(t)$ vs. U-Pb zircon spot analyses results for enclave sample BG15 from the middle unit, leucogranite sample BG19 from inner unit, granite samples BG2, BG3 & BG26 (middle unit) and granodiorite samples BG13, BG35 & BG 48 (outer unit) from the Buddusò pluton. Values for Depleted Mantle (DM) and Chondritic Uniform Reservoir (CHUR) shown on figure were according to Vervoort et al. (2000) and Blichert & Albarède (1997) respectively. TDM ages extrapolated to the DM, TDM ages based on assumed magmatic age of 293 Ma for samples with no U-Pb data.....57
20. Mixing model; a test to investigate if the compositions of the more mafic granites (granodiorites from the outer unit and intermediate granites from the middle units) can be shaped by mixing the most leucocratic granite and mafic magma(s) represented by the enclaves composition. The most leucocratic granite BG 32 is mixed with each enclave in 5 wt. % increments (refer to Appendix V for mixing calculations).....60
21. $\epsilon^{(176/177)}\text{Hf}$ of magmatic zircon plotted over whole rock $\text{MgO} + \text{FeO}$. Large solid circles represent granitic samples, increasing in maficity from green to blue and the small black open circles displays an enclave sample. Magmatic age of 293 Ma has been assumed for samples with Lu-Hf data without corresponding U-Pb data. Red arrows represent 2σ error values on maximum and minimum $\epsilon^{(176/177)}\text{Hf}$ compositions for each sample. Refer to Appendix IV for all 2σ error values.....62
22. $\text{FeO}t$ vs $\text{FeO}t/\text{MgO}$, for all samples from the Buddusò Pluton, using $\text{FeO}t$ content as a discriminator for hybridisation (Zorpi eta 1989).....65
23. Animation representing fractionation model process, with A) as the starting bulk compositions of the reactive system, D) the magma extracted from the reactive system to form the extract system and B-C) representing the evolving compositions of the shrinking reactive system. Modelling was done at same pressure of 3kbar at various temperatures; 700°C, 800°C and 900°C run for two different starting compositions; BG27 (granite from the middle unit) and BG34(granodiorite from the outer unit).....68
24. Fractionation model using starting parameter BG34, assuming isobaric conditions at 3 kbar for three heating paths at 700, 800 and 900°C. Fractionation was scaled along each path by extracting 5 wt. % magma present in the reactive subsystem at each step. This data was then superimposed on corrected natural samples. The blue dotted line (700°C) represents the best fit with respect to the fractionation model results and the natural samples. Refer to Appendix V for calculations.....71
25. Fractionation model using starting parameter BG27, assuming isobaric conditions at 3 kbar for three heating paths at 700, 800 and 900°C. Fractionation was scaled along each path by extracting 5 wt. % magma present in the reactive subsystem at each step. This

data was then superimposed on corrected natural samples. The blue dotted line (700°C) represents the best fit with respect to the fractionation model results and the natural samples. Refer to Appendix V for calculations.....73

26. Major elements A) K₂O and B) TiO₂ plotted against FeO + MgO for all granite and mafic enclave samples from the Buddusò Pluton.....74

27. Graphs A-E showing the phase proportions and mineral assemblages of the two different fractionation models using starting parameters BG27 and BG34 at different temperatures. The proportion of each mineral phase and magma is plotted as a percentage against the steps of incremental magma loss. Each step indicates 5wt. % magma extraction. For full values and calculations refer to Appendix V.....75

List of Tables

Tables	Pages
1. Lithological units identified by different authors with their corresponding names given.....	6
2. A sample list of localities, rock types and the different analytical techniques used individually, (a) Whole rock and trace element geochemistry, (b) Thinsection, (c) Mineral Chemistry, (d) U-Pb isotope analysis and (e) Lu-Hf isotope analysis.....	8
3. Representative analyses of the K-feldspar from enclaves. (2 spots analysis were chosen for each sample based on the best totals, complete analyses of all spots can be found in Appendix III). Formula based on 8 O atoms.....	32
4. Representative analyses of K-feldspar from granites. (2 spots analysis were chosen for each sample based on the best totals, complete analyses of all spots can be found in Appendix III). Formula based on 8 O atoms.....	33
5. Representative analyses of biotite from enclaves. (2 spots analysis were chosen for each sample based on the best totals, complete analyses of all spots can be found in Appendix III). Formula based on 22 O atoms.....	34
6. Representative analyses of biotite from granites. . (2 spots analysis were chosen for each sample based on the best totals, complete analyses of all spots can be found in Appendix III). Formula based on 22 O atoms.....	35
7. Representative analyses of the hornblende from enclave. . (2 spots analysis were chosen for each sample based on the best totals, complete analyses of all spots can be found in Appendix III). Formula based on 23 O atoms.....	36
8. Representative analyses of hornblende from granite. .(2 spots analysis were chosen for each sample based on the best totals, complete analyses of all spots can be found in Appendix III). Formula based on 23 O atoms.....	37
9. Whole-rock major (wt.%) and trace (ppm) element analyses of enclaves and mixed samples from the Buddusò Pluton.....	38
10. Whole-rock major (wt. %) compositions of granite samples from the Buddusò Pluton.....	39
11. $\epsilon_{\text{Hf}}(t)$ range, $^{176}\text{Hf}/^{177}\text{Hf}$ range and TDM range for magmatic enclave and granite samples. Magmatic age of 293 Ma was assumed for Lu-Hf isotopes that did not have U-Pb data.	56
12. Starting compositions used in fractionation modelling, BG27 and BG34.....	67

List of Abbreviations and Terms

K-feldspar	Potassium Feldspar
Pl	Plagioclase
Bt	Biotite
Qtz	Quartz
Ms	Muscovite
Ep	Epidote
Sph	Sphene
Ap	Apatite
Hbl	Hornblende

Chapter 1: Introduction

1.1 Granites; the debate around I-types and their sources

Chappell and White (1974) revealed that there are two different classes of granitic rocks based on their respectively different mineralogical, isotopic and chemical features. The authors coined the terms S-type and I-type granites. I-type granites described as less aluminous (Al) rocks with less radiogenic isotope compositions, higher sodic concentrations and show a wider spectrum in compositions from felsic to mafic with meta-igneous protoliths (Clemens et al., 2011 & Chappell & White, 2001). S-type granites are generally restricted only to high silica compositions, have relatively low sodic concentration and were concluded to have meta-sedimentary protoliths (Chappell & White, 2001). The debate regarding how I-type granites achieved their compositional variation remains very enigmatic. The granite controversy indulges three prevalent processes/models surrounding the typical range in chemistry portrayed by common I-type granites;

- 1) Magma mixing/mingling (e.g. Chappell, 1996)
- 2) Differential entrainment of material from the source (e.g. Chappell & White, 1992 and Clemens & Stevens, 2012).
- 3) Crystal fractionation or Fractional crystallisation from the source (e.g. Chappell and Wyborn, 2004)

Clemens and Stevens (2012) briefly summarise the other variation mechanisms that have been suggested by several authors to explain the variation in chemistry displayed by common I-types; wall-rock assimilation, liquid immiscibility, vapour-phase alkali leaching, double-diffusive convection and Soret diffusion, deep –seated magma hybridisation in mash or hot zones, shallow magma mixing and mingling, progressive partial melting, crystal fractionation and phenocryst unmixing, crystal entrainment and unmixing and restite unmixing and peritectic assemblage entrainment.

1.2 Mafic Enclaves as a petrogenetic tool

The term enclave was forged by Didier (1973) and was used to describe mesoscopic rock bodies enclosed within granitic rocks. Enclaves share similar compositions to their host rocks and often contain a higher proportion of mafic minerals with a finer-grained texture than their host counterpart. Enclaves are related to their host rocks and their linkage and petrogenetic significance has been studied widely by several authors (e.g. Didier, 1973; Vernon, 1983; Didier and Barbarin, 1991,). Various authors have used various names to describe enclaves; microgranular enclaves, igneous microgranular enclaves or mafic magmatic enclaves; this terminology is independent of location or characteristics, as most enclaves show similar characteristics independent of location or tectonic environment. The different terminology is more suited to individual authors and these enclosed rock bodies will be referred to as 'mafic enclaves' in this study. The term 'mafic enclaves' used in this study does not refer to mineral inclusions or xenoliths where the chemistries of the enclosed material are different and unrelated to the host rock. Mafic enclaves have over the years, started to play a considerable role in understanding the evolution of granitic magmas. There are three predominant theories which describe the petrogenesis of mafic enclaves:

- 1) Settling of early crystals from the host magma or crystallisation from cumulate fragments. (e.g. Dodge and Kistler, 1990 and Dahlquist, 2002)
- 2) Globules of hybrid magma which represent the mixture of a more mafic magma mixing with a more felsic host magma.(e.g. Vernon, 1984 and Barbarin, 1999, 2005)
- 3) Mafic enclaves represent fragments of recrystallized metamorphic rocks (or restite blocks) inherited from the source during partial melting of it (the source). (e.g. Chappell et al., 1987 and Kocak, 2006)

Many authors (Didier and Barbarin, 1991; Dahlquist, 2002; Perugini et al., 2003; Kocak, 2006; Kocak et al., 2011,) have used mafic enclaves as evidence supporting processes which are responsible for shaping the chemistry of the respective granitic plutons. It is imperative to note that magma interaction either via mixing or hybridization between mafic enclave magma and felsic host granite magma is a dominant mechanism proposed by many authors to explain mafic enclave genesis. Such case studies will be explored in greater detail in a later section. The genetic relationship proposed to exist between mafic enclaves and their host rocks from previous studies suggests that the study of mafic enclaves as well as their host rocks can be significant in finding out the processes that shape the petrogenesis of a granitic pluton or body.

1.3 The Buddusò Pluton; a perfect study area with common I-type granites hosting mafic enclaves

The area of study is the Buddusò Pluton in Sardinia, Italy. It is an I-type granitic pluton which is subdivided into three units (Barbey et al., 2008); an inner unit comprised of leucogranites (SiO₂ concentration ranging between 74.00 and 77.01 wt. %), a middle unit comprised of granitic compositions (SiO₂ concentration ranging between 68.06 and 74.04 wt. %) and an outer unit comprised of granodiorites (SiO₂ concentration ranging between 64.48 and 66.81 wt. %). Mafic enclaves exist throughout the pluton, increasing in abundance proportionally to the decreasing silica concentration of the pluton (from the inner to outer unit). Mafic enclaves show a similar mineral assemblage to the granites (*sensu lato*) with a higher proportion of mafic minerals. The Buddusò pluton has been proposed to have formed by interaction between felsic and mafic magmas (Zorpi et al., 1989 and Barbey et al., 2008).

The Buddusò Pluton is a perfect example of a common I-type granitic body with mafic enclaves. This study will make use of a blend of geo-analytical techniques; field relations, whole rock geochemistry, petrography, mineral chemistry, zircon geochronology and Lu-Hf and U-Pb isotopic analysis of the zircons from both mafic enclaves and granites to aid in meeting the aims of the study, which are to:

- 1) Explain the origin of the compositional variation seen in the granitic units
- 2) Explain the origin of the composition of the mafic enclaves
- 3) Constrain the most consistent model for the petrogenesis of the Buddusò Pluton
- 4) Assess the significance of using mafic enclaves as a petrogenetic tool

Chapter 2: Geological Setting and Past Work

The town of Buddusò is located in northern Sardinia in the province of Sassari (represented by the black box on the inset image in Fig.1). There are several quarries (1-9 in Fig.1) throughout the pluton that mine granite, which offers a great opportunity to study and obtain good, fresh samples as well as study structures and textures.

2.1 Geological Setting

The Sardinia- Corsica batholith was formed between 320Ma to 300Ma, during the Hercynian orogeny (Poli et al., 1989., Zorpi et al., 1991). During the Oligocene, Corsica-Sardinia broke away from the Iberian plate as one lithospheric block and rotated counter-clockwise to reach its present position. This drift subsequently caused the opening of the Liguro-Provencal back-arc basin which lead to subduction under Sardinia along the Franco-Spanish margin and a volcanic cycle until the Mid Miocene (Carminati et al., 2010). Towards the end of the Oligocene, the Corsica- Sardinia block migration was stopped by the Adriatic continental plate and during the Plio-oleistocene, the opening of the Tyrrhenian Basin subsequently caused a new volcanic cycle. Sardinia-Corsica is presently bounded by the Ligurian-Provencal Basin (West), Tyrrhenian Sea (East) and Northern Algerian Basin (South) (Carminati et al., 2010). All these basins represent thinned continental to oceanic basins and formed during the Neogene.

The Sardinia-Corsica batholith extends over if ca. 120000 km² and belong to a calc-alkaline suite which intrudes the metamorphic basement that underwent repeated cycles of deformation during the Hercyian orogenesis. After Cenozoic drifting of the Sardinia-Corsica block, the basement shows a NW-SE trend; increasing in metamorphic grade from SW to NE (Poli et al., 1989). The batholith is sub-divided into two magmatic associations; the sub-alkaline association in northwest Corsica and the calc-alkaline association in central and southern part of the Sardinia-Corsica batholith. All plutons are heterogeneous and differ in composition, abundance of mafic enclaves, age and degree of deformation.

The Buddusò pluton belongs to the above mentioned calc-alkaline plutonic association aged ca. 305 – 290 Ma (Barbey et al., 2008). An Rb-Sr isochron analysed by Cocherie (1984) gives an emplacement age of 281+/- 5 Ma. The pluton has three petrographic groups; granodiorites, tonalities and monzogranites with plentiful microgranular mafic enclaves (Rossi and Cocherie, 1991). The pluton is approximately 15km in length, and crops out over an area of 70km². It is bound by the Aladei Sardi pluton to the North, Concas pluton to the right and Benetutti pluton to the South (Fig.1). The Benetutti's intrusions are near synchronous with those of the Buddusò

Pluton and are comprised of granodiorites and two types of monzogranites; one with megacrystals of K-feldspar and one with biotite and muscovite. Enclaves are sporadic and exist in all granodiorites and monzogranites. Aladei Sardi is of granodiorite composition and is suggested to have intruded simultaneously (Orsini & Fernandez, 1987). The Buddusò pluton is crosscut by the Concas pluton, which is comprised of leucogranites with garnet ± muscovite and mafic enclaves are uncommon in this pluton. Rb/Sr geochronological dating revealed an emplacement age of 275 ± 4 Ma (Cocherie, 1978) for the Concas pluton.

2.2 Past work

2.2.1 Sardinia-Corsica Batholith

Many authors studied various plutons of the Sardinia-Corsica batholith and its mafic enclaves to understand the petrogenesis of the batholith as a whole (Orsini & Fernandez, 1976, Orsini et al., 1977, Bruneton & Orsini, 1977, Orsini et al., 1987, Cocirta & Michon, 1989, Zorpi et al., 1989, Poli et al., 1989, Zorpi et al., 1991) and more recently Barbey et al. (2008) and Rocco et al. (2012). Some of these authors focused specifically on the Buddusò pluton and its mafic enclaves (Orsini, 1976, Bruneton & Orsini, 1977, Orsini & Fernandez, 1987 and Barbey et al., 2008).

Orsini (1976) described two magmatic associations; sub-alkaline potassic in the northwest Corsica and a larger calc-alkaline series in the central and southern part of Sardinia-Corsica. Three major groups were recognised based on composition into groups G1, G2 and G3. This labelling by Orsini (1976) was used by many authors who studied the Sardinia-Corsica Batholith thereafter (Bruneton & Orsini, 1977, Orsini and Fernandez, 1987, Cocirta & Michon, 1989 and Barbey et al., 2008). G1 was described by Orsini (1976) as consisting of homogenous to slightly differentiated intrusions of tonalites and granodiorites characterised by the presence of amphibole. G2 was described as being concentrically zoned from leucogranites in the inner, increasing in maficity to a granodioritic outer unit. All plutons within the G2 suite show this zonation or part thereof (Zorpi et al., 1989). The G2 suite is most represented in the calc-alkaline association and the Buddusò pluton falls completely within this suite (Cocirta & Michon, 1989, Barbey, 2008). This group was characterised by K-feldspar megacrystals. G3 was described as being mainly composed of leucogranites and characterised by the occurrence of garnet ± muscovite. G3 is the youngest of the three groups of granites with an Rb/Sr age of 275 ± 4 My, G2; 292 ± 5 My and the oldest age represented by G1 of 297 ± 6 My (Del Moro et al., 1975, Cocherie, 1978).

Cocirta & Michon (1989) describe two different groups of mafic enclaves; the first group of mafic enclaves labelled E1 are found only within the G1 granitoids and are dioritic in composition. The second group of mafic enclaves labelled E2 (quartz diorites) and mafic enclaves labelled E3 (tonalites) are found in the corresponding G2 and G3 granite hosts. The mafic enclaves from the second group decrease in MgO, CaO, TiO₂ and total Fe as the silica concentration increases in their respective host rocks. Mafic enclaves are common in the G1 and G2 granite groups but are rare in the G3 granite group.

2.2.2 The Buddusò Pluton

2.2.2.1 The three magmatic units of the Buddusò pluton

Table 1: Lithological units in the Buddusò Pluton as identified by different authors with the corresponding terminology used.

Authors	Lithological units					
This Study	Inner Unit (Iu) Leucogranites	Middle Unit (Mu) Granites		Outer Unit (Ou) Granodiorites		
Orsini, (1976), Bruneton & Orsini, (1977), Zorpi et al. (1989)	Unit III	Unit II		Unit I		
	Leucogranites	Ia Biotite Monzogranites	Ib Monzogranites	Ia Tonalites	Ib Granodiorites	Ic Granites with megacrystals of K-feldspar
Barbey et al. (2008)	Inner Unit (Iu)	Middle Unit (Mu)		Outer Unit (Ou)		
	Leucocratic monzogranites	Mu1 Biotite Monzogranites	Mu2 Monzogranites	Ou1 Hbl-bearing tonalities granodiorites	and	Ou2 Biotite Monzogranites

There are three magmatic units that have been identified by several authors (Table 1) which constitute the Buddusò pluton (Fig.1). Authors are in agreement that the Buddusò pluton is concentrically zoned with the units becoming more felsic towards the centre (inner unit) of the pluton (Zorpi et al., 1989) with mafic enclaves also decreasing in abundance in the same direction.

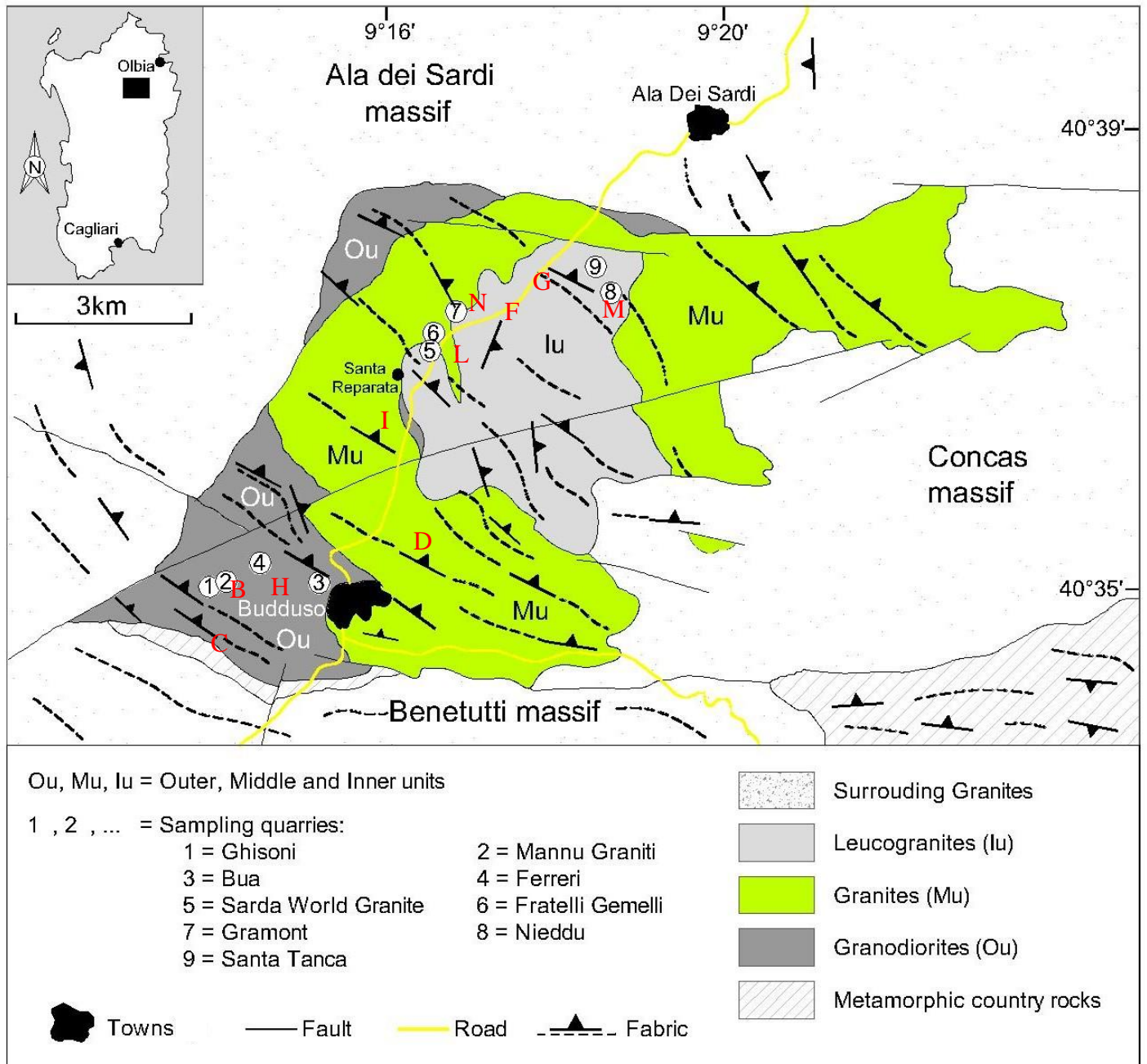


Figure 1 : Geological map of the Buddusò pluton (redrawn from Barbey et al., 2008) showing sites B-D, F-I and L-N, where samples were collected from. Corresponding GPS locations can be found in Table 2.

2.2.2.2 Bruneton & Orsini (1977)

Bruneton & Orsini (1977) differentiate the lithological units as described in Table 1 above. In unit I enclaves showed wide centres which tapered towards the ends, planar magmatic fluidity was recorded by the orientation of coloured minerals and K-feldspar. In Unit II the monzogranites are differentiated on their biotite content, mafic enclaves are always arranged according to planar magmatic fluidity. In unit I and II, the planes of magmatic fluidity are directed towards the centre of the pluton (redrawn as fabric on Fig.1). Plagioclase was recorded to show zoning, and its maficity gradually decreases from An 54 (unit I) to An 24 (unit III). A wide array of compositions in biotites were documented resulting in a gradual enrichment of total Fe from the unit III through to unit I. K-feldspar displayed a constant composition throughout all units (Or 90, Ab 10). Bruneton & Orsini (1977) proposed that with the evidence found, these magmatic units did not form from successive intrusions. The presence of fusiform enclaves, the orientation of the planar magmatic fluidity parallel to cartographic boundaries as well as the absence of net contacts, fine grained edges and angular enclaves all favour a single intrusion argument. The study concluded that the Buddusò pluton was an alloctonous post-tectonic intrusion that is composed of different portions of the same calc-alkaline magma that was differentiated at depth; fractional crystallisation was the dominant magmatic mechanism proposed.

2.2.2.3 Barbey et al. (2008)

Barbey et al. (2008) investigated the origin of the proposed igneous layering present in the pluton and the extent to which the proposed layering reflects mafic and felsic magma interactions. The three magmatic units were defined as per Table 1 above. All units show a mineral assemblage; Quartz+ K-feldspar + Plagioclase + Biotite, with the outer unit (Ou) showing a higher variation in biotite and plagioclase normative contents. Hornblende is a mineral characteristic of the outer unit distinguishing the increasing maficity from the inner unit (Iu) through to the outer unit (Ou). Two compositions of enclaves are recognised; dioritic; plagioclase + biotite + amphibole and quartz dioritic, tonalitic; plagioclase + biotite + quartz. The dioritic enclaves found in the outer unit exhibit a homogenous texture and the quartz dioritic and tonalitic enclaves are found in the middle (Mu) and inner units. Enclaves show crystal capture, plagioclase crystals detailing resorbed cores and reaction rims and ocelli quartz; all proposed to be evidence of interaction of the enclave mafic magma with the host magma. This assumption is made irrespective of the sharp contacts noted by the authors between the mafic enclave and its host granites. In the direction from the outer to the inner unit there is; a decrease in most oxides with an increase in SiO₂ apart from K₂O, a decrease in light REE, constant heavy

REE patterns all suggesting an increasing degree of differentiation of units in the same direction (major and trace element compositions from Barbey et al. (2008) can be found in Fig.8-11).

$^{87}\text{Rb}/^{86}\text{Sr}$ and $^{87}\text{Sr}/^{86}\text{Sr}$ ratios yielded ages of 286 ± 10 Ma ($\text{Sr}_i=0.4090\pm 4$, $\text{MSWD}= 1.65$) and $^{143}\text{Nd}/^{144}\text{Nd}$ isotopic ratios yielded ages of 286 ± 16 Ma ($\epsilon_{\text{Nd}(t)}=-5.6\pm 0.1$, $\text{MSWD}=1.3$) (Fig.2). The above yielded ages which were concordant with the emplacement sequence of the Sardinia-Corsica Batholith described by Rossi and Cocheri (1991).

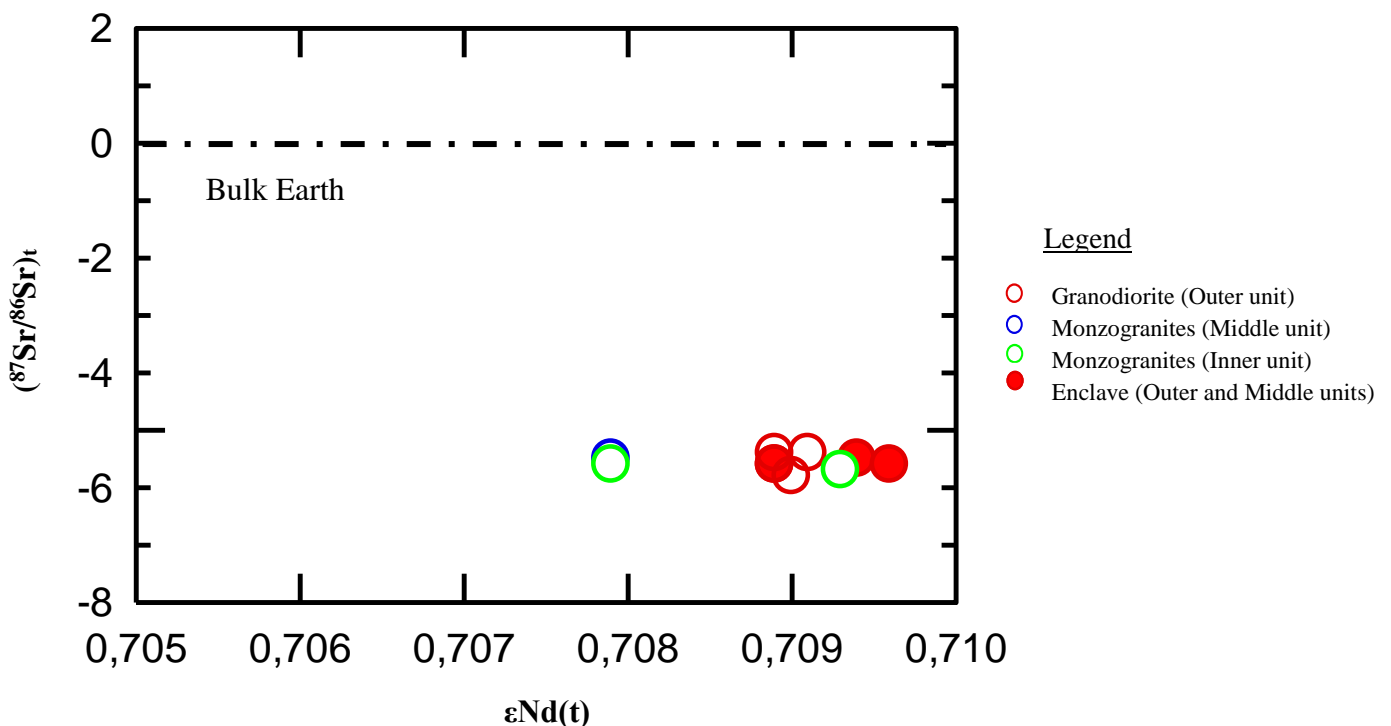


Figure 2: Graph showing Sr-Nd isotopic data for the Buddusò Pluton for granites and mafic enclaves. $^{87}\text{Sr}/^{86}\text{Sr}$ initial ratios and $\epsilon_{\text{Nd}(t)}$ values were calculated for 286 Ma, values are from Barbey et al. (2008).

Field relations of the entire pluton revealed a preferred orientation in biotite, K-feldspar and mafic enclaves which constituted to a well-developed submagmatic planar fabric in the outer unit. Quartz show elongated grains and are indicative of subsolidus deformation. Faults showing higher proportions of biotite were noted with respect to the host granites and was interpreted as evidence of magma removal. Two types of layering was seen in the outer and middle units based on the distribution of biotite; isomodal layering showing alternating layers of homogenous biotite layers and biotite-free layers and mineral-graded granodioritic layers showing

heterogeneous dispersal of biotite. In all three units schlieren was observed. In the middle unit mafic enclaves are stretched in monzogranites and are seen grading into biotite schlieren. Mafic enclaves are dispersed heterogeneously throughout the outer unit but show an increased occurrence near contacts with surrounding country rocks. The layering and field relations are discussed very briefly here, however layered structures involving dykes, shear zones and schlieren found in both the outer and middle units are complex and the detailed study undertaken by Barbey et al. (2008) should be consulted should the reader require a more comprehensive outline.

The volume proportions of each unit in comparison to the overall evolution in chemistry from the outer unit towards the inner unit, as well as the decrease in deformation in the same direction implies, according to the authors, an argument prohibiting in situ differentiation. The decreasing deformation from the outer unit inwards, suggest incremental magmatic pulses with the outer unit being emplaced first. Similar mineral compositions analysed in the enclaves and host granites, captured crystals and reaction rims show interaction between two magmas. However homogeneous initial isotope concentrations (Fig.2) and partial re-equilibration of certain mineral phases oppose the theory of two magmas of different compositions mixing. Magma mixing could produce homogeneous isotopic compositions when mixed:

- 1) If both magmas had identical Nd isotopic compositions and differed in their LREE concentrations
- 2) Via isotopic exchange by diffusion during magma mixing (Baker, 1989)
- 3) The magmas that underwent mixing were cogenetic.

Isotope homogeneity is uncommon for Sr and Nd in granites and their enclaves (Flinders and Clemens, 1996).

The modally-graded layering was attributed to two possible theories; magma segregation via compaction or deformation and convection related crystal sorting. Fractional crystallisation was ruled out as biotite shows no zoning or systematic change in X_{Fe} values and the different compositions preserved by the minerals in the rocks throughout the pluton ruled out late stage re-equilibration of the minerals. The isomodal layering seen also opposed the idea of crystal fractionation due to the absence of chemical evolution from one layer to the other. Two interpretations for the isomodal layering were suggested; mingling and stretching of a biotite rich magma with a more differentiated magma or by flow banding - “deformation assisted magma segregation with redistribution of interstitial evolved residual magma.”

Important conclusions about the processes of the construction of the pluton from the study included;

- 1) Variation in the granite compositions is attributed to magma pulses of differentiated but isotopically homogeneous magmas with an array of compositions between granodiorites (Ou) to leucomonzogranites (Iu) successively emplaced.
- 2) Enclaves represent hybrids which formed due to magma mingling and hybridization related to viscous flow which occurred prior to final emplacement.
- 3) Modal-layering is caused by material transfer within parts of the pluton due to density currents.
- 4) Isomodal layering is caused by deformation assisted magma segregation or flow banding.

All the above processes are explained by the authors to never affect the entire pluton body and are limited to specific parts of the body. The partial or incomplete re-equilibration of some minerals suggests that hybridisation or fragmentation of the mafic magma happened either deeper in the chamber or occurred just before emplacement.

2.2.3 Using the Buddusò pluton; a case study to aid understanding the petrogenesis of the Sardinia-Corsica Batholith

2.2.3.1 Zorpi et al. (1989)

Zorpi et al. (1989) undertook a study on four compositionally zoned plutons from the G2 calc-alkaline association mentioned above; one of them being the Buddusò pluton. The aim of the study was to understand if there was a link between the zonation of the plutons and the abundance of mafic enclaves and to assess which differentiation mechanisms played a role in producing the zoning of the plutons. On investigation of the Buddusò pluton the study identified the three magmatic units as described by Bruneton & Orsini (1977) in Table 1 above. There is an increase in silica content; quartz and K-feldspar from the outer unit I through to the inner unit III, with a decrease in amphibole and modal proportion of biotite in the same direction. Mafic enclaves show a wide range in compositions and range between 45% and 69% with respect to their SiO₂ content; they are alkali rich and Ca poor. K₂O decreases with decreasing maficity. Zorpi et al. (1989) based their study on mineralogical, petrographical, chemical and field evidence found by Orsini (1979), Cocirta & Orsini (1986) and Concirta (1986). The paper summarised their findings:

- 1) Mineralogies of mafic enclaves and host granites are identical and differ in modal proportions. Compositions of minerals in both mafic enclaves and host granites are also similar; this similarity supposedly supports the idea that minerals in both mafic enclave and host granite, crystallised under the same physical conditions after the mafic magma was incorporated into the felsic magma.
- 2) Remnant minerals; corroded plagioclase cores, clinopyroxene partially replaced by hornblende, clots of Mg-rich hornblende, all are proposed to represent evidence of early formed minerals that were destabilized after the mafic magma mixed with the felsic magma.
- 3) Existence of “disequilibrated crystals” in host granites and mafic enclaves; two textures of apatite seen; acicular and short prisms, ocelli quartz inclusions penetrated by mafic inclusions which are often surrounded by hornblende \pm biotite reaction rims; were all proposed to imply mechanical transfer between host granite and mafic enclave and vice versa.

When comparing all data for the four different plutons, the mafic enclaves that belonged to each of the plutons showed a corresponding narrow range of FeO_t/MgO and the authors used FeO_t and MgO contents of mafic enclaves and host granites as discriminants to categorise each pluton and its mafic enclaves. They also suggest that this FeO_t/MgO ratio of each pluton portrays intrusive events linked to the mingling of felsic magma with the mafic magma. The enclaves show a wide range in Mg and Fe content, and some compositions are close to the host granites, the authors attribute this variation in composition to the degree or extent of hybridization seen in the enclave by the felsic granite magma. The authors suggest that for the Sardinia-Corsica batholith the FeO_t/MgO ratio demonstrates the hybridization process between the two components. The reader is referred to Figures 1 and 2 in Zorpi et al. (1989).

The authors proposed the following mechanisms of mixing and mingling;

- 1) Mechanical exchange of crystals between the two magmas resulting in a modification of the mafic enclave magma as it is smaller in volume. Host granites from Unit I (outer unit) show a higher degree of hybridization by the mafic enclave magma because of the higher proportion of mafic enclaves and the lower compositional contrast between mafic enclave and host granite.
- 2) Volatile migration from felsic magma to mafic magma exhibited by abundance of biotite and amphibole and a general Si, K, Rb, Cs, P, Zr enrichment in the enclaves and Ca, Fe and Mg impoverishment in comparison to host granites.

- 3) Chemical exchange via diffusion displayed by aureoles of leucocratic composition found at contacts with enclaves in the host granite matrix, dark peripheral zone in enclaves. Both textures showing chemical migration.
- 4) Expulsion of residual liquid into host granite which migrated from the cores of inclusions.

The research concluded that there is a close relationship that exists between the composition of the plutons and the quantity of the mafic enclaves. Most of the plutons were zoned and became more felsic towards the core, with a parallel decrease in the amount of mafic enclaves. Mixing of felsic and mafic magmas was proposed to occur at several stages in the pluton's history from injection of basaltic magma into the chamber until final emplacement of the pluton. Mixing and mingling was assisted by the above mentioned mechanisms during ascent and upon final emplacement. The pluton cooled and solidified from the outer (unit III) to inner (unit I).

2.3 Recent work published using mafic enclaves to understand petrogenetic processes of magmatic bodies

Detailed studies involving petrographic, geochemical analysis, mineral chemical analysis and field evidence of both mafic enclaves and host rocks can shed light on petrogenetic processes and could possibly give valuable information on both the magma that generated the enclaves and the granites that would otherwise not be readily available from the granites itself. Hence the study of mafic enclaves has popularly become the subject of widespread research. For the context of the reader, the prevalent theories for petrogenesis of I-type granites will be reviewed.

2.3.1 Magma mixing or mingling

Various authors have ascribed the presence of mafic enclaves in I-type granites to the process of magma mixing or mingling between a felsic and mafic magma (Zorpi et al., 1989, Kocak et al., 2011 and Ghaffari & Omran, 2015). Further petrographical and geochemical evidence for magma mixing summarised from studies (Kocak et al., 2011 and Ghaffari & Omran, 2015) are as follows;

- 1) The enclaves' contact morphology; presence of chilled margins or diffused contacts with host granites presents evidence of a mafic enclave magma quenching against a cooler felsic host. The absence of chilled margins in some enclaves is explained as a consequence of having been formed from the breakdown of larger enclaves with chilled margins.
- 2) The morphologies of zoned plagioclase, acicular apatite, bladed biotite and quartz xenocrysts are all suggestive of magma mixing processes (Hibbard, 1981). The acicular apatite morphology was suggested as being indicative of mafic magma quenching and igneous microtextures; bladed biotite and zoned plagioclase are evidence of mafic components added to felsic magma chamber (Eichelberger, 1980)
- 3) The ellipsoidal shape of the enclaves with their pillow like textures and slightly diffused contact with the host granodiorite were proposed to be evidence of quenched globules which were formed from a mafic magma via the process of magma mixing or mingling.
- 4) Plagioclase crystals show corroded cores with An zoning and compositional spikes. Plagioclase can become corroded when it exists in magma that it is not in equilibrium. New rims of that magma's composition will crystallise around the plagioclase's corroded

cores resulting in zones of differing An composition as equilibration occurs (Wieber, 1968). This texture could also be formed on magma ascent to the surface via decompression (Stormer, 1972).

- 5) The xenocrysts of host material seen in the enclaves suggest magma-hybridisation and were mechanically transferred to these mafic magma globules during magma mixing.

2.3.2 Fractional Crystallisation

Another accepted hypothesis for the presence of mafic enclaves in I-type granites is fractional crystallisation. The evidence for fractional crystallisation is as follows;

- 1) The similarity in mineralogy and mineral composition between mafic enclave and host granites is indicative of similar chemical and physical conditions of crystallization for both the mafic enclave and host granites (Dahlquist, 2002). Mafic enclave magma is segregated from the parent magma leaving a slightly differentiated host granite magma.
- 2) Isotopic homogeneity in initial Sr and Sm/Nd ratios of mafic enclaves and host granites suggests partial melting of the same source with the same isotopic signature.
- 3) Major and trace element data for enclaves do not show linear mixing arrays and plot of trends defined by their host granites (Akal & Helvci, 1999).

2.3.3 A combination of several processes, case study ; Central Victoria, Australia, Clemens et al. (2016a)

Clemens et al. (2016a) studied the granites and their mafic enclaves from the Central Victoria in south-eastern Australia. A large analytical database of several other authors' work on the various plutons of Central Victoria was studied. This database was used to look at chemical variations between granites and their mafic enclaves; mainly variations between titanium and iron + magnesium. These variations were explored to investigate the petrogenetic processes of both granites and mafic enclaves. It has been documented that these three elements are present in granitic rocks at varying concentrations. Through studies of magma inclusions within peritectic minerals as well as partial melting experiments (Stevens et al., 1997 & Bartoli et al., 2013), these three elements only “occur at low concentrations in the magmas that form the liquid parts of granitic magma” (Clemens et al., 2016a). This allowed the authors, based on the concentration of these elements, to assess “which rocks crystallised from liquid magmas and which rocks crystallised from magmas that contained source-inherited crystalline material” (Clemens et al., 2016a). The authors' work is based on the assumption that leucogranites

represent magmas which are almost completely pure magma and therefore granodiorites are composed of mixtures of magma and ferromagnesian crystals. This mixture is achieved either via crystal fractionation of ferromagnesian crystals from granite magma, mixing of mafic and felsic magmas or entrainment of ferromagnesian minerals into the granite magma at the source. The concentrations of these elements are higher in the mafic enclaves in comparison to host rock. The study of the trends between them allowed the authors to investigate which process generated the enclaves and the granites and to assess if the processes were the same for both the granites and enclaves. Mol. of element per 100g values was used and lines defined on graphs are independent of Mg# of minerals or magma. The reader is advised to refer to the paper in discussion, for a better understanding. It is important to note that the paper studied both S-type and I-type granites, they were however dealt with separately and only the results on I-type granites and their mafic enclaves will be presented as it is relevant to this study.

I-type rocks and enclaves from the Cowbar, Tynong and Harcourt batholiths were analysed according to their ferromagnesian content as explained above. The Cowbar and Tynong batholiths' mafic enclaves showed non-linear trends in comparison to its host rocks. However mafic enclaves from the Harcourt Batholith showed a good correlation and a similar slope to the host granites. Magma mixing between the mafic enclave magma and the host rock magma could explain the variation seen in the rocks. However the study suggests that when other chemical and isotopic evidence were analysed; magma mixing did not become a viable mechanism for the chemical variation seen between the rocks. Geochemical data plotted for the same host granites and their enclaves showed a poor correlation with a two-end member mixing model seeming highly unlikely.

There were several conclusions drawn about the mafic enclaves;

- 1) Mafic enclaves have a fine-grained texture and a mafic composition, too mafic to have arisen from crustal magmas suggesting that the parental mafic enclave magma was mantle-derived. (Stevens et al., 2007)
- 2) The lack of correlation between elements in mafic enclaves suggests a "chaotic" interaction between mantle-derived mafic enclave magma and crustal magma prior to emplacement, to create mafic enclave parent magmas which then were engulfed by the host granites.
- 3) Mafic enclaves and host granites further interacted at/near emplacement both mechanically; due to the captured crystals of host granite found in the enclaves and chemically; evidence of diffusive exchange of magma components.

The study concludes that the differentiation processes that acted on the mafic enclaves and host granites are completely different. The host granite's chemical variation can be ascribed to a mixture of mechanisms; crystal fractionation, peritectic mineral entrainment and magma mixing/mingling which are absent in the mafic enclaves. Mantle derived mafic enclave magma mixed with crustal materials at a depth before emplacement and incorporation into the felsic granite host magma. Once the mafic magma was emplaced, further chemical interaction; noted by the authors as chaotic mineral entrainment and diffusional exchange, took place with the host granite magma resulting in irregular chemical changes. These irregular chemical changes make it complicated to study the origin of the mafic enclaves.

Chapter 3: Analytical Techniques

3.1 Field work and sampling

Dr Federico Farina of University of Geneva, Genève and Professor Gary Stevens of Stellenbosch University undertook the fieldwork in Sardinia, Italy in September 2010. The localities of the sample are shown in Fig.1.

Table 2: A sample list of localities, rock types and the different analytical techniques used individually, (a) Whole rock and trace element geochemistry, (b) Thinsection, (c) Mineral Chemistry, (d) U-Pb isotope analysis and (e) Lu-Hf isotope analysis. (Sample localities were not recorded/lost for 12 samples.)

Sample	Latitude	Longitude	Locality	Unit	Rock Type	WR + TE ^(a)	ThinS. ^(b)	Min. Chem. ^(c)	U-Pb ^(d)	Lu-Hf ^(e)
BG1	40° 37' 48.0166" N	9° 17' 45.2479" E	G	Inner	Leucogranite	X				
BG10	40° 37' 19.5308" N	9° 17' 24.1354" E	F	Inner	Leucogranite	X	X	X		
BG18	40° 37' 35.112" N	9° 18' 19.2197" E	M	Inner	Leucogranite	X	X			
BG19	40° 37' 35.112" N	9° 18' 19.2197" E	M	Inner	Leucogranite	X				X
BG25	40° 35' 19.1677" N	9° 16' 6.1651" E	D	Inner	Leucogranite	X	X			
BG32	40° 37' 28.5002" N	9° 16' 57.3157" E	N	Inner/Middle	Leucogranite	X	X			
BG2	40° 36' 29.0239" N	9° 16' 3.9076" E	I	Middle	Granite	X				X
BG3	40° 36' 29.0239" N	9° 16' 3.9076" E	I	Middle	Granite	X	X			X
BG23	40° 35' 19.1677" N	9° 16' 6.1651" E	D	Middle	Granite	X				
BG24	40° 35' 19.1677" N	9° 16' 6.1651" E	D	Middle	Granite	X	X			
BG26	40° 35' 19.1677" N	9° 16' 6.1651" E	D	Middle	Granite	X	X	X	X	X
BG27	40° 35' 19.1677" N	9° 16' 6.1651" E	D	Middle	Granite	X				
BG30	40° 37' 28.5002" N	9° 16' 57.3157" E	N	Middle	Granite	X				
BG31	40° 37' 28.5002" N	9° 16' 57.3157" E	N	Middle	Granite	X	X			
BG15mix	40° 34' 23.8285" N	9° 13' 52.5619" E	C	Middle/Outer	Enclave	X	X		X	X
BG15mme	40° 34' 23.8285" N	9° 13' 52.5619" E	C	Middle/Outer	Enclave	X	X	X	X	X
BG16mix	40° 34' 23.8285" N	9° 13' 52.5619" E	C	Middle/Outer	Enclave	X				
BG16mme	40° 34' 23.8285" N	9° 13' 52.5619" E	C	Middle/Outer	Enclave	X				
BG13	40° 34' 23.8285" N	9° 13' 52.5619" E	C	Outer	Granodiorite	X	XX	X		X
BG14	40° 34' 23.8285" N	9° 13' 52.5619" E	C	Outer	Granodiorite	X				
BG33	40° 34' 49.0494" N	9° 14' 22.155" E	H	Outer	Granodiorite	X	X			
BG34	40° 34' 49.0494" N	9° 14' 22.155" E	H	Outer	Granodiorite	X				
BG35	40° 34' 49.0494" N	9° 14' 22.155" E	H	Outer	Granodiorite	X			X	X
BG36	40° 34' 49.0494" N	9° 14' 22.155" E	H	Outer	Granodiorite	X	X			
BG48	40° 34' 41.7907" N	9° 13' 49.7813" E	B	Outer	Granodiorite	X	X			X
BG8	40° 37' 19.5308" N	9° 17' 24.1354" E	F	Outer	Enclave	X	X			
BG9	40° 37' 19.5308" N	9° 17' 24.1354" E	F	Outer	Enclave	X	XX			
BG21	40° 35' 19.1677" N	9° 16' 6.1651" E	D	Outer	Enclave	X	X			
BG22	40° 35' 19.1677" N	9° 16' 6.1651" E	D	Outer	Enclave	X	X			
BG29	40° 35' 19.1677" N	9° 16' 6.1651" E	D	Outer	Enclave	X	X	X		
BG38	40° 34' 49.0494" N	9° 14' 22.155" E	H	Outer	Enclave	X	X			
BG4A	40° 37' 0.2633" N	9° 16' 48.0302" E	L	/	Country rock	X	X			
BG4B	40° 37' 0.2633" N	9° 16' 48.0302" E	L	/	Country rock	X	X			
BG6	40° 37' 0.2633" N	9° 16' 48.0302" E	L	/	Country rock	X	X			
BG7	40° 37' 0.2633" N	9° 16' 48.0302" E	L	/	Country rock	X	X			
BG49	40° 37' 0.2633" N	9° 16' 48.0302" E	L	/	Country rock	X	X			
BG11							X			
BG12							XXXX	XX		
BG17							XXX	X		
BG20							X			
BG28							X			
BG37							XX			
BG39							XX			
BG41							X			
BG42A							X			
BG44							X	X		
BG43							X			
BG46							X	X		

3.2 Microscopic petrography

Forty-six thin sections were made at the Department of Geological Sciences, University of Cape Town. Some samples have more than one thin section, this is due to the different textures seen in the rock hand sample (refer to Table 2). Thin sections were made of the three different types of host rocks seen as well as the different enclave textures. There are also a few thin sections which cover contact between host granites and mafic enclaves so as to inspect their interaction. The thin sections were used to identify mineral assemblages and to describe textures of interest between the minerals.

3.3 Mineral chemical analysis

Mineral chemical analysis was undertaken at Stellenbosch University's Central Analytical Facility (CAF). Sample preparation requires the samples to be properly cleaned and carbon coated before being imaged and analysed. Plagioclase, K-feldspar, biotite and hornblende mineral major element compositions were analysed by quantitative energy-dispersive X-ray spectroscopy (EDS) analysis using a Zeiss EVO MA 15 Scanning Electron Microscope (SEM). The SEM is fitted with an Oxford Instrument 20mm² detectors and uses Oxford INCA Software. Beam conditions used during analysis were; 1) an acceleration voltage of 20.00kV and approximately 1.0A probe current, 2) a working distance of 8.5mm and 3) a specimen beam current of -20.00nA. Accuracy of analytical data was confirmed by using a mineral standard of known composition as unknowns. Natural standards for each mineral can be found within the Appendix (Astimex Scientific limited, MINM25-53 #05-010) under Zeiss EVO MA 15 SEM mineral standards. Mineral stoichiometries were calculated from mineral phases to obtain mineral formulae in Microsoft Office Excel 2010. The analyses falling below ± 0.02 of ideal stoichiometry was rejected.

SEM analysis was used to determine the mineral compositions in samples as well as compare the compositions of plagioclase, K-feldspar, biotite and hornblende between samples. In some samples traverses of points across crystals were analysed to identify compositional changes or zoning within a sample (Fig.8&9).

3.4 Whole-rock geochemistry

3.4.1 Sample preparation

The fusion disk is prepared for XRF analysis by an automatic Claisse M4 Gas Fusion instrument and ultrature Claisse Flux; a ratio of 1:10 sample: flux is used. This sample + flux mix is coarsely crushed and a piece of sample was mounted along with a number of other samples in a 2.4cm round resin disk. The mount is then mapped and polished for analysis.

3.4.2 LA-ICPMS

Major and trace element compositions were obtained from the Laser Ablation-Inductively-Coupled-Mass-Spectrometry (LA-ICPMS) laboratory at Stellenbosch University's CAF. A NewWave 213nm laser connected to an Agilent 7500ce ICP-MS is used to analyse trace elements in bulk rock samples and on single grains. Laser ablation is executed in He gas at a flow rate of 0.9L/min. Before introduction into the ICP plasma it is mixed with argon (0.9L/min). For traces in fusions, 3 spots of 110µm each is ablated on each sample using a frequency of 10Hz and ~100mJ energy.

The trace elements are quantified using NIST 612 for calibration. The percentage SiO₂ from XRF measurement was used as an internal standard. A quality control standard was run at the beginning of the sequence with calibration standards having run throughout; BCR-2 or BHVO 2G, both basaltic glass certified reference standards produced by USGS (Dr Steve Wilson, Denver, CO 80225). A fusion control standard from certified basaltic reference material (BCR-2, also from USGS) was also analysed in the beginning of a sequence to verify the effective ablation of fused material.

Data was processed using Glitter software, distributed by Access Macquarie Ltd., Macquarie University NSW 2109. Trace element compositions were analysed using Microsoft Excel 2010 and geochemical plots were made using IgPet06 software.

3.5 Isotope analysis of zircons

3.5.1 Zircon sample preparation

Rock samples were crushed using the jaw crusher and sieved. The samples were hand washed several times before being gravitationally separated on the Super Panner which is a machine designed to separate minerals with distinct density differences. Samples are put in an oven to dry overnight. The samples are separated using a magnet to free the non – magnetic minerals (which include Zircon) from the magnetic minerals. Then non-magnetic portion of the samples go through heavy liquid separation, which is used to further concentrate the heavy minerals. At CAF two types of heavy liquids are used Tetrabromoethane (TBE), density 2.96gm/cc and Diiodinemethane (DIM), density 3.3 gm/cc. Zircon has a density of 4.85gm/cc therefore the DIM was used as the separate, causing the heavier concentrate which included zircon to settle to the bottom of the liquid mixture. The concentrate left over was put into an oven overnight. Zircon crystals were handpicked under a binocular microscope and mounted onto a glass slide using double sided tape. The mount is filled with Epoxy made from a mixture of 25 parts Epofix resin into 3 parts of Epofix hardener. The mount was left to cure for twelve hours and then ground down to expose the middle of zircon grains. The mount was polished with MD-polishing cloths which were compatible with Struers DiaPro Suspensions and required no water during polishing. The disks were imaged by cathodoluminescence using a Leo 1430VP SEM at the CAF.

3.5.2 U-Pb Isotope analysis

Zircon U–Pb isotope analyses were undertaken at the GEUS in Copenhagen (Denmark) and at the CAF of the University of Stellenbosch (South Africa) following the method described in Gerdes and Zeh (2006, 2009) and Frei and Gerdes (2009). An Element 2 sector field ICP–MS coupled to a New Wave Research UP-213 ultraviolet laser system was used to analyse uranium, thorium and lead isotopes. Data were acquired in time-resolved, peak-jumping, pulse-counting mode during 30 second background measurement followed by 30 second sample ablation (Farina et al., 2014).

3.5.3 Lu-Hf-Yb Isotope analysis

Lutetium–hafnium–ytterbium isotopes were measured at the Goethe University of Frankfurt. A Thermo-Finnigan Neptune multicollector ICP–MS coupled to an M-50 Resonetics 193 nm ArF Excimer laser system (CompexPro 102, Coherent) equipped with two-volume ablation cell (Laurin Technic, Australia) was used. The method carried out followed the procedure described by Gerdes and Zeh (2006, 2009). All Data was collected in static mode (^{172}Yb , ^{173}Yb , ^{175}Lu , ^{176}Hf –Yb–Lu, ^{177}Hf , ^{178}Hf , ^{179}Hf , ^{180}Hf) during 55 seconds of laser ablation. A 40- μm diameter laser spot was drilled on top of the 30- μm U–Pb laser spot previously analysed to get the Lu-Hf-Yb analysis. Careful attention was kept to drill exactly in the same growth zone, which was previously used for U–Th–Pb isotope analyses as described by Farina et al. (2014).

Initial $^{176}\text{Hf}/^{177}\text{Hf}$ and ϵHf ratio calculations for each spot was done by using either their individual LA–ICP–MS ^{206}Pb – ^{238}U spot or their or ^{207}Pb – ^{206}Pb ages. Calculations made use of a ^{176}Lu decay constant of $1.867 \times 10^{-11} \text{ year}^{-1}$ (Scherer et al. 2001) and present-day CHUR compositions of $^{176}\text{Hf}/^{177}\text{Hf} = 0.282785$ and $^{176}\text{Lu}/^{177}\text{Hf} = 0.0336$ (Bouvier et al. 2008)

A detailed description of the analytical procedures for both U–Pb and Lu–Hf isotope systems can be found in the reference material. Further analysis of the data was processed in Microsoft Excel 2010 and geochemical plots were derived using Isoplot version 4.15 created by Kenneth R. Ludwig of the Berkley Geochronology Centre (Ludwig, 1990).

Chapter 4: Results

4.1 Field Relations



Figure 3: Plates A-H showing various granitic textures seen in the field. Plates E-H showing various enclave textures seen in the field. A) A contact close by the area of Santa Reparata can be seen, the contact shows a leucocratic granite (bottom left) and a more mafic granite (top right). B) Shows an undeformed igneous texture showing quartz, plagioclase and potassium feldspar crystals. C) shows the textural differences seen in the granites; the leucocratic granite (bottom left) has a finer grained texture compared to the more coarse grained mafic granite (top right). D) The finer grained enclave shows an elongated protuberance. E) Plate E shows an xenolith that has cusps and flames. F & G) the feldspar crystals in the enclaves are euhedral and are similar in size to the feldspar microphenocrysts seen in the granites. H) Coarser grained enclave

It is important to state that the field work was conducted by Professor Gary Stevens and Dr Federico Farina in setting up the current research project. The field photos, samples and sample sites were handed over to Roxanne Soorajlal to continue the study.

The field relations observed are largely in agreement with the previous literature; the three magmatic units exist and can be defined by the three different types of granites and the contacts that occur between them (Fig.3 Plates A & C). These different types of granites are easily distinguished based on the different amounts of mafic minerals, Plates F and G from a granodiorite in the outer unit, show a close up where the abundance of mafic minerals (hornblende and biotite) can be clearly seen. The samples taken were in agreement with the published map in Fig.1.

Two main types of enclaves were noted in the field; enclaves with a finer grained texture in relation to the granites (Fig.3 Plate D, E & G) and a coarser grained texture almost similar to that of the granite host (Fig.3 Plate F&H).

There are contacts between enclaves and granites in the pluton that are quite sharp but appear to involve two comagmatic magmas based on the textural evidence; elongated enclave protuberance in Plate D and cusped edges in plate E. Both textures are indicative of showing that the enclave was semi-plastic whilst the granite magma was flowing hence the deformed patterns by magma flow. Equal mineral crystal sizes seen in both the mafic enclaves and in the granites (Fig.3 Plate F&G) also suggest these crystals either started to grow at the same time or were captured from the granites.

4.2 Petrography

4.2.1. Granites

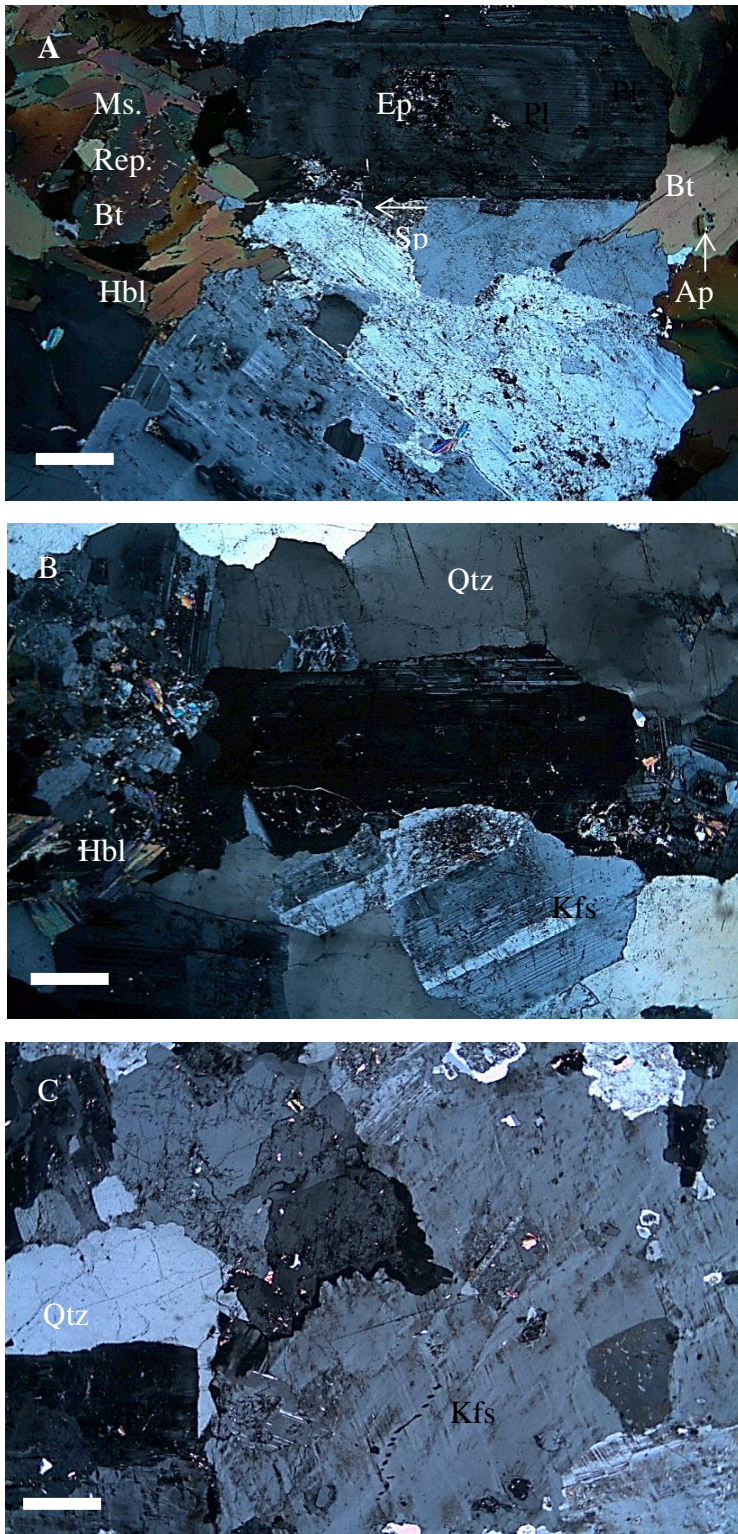


Figure 4: Thin section photographs of granites in XPL (a-c) showing similar coarse grained textures with varying mineral assemblages; a) granodiorites from the outer unit (BG48), b) granite from the middle unit (BG23) and c) leucogranite from the inner unit (BG25). Scale bar=100µm. Ms.;Muscovite, Bt;Biotite, Ep;Epidote, Ap;Apatite, Hbl;Hornblende, Sp; Spheene, Pl;Plagioclase, Qtz;Quartz and Kfs;K-feldspar.

The granitic rocks of the Buddusò Pluton share a similar coarse-grained texture. All three different types of granites described in the whole rock chemistry share a similar mineral assemblage differentiated by the proportion of mafic minerals. The leucogranites found in the inner unit (Fig.4C) are composed of quartz (20 – 40 % vol.) plagioclase (35 – 55 %), K-feldspar (30 – 40 %), biotite (0 – 10 %) and hornblende (0 – 5 %). The granites found in the middle unit (Fig.4B) are composed of quartz (15 – 30 %), plagioclase (30 – 45 %), K-feldspar (25 – 40 %), biotite (10 – 15 %) and hornblende (0 – 10 %). The granodiorites found in the outer unit (Fig.4A) are characterized by quartz (15 – 25 %), plagioclase (25 – 40 %), K-feldspar (20 – 35 %), biotite (10 – 25 %), and amphiboles (5 – 15 %).

Quartz occurs as subhedral crystals and showed undulose extinction in some samples (Fig.4B). Plagioclase crystals occur as zoned euhedral crystals (Fig.4A) and unzoned subhedral crystals (Fig.4B). Epidote occurs as inclusions in the zoned plagioclase, epidote inclusions are often concentrated in the plagioclase crystals' core (Fig.4A, Fig.6A-B).

K-feldspar occurs as both an interstitial phase (Fig.4C) showing a microcline texture and as subhedral phenocrysts (Fig.4B). Plagioclase and K-feldspar sometimes show an intergrown perthite texture which is altered with respect to the rest of the minerals in the sample. Biotite occurs as euhedral to subhedral crystals and shows varying degrees of alteration with respect to the other minerals, in both the granites and the enclaves. Biotite was observed as inclusions in plagioclase and exists with or without inclusions of apatite. Sphene reaction rims are also seen around biotite crystals. Hornblende occurs as massive crystals usually unaltered.

The accessory minerals are zircon, ilmenite, titanite, apatite, sphene and allanite. All the granite samples show oscillatory zoned apatite, zoned subhedral allanite which sometimes have epidote rims, euhedral oscillatory zoned zircon with apatite inclusions and ilmenite crystals. Chlorite and muscovite occur as secondary textures, generally seen replacing biotite (Fig.4A) and rarely seen replacing K-feldspar inclusions in plagioclase phenocrysts. Sphene occurs at the rims of different minerals forming a reaction rim (Fig.4A). Leucogranites show little to no alteration whilst the granites and mafic granites show varying degrees of seritization and chloritization.

4.2.2 Enclaves

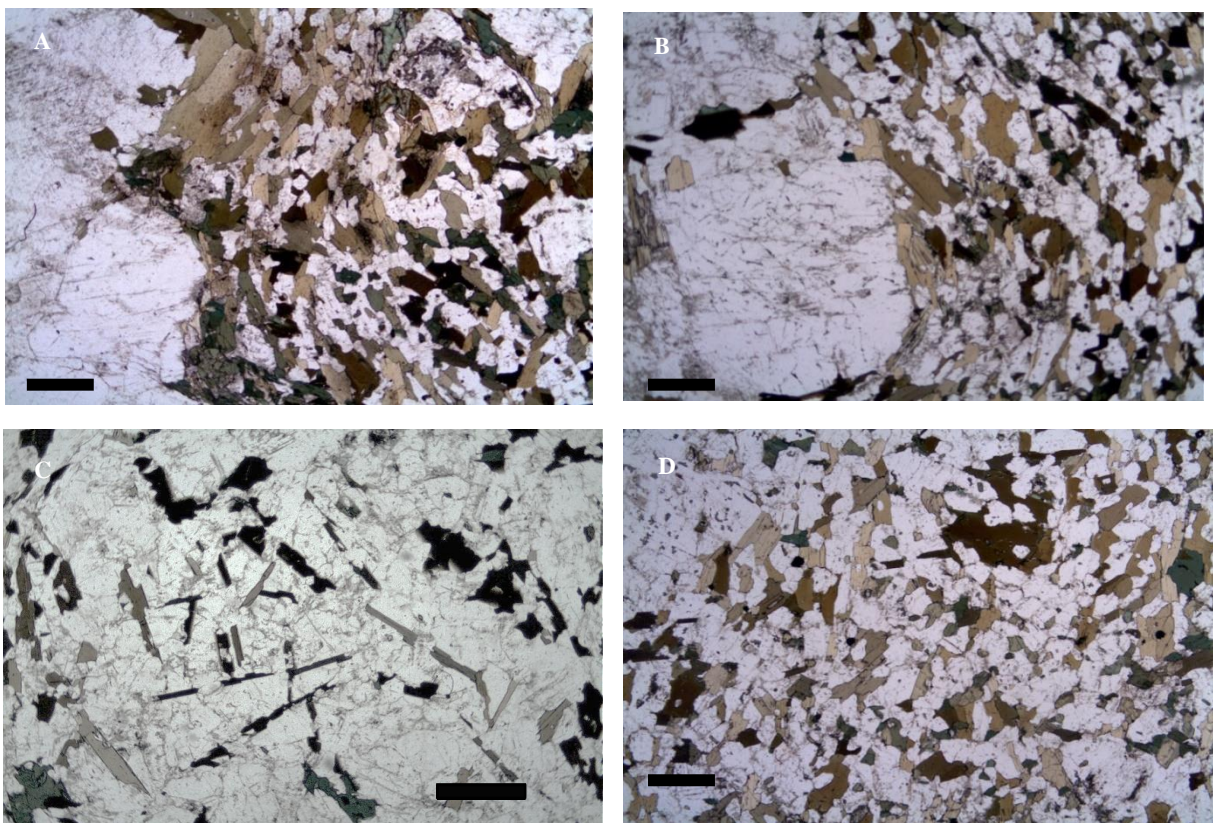


Figure 5: Thin section photographs of enclaves in PPL: A-B) contact between granite (left) and enclave (right) showing a high concentration of amphiboles and biotite, enclave show a foliation which is absent in the granite, (BG44) C) enclave showing a higher ratio of felsic:mafic minerals(BG22), D) enclave showing a fine grained, homogenous intergranular texture. (BG12D) (A), (B), (C) are from the middle unit and (D) is from the outer unit.

The mineral assemblages of the enclaves with respect to their host granites are the same but the mineral modes differ. Dominant phases seen in the mafic enclaves were; plagioclase, K-feldspar, biotite and amphiboles. Quartz exists as a minor phase and accessory minerals are apatite and zircon.

The foliation of the enclave in some samples bend around these phenocrysts (Fig.5A) whilst in other samples the foliation does not bend around the phenocrysts (Fig.5B). Albite and Albite-Carlsbad twinning is characteristic of plagioclase, both plagioclase and K-feldspar occur as large subhedral phenocrysts in the enclaves (Fig.5B). Biotite varies from lath like, unaltered euhedral crystals within the enclave (Fig.5C) to larger altered subhedral crystals (Fig.4A) at the contact with the granite host. Hornblende and epidote form subhedral crystals with a general abundance of amphiboles at the contact between the granite and enclave (Fig.5A&B). Quartz occur as an interstitial phase with zoned acicular apatite and euhedral zircon.

Enclaves can be separated into two groups based on the amount of mafic minerals; with some samples (Fig.5C) containing more leucocratic material and other samples composing of less felsic and more mafic material (Fig.6B). Enclaves vary from medium to fine grained textures. Some enclave samples show a foliation (Fig.5A&B, Fig.6B) which is absent in all of the granitic samples whilst other enclave samples show no foliation (Fig.5D).

4.2.3 Plagioclase

Two types of plagioclase crystals exist in both the granites and enclave samples. Plagioclase exist as small subhedral crystals that exhibit albite or Carlsbad twinning (Fig. 6B) and as large euhedral phenocrysts (Fig.6A-D) which show complex zoning with varying compositional patterns. These complexly zoned plagioclase crystals are found in both the granite (Fig.6C&D) and enclaves (Fig.6A). The plagioclase phenocrysts show four basic compartments, the core has hornblende and epidote inclusions. Outside the core is a zone of plagioclase which is surrounded by an epidote rim. Epidote inclusions are arranged along specific crystal planes in the plagioclase and may coincide with chemical zonation patterns. The fourth compartment is a plagioclase overgrowth which surround the epidote rims (Fig.6C).

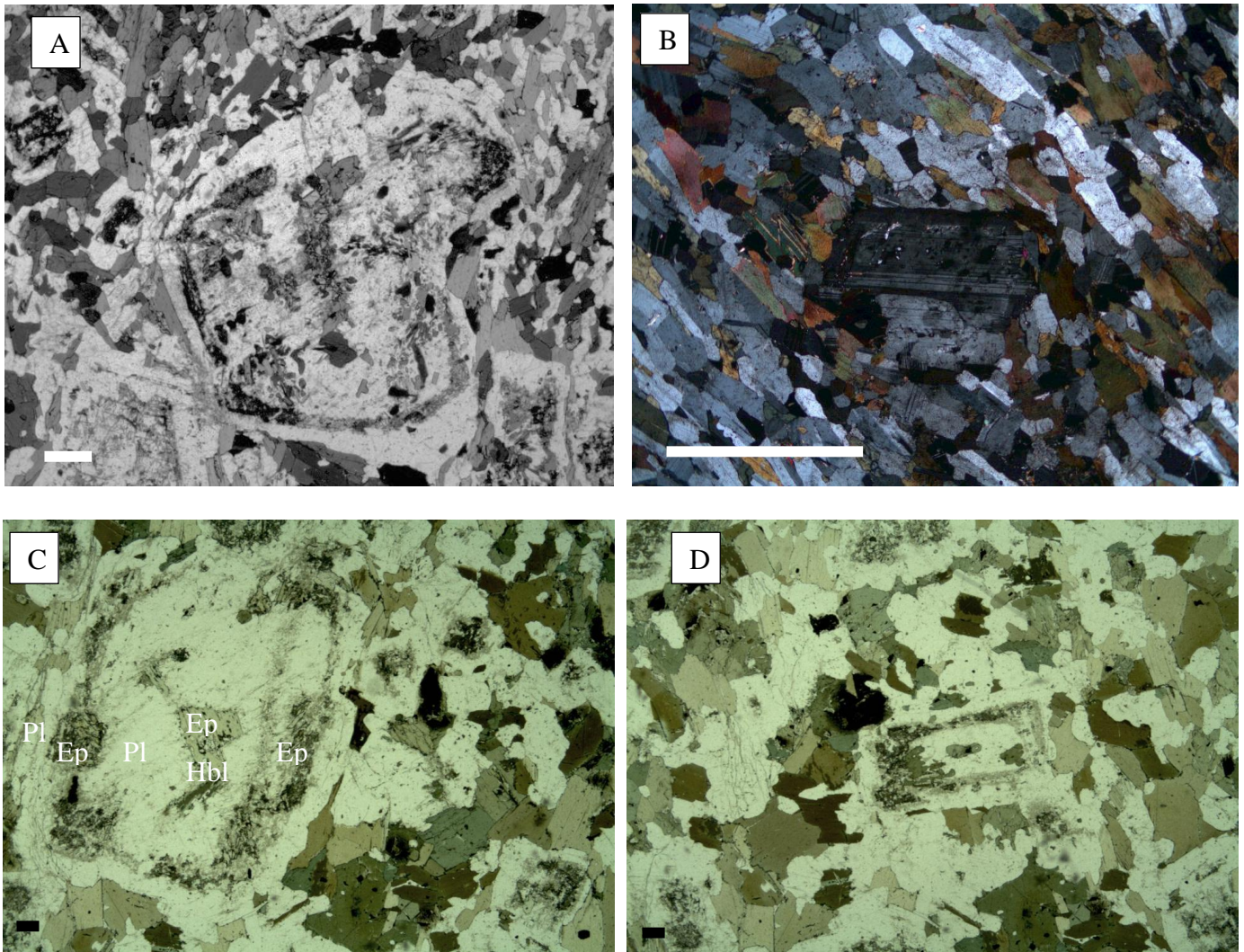


Figure 6: Plagioclase crystals showing A) epidote inclusions concentrated in the core and epidote rims, with foliation bending around phenocryst in PPL) B) Carlsbad twinning with foliation uninterrupted by phenocrysts in XPL in enclave sample BG16 C&D) plagioclase crystals in PPL showing epidote core and rims in granite sample BG12C2. Scale bar= 100um*

4.3 Mineral Chemistry

4.3.1 Plagioclase

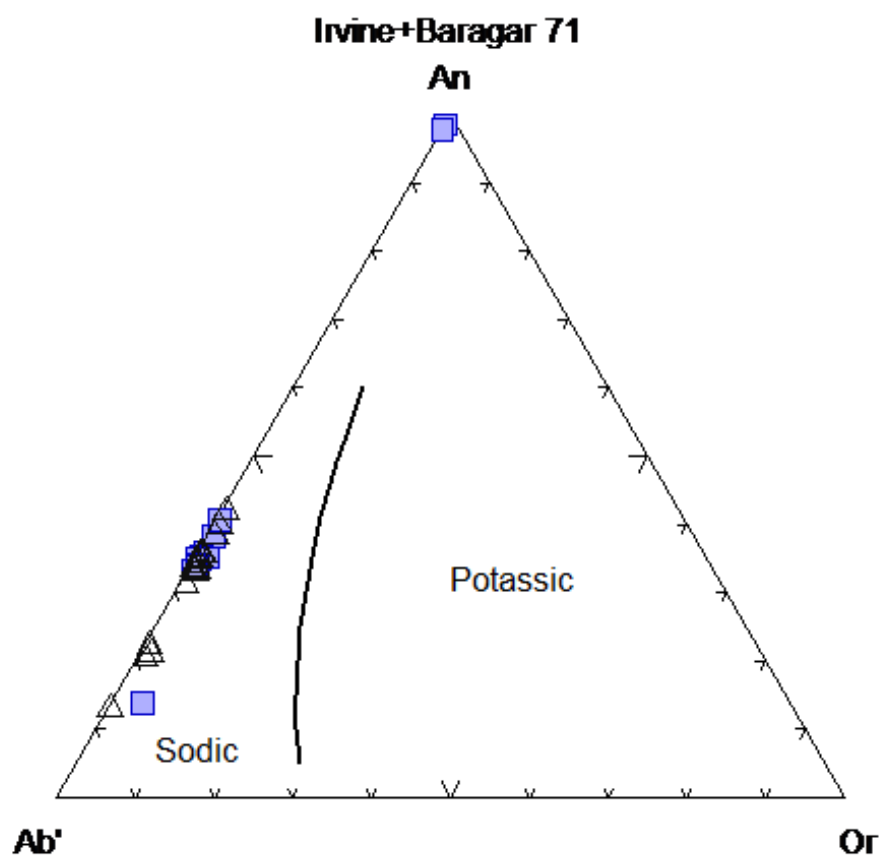


Figure 7: Representative compositions of the plagioclase from enclaves (blue squares) and granites (black triangles). Formula based on 8 O atoms. A full set of all mineral compositions generated in the study can be found Appendix III. Diagram based on Irvine and Baragar, 1971. An = Anorthite, Ab =Albite, Or=Orthoclase

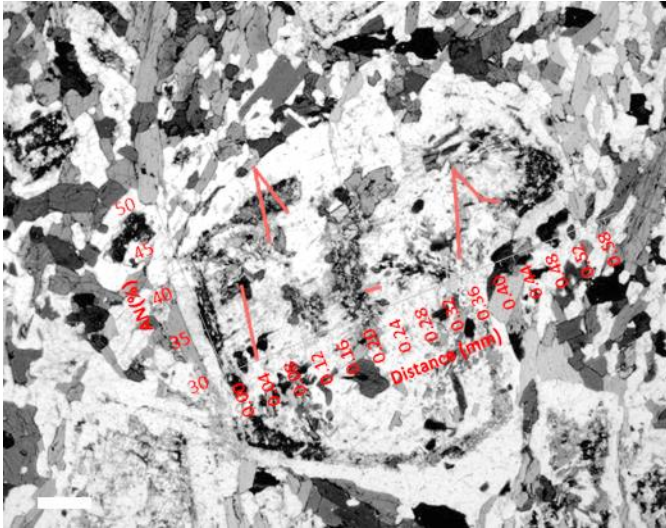


Figure 8: Plagioclase crystals showing A) epidote core and rims in PPL overlaid by a traverse showing anorthite (An %) content for plagioclase only. $An = \frac{Ca}{Ca+Na+K} * 100$ (BG44) An calculations can be found in Appendix III.

Mineral chemical analysis was done on the two different types of plagioclase crystals found in both the enclaves and granites; 1) normally zoned and unzoned plagioclase crystals and 2) complexly zoned plagioclase crystals with four zones and epidote and hornblende inclusions.

The spot analyses shown in Fig.7 are of normally zoned and unzoned plagioclase crystals found in both the granites and enclaves. Normally zoned plagioclase crystals show An content ranges between 31.46 % to 35.92 % for the enclaves and between 20.42 % and 39.84 % in the granites. The plagioclase crystals commonly show inclusions of amphiboles and epidote and sphene reaction rims.

Complexly zoned plagioclase crystals which show the four zones and occur in both the granite and the enclave have more calcic-rich plagioclase compositions in the cores than in the rims. An content of the granite (Fig.9A-D) in the rims are between 50 % - 54 % whilst the cores show varying spikes between 45 % to 60 %. An content of the enclave (Fig.8) show a compositional range of 30 % to 40 % in the rims and 40 % to 50 % in the core. Many plagioclase phenocrysts reveal distinct increases in An content which are described as spikes by Wiebe (1968) which disturb normally zoned plagioclase coinciding with the different zones within the plagioclase crystals optically described in section 4.2.3.

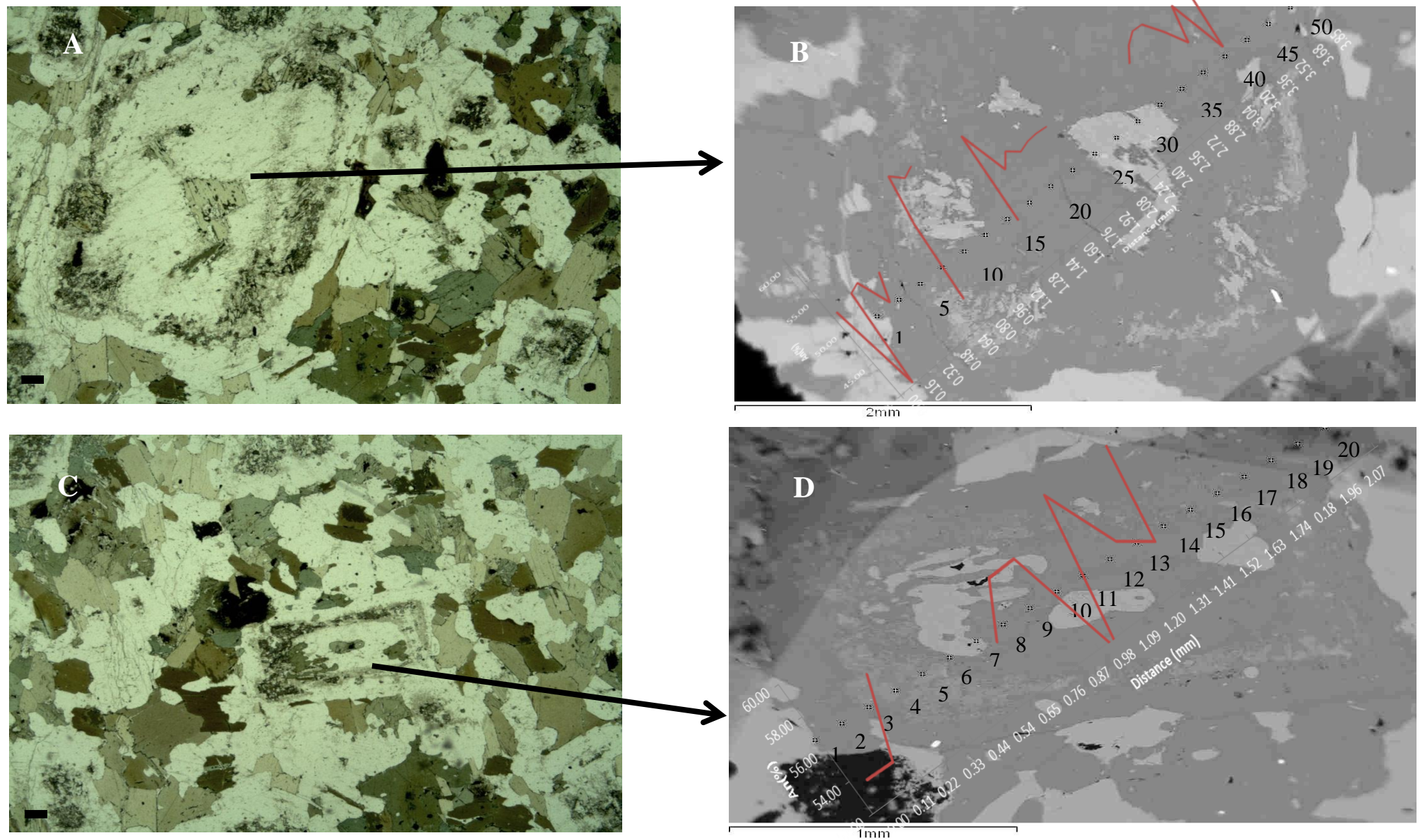


Figure 9: Thins section photos in PPL (A&C) of plagioclase phenocrysts in granite sample BG12C2 with backscatter electron images of the same crystals in (B&D) overlaid by a traverse showing anorthite (An%) content for plagioclase only. $An = \frac{Ca}{Ca+Na+K} * 100$, Numbers in black are spot no. analyses, Scale bar =200um (A&C). *An calculation scan be found in Appendix III.

4.3.2 Potassium Feldspars

Table 3: Representative analyses of K-feldspar from enclaves. (2 spots analysis were chosen for each sample based on the best totals, complete analyses of all spots can be found in Appendix III). Formula based on 8 O atoms.

Type	Enclave							
Sample	BG12D		BG15A		BG29		BG44	
Spot No.	8	10	3	12	7	9	7	11
SiO ₂	62.72	63.62	65.46	65.33	64.81	65.04	65.41	64.97
TiO ₂	0.00	0.00	0.00	0.00	0.00	0.00	0.00	0.00
Al ₂ O ₃	20.28	20.04	17.93	17.84	17.92	18.24	17.98	18.57
FeO	0.18	0.00	0.00	0.14	0.17	0.16	0.00	0.00
CaO	0.71	0.17	0.12	0.12	0.18	0.00	0.14	0.65
BaO	1.66	0.00	0.00	0.00	0.32	0.39	0.31	0.28
Na ₂ O	0.49	0.51	0.34	0.39	0.90	0.38	0.38	1.14
K ₂ O	14.59	15.45	16.47	16.35	15.46	16.07	16.41	14.84
Total	100.64	99.79	100.32	100.18	99.77	100.27	100.62	100.46
Si	2.91	2.94	3.02	3.02	3.00	3.01	3.01	2.99
Ti	0.00	0.00	0.00	0.00	0.00	0.00	0.00	0.00
Al	1.11	1.09	0.97	0.97	0.98	0.99	0.98	1.01
Fe ²⁺	0.01	0.00	0.00	0.01	0.01	0.01	0.00	0.00
Ca	0.04	0.01	0.01	0.01	0.01	0.00	0.01	0.03
Ba	0.03	0.00	0.00	0.00	0.01	0.01	0.01	0.01
Na	0.04	0.05	0.03	0.04	0.08	0.03	0.03	0.10
K	0.86	0.91	0.97	0.96	0.91	0.95	0.96	0.87
An	3.76	0.85	0.61	0.57	1.00	0.00	0.69	3.19
Ab	4.71	4.73	3.03	3.51	8.00	3.00	3.38	10.15
Or	91.53	94.41	96.37	95.92	91.00	97.00	95.93	86.66

An contents range from 0 % to 3.76 % in the enclaves and from 0 % to 0.66 % in the granites (Table 3 and 4). Both the enclaves and granites both fairly similar feldspar compositions; granites have a slightly higher K₂O content between 15.28 wt. % and 16.67 wt. % compared to enclaves K₂O range falling between 14.59 wt. % and 16.47 wt. %.

Table 4: Representative analyses of K-feldspar from granites. (2 spots analysis were chosen for each sample based on the best totals, complete analyses of all spots can be found in Appendix III). Formula based on 8 O atoms.

Type	Granite													
Sample	BG10		BG12D		BG13A		BG15B		BG26		BG44		BG46A	
Spot No.	1	2	3	12	3	4	3	4	4	5	6	7	9	10
SiO ₂	65.01	65.18	65.21	64.65	64.28	65.35	64.63	64.46	64.84	64.30	65.43	65.12	64.83	64.96
TiO ₂	0.00	0.00	0.00	0.00	0.00	0.00	0.00	0.00	0.00	0.00	0.00	0.00	0.00	0.00
Al ₂ O ₃	17.77	17.99	18.07	18.18	17.99	18.01	18.06	18.10	17.83	18.26	18.05	17.98	18.13	18.32
FeO	0.00	0.00	0.00	0.00	0.00	0.00	0.00	0.00	0.00	0.00	0.00	0.00	0.00	0.00
CaO	0.00	0.00	0.00	0.00	0.12	0.00	0.00	0.00	0.00	0.13	0.00	0.12	0.00	0.00
BaO	0.00	0.00	0.34	0.62	0.67	0.39	0.00	0.00	0.50	0.87	0.46	0.55	0.44	0.79
Na ₂ O	0.28	0.38	0.48	0.58	0.79	0.55	0.55	0.55	0.91	0.81	0.49	0.35	0.59	0.71
K ₂ O	16.57	16.28	16.17	15.86	15.28	15.92	15.99	16.20	15.48	15.48	16.11	16.52	15.69	15.67
Total	99.63	99.83	100.27	99.89	99.13	100.23	99.23	99.31	99.56	99.85	100.55	100.65	99.68	100.46
Si	3.02	3.02	3.01	3.00	3.01	3.02	3.01	3.00	3.01	2.99	3.02	3.00	3.01	3.00
Ti	0.00	0.00	0.00	0.00	0.00	0.00	0.00	0.00	0.00	0.00	0.00	0.00	0.00	0.00
Al	0.97	0.98	0.98	0.99	0.99	0.98	0.99	0.99	0.98	1.00	0.98	0.98	0.99	1.00
Fe ²⁺	0.00	0.00	0.00	0.00	0.00	0.00	0.00	0.00	0.00	0.00	0.00	0.00	0.00	0.00
Ca	0.00	0.00	0.00	0.00	0.01	0.00	0.00	0.00	0.00	0.01	0.00	0.01	0.00	0.00
Ba	0.00	0.00	0.01	0.01	0.01	0.01	0.00	0.00	0.01	0.02	0.01	0.01	0.01	0.01
Na	0.03	0.03	0.04	0.05	0.07	0.05	0.05	0.05	0.08	0.07	0.04	0.03	0.05	0.06
K	0.98	0.96	0.95	0.94	0.91	0.94	0.95	0.96	0.92	0.92	0.95	0.97	0.93	0.92
An	0.00	0.00	0.00	0.00	0.60	0.00	0.00	0.00	0.00	0.66	0.00	0.61	0.00	0.00
Ab	2.49	3.38	4.32	5.25	7.20	5.00	5.01	4.91	8.19	7.34	4.40	3.11	5.37	6.46
Or	97.51	96.62	95.68	94.75	92.20	95.00	94.99	95.09	91.81	91.99	95.60	96.28	94.63	93.54

4.3.3 Biotite

Table 5: Representative analyses of biotite from enclaves. (2 spots analysis were chosen for each sample based on the best totals, complete analyses of all spots can be found in Appendix III) Formula based on 22 O atoms.

Type	Enclave					
Sample	BG12D		BG15A		BG44	
Spot No.	3	5	3	5	5	6
SiO ₂	36.18	36.39	35.76	35.15	35.58	35.70
TiO ₂	2.25	2.59	3.38	3.23	3.63	3.62
Al ₂ O ₃	15.38	15.86	15.23	14.98	15.00	14.96
FeO	24.39	23.42	23.87	24.35	24.56	23.98
MnO	0.67	0.68	0.80	0.97	0.68	0.77
MgO	8.05	8.06	7.36	7.12	7.25	7.32
CaO	0.00	0.00	0.00	0.00	0.00	0.14
Na ₂ O	0.00	0.00	0.19	0.20	0.00	0.17
K ₂ O	9.43	9.51	9.27	9.10	9.21	9.25
Total	96.36	96.50	95.85	95.10	95.92	95.91
Si	2.80	2.80	2.79	2.77	2.78	2.78
Al ^{IV}	1.20	1.20	1.21	1.23	1.22	1.22
∑ Z	4.00	4.00	4.00	4.00	4.00	4.00
Al ^{VI}	0.21	0.24	0.18	0.17	0.16	0.16
Ti	0.13	0.15	0.20	0.19	0.21	0.21
Fe ²⁺	1.58	1.51	1.55	1.61	1.60	1.56
Mn	0.04	0.04	0.05	0.06	0.05	0.05
Mg	0.93	0.92	0.85	0.84	0.84	0.85
∑ X	2.90	2.86	2.84	2.87	2.86	2.83
Ca	0.00	0.00	0.00	0.00	0.00	0.01
Na	0.00	0.00	0.03	0.03	0.00	0.03
K	0.93	0.93	0.92	0.92	0.92	0.92
∑ Y	0.93	0.93	0.95	0.95	0.92	0.96
X _{Mg} ^a	0.37	0.38	0.35	0.34	0.34	0.35
X _{Mg(divalent)} ^b	0.36	0.37	0.35	0.33	0.34	0.34

$$X_{Mg}^a = Mg/(Fe^{2+}+Mg), X_{Mg(divalent)}^b = Mg/(Fe^{2+}+Mn+Mg+Ca)$$

Biotite in both granites and enclaves show similar compositions in FeO =23.84 to 25.40 wt. %, Al₂O₃ = 13.96 to 15.86 wt. % and K₂O =9.06 to 9.52 wt. % (Tables 5 and 6). Biotites are rich in Ti, with enclave contents ranging between 2.25 and 3.63 wt. % and granite contents between 2.5 and 3.44 wt.%. The Al^{IV} and Fe²⁺ are in the same range (1.18 to 1.23 and 1.51 to 1.66 respectively) for both granites and enclaves and are characteristic of the biotite subgroup; siderophyllite (Tischendorf et al., 1997).

Table 6: Representative analyses of biotite from granites. . (2 spots analysis were chosen for each sample based on the best totals, complete analyses of all spots can be found in Appendix III). Formula based on 22 O atoms.

Type	Granite															
Sample	BG10		BG12D		BG13A		BG15B		BG26		BG29		BG44		BG46A	
Spot No.	1	3	5	6	1	3	5	8	2	3	1	4	4	5	5	9
SiO ₂	35.48	35.46	36.24	36.30	36.09	35.63	35.48	35.69	35.61	35.67	35.62	36.00	35.85	35.79	35.69	35.57
TiO ₂	3.10	3.44	2.71	3.15	2.94	3.20	2.50	2.55	3.35	3.38	3.58	3.72	2.91	3.24	3.20	3.21
Al ₂ O ₃	15.50	14.85	15.48	14.99	15.10	14.77	15.19	15.25	14.46	14.46	14.47	13.96	15.38	15.41	15.25	15.08
FeO	25.40	25.10	24.21	24.43	23.84	24.48	24.77	24.07	24.43	24.39	24.45	24.67	23.96	24.00	24.58	24.66
MnO	1.65	1.69	0.71	0.72	0.44	0.29	0.59	0.64	1.15	1.02	0.87	1.09	0.73	0.71	0.59	0.82
MgO	6.06	6.17	7.76	7.67	7.58	7.34	6.95	7.76	7.05	7.28	7.30	7.22	7.39	7.39	7.51	7.13
CaO	0.00	0.15	0.00	0.00	0.00	0.00	0.00	0.00	0.13	0.00	0.11	0.00	0.11	0.00	0.00	0.00
Na ₂ O	0.00	0.00	0.00	0.00	0.00	0.00	0.00	0.00	0.28	0.21	0.17	0.00	0.00	0.00	0.00	0.00
K ₂ O	9.12	9.19	9.35	9.52	9.59	9.66	9.06	9.25	9.19	9.10	9.31	9.22	9.33	9.23	9.26	9.23
Total	96.30	96.04	96.46	96.77	95.58	95.37	94.53	95.20	95.65	95.51	95.89	95.87	95.67	95.78	96.08	95.69
Si	2.78	2.79	2.80	2.80	2.82	2.80	2.81	2.80	2.80	2.80	2.79	2.82	2.80	2.79	2.78	2.79
Al ^{IV}	1.22	1.21	1.20	1.20	1.18	1.20	1.19	1.20	1.20	1.20	1.21	1.18	1.20	1.21	1.22	1.21
∑ Z	4.00	4.00	4.00	4.00	4.00	4.00	4.00	4.00	4.00	4.00	4.00	4.00	4.00	4.00	4.00	4.00
Al ^{VI}	0.21	0.16	0.21	0.17	0.20	0.17	0.23	0.21	0.14	0.14	0.12	0.11	0.21	0.20	0.18	0.18
Ti	0.18	0.20	0.16	0.18	0.17	0.19	0.15	0.15	0.20	0.20	0.21	0.22	0.17	0.19	0.19	0.19
Fe ²⁺	1.66	1.65	1.57	1.58	1.56	1.61	1.64	1.58	1.61	1.60	1.60	1.62	1.56	1.56	1.60	1.61
Mn	0.11	0.11	0.05	0.05	0.03	0.02	0.04	0.04	0.08	0.07	0.06	0.07	0.05	0.05	0.04	0.05
Mg	0.71	0.72	0.89	0.88	0.88	0.86	0.82	0.91	0.83	0.85	0.85	0.84	0.86	0.86	0.87	0.83
∑ X	2.87	2.85	2.87	2.86	2.84	2.84	2.88	2.88	2.84	2.86	1.99	2.01	2.85	2.86	2.87	2.87
Ca	0.00	0.01	0.00	0.00	0.00	0.00	0.00	0.00	0.01	0.00	0.01	0.00	0.01	0.00	0.00	0.00
Na	0.00	0.00	0.00	0.00	0.00	0.00	0.00	0.00	0.04	0.03	0.03	0.00	0.00	0.00	0.00	0.00
K	0.91	0.92	0.92	0.94	0.95	0.97	0.92	0.93	0.92	0.91	0.93	0.92	0.93	0.92	0.92	0.92
∑ Y	0.91	0.93	0.92	0.94	0.95	0.97	0.92	0.93	0.97	0.94	0.96	0.92	0.94	0.92	0.92	0.92
X _{mg}	0.30	0.30	0.36	0.36	0.36	0.35	0.33	0.36	0.34	0.35	0.35	0.34	0.35	0.35	0.35	0.34
X _{mg(divalent)}	0.29	0.29	0.36	0.35	0.35	0.34	0.32	0.35	0.33	0.34	0.34	0.33	0.35	0.35	0.35	0.33

4.3.4 Hornblende

Table 7: Representative analyses of hornblende from enclaves. (2 spots analysis were chosen for each sample based on the best totals, complete analyses of all spots can be found in Appendix III). Formula based on 23 O atoms.

Type	Enclave							
Sample	BG12D		BG15A		BG29		BG44	
Spot No	6	9	1	6	5	7	1	4
SiO ₂	42.71	42.21	41.99	43.33	42.99	42.70	42.54	40.31
TiO ₂	0.97	1.19	1.32	1.12	0.94	1.03	0.96	0.79
Al ₂ O ₃	10.07	10.25	10.06	9.32	9.49	9.89	9.46	11.79
FeO	22.79	22.74	23.08	23.03	24.12	23.83	23.61	24.70
MnO	0.61	0.69	0.75	0.61	0.83	0.84	0.66	0.53
MgO	6.75	6.67	6.61	6.95	6.19	6.28	6.96	5.91
CaO	11.90	12.11	11.73	11.94	11.27	11.38	12.00	11.92
Na ₂ O	1.13	0.97	1.39	1.11	1.35	1.51	1.07	1.24
K ₂ O	1.14	1.21	1.23	1.09	1.19	1.12	1.03	1.21
Total	98.07	98.04	98.17	98.50	98.36	98.58	98.30	98.40
Si	6.60	6.53	6.51	6.67	6.66	6.60	6.59	6.29
Al ^{IV}	1.40	1.47	1.49	1.33	1.34	1.40	1.41	1.71
Al ^{VI}	0.43	0.40	0.35	0.35	0.39	0.40	0.32	0.46
Ti	0.11	0.14	0.15	0.13	0.11	0.12	0.11	0.09
Fe ²⁺	2.94	2.94	2.99	2.96	3.13	3.08	3.06	3.23
Mn	0.08	0.09	0.10	0.08	0.11	0.11	0.09	0.07
Mg	1.55	1.54	1.53	1.59	1.43	1.45	1.61	1.38
Ca	1.97	2.01	1.95	1.97	1.87	1.89	1.99	1.99
Na	0.34	0.29	0.42	0.33	0.41	0.45	0.32	0.37
K	0.23	0.24	0.24	0.21	0.23	0.22	0.20	0.24
X _{Mg}	0.35	0.34	0.34	0.35	0.31	0.32	0.34	0.30

X_{Mg}=Mg/(Fe²⁺+Mg),

In comparison with the enclaves, the granites have generally higher Al, Ti, Mg and Na contents (Table 7 and 8). Enclaves and granites show overlapping compositions with respect to Si, K and Ca content. Granites show a larger variation in CaO content from 9.87 to 11.95 wt. %. X_{Mg} values ranging between 0.30 and 0.35 for both enclaves and granites are characteristic of the magnesiohornblende compositions (Leake et al., 1997).

Table 8: Representative analyses of hornblende from granite. (2 spots analysis were chosen for each sample based on the best totals, complete analyses of all spots can be found in Appendix III). Formula based on 23 O atoms.

Type	Granite									
Sample	BG12C2		BG12D		BG15B		BG44		BG46A	
Spot No	1	5	5	6	4	7	4	8	2	6
SiO ₂	40.75	42.09	40.54	41.70	42.14	40.34	42.22	41.63	42.87	41.99
TiO ₂	2.16	1.20	0.89	0.97	1.10	0.96	1.14	1.65	1.17	1.67
Al ₂ O ₃	10.46	10.49	12.18	10.65	9.29	11.01	9.54	9.94	10.03	10.23
FeO	23.57	23.52	24.11	22.63	24.01	24.33	23.76	23.69	22.60	22.77
MnO	0.56	0.44	0.65	0.65	0.79	0.63	0.72	0.52	0.64	0.70
MgO	6.46	6.83	7.37	6.49	6.69	5.87	6.59	6.50	6.43	6.47
CaO	11.35	11.48	9.87	11.89	11.78	11.95	11.69	11.75	11.92	12.02
Na ₂ O	1.53	1.11	1.08	1.21	1.15	1.24	1.18	1.29	1.28	1.33
K ₂ O	0.99	1.08	0.98	1.19	1.01	1.17	1.17	1.11	1.24	1.23
Total	97.81	98.24	97.66	97.37	97.96	97.50	98.01	98.08	98.17	98.42
Si	6.36	6.50	6.30	6.50	6.57	6.36	6.57	6.48	6.62	6.49
Al	1.64	1.50	1.70	1.50	1.43	1.64	1.43	1.52	1.38	1.51
Al	0.29	0.42	0.54	0.46	0.28	0.40	0.32	0.30	0.44	0.35
Ti	0.25	0.14	0.10	0.11	0.13	0.11	0.13	0.19	0.14	0.19
Fe ²⁺	3.08	3.04	3.14	2.95	3.13	3.21	3.09	3.08	2.92	2.94
Mn	0.07	0.06	0.09	0.09	0.10	0.08	0.09	0.07	0.08	0.09
Mg	1.50	1.57	1.71	1.51	1.56	1.38	1.53	1.51	1.48	1.49
Ca	1.90	1.90	1.64	1.99	1.97	2.02	1.95	1.96	1.97	1.99
Na	0.46	0.33	0.32	0.37	0.35	0.38	0.36	0.39	0.38	0.40
K	0.20	0.21	0.19	0.24	0.20	0.24	0.23	0.22	0.24	0.24
X _{mg}	0.33	0.34	0.35	0.34	0.33	0.30	0.33	0.33	0.34	0.34

4.4 Whole-rock Geochemistry

Table 9: Whole-rock major (wt. %) and trace (ppm) element analyses of enclaves and mixed samples from the Buddusò Pluton

Type	Enclaves						Mix ^(a)			
Unit	Outer						Middle			
Sample	BG8	BG9	BG21	BG22	BG29	BG38	BG15mme	BG16mme	BG15mix	BG16mix
SiO ₂	49.45	49.10	64.02	63.86	56.77	51.77	52.77	52.68	60.81	54.97
Al ₂ O ₃	16.90	17.04	16.69	16.80	19.15	20.77	20.00	21.80	18.79	19.49
Fe ₂ O ₃	10.61	10.65	5.46	5.59	7.61	8.91	8.97	7.27	4.98	7.95
MnO	0.18	0.17	0.12	0.13	0.18	0.16	0.16	0.12	0.10	0.14
MgO	5.39	5.63	1.08	1.31	1.68	2.37	2.25	1.87	1.26	2.05
CaO	7.30	7.61	3.88	4.38	5.03	6.74	6.71	5.53	4.56	5.87
Na ₂ O	3.76	3.55	3.90	4.28	4.77	4.62	4.36	4.99	4.14	4.17
K ₂ O	0.87	1.23	2.95	1.73	2.10	2.20	2.06	2.59	2.84	2.57
TiO ₂	1.89	1.91	0.50	0.62	0.78	0.90	0.88	0.90	0.60	0.83
P ₂ O ₅	0.52	0.51	0.22	0.24	0.31	0.42	0.38	0.34	0.22	0.33
Cr ₂ O ₃	0.01	0.01	BD	BD	BD	BD	BD	BD	BD	BD
LOI	2.33	1.94	0.79	0.65	0.69	0.67	0.90	0.98	0.73	0.85
H ₂ O-	0.20	0.15	0.10	0.05	0.12	0.05	0.13	0.16	0.06	0.08
Sum	99.42	99.50	99.71	99.64	99.19	99.60	99.58	99.23	99.11	99.31
Total	96.88	97.41	98.82	98.94	98.38	98.88	98.56	98.10	98.32	98.38
Ba	464.15	488.76	665.20	261.85	289.51	392.82	470.48	330.36	797.20	741.13
Co	52.73	74.51	88.84	90.21	55.15	55.08	64.28	58.71	72.95	66.44
Sc	33.61	35.82	16.44	14.14	21.41	49.29	43.98	12.84	13.31	35.30
Cu	32.17	49.25	7.01	19.43	9.25	9.16	8.80	2.55	4.13	7.90
W	104.84	218.09	511.38	514.00	268.04	222.23	292.08	257.24	416.01	310.88
Pb	8.27	6.92	16.36	13.32	14.83	11.80	10.34	13.72	14.94	12.08
Cr	109.31	113.14	9.45	10.43	9.90	11.82	10.78	12.46	11.38	13.14
Cs	0.53	1.18	1.27	1.64	2.52	1.96	1.81	6.41	4.00	1.93
Hf	6.81	6.92	6.65	6.61	11.60	11.01	10.32	25.24	18.55	10.72
Nb	18.21	18.28	13.88	15.56	19.79	23.77	20.80	20.76	14.52	18.62
Sn	2.92	3.24	4.29	3.63	4.78	5.07	10.73	6.66	4.82	10.40
Ni	48.20	50.10	8.19	9.75	5.17	8.15	5.67	8.51	6.29	7.59
Rb	20.14	29.85	124.22	126.43	153.37	116.32	109.65	160.14	123.63	118.97
Sr	461.32	509.44	205.34	200.49	197.74	266.21	274.80	273.83	255.05	259.37
Th	4.41	4.50	16.78	14.25	15.28	2.24	3.78	36.79	30.91	10.60
U	0.75	1.14	3.19	0.81	0.92	0.74	1.10	2.58	2.94	1.14
V	224.53	237.41	57.13	60.74	47.90	119.96	106.38	104.51	73.43	97.23
Y	48.97	47.64	41.49	27.40	50.72	84.62	65.52	54.48	36.17	54.93
Zn	84.29	101.51	63.35	93.37	86.86	102.03	99.98	100.29	68.72	96.23
Zr	324.38	327.15	268.99	306.19	556.54	509.45	479.07	1052.51	741.96	479.98
La	36.30	36.80	56.07	58.59	49.57	11.51	20.24	143.39	113.62	48.53
Ce	78.66	82.12	105.64	108.29	96.63	30.18	51.16	258.00	211.33	95.03
Pr	10.28	10.39	11.94	11.51	11.45	5.56	8.06	27.60	22.67	11.76
Nd	44.73	47.24	46.34	41.79	47.49	33.71	43.09	101.25	82.22	51.58
Sm	9.89	10.57	9.74	7.84	10.88	13.62	13.35	15.48	12.85	12.34
Eu	2.48	2.72	1.30	1.16	1.25	2.17	2.18	1.91	1.63	1.93
Gd	9.33	9.61	9.09	6.78	10.86	15.66	12.51	11.62	9.20	11.24
Tb	1.38	1.42	1.31	1.01	1.56	2.51	2.04	1.59	1.22	1.76
Dy	9.06	9.15	8.29	5.67	9.71	16.39	13.19	9.83	7.16	11.02
Ho	1.76	1.84	1.50	1.08	2.00	3.24	2.54	1.98	1.39	2.11
Er	5.10	5.29	4.32	2.75	4.92	8.75	6.78	5.87	3.97	5.69
Tm	0.72	0.72	0.57	0.33	0.64	1.22	0.94	0.80	0.60	0.77
Yb	4.77	4.70	3.45	2.08	4.00	7.28	5.86	6.10	4.15	4.98
Lu	0.68	0.77	0.47	0.28	0.56	0.96	0.81	1.03	0.62	0.70
Ta	0.92	0.99	0.78	0.58	0.85	0.72	0.63	1.22	0.87	0.64
Mo	1.35	1.95	0.86	0.97	1.01	0.87	0.87	1.04	0.89	0.77
LREE	191.66	199.45	240.12	235.96	228.13	112.41	150.61	559.25	453.52	232.42
HREE	23.48	23.87	19.90	13.20	23.39	40.36	32.16	27.20	19.11	27.03
Eu/Eu*	0.15	0.15	0.15	0.16	0.15	0.16	0.16	0.15	0.15	0.16

(a) Mix between granites and enclaves. (b) Total iron as Fe³⁺. (c)BD= below detection limit. (d)LOI=Loss on ignition. Refer to

Table 10: Whole-rock major (wt. %) compositions of granite samples from the Buddusò Pluton

Type	Granites																				
Unit	Inner						Middle							Outer							
Sample	BG1	BG10	BG18	BG19	BG25	BG32	BG2	BG3	BG23	BG24	BG26	BG27	BG30	BG31	BG13	BG14	BG33	BG34	BG35	BG36	BG48
SiO ₂	74.00	74.50	75.96	75.80	75.03	77.01	69.82	73.71	71.00	69.37	68.06	71.88	74.04	73.99	66.81	66.76	67.55	65.70	65.78	66.48	64.56
Al ₂ O ₃	13.69	12.89	13.01	12.87	13.15	12.19	14.64	13.47	14.53	14.18	15.57	13.88	13.28	13.28	15.77	15.62	15.33	16.14	15.65	15.69	16.60
Fe ₂ O ₃ ^(b)	1.50	1.36	1.11	1.13	1.06	0.73	3.40	1.98	2.42	2.88	3.98	2.63	1.99	2.14	3.91	4.24	4.34	4.61	4.87	4.45	4.80
MnO	0.06	0.05	0.04	0.05	0.03	0.02	0.07	0.05	0.06	0.08	0.11	0.08	0.06	0.06	0.07	0.08	0.08	0.09	0.08	0.08	0.08
MgO	0.16	0.17	0.08	0.09	0.06	0.00	0.61	0.31	0.49	0.62	0.88	0.55	0.33	0.32	0.98	1.07	1.11	1.18	1.24	1.13	1.27
CaO	1.37	1.27	1.22	1.16	1.07	0.46	2.35	1.54	2.27	2.40	3.59	2.42	1.50	1.65	3.70	3.66	3.85	3.91	4.03	3.73	4.32
Na ₂ O	3.31	2.92	3.06	3.06	2.30	2.24	3.43	2.83	3.06	2.99	3.40	3.08	3.06	3.17	3.14	3.06	3.20	3.26	3.33	3.14	3.23
K ₂ O	4.81	4.85	4.72	4.79	6.46	6.44	3.71	4.97	4.58	4.08	2.84	3.61	4.51	4.08	3.26	3.31	2.53	3.15	2.39	3.17	2.85
TiO ₂	0.11	0.11	0.09	0.10	0.07	0.04	0.30	0.17	0.25	0.30	0.40	0.27	0.19	0.19	0.44	0.47	0.50	0.52	0.56	0.53	0.57
P ₂ O ₅	0.03	0.03	0.02	0.02	0.02	0.01	0.09	0.05	0.06	0.08	0.10	0.08	0.05	0.05	0.12	0.13	0.13	0.14	0.15	0.13	0.16
Cr ₂ O ₃	BD ^(a)	BD	BD	BD	BD	BD	BD	BD	BD	BD	BD	BD	BD	BD	BD	BD	BD	BD	BD	BD	BD
LOI ^(c)	0.99	1.17	0.61	0.58	0.78	0.35	0.96	0.93	1.19	0.92	0.82	0.78	0.78	0.66	0.75	0.85	0.72	0.70	0.71	0.81	0.80
H ₂ O ⁻	0.27	0.20	0.07	0.12	0.13	0.12	0.26	0.22	0.17	0.15	0.10	0.10	0.15	0.11	0.07	0.10	0.08	0.06	0.09	0.11	0.02
Sum	100.29	99.53	99.98	99.76	100.16	99.61	99.64	100.24	100.09	98.06	99.85	99.36	99.93	99.69	99.01	99.34	99.41	99.44	98.88	99.44	99.27
Total	99.03	98.16	99.30	99.06	99.24	99.15	98.42	99.08	98.73	96.99	98.93	98.48	99.00	98.92	98.20	98.39	98.61	98.69	98.08	98.52	98.45
Ba	259.24	316.35	227.49	201.62	950.99	521.91	769.83	719.78	1147.75	1151.99	650.71	723.47	583.11	477.05	1281.62	1222.49	840.83	1235.99	674.89	1234.41	1319.49
Co	157.56	165.22	163.15	169.39	143.89	132.73	161.94	147.95	141.01	131.09	117.13	135.07	151.58	195.03	110.25	136.55	124.61	108.17	109.28	118.80	113.25
Sc	7.72	6.85	5.74	6.30	4.42	3.79	11.23	7.99	8.08	9.01	16.00	8.11	10.38	8.20	13.50	15.09	15.54	16.40	15.15	15.88	15.41
Cu	4.19	3.89	3.77	3.54	2.89	2.80	16.85	5.46	7.30	9.75	8.12	6.58	4.36	8.00	6.29	13.39	12.10	2.79	6.49	13.25	11.48
W	962.19	1069.10	1007.09	1028.28	888.65	842.18	985.76	923.74	854.60	828.70	710.41	876.73	928.59	1229.16	667.27	802.03	715.91	618.23	649.63	674.43	693.45
Pb	38.04	35.66	32.66	37.71	35.47	40.73	19.88	24.63	23.24	24.81	17.17	25.99	26.42	24.82	13.40	10.93	12.11	13.88	11.95	13.86	12.39
Cr	10.53	10.96	11.02	14.82	11.43	10.28	17.27	12.62	14.11	13.32	14.02	10.95	15.74	11.95	12.77	12.76	13.77	18.17	14.96	19.31	15.29
Cs	1.61	1.95	1.62	1.90	1.98	1.63	2.28	1.81	1.65	1.83	1.54	2.42	1.64	2.04	1.58	1.68	1.35	1.73	1.45	1.40	1.86

Table 10 (continued).

Type	Granites																					
Unit	Inner						Middle								Outer							
Sample	BG1	BG10	BG18	BG19	BG25	BG32	BG2	BG3	BG23	BG24	BG26	BG27	BG30	BG31	BG13	BG14	BG33	BG34	BG35	BG36	BG48	
Hf	2.52	3.20	2.69	2.52	3.14	2.76	4.46	3.25	4.26	5.01	5.34	3.26	4.27	4.20	5.45	5.01	6.33	6.53	6.78	6.35	6.93	
Nb	10.22	6.96	8.26	7.66	3.30	3.35	13.88	7.85	9.43	11.62	13.49	10.30	11.95	11.82	10.79	10.32	12.80	14.86	15.08	14.73	11.88	
Sn	1.52	2.57	3.44	3.22	1.57	1.64	2.96	1.83	3.52	3.61	3.33	3.39	2.95	2.87	2.45	2.20	3.40	3.17	3.70	3.36	4.04	
Ni	7.14	6.20	7.79	8.53	6.49	6.40	8.07	7.76	7.86	8.38	9.06	7.43	5.69	6.69	7.82	5.94	9.96	8.40	8.33	7.43	6.72	
Rb	158.25	146.21	158.93	164.60	180.58	177.30	125.06	124.08	147.77	156.82	129.28	145.94	139.06	137.27	90.75	92.39	96.26	109.14	101.92	110.03	95.58	
Sr	52.96	58.69	47.93	42.68	126.67	68.94	128.15	99.52	173.19	181.92	199.14	130.75	96.14	102.08	214.45	204.79	230.31	243.14	229.24	239.35	268.96	
Th	9.64	10.27	17.50	14.44	11.03	18.74	11.58	12.34	17.49	19.56	11.66	11.45	18.72	14.64	10.77	11.94	14.03	15.24	16.48	15.20	14.14	
U	2.46	2.91	2.64	2.77	2.79	3.83	1.61	1.70	1.61	1.56	2.32	2.19	1.85	2.24	1.94	2.16	1.72	1.53	1.75	1.51	1.86	
V	13.50	14.20	9.76	12.12	20.69	14.21	34.29	22.07	35.20	41.49	58.32	35.39	19.30	23.00	55.21	60.34	66.32	69.52	74.55	67.70	74.37	
Y	9.44	13.75	14.26	13.03	11.70	17.75	16.89	11.78	13.30	15.29	26.71	9.22	20.85	19.74	19.60	19.85	24.83	28.65	27.30	27.29	23.70	
Zn	31.67	52.17	31.25	31.13	22.76	16.04	72.50	45.58	38.48	63.21	58.75	44.22	44.05	52.62	48.56	49.01	51.68	63.18	64.14	56.43	58.04	
Zr	75.96	93.37	76.98	74.74	99.20	65.08	169.22	114.35	152.75	181.39	218.61	121.41	142.02	138.59	210.33	197.88	245.00	266.31	276.70	257.09	283.98	
La	14.56	15.71	12.23	10.85	20.43	13.59	35.42	29.37	46.14	50.62	33.85	28.21	42.40	30.00	42.16	50.51	54.10	59.10	66.26	65.66	67.70	
Ce	35.31	35.38	26.35	23.98	45.76	30.83	67.89	60.99	87.35	98.08	66.29	62.42	82.98	61.05	79.46	96.25	100.13	109.88	123.00	118.88	122.15	
Pr	3.78	3.99	2.98	2.65	4.94	3.51	7.46	6.66	9.70	10.80	7.21	6.26	9.51	6.90	8.58	10.15	10.90	12.13	13.45	13.27	13.26	
Nd	14.57	14.57	11.87	10.73	18.14	13.08	27.02	24.26	36.10	39.23	28.73	22.23	36.36	26.53	31.97	37.81	42.84	46.97	51.58	47.92	49.33	
Sm	3.07	3.22	2.86	2.66	3.41	2.78	5.04	3.97	6.15	6.17	5.79	3.89	6.54	4.97	5.87	6.02	8.05	8.83	8.83	7.89	7.83	
Eu	0.37	0.50	0.43	0.37	0.68	0.45	0.81	0.67	1.05	1.08	1.16	0.74	0.66	0.79	1.31	1.22	1.37	1.41	1.43	1.45	1.65	
Gd	2.41	2.47	2.60	2.15	2.32	2.43	4.29	2.80	4.33	4.95	5.88	2.82	5.15	3.91	4.38	4.92	5.99	6.67	6.65	6.51	6.14	
Tb	0.31	0.33	0.42	0.35	0.33	0.41	0.57	0.39	0.50	0.59	0.84	0.36	0.61	0.51	0.64	0.62	0.75	0.88	0.93	0.84	0.78	
Dy	1.73	2.06	2.84	2.28	2.07	2.76	3.10	2.11	2.84	3.57	5.27	1.94	3.72	3.44	3.98	3.44	4.96	5.90	5.31	5.08	4.70	
Ho	0.33	0.44	0.55	0.44	0.43	0.59	0.60	0.42	0.54	0.64	1.03	0.36	0.67	0.68	0.75	0.74	0.96	1.09	1.08	0.98	0.91	
Er	1.05	1.49	1.37	1.15	1.29	2.01	1.67	1.12	1.29	1.41	2.83	0.87	2.26	2.18	2.22	1.98	2.61	3.00	2.83	2.88	2.50	
Tm	0.18	0.24	0.23	0.17	0.20	0.36	0.26	0.18	0.16	0.20	0.41	0.12	0.37	0.36	0.33	0.29	0.38	0.41	0.39	0.36	0.33	
Yb	1.19	2.07	1.50	1.20	1.48	2.55	1.51	1.24	1.20	1.35	2.44	0.75	2.26	2.29	2.20	1.84	2.64	2.78	2.57	2.56	2.30	
Lu	0.20	0.34	0.27	0.19	0.23	0.41	0.23	0.18	0.13	0.18	0.36	0.11	0.34	0.34	0.30	0.29	0.35	0.38	0.35	0.36	0.36	
Ta	0.42	0.59	0.79	0.70	0.37	0.40	0.71	0.47	0.53	0.60	0.75	0.51	0.75	0.79	0.61	0.52	0.63	0.65	0.72	0.71	0.54	
Mo	1.04	0.87	0.81	0.99	0.83	1.07	0.92	0.91	1.02	1.04	0.99	0.85	0.70	0.88	0.93	1.01	1.12	1.22	0.90	1.00	0.78	
LREE	74.07	75.84	59.32	53.39	95.67	66.66	147.92	128.73	190.81	210.93	148.91	126.56	183.60	134.15	173.72	206.89	223.38	244.98	271.21	261.58	268.05	
HREE	4.98	6.97	7.17	5.79	6.02	9.09	7.95	5.64	6.66	7.94	13.19	4.52	10.24	9.81	10.42	9.20	12.65	14.44	13.45	13.07	11.88	
Eu/Eu*	0.15	0.15	0.15	0.16	0.15	0.16	0.16	0.16	0.14	0.14	0.15	0.15	0.14	0.14	0.15	0.15	0.14	0.14	0.16	0.15	0.14	

4.4.1 Major element geochemistry

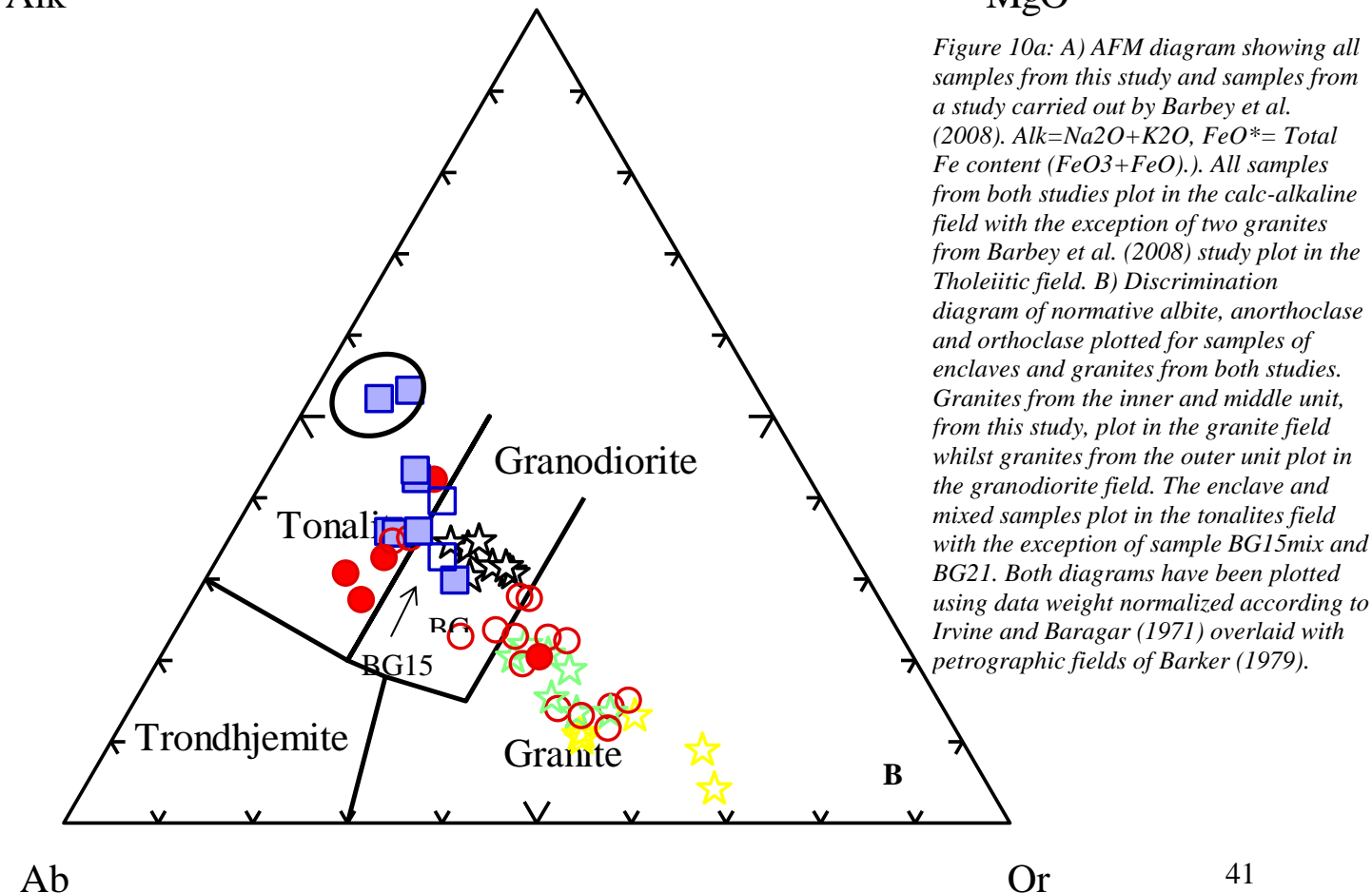
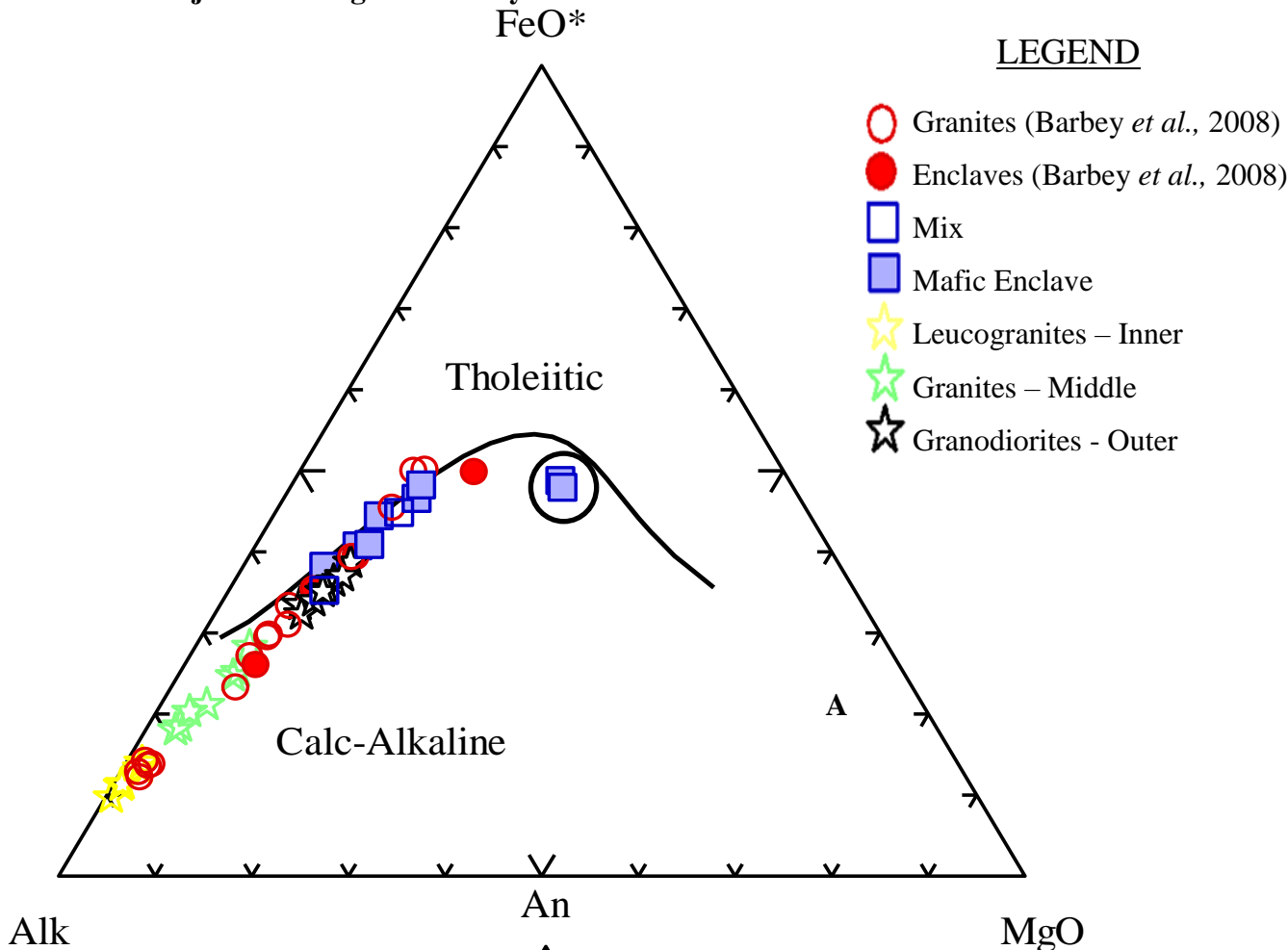


Figure 10a: A) AFM diagram showing all samples from this study and samples from a study carried out by Barbey *et al.* (2008). Alk=Na₂O+K₂O, FeO*= Total Fe content (FeO₃+FeO). All samples from both studies plot in the calc-alkaline field with the exception of two granites from Barbey *et al.* (2008) study plot in the Tholeiitic field. B) Discrimination diagram of normative albite, anorthoclase and orthoclase plotted for samples of enclaves and granites from both studies. Granites from the inner and middle unit, from this study, plot in the granite field whilst granites from the outer unit plot in the granodiorite field. The enclave and mixed samples plot in the tonalites field with the exception of sample BG15mix and BG21. Both diagrams have been plotted using data weight normalized according to Irvine and Baragar (1971) overlaid with petrographic fields of Barker (1979).

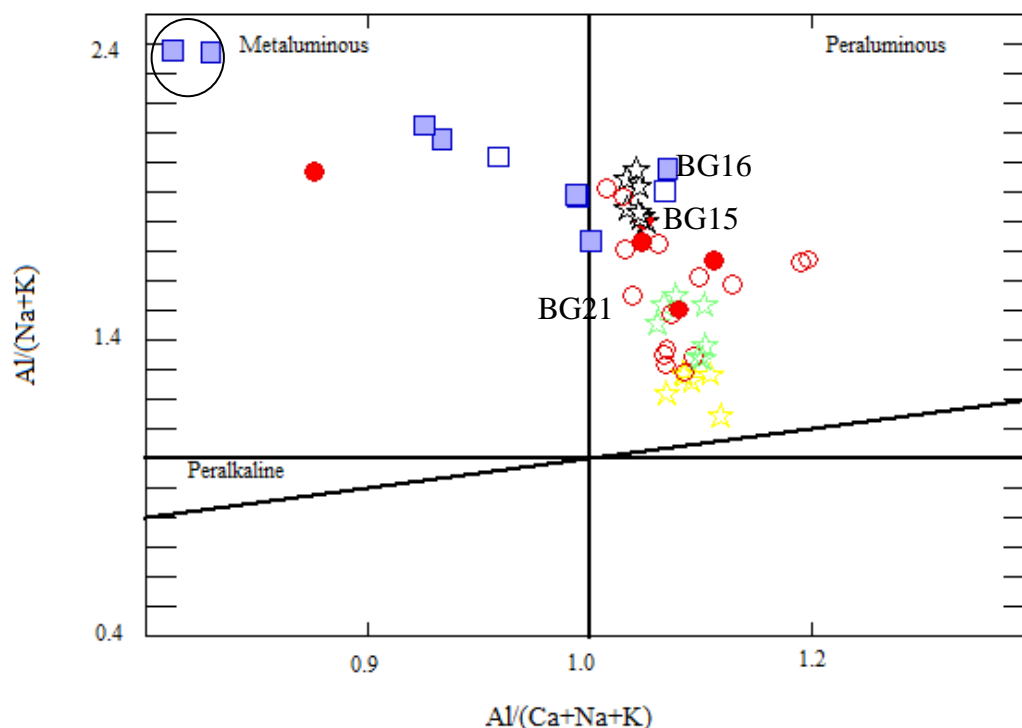


Figure 10b: Discrimination diagram showing $Al/(Na+K)$ vs $Al/(Ca+Na+K)$. All granite samples from this study plot in the peraluminous section and enclaves plot in the metaluminous field with exception of samples BG15mix and BG16mme plotting in the peraluminous field. Diagram uses Shand's Index (1943) superimposed by discrimination fields of Maniar and Piccoli (1989) using molar proportions.

4.4.1.1 Granites

Leucogranites from the inner unit plot lowest in the peraluminous field (Fig.10b) reflecting the group's low Al_2O_3 content (12.19 % - 13.69 %) and CaO content (0.46 % - 1.37 %) and high K_2O content (4.81 % - 6.46 %) The granodiorites from the outer unit plot the highest in the peraluminous field reflecting the group's relatively higher Al_2O_3 content (15.62 % - 16.60 %) and CaO content (3.70 % - 4.32 %) and lower K_2O content (2.39 % - 3.26 %) (Table 10). This is reasonably unusual for I-type granites which usually have an inverse correlation between $FeO+MgO$ vs. A/CNK with granodiorites being significantly metaluminous.

Granites from all units show negative correlations for all major elements except K_2O with respect to SiO_2 . They show an increase in Al_2O_3 , CaO, FeO, MgO, TiO_2 and, P_2O_5 with decreasing SiO_2 from the inner unit through to the outer unit (Fig.11). Granite samples show an increase in K_2O with an increase in SiO_2 . The three groups of granites are enriched in SiO_2 and K_2O in comparison to the enclaves.

4.4.1.2 Mafic enclaves

The enclaves and mix samples from this study plot mostly in the metaluminous field on Fig.10b with the exception of BG16mme and BG15mix which plot in the peraluminous fields and BG21

which plot on the border of both fields. All three of these samples show a lower CaO content in relation to the rest of the enclaves, with a CaO content of 5.53 %, 4.56 % and 3.88 % respectively. BG21 plots on the border because the sample's low CaO content is paired with a lower Al₂O₃ concentration (16.69 %) with respect to the rest of the enclaves (Table 9).

The two enclave samples circled on Fig.10a and Fig.10b are samples BG8 and BG9; both samples exhibit an interesting chemistry which is unlike the rest of the enclave samples. The sample's relatively higher CaO content (7.30 % & 7.61 % respectively) and lower K₂O content (0.87 % & 1.23 % respectively) position the samples higher in the metaluminous field distinguishing them from the rest of the enclaves. These samples display various other differences in their major element chemistry in comparison to the other enclave samples; lower SiO₂ and Na₂O, higher Fe₂O₃, MnO, MgO, TiO₂ and P₂O₅ (Table 9, Fig.11).

In Fig.11, enclaves define continuous patterns showing an increase in Al₂O₃, CaO, FeO, MgO, Na₂O, TiO₂ and, P₂O₅ with a decrease in the SiO₂ content. Mafic enclaves are more enriched in Al₂O₃, CaO, FeO_{tot}, MgO, Na₂O, TiO₂ and P₂O₅ in comparison with the granites. Enclaves show no correlation with respect to SiO₂ vs. K₂O. An interesting point observed from the major element chemistry; enclaves from this study show a wider range in compositions seen by their dispersive patterns in Fig.11 whilst the granites share a smaller range in compositions seen by their tightly concentrated patterns.

Granites and enclave compositions from Barbey et al. (2008) show continuous patterns showing an increase in Al₂O₃, CaO, FeO, MgO, Na₂O, TiO₂ and, P₂O₅ with a decrease in the SiO₂ content (Fig 11). With respect to SiO₂ vs. K₂O both enclaves and granites from Barbey et al. (2008) study show no correlation. Both datasets show little correlation for SiO₂ vs. Na₂O (R= -0.36, R' = -0.61 & r = -0.82 and r' = -0.86). Granodiorites from this study show higher CaO contents and Na₂O and Zn contents for a given SiO₂ content in comparison with granites from Barbey et al. (2008).

Generally the samples of both enclaves and granites from this study show a tighter correlation with respect to the samples from Barbey et al. (2008), with the exception of the coefficient correlation values for MgO vs. SiO₂ and TiO₂ vs. SiO₂. In these plots, correlation coefficients are lower (r = -0.86, r' = 0.98 & R = -0.90, R' = -0.98) than values from Barbey et al. (2008) (R = -0.98, R' = -0.96 & R = -0.96, R' = 0.95). This could be due to samples BG8 and BG9's much higher MgO and TiO₂ content which skews the correlation calculations.

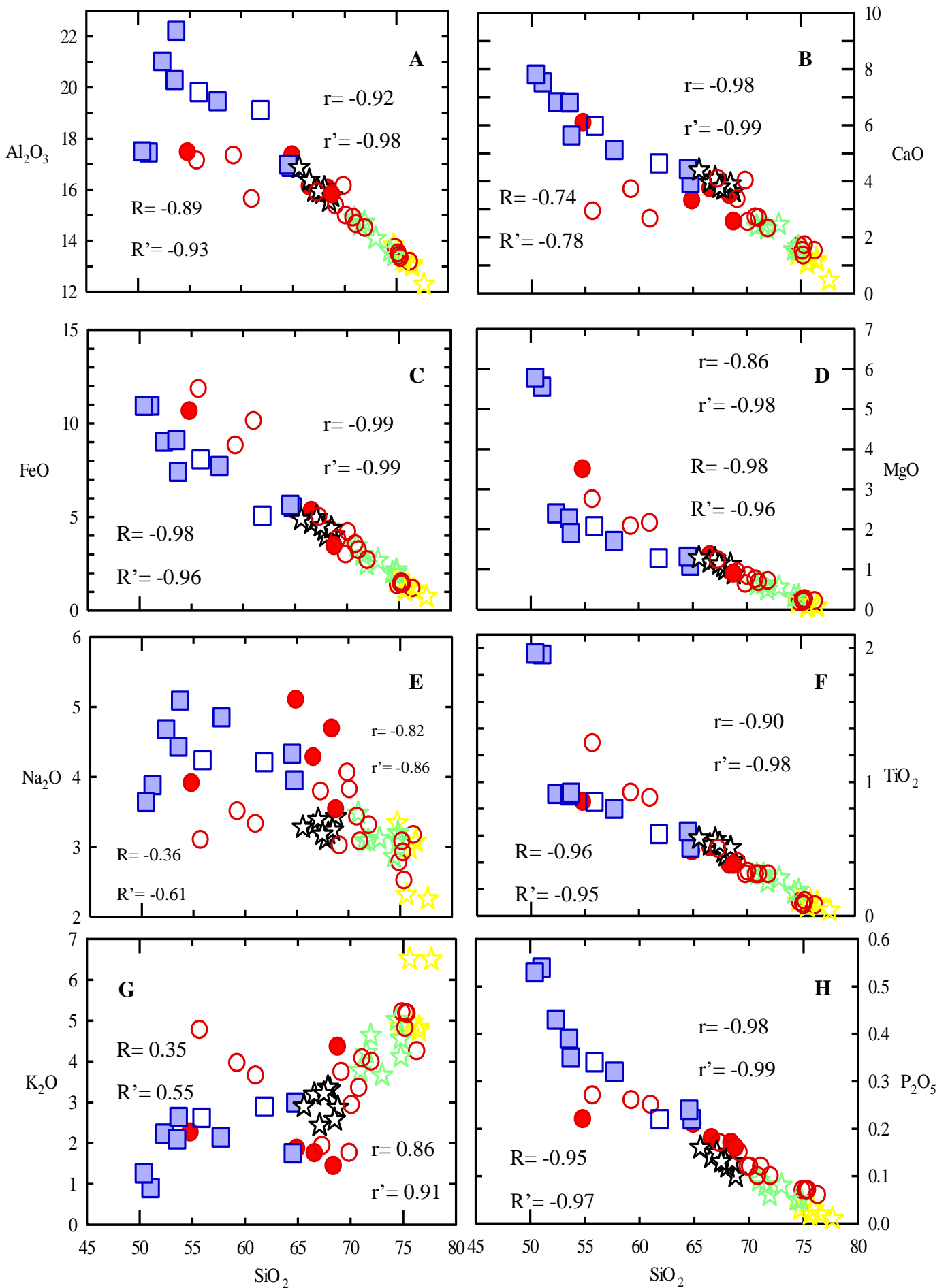


Figure 11: Harker plots comparing granite and enclave compositions from this study with those from the study conducted by Barbey et al. (2008). Pearson's coefficient (R) and Spearman's rank order coefficient (R') values are given for the data from Barbey et al. (2008) and Pearson's coefficient (r) and Spearman's rank order coefficient (r') values are given for the samples from this study. Refer to Appendix II for full regression parameters and graphs.

4.4.2 Trace element geochemistry

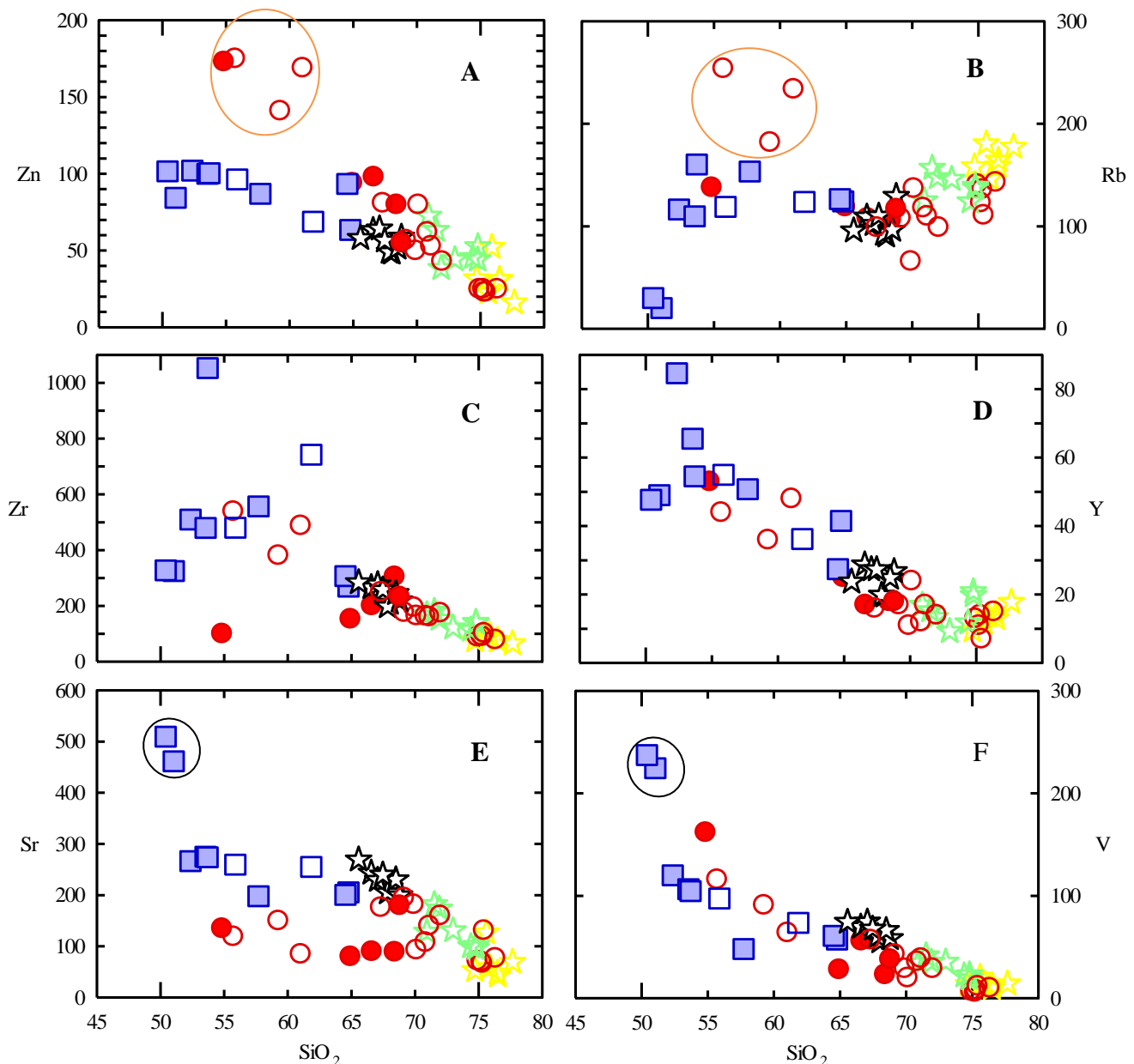


Figure: 12a Harker plots comparing granite and enclave compositions from this study with those from the study conducted by Barbey et al. (2008). All trace elements plotted are measured in ppm. Refer to Appendix II for full data set.

4.4.2.1 Granites

Fig.12a & 12b show trends for trace elements vs. SiO_2 , which are less well defined than the major elements. High field strength elements (HFS); heavy rare earth elements (HREE), Zr and Nb show negative correlations with SiO_2 in granites. Low field strength elements (LFSE); Rb, Sr and Eu^{2+} show positive correlations with SiO_2 whilst LFSE Ba displays a negative correlation with SiO_2 . Granites show a general increase in Zn, Zr, Y, Sr, V, Eu, Nb and all REE from the inner unit through to the outer unit with decreasing SiO_2 . Granites show low Ni concentrations.

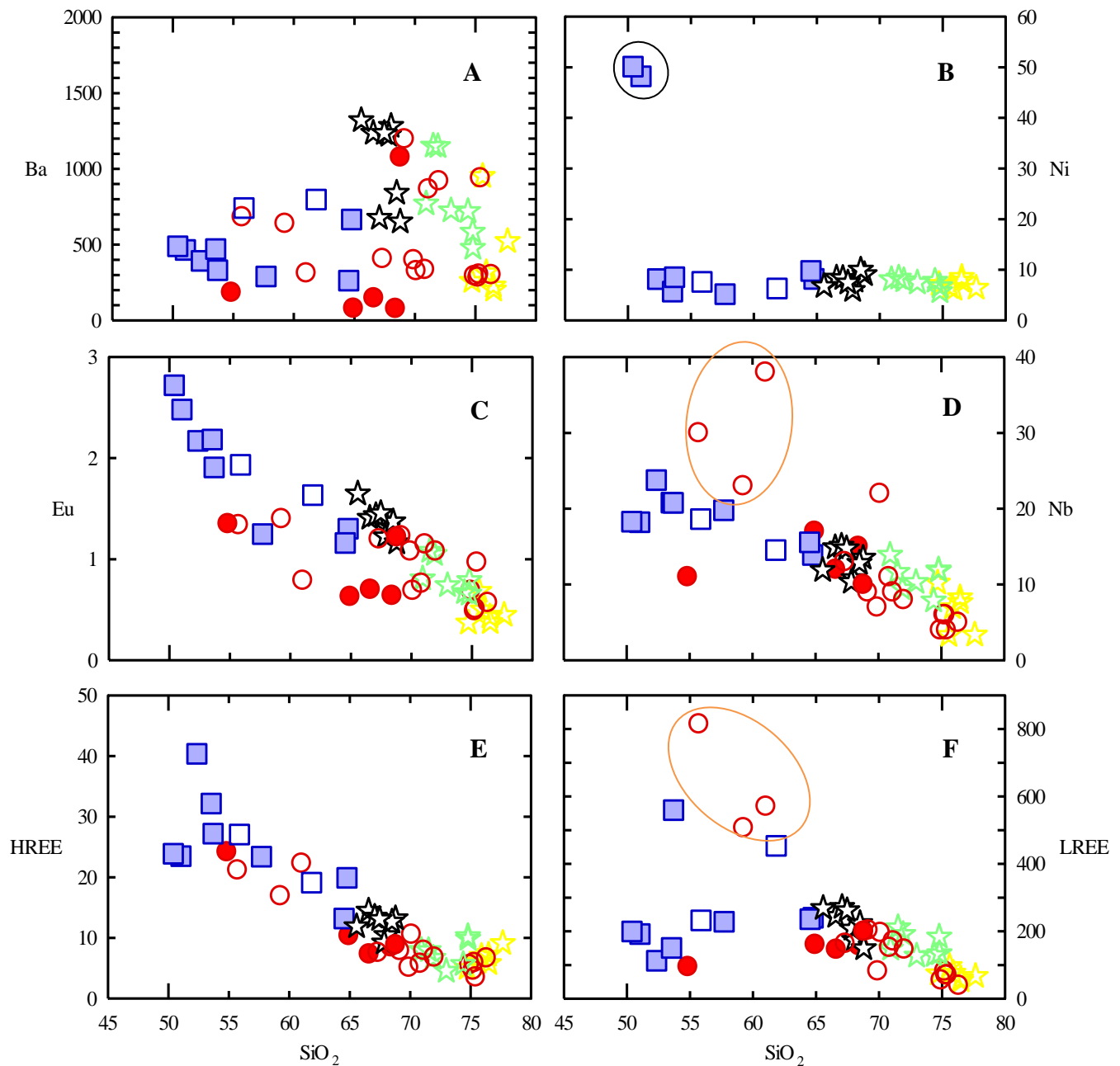


Figure 12b: Harker plots of granite and enclave compositions from this study with those from the study conducted by Barbey *et al.* (2008). All trace elements plotted are measured in ppm. Refer to Appendix: II for full dataset. $LREE = La + Ce + Pr + Nd + Sm + Eu + Gd$, $HREE = Tb + Dy + Ho + Er + Tm + Yb + Lu$

With regard to Fig.13B-D granites all share a negative slope indicative of enrichment in light rare earth elements (LREE) over HREE. Within the three units; there is a decrease in the sum of HREE and LREE in the direction of the outer unit through to the inner unit corresponding to a decrease in mafic minerals (hornblende and epidote) from the outer unit through to the inner unit. All granite groups share a negative Eu anomaly suggestive of plagioclase fractionation with the leucogranites from the inner unit having the lowest Sr values (Fig.12a) reflecting its high felsic proportion. Enrichment in La increases from the inner unit (40 to 100 times chondritic range) through to the outer unit (110 to 120 times chondritic range). Granites from the middle unit are less enriched in Lu (4 to 20 times chondritic range). Granites are

characterized by negative Rb, Ta, Nb, Sr, P and Eu anomalies with Rb, Th-U, La-Ce, Pb and Nd peaks (Fig.13F-H) all correlating to the various amounts of apatite, plagioclase and ilmenite seen in the samples.

4.4.2.2 Enclaves

Enclaves show an increase in HREE and Nb with decreasing SiO₂ content. Rb, Ba and Sr show no correlation with SiO₂ whilst LFSE Eu²⁺ displays a positive correlation. Enclaves are more enriched in elements Zn and Y in comparison to granites. Both granites and enclaves share almost the same Ni content (with the exception of enclave samples BG8 and BG9). In comparison to the granites, enclaves are more enriched in Zr, Eu²⁺, Nb and HREE with respect to SiO₂ content. Enclave samples BG8 and BG9 show considerably higher concentrations in Sr, V and Ni (circled in black) in comparison to the other enclave and granite samples. Enclaves show low Ni concentrations.

Enclaves are characterized by a wider range in La enrichment (varying from 30 to 980 times the chondritic range) and have a weaker depletion in Lu in comparison to the granites (Fig.13E). Enclave samples share Nb-Ta and Sr-P troughs and a Pb peak. All enclave samples share Eu and Sr anomalies and Zr peaks with the exception of samples BG8 and BG9 (Fig.13E1). Samples from Fig.13E2 & 13E4 share a negative Rb anomaly and a Th peak. Enclave samples in Fig. 13E2 show the strongest Lu depletion.

Samples from Barbey et al. (2008) show fairly similar correlation patterns with respect to SiO₂ but enclaves show a smaller range in composition, with the exception of a few granite samples (circled in orange) showing enrichment in Zn, Rb, Nb and LREE (Fig.12).

It is important to note that proposed enclave sample BG8 and BG9 have been removed from all modelling explored here forth based on the assumption that their distinctive chemistry (Fig.10-13) is suggestive of them being xenoliths of country rock rather than the mafic enclaves being investigated.

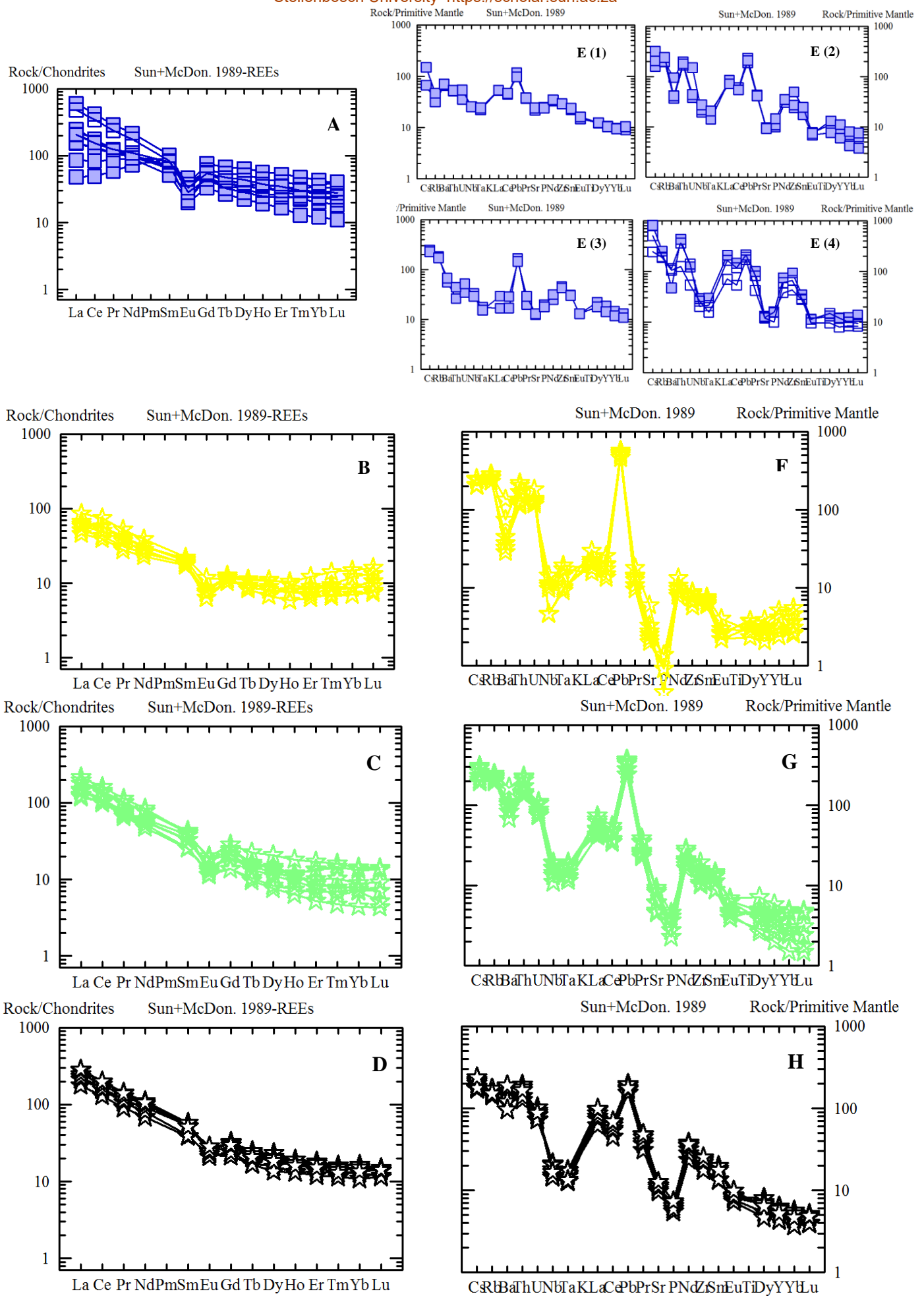


Figure 13: A-D) Chondrite-normalized REE patterns and E-H) Primitive mantle-normalized trace element diagrams. Primitive mantle-normalized trace element diagrams for enclave samples BG8 and BG9 (E1), BG21, BG22 and BG29 (E2), BG38 and BG15mm (E3) and BG16mm, BG15mix and BG16mix (E4). Normalization values are from McDonough and Sun (1995) for primitive mantle and from Sun and McDonough (1989) for Chondrite.

Chapter 5: Using Zircon as a tool to understand the petrogenesis of the Buddusò Pluton

Scenarios where both the granitic rocks and their source rocks are preserved are rare. The large amount of zircon crystals present in granitic source rocks as well as zircon's refractory nature allow them to be commonly entrained in the magma during magma separation from the source (e.g. Villaros et al., 2012). The U-Pb isotope ratios in magmatic zircon were analysed to determine the crystallization ages of the different varieties of granite and the enclaves. The U-Pb isotope data from inherited cores will be studied to determine the crystallisation ages of the rocks that form components of the source of the magma. The Lu-Hf isotopic data from both magmatic and inherited zircons will be used to provide a model age for the age of separation of the material from which the granite was derived.

5.1 Zircon Crystals

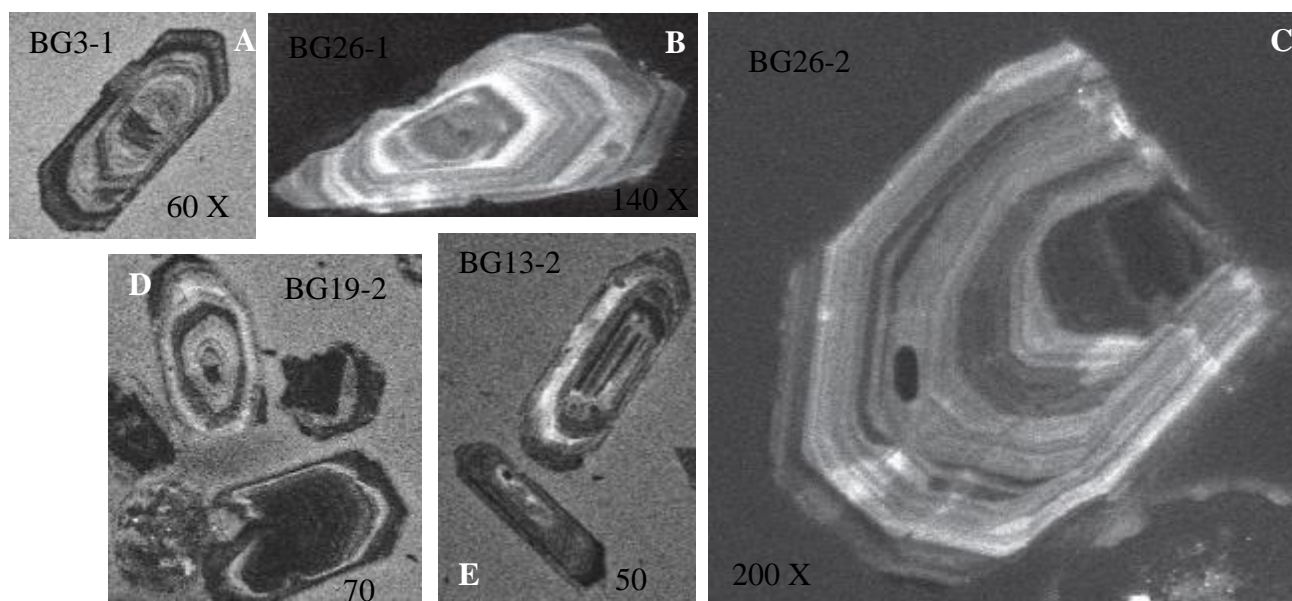


Figure 14: Cathodoluminescence images of zircon crystals from granites. Sample names and magnification included on each image. Zircon crystals are subhedral to euhedral in shape and show strong oscillatory zoning. Apatite inclusions can be seen in Figures E and C.

5.2 U-Pb Isotope analysis

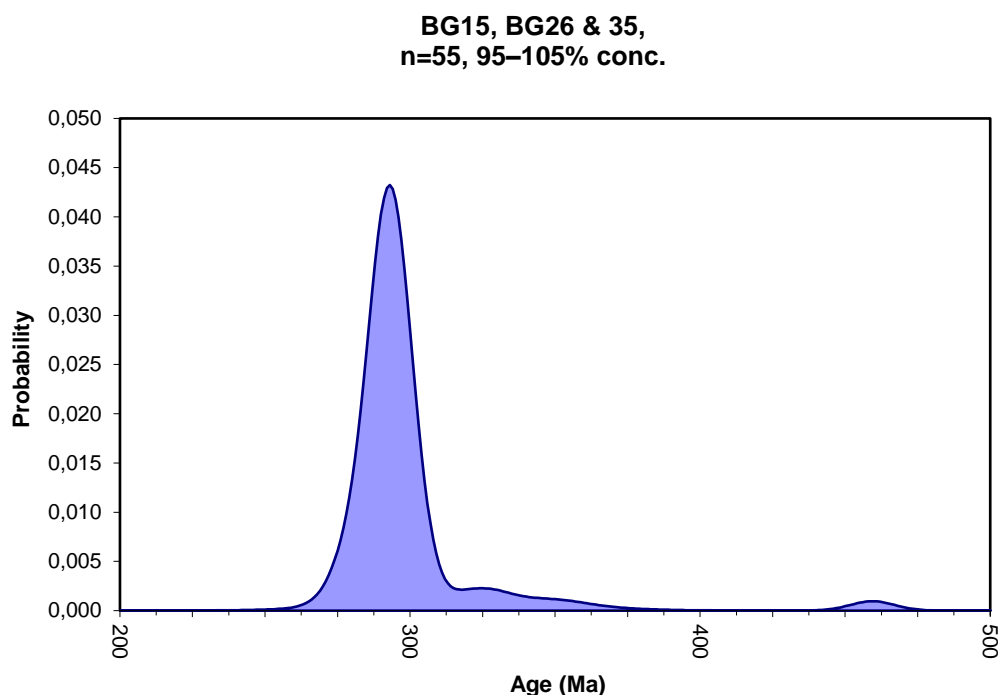


Figure 15: Relative probability plot showing distribution of ages for the concordant magmatic zircons crystals from samples BG15, BG26 and BG35. n refers to the number of concordant crystals, with concordance measured between 95 – 105%. Uncertainty on individual age analyses can be found in Appendix IV.

The Buddusò pluton belongs to calc-alkaline plutonic association aged ca. 305 – 290 Ma (Barbey et al., 2008). An Rb-Sr isochron analysed by Cocherie (1984) gives an emplacement age of 281 ± 5 Ma. The Benetutti intrusion to the south and Aladei Sardi pluton to the north is proposed to have the same emplacement age (Orsini et al., 1977). The Buddusò pluton is crosscut by the Concas pluton to the east with an emplacement Rb-Sr age of 275 ± 4 Ma (Cocherie, 1978).

Poli et al. (1989) studied various plutons and established the granodiorites from the outer unit have an emplacement age of 299 ± 21 Ma, the granodiorites from the middle unit; 281 ± 5 and the leucogranites from the inner unit have an emplacement age of 289 ± 1 . All ages are from Rb-Sr isochrons.

Seventy-seven U-Pb ages were obtained from zircon grains of the Buddusò pluton. Fig.15&16 show the fifty-five concordant U-Pb ages, the complete dataset is provided in Appendix IV. Fig.15 shows that the zircon population is strongly dominated by dates between the ranges 256Ma to 312Ma. There are a few grains which record dates 444Ma to 466Ma indicating that the zircon grains sampled show little inheritance. Fig.16 show Concordia diagrams for samples BG15 (enclave from the middle unit), BG26 (granite from middle unit) and BG35 (granodiorite from outer unit) respectively. From the twenty-two U-Pb analyses recorded from Sample BG15 (Fig.16A) only sixteen analyses passed the <5% discordancy test showing spot dates between 289Ma and 304Ma. Two of the grains represented inherited zircon dates of 328Ma and 346Ma. Thirty four U-Pb analyses out of the initial forty four that were sampled from BG26 (Fig.16B) passed the <5% discordancy test. Those grains showed spot dates that vary between 277Ma and 319Ma with two of the inherited grains indicating dates of 347Ma and 334Ma. Five out of the eleven grains from sample BG35 passed the <5% discordancy test (Fig. 16C). Analyses showed spot dates ranging between 277Ma to 297Ma with one grain indicating an inherent date of 457Ma.

It is interesting to note that enclave sample BG15 (Fig.16A) and granite sample BG26 (Fig.16B) from the middle unit show similar weighted mean $^{206}\text{Pb}/^{238}\text{U}$ ages of $294\pm 2\text{Ma}$ (MSWD=0.55) and $291\pm 2\text{Ma}$ (MSWD=0.47) respectively. This age is considered as the magmatic age of the pluton. However sample BG35 (Fig.16C) shows a slightly younger weighted mean $^{206}\text{Pb}/^{238}\text{U}$ date of $287\pm 3\text{Ma}$ (MSWD=1.7). This could also be due to the one date represented as the yellow circle which skews the Concordia age.

The U-Pb data from the inherited zircon grains show that the source of the magma was fairly close in age to the granites because the age of the source of the granites is defined by the youngest inherited zircon age which on Fig.15, is fairly close to the age of the granites. The reader is urged to keep in mind that the sample population was small with an even smaller subset of inherited zircon grains therefore true representivity of the zircon population in the source is limited.

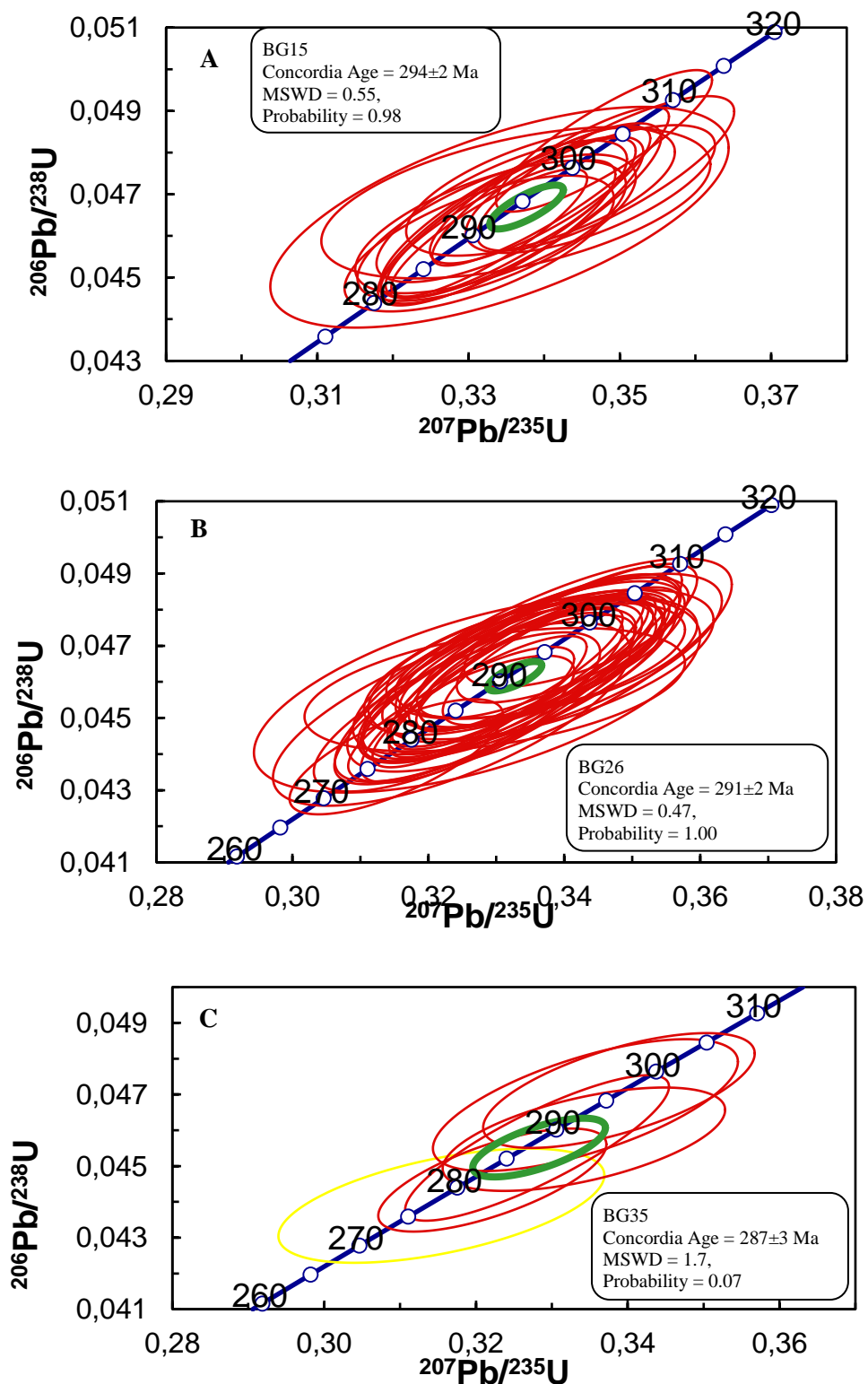


Figure 16: Wetherill Concordia diagrams for magmatic zircon crystals of the three samples; A) BG15, B) BG26 and C) BG35. Error ellipses are plotted at 2σ .

5.3 Lu-Hf Isotope analysis

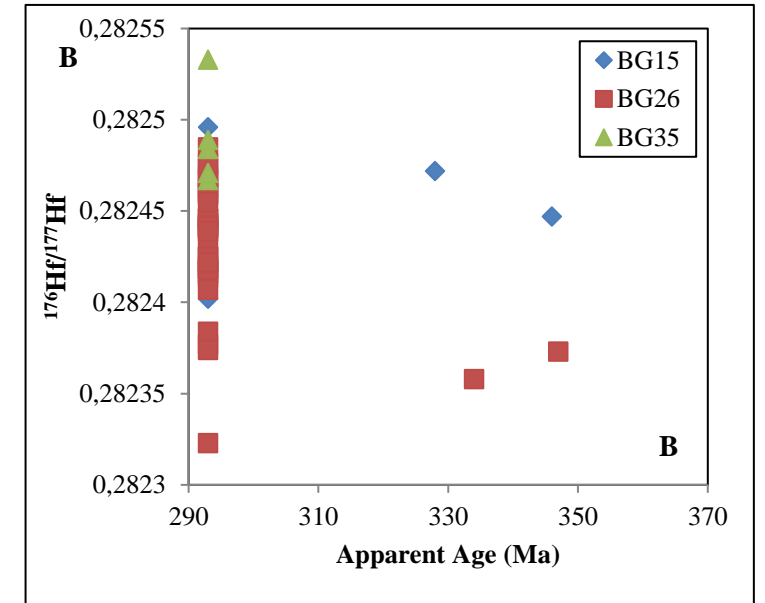
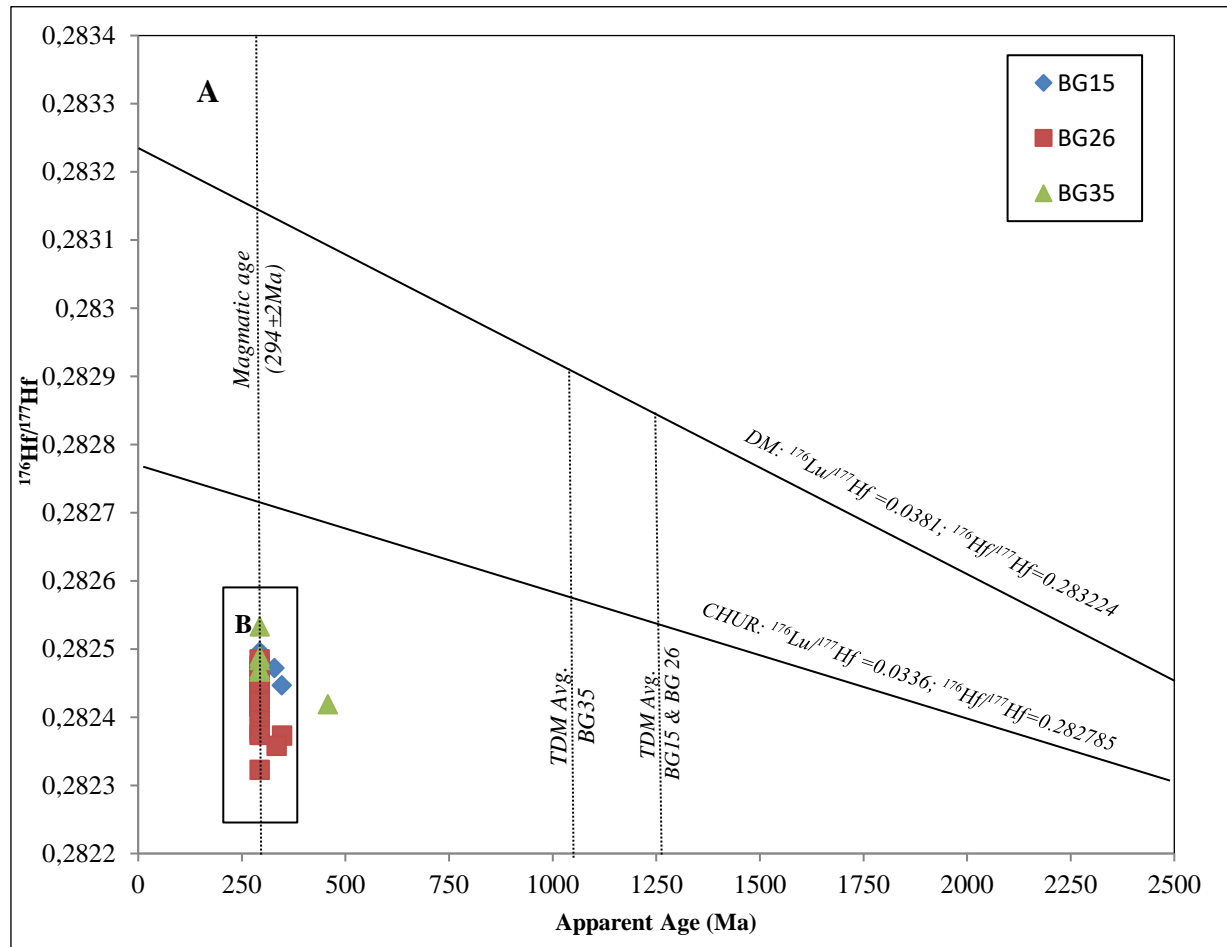


Figure 17A: Lu-Hf and U-Pb zircon results for enclave sample BG15 from the middle unit and granite samples BG26 (middle unit) and BG35 (outer unit) from the Buddusò pluton. Values for Depleted Mantle (DM) and Chondritic Uniform Reservoir (CHUR) shown on figure were according to Vervoort et al. (2000) and Blichert-Toft & Albarède (1997) respectively. Magmatic age refers to the age of proposed age of granite crystallisation. TDM is referred to as the crustal residence age which estimates the time elapsed since the crustal domain hosting the zircon was extracted from the depleted mantle Scherer (2007). B) Magnified image to show spread of zircon population represented in box B on Fig.14A.

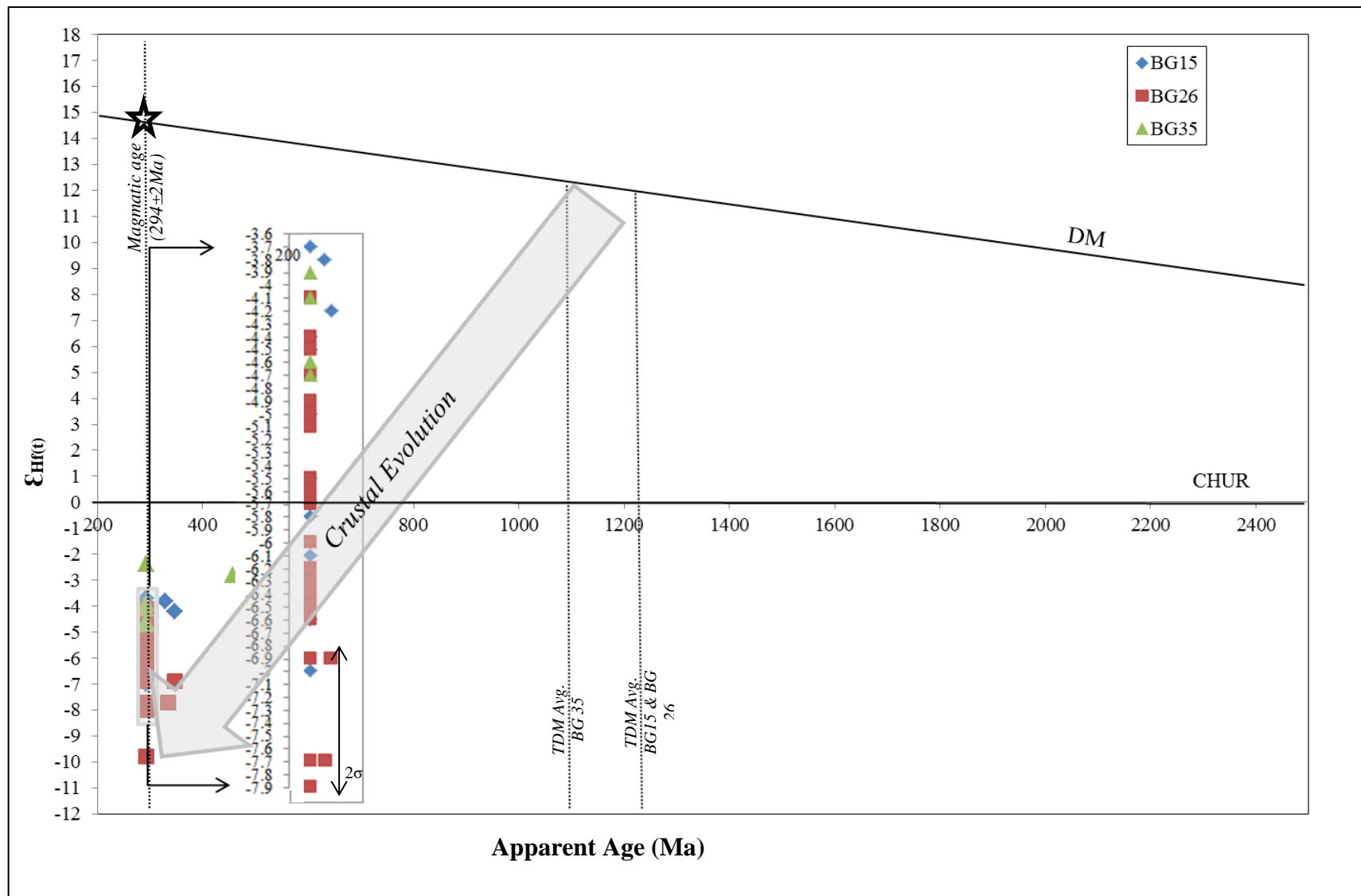


Figure 18: $\epsilon_{\text{Hf}(t)}$ vs. U-Pb zircon results for enclave sample BG15 from the middle unit and granite samples BG26 (middle unit) and BG35 (outer unit) from the Buddusò pluton. Values for Depleted Mantle (DM) and Chondritic Uniform Reservoir (CHUR) shown on figure were according to Vervoort et al. (2000) and Blichert-Toft & Albarède (1997) respectively. Inset shows the composition of the majority zircon population of magmatic zircons analysed. The 2σ error on Hf isotope estimated ca. 1 ϵ unit (refer to Appendix VI). Magmatic age refers to the age of proposed age of granite crystallisation. TDM is referred to as the crustal residence age which estimates the time elapsed since the crustal domain hosting the zircon was extracted from the depleted mantle (Scherer, 2001)

The deviation of the $^{176}\text{Hf}/^{177}\text{Hf}$ from the chondritic (CHUR) values for samples in Fig.18 (indicated by the Epsilon (ϵ) notation) is calculated (Matteini et al., 2010):

$$\epsilon_{\text{Hf}} = \left[\frac{\left(\frac{^{176}\text{Hf}}{^{177}\text{Hf}} \right)_{\text{sample}}}{\left(\frac{^{176}\text{Hf}}{^{177}\text{Hf}} \right)_{\text{CHUR}}} - 1 \right] \times 10^4$$

For $\epsilon_{\text{Hf}}(t)$: t is the crystallization age, so $\epsilon_{\text{Hf}}(t)$ represents the zircon's initial Hf isotope composition (the isotopic composition of the magma from which the zircon crystallized).

Model or crustal residence age (TDM) (Fig.17 &18) is calculated with respect to the DM using the following formula (Matteini et al., 2010):

$$\text{Hf } T_{\text{DM}} = \left(\frac{1}{\lambda} \right) \ln \left\{ \frac{\left(\frac{^{176}\text{Hf}}{^{177}\text{Hf}} \right)_{\text{sample}} - \left(\frac{^{176}\text{Hf}}{^{177}\text{Hf}} \right)_{\text{DM}}}{\left(\frac{^{176}\text{Lu}}{^{177}\text{Hf}} \right)_{\text{sample}} - \left(\frac{^{176}\text{Lu}}{^{177}\text{Hf}} \right)_{\text{DM}}} + 1 \right\}$$

Values of $^{176}\text{Lu}/^{177}\text{Hf} = 0.0381$; $^{176}\text{Hf}/^{177}\text{Hf} = 0.283224$ (Vervoort et al., 2000) for the DM and $^{176}\text{Lu}/^{177}\text{Hf} = 0.0336$; $^{176}\text{Hf}/^{177}\text{Hf} = 0.282785$ (Blichert-Toft & Albaréde 1997) for CHUR were used in the calculations.

The zircon population sampled display a wide array of $\epsilon_{\text{Hf}}(t)$ for magmatic zircons with values ranging between -2.4 (293 Ma, $^{176}\text{Hf}/^{177}\text{Hf} = 0.282489$) and -9.8 (293 Ma, $^{176}\text{Hf}/^{177}\text{Hf} = 0.282323$) (Fig.17&18).

Enclave sample BG15 from the middle unit shows a range of $\epsilon_{\text{Hf}}(t)$ values between -7 (293 Ma, $^{176}\text{Hf}/^{177}\text{Hf} = 0.282402$) and -3.6 (293 Ma, $^{176}\text{Hf}/^{177}\text{Hf} = 0.282496$). Granite sample BG26 from the middle unit displays the widest range of $\epsilon_{\text{Hf}}(t)$ values between -9.8 (293 Ma, $^{176}\text{Hf}/^{177}\text{Hf} = 0.282323$) and -4.1 (293 Ma, $^{176}\text{Hf}/^{177}\text{Hf} = 0.282485$). Granite sample BG35 from the outer unit exhibits the smallest array of $\epsilon_{\text{Hf}}(t)$ values from -4.7 (293 Ma, $^{176}\text{Hf}/^{177}\text{Hf} = 0.282467$) and -2.4 (293 Ma, $^{176}\text{Hf}/^{177}\text{Hf} = 0.282533$). It is important to note that the enclave has a large range in Hf isotopic compositions which almost completely overlaps with the granites.

T_{DM} values overlap and are fairly similar; T_{DM} of granite sample BG35 from the outer unit is between 1.07 - 1.25 Ga, the T_{DM} of granite sample BG26 from the middle unit is between 1.17 - 1.48 Ga and the T_{DM} of enclave sample BG15 is 1.14 - 1.33 Ga. The inherited crystals fall within these overlapping ranges. Most of the inherited zircons correlate on a crustal evolution

trend with the most crustal Hf isotopes in the magmatic zircons. BG 35 therefore is the closest resemblance of mantle-like composition and BG 26 represents the most crustal compositions; this corresponds with the trace element data portrayed in Fig.12A-D showing granites from the middle unit having lower Lu contents. Even though BG35 resembles the closest mantle-like composition, it still displays a very crustal signature; 1) $\epsilon_{\text{Hf}(t)}$ isotopic composition of a magma at 294 ± 2 Ma magmatic age (portrayed by the black star on Fig.18) is extremely more mantle-like in composition and 2) its composition overlaps with the most crustal Hf composition BG26. Although the sample population of zircon grains is small and representivity is limited, inferences can be made with respect to the data that does exist. The Hf composition seems to be fairly homogenous over the different granitic units and enclaves in the pluton. The magmatic age can be confidently interpreted to be 294 ± 2 Ma and the rock Hf compositions show overall crustal signatures.

Fig.19 shows $\epsilon_{\text{Hf}(t)}$ vs. apparent age for magmatic zircons from samples BG15, BG26 and BG15 as well samples BG2, BG3, BG13, BG19 and BG48. It is important to note that samples BG2, BG3, BG13, BG19 and BG48 (Fig.19) from this study have only been analysed for Lu-Hf isotopes and not U-Pb isotopes therefore making the Hf isotopic concentrations of those samples unconstrained by the quality of U-Pb data. However from the U-Pb constrained data that exists for BG15, BG26 and BG35, a magmatic age of 293 Ma was assumed to constrain the Lu-Hf data for samples BG2, BG3, BG13, BG19 and BG48. More magmatic grains from more samples increases the representivity of the dataset. Table 11 shows the Hf compositional ranges for the respective granitic units and the mafic enclaves. The magmatic data shows that the Hf isotopic compositions and TDM ranges overlap suggesting the Hf isotopic composition is the same throughout the Buddusò pluton. An interesting observation from the additional magmatic data is the $\epsilon_{\text{Hf}(t)}$ range gets larger from the inner unit through to the middle unit.

Table 11: $\epsilon_{\text{Hf}(t)}$ range, $^{176}\text{Hf}/^{177}\text{Hf}$ range and TDM range for magmatic enclave and granite samples. Magmatic age of 293 Ma was assumed for Lu-Hf isotopes that did not have U-Pb data.

Sample	Rock type/Unit	$\epsilon_{\text{Hf}(t)}$ range	$^{176}\text{Hf}/^{177}\text{Hf}$ range	TDM range (Ga)
BG19	Leucogranite (lu)	-6.2 to -4.3	0.282424 to 0.282478	1.28 to 1.18
BG3		-7.7 to -5.2	0.282348 to 0.282454	1.36 to 1.23
BG2	Granite (Mu)	-6.6 to -5.1	0.282418 to 0.282458	1.30 to 1.22
BG26		-9.8 to -4.1	0.282323 to 0.282485	1.50 to 1.20
BG13		-5.6 to -3.9	0.282441 to 0.282489	1.25 to 1.16
BG48	Granodiorite (Ou)	-11.2 to -4.7	0.282284 to 0.282469	1.55 to 1.20
BG35		-6.0 to -2.4	0.282431 to 0.282583	1.27 to 1.10
BG15	Enclave (Mu)	-7.0 to -3.7	0.282402 to 0.282496	1.33 to 1.10

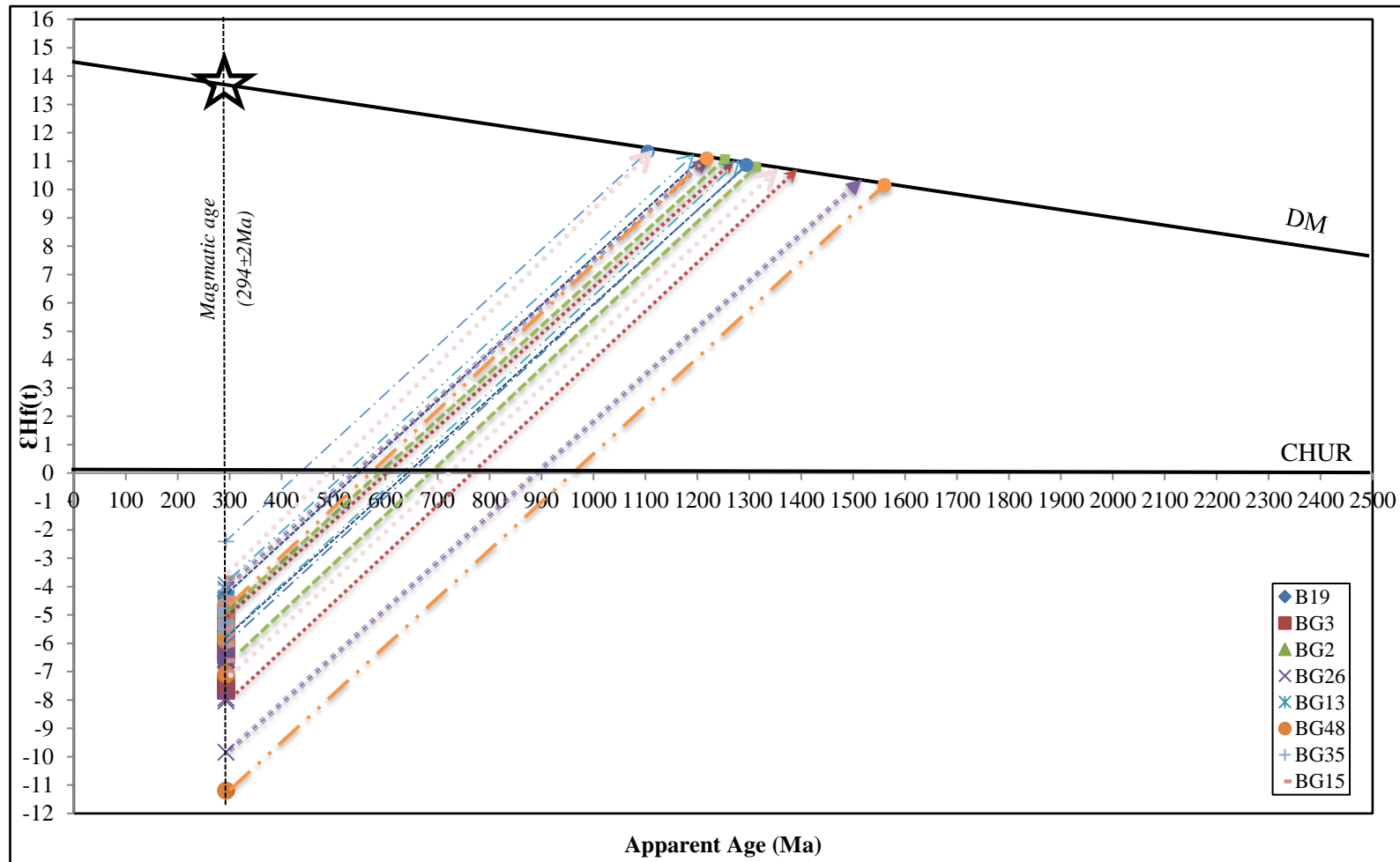


Figure 19: $\epsilon_{\text{Hf}(t)}$ vs. U-Pb zircon spot analyses results for enclave sample BG15 from the middle unit, leucogranite sample BG19 from inner unit, granite samples BG2, BG3 & BG26 (middle unit) and granodiorite samples BG13, BG35 & BG 48 (outer unit) from the Buddusò pluton. Values for Depleted Mantle (DM) and Chondritic Uniform Reservoir (CHUR) shown on figure were according to Vervoort et al. (2000) and Blichert-Toft & Albarède (1997) respectively. Extrapolated magmatic zircon grains to point of separation from the DM, TDM ages based on assumed magmatic age of 293 Ma for samples with no U-Pb data. Black star represents $\epsilon_{\text{Hf}(t)}$ composition of a mantle-like magma at age 294 ± 2 Ma.

Chapter 6: Discussion and Interpretations

6.1 Magma mixing as a mechanism for shaping the petrogenesis of the Buddusò Pluton

The idea that a felsic crustal magma mixed with a mafic mantle derived magma to produce the compositional variations seen in I-type granites and their mafic enclaves is dominant theory in the research world (as described in sections 2.2 & 2.3) as well as with respect to the petrogenesis of the Buddusò pluton (Zorpi et al., 1989 and Barbey et al., 2008). In the following section, the evidence for magma mixing and/or mingling will be considered to determine if the Buddusò Pluton was shaped by this petrogenetic process.

6.1.1 Evidence of mafic enclave magma and felsic granite magma interaction

6.1.1.1 Field Evidence

There is field evidence that is proposed to represent evidence of magma mixing in the granitic units. Magma interaction can be seen in Fig.3 Plate D & E by the presence of elongated and cusped margins which is suggestive of enclave magma quenching against cooler felsic granitic magma (Kumar et al., 2003). The margins seen between the granites shown in Fig.3 Plates A-C merge towards the contact and show no sharp intrusive line implying the contact is not intrusive but rather comagmatic. Similar mineral crystal sizes seen in both the mafic enclaves and the granites (Fig.3 Plate F&G) suggests either these crystals started to grow at the same time or there was crystal exchange between the two magmas.

6.1.1.2 Petrographic Evidence

There are enclaves that show a foliation which is absent in the granite series (Fig. 5A&B, Fig.6B); suggesting that the enclave foliation formed prior to intrusion. Little deformation is seen in the enclaves, no cataclasis and no evidence of grain size reduction which suggests that the foliation fabric was created by a magmatic process (magma flow). However, the deformation fabrics that do exist – the magmatic fabric wrapping around the crystals, suggest that it was not solid-state deformation. Foliations in the enclaves are seen bending around large plagioclase and K-feldspar phenocrysts (Fig.5 A&B) The textural similarity of these plagioclase and K-feldspar phenocrysts within the mafic enclaves in comparison to the plagioclase and K-feldspar phenocrysts in the granites; suggest the crystals could have been captured from the granitic magma. The existence of this fabric suggest that crystal capture could not have occurred at the level of the intrusion, it must have occurred before the enclave magma mingled with the granite

magma either upon ascent or near/at emplacement level because it would have otherwise disturbed the fabric. Pieces of granitic grain have also entered into the enclaves which lie across the undisturbed foliation (Fig.6B). This texture suggest that it is a growth of a crystal within the enclave due to diffusion of elements from the granite via a magma which was present on the crystal boundaries; displaying evidence of magma interaction. Samples which show the contact between granite and enclave display large amounts of amphibole at the contact with a lot of epidote inclusions (Fig.5A&B). This is also evidence of interaction between enclave and granitic magma; epidote being the reaction mineral that formed from the breakdown of the amphiboles as the granitic magma came into contact with the enclave magma (Johnston & Wyllie, 1988; Wiebe, 1994 & Kumar et al., 2003). It is important to note that careful consideration has to be taken when interpreting foliations as the orientation of how the samples were cut relative to the fabric is unknown.

Both the granites and mafic enclaves share the same mineral chemistry but differ in mineral mode. The mafic enclaves are divided petrographically into two groups; finer grained with less mafic minerals and coarser grained with more mafic minerals. In both groups but at varying amounts there is acicular apatite, bladed biotite and compositionally zoned atoll inclusion array plagioclase phenocrysts. These textures are proposed to be indicative of magma interaction (Vernon, 1990 & Hibbard, 1991). This could be interpreted as some mafic enclaves showing a higher degree of interaction with the felsic granite magma or equilibration between mafic enclave magma and host granite magma (Fourcade and Allegrè, 1981).

6.1.1.3 Whole Rock Geochemical Evidence

Granites show a tighter correlation with respect to major and trace elements than the mafic enclaves do (Fig.11-13), except with respect to Na₂O and K₂O elements. Granites show increasing maficity from the outer unit towards the inner unit which is characterised by a decrease in SiO₂, Al₂O₃, CaO, FeO, MgO, TiO₂ and P₂O₅ in the same direction. The enclaves follow the above major element chemistry however they show a larger variation in their composition. With respect to REE and multi-element patterns, the mafic enclaves show a generally similar pattern to the granites; this could be due to re-equilibration of REE, LILE and HFSE between enclaves and granites (Ibyeli & Pearce, 2005). Enrichment in HREE and Zr in the enclaves over the granites argues volatile migration between the magmas from the felsic magma into the mafic magma (Fig.11-13) (Zorpi et al., 1989). However Rb and Ba show depletion in the enclaves with respect to the granites this does not coincide with volatile migration between magmas (Fig. 11-13).

The enclaves' wider compositional scatter with respect to major and trace elements is not evidence suggestive of a linear magma mixing array between enclave magma and granite magma. This opposes the theory that the enclaves could be potential mixing candidates for the granite series. A model was set up to investigate this (Fig.20), which mixed each of the enclave compositions with the most leucocratic granite (sample BG32) in 5wt. % increments.

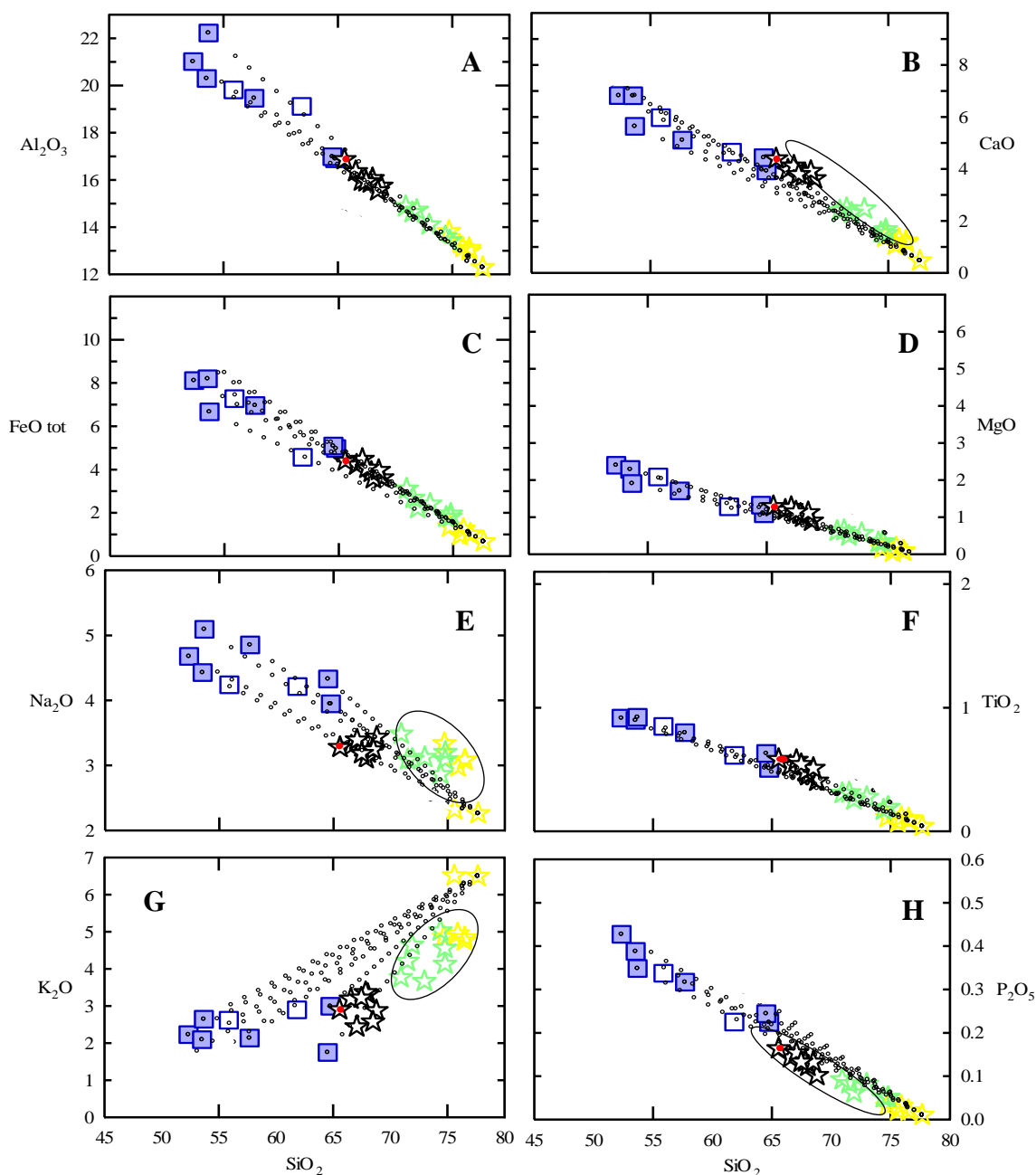


Figure 20: Mixing model; a test to investigate if the compositions of the more mafic granites (granodiorites from the outer unit and intermediate granites from the middle units) can be shaped by mixing the most leucocratic granite and mafic magma(s) represented by the enclaves composition. The most leucocratic granite BG 32 is mixed with each enclave in 5 wt. % increments (refer to Appendix V for mixing calculations).

It is clear that in some of the plots, Al_2O_3 , FeO, MgO, TiO_2 , (Fig.20A, C, D & F) some enclaves are possible mixing candidates, however as illustrated by the red dot on sample BG48, the

mixing arrays does not fit throughout the samples' entire chemical composition. CaO and P₂O₅ (Fig.20B&H) show linear array patterns that are slightly off but could still fit for some enclaves and there is a poor linear fit with respect to Na₂O and K₂O and (Fig.20E&G). Na₂O and K₂O are mobile elements and could have changed concentrations post-crystallisation. The abundance of K₂O and Na₂O seen in the granites, especially in the granites from the middle unit argues against element mobility being a reasonable justification for magma mixing. With the spread in composition shown, the granodiorites would need to be made up of between 50% (for the higher silica enclaves) and 80% (for the lower silica enclave) enclave magma. It is important to note that the quantity ratios of mafic magma: granite magma cannot be constrained and is assumed based on the larger physical volume of granites to mafic enclaves seen in outcrops as well as the difference in the major element compositions between the two. Proportions of 50 to 80% enclave magma are not feasible considering that there is a higher volume of granitic magma interacting with a smaller volume of enclave magma at any given time. However, if there was more of the mafic enclave magma (more than that which is recorded by the volume of the enclaves in the outcrops) that was available to mix, the compositions of the granites and the enclaves would share a tighter correlation. This is also based on the assumption that the enclave magma was a single composition.

6.1.1.4 Mineral Chemical Evidence

The complexly zoned atoll inclusion arrays in plagioclase phenocrysts observed in some enclave samples (Fig.6,8&9) show complexly zoned plagioclase with spikes in their An content and reaction texture between crystals which are not in equilibrium with the magma around it. Resorption and subsequent crystallisation of An zones with differing compositions of plagioclase can be caused by multiple processes; 1) recharge of more mafic magma thus altering the magma composition and allowing new rims of a different An concentration to grow. 2) Transfer of crystals between different magmas – if the plagioclase crystal is put into a magma it is not in equilibrium with, its cores will become corroded, allowing the new magma to move into the crystal structure, plagioclase of a new composition will form with rims possibly forming around the corroded core (Kocak et al., 2011). 3) Plagioclase originating from the mafic magma comes into contact with the felsic magma, changes towards a sodic composition as equilibration takes place (Hibbard, 1995). 4) Increases in temperature and changes in water fugacity (Pietranik, A & Koepcke, J. 2014.) or 5) by decompression upon magma ascent (Stormer, 1972).

Plagioclase (not the complexly zoned phenocrysts discussed above), K-feldspar and biotite all share similar mineral compositions in the mafic enclaves and host granites and are interpreted to reflect mineral equilibration during magma mixing (Ghaffari & Omran, 2015) However with respect to hornblende; host granites show higher Al, Ti, Mg and Na contents with respect to their mafic enclaves and appear to be equilibrated. This could be explained as the mafic enclaves' hornblende being xenocrysts and it was transferred from the mafic enclaves to host granites during magma mixing (Kocak et al., 2011).

6.1.1.5 Isotopic Evidence

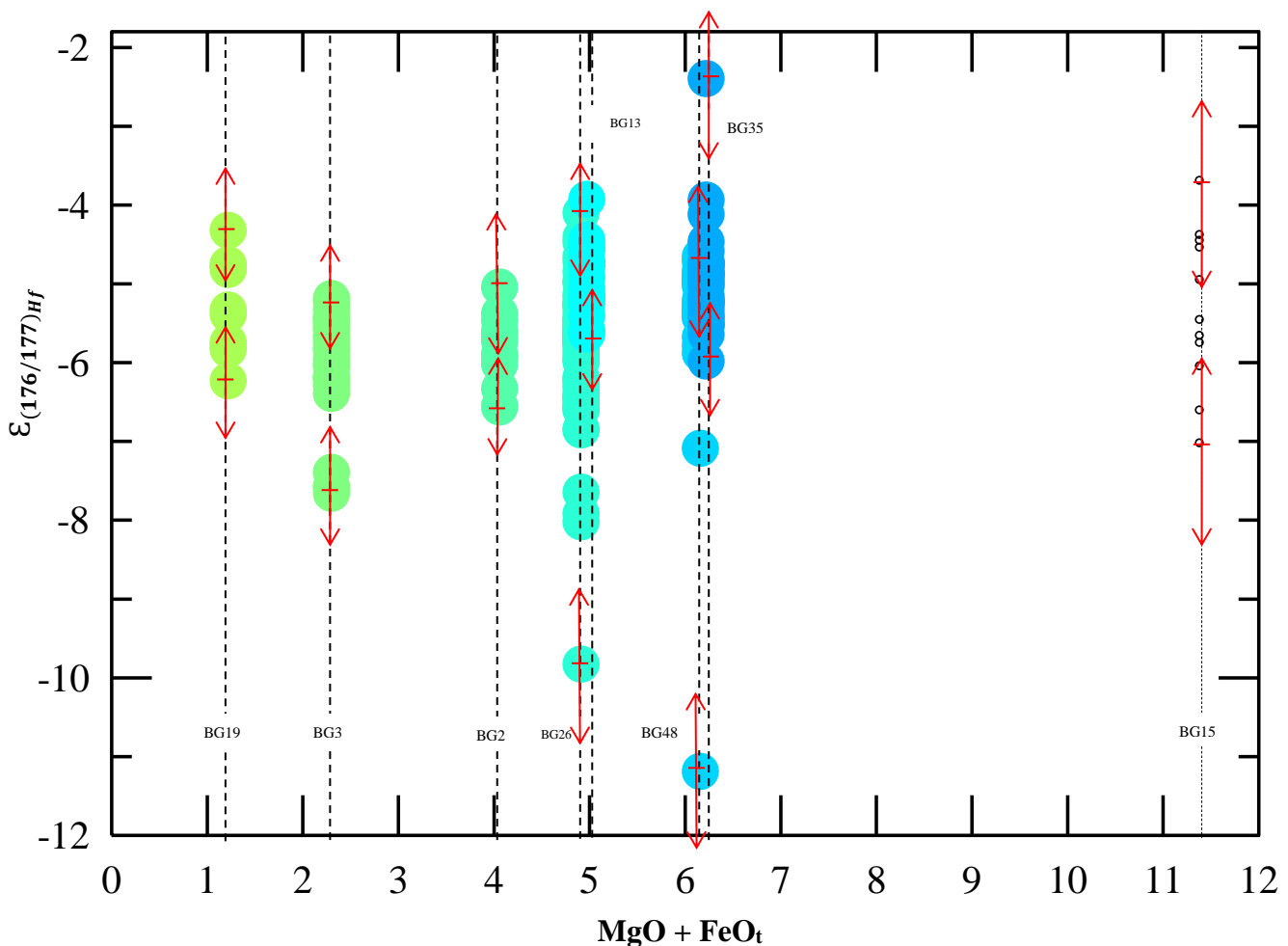


Figure 21: $\epsilon_{(176/177)Hf}$ of magmatic zircon plotted over whole rock $MgO + FeO_t$. Large solid circles represent granitic samples, increasing in maficity from green to blue and the small black open circles displays an enclave sample. Magmatic age of 293 Ma has been assumed for samples with Lu-Hf data without corresponding U-Pb data. Red arrows represent 2σ error values on maximum and minimum $\epsilon_{(176/177)Hf}$ compositions for each sample. Refer to Appendix IV for all 2σ error values.

Fig.21 explores $\epsilon_{(176/177)Hf}$ against increasing mafic content; the graph shows that the Hf isotopic composition of the granites are not influenced by how mafic the granites become. The

isotopic signature becomes more variable with increasing maficity. The question arises; could the array of Hf isotopic compositions seen in Fig.19&21 be produced by mixing a crustally derived magma with a mantle derived magma? The Hf isotopic compositions exhibited by the granite samples and enclave sample are very crustal, the closest composition to a mantle-like magma is sample BG35 which is not close to the extrapolated composition of a mantle derived magma at magmatic age 293Ma (showed by a black star on Fig.19). The enclave BG15 shows a very crustal $\epsilon_{(176/177)Hf}$ range and with respect to the mixing model in Fig.20 does not adequately represent a mantle-like derived magma, unless the mantle has been heavily hybridised.

Crustal contamination at subduction zones can cause uncertainty in the Hf isotopic composition of mantle derived magmas. Hf isotopic concentrations in uncontaminated mantle magmas are lower than in felsic magmas. A simple mixing ratio where the more mafic component would have a more mantle like $\epsilon_{(176/177)Hf}$ value and the more felsic components would have a crustal like $\epsilon_{(176/177)Hf}$ value does not scale into the isotopic composition in a linear way. This makes interpreting this isotopic data with respect to mixing complicated.

As the maficity of the samples increase; the $\epsilon_{(176/177)Hf}$ range also increases. This opposes a mixing theory, as most Hf diversity comes from crustally derived magmas therefore the leucogranites (least mafic) should show the widest range in $\epsilon_{(176/177)Hf}$. Again, the degree of crustal contamination and Hf isotopic concentration in the mantle magma could provide homogenous Hf isotopic concentrations. However, to achieve this homogenous overall $\epsilon_{(176/177)Hf}$ array, a mantle magma with essentially no Hf in it would have to be mixed in because if there is no Hf in the mantle derived magma, the Hf isotopic composition remains unaffected, this however seems fairly improbable.

If a simple mixing scenario is considered, one would expect there would be a good correlation of $\epsilon_{(176/177)Hf}$ with maficity because the more mafic magma that is added into the mixing system, the more mafic the bulk rock system becomes and the more mantle-like the Hf isotopic signature should also become, in theory. However Fig.21 shows the most mafic granite with a value of MgO + FeO tot. = 6.25 wt. % is just as crustal as the most felsic granite with MgO + FeO tot. = 1.2wt%. The amount of mafic magma that would need to be mixed in to achieve that kind of variation would be a large amount; even at MgO +FeO tot. contents (as high as 20%), a third of the magma would need to be mixed in.

Small scale variations in $\epsilon_{(176/177)Hf}$ exist within each sample, these variations although increasing towards the more mafic samples generally display overlapping $\epsilon_{(176/177)Hf}$ ranges and TDM ranges (Table 11). 2σ error values on maximum and minimum $\epsilon_{(176/177)Hf}$ compositions show that most samples display small scale isotopic variation irrespective of errors. Sample BG2 is an exception where the 2σ error values on maximum and minimum $\epsilon_{(176/177)Hf}$ compositions overlap. In a complete mixing scenario – the magmatic zircon Hf isotopic compositions and whole rock chemistry would be correlated. Small scale Hf isotopic variations would not exist in any samples as magma mixing would homogenise the composition of the magma (Farina et al., 2014). Zircon populations could represent crystals assembled from a range of different magma batches, however the study rules this possibility out due to;

- 1) Zircons within individual hand specimens contained this isotopic variation
- 2) The small size of zircon crystals as well as the high viscosity of the felsic magma at the temperature of zircon crystallisation would make independent movement of zircon crystals through felsic magmas highly improbable. (The reader is referred to Farina et al., 2014 for calculations).

Fig.18, 19&21 suggests that the small scale heterogeneity seen in $\epsilon_{(176/177)Hf}$ is produced by mixing of components with fundamentally different Hf isotopic ratios, possibly the source.

6.1.2 Hybridisation

The evidence provided in the above sections imply that magma mixing between mafic enclave magma and felsic granitic magma was not the mechanism responsible for the compositional variation seen in the granitic units. However field and petrographical evidence; contact morphologies, presence of reaction minerals, crystal exchange, presence of acicular apatite, bladed biotite, and compositionally zoned plagioclase all suggest that the mafic enclave magma did see interaction with the granitic magma most probably prior to emplacement.

However the geochemical and mineral data suggest that this interaction was limited. Some mafic enclaves show a closer chemical composition to the granodiorites as portrayed in Fig.22. Fig.22 is based on a study undertaken by Zorpi et al. (1987) in which the authors made use of FeO_t/MgO ratio as a discriminator to link mafic enclaves to their respective plutons in the Sardinia-Corsica Batholith. The figure shows a gap in the enclaves, with some enclaves having a closer composition to the granodiorites and this is true for all other major and trace elements

(Fig.11&12). The equilibration of plagioclase, biotite and K-feldspar and the incomplete chemical re-equilibration of hornblende in both host granites and mafic enclaves suggest that hybridisation was limited.

The enclave samples (BG21 and BG22) which do share very similar chemistries are texturally different possessing finer grained textures (Fig.5C&D, Fig.3 Plate F&H), no foliation, contain the least mafic minerals out of the enclave population and contain the complexly zoned plagioclase phenocrysts discussed earlier, which reiterates that hybridisation of the enclave magma by interaction with the granitic magma has brought some of the enclave compositions closer to that of the granite. It is important to note that these complexly zoned plagioclase phenocrysts only exist in some of the enclave population. If these zoned plagioclase phenocrysts are evidence of granitic and enclave magma interaction then this interaction was limited. The enclaves consisting of these plagioclase structures would show a higher degree of hybridisation leaving the other enclaves less hybridised with compositions closer to that of the original mafic enclave magma.

Hybridisation of the mafic enclaves could also cause the granite compositions to plot off the mixing line trends in the mixing model in Fig.20. The enclave compositions used were not complete representatives of the enclave magma, rather an already mixed composition of enclave and granitic magma. However looking at the scatter of the data, this does not become a feasible argument for magma mixing. If the enclave compositions presented represented an already hybridised enclave magma, then then composition of the original mafic enclave magma would move even further away from the granite series and would therefore still contribute higher proportions in the mixing scenario.

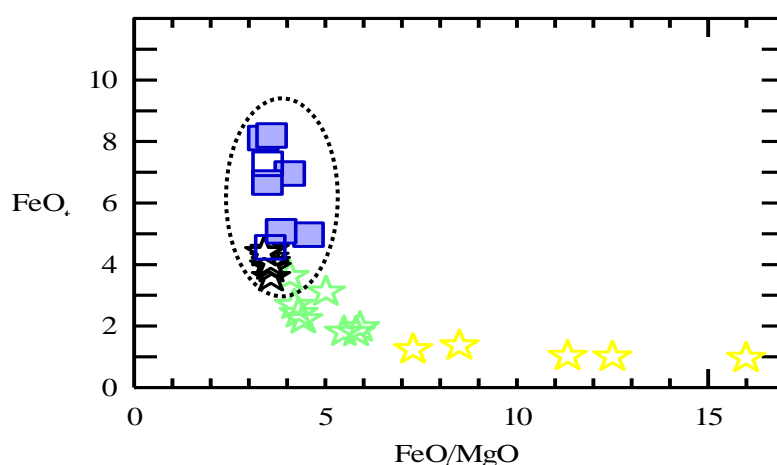


Figure 22: FeO_t vs FeO_t/MgO , for all samples from the Buddusò Pluton, using FeO_t content as a discriminator for hybridisation (Zorpi et al., 1989).

6.2 Phase Equilibrium modelling: Evaluating the role of Crystal Fractionation

6.2.1 Fractional crystallization vs. Crystal fractionation

Fractional crystallisation involves a process whereby crystals are removed from the magma as it crystallises. These early formed crystals are not equilibrated with the magma from which they grew from and result in a succession of residual liquids of different compositions with the magma composition continuously becoming the new bulk composition as crystals crystallise (Chappell & Wyborn, 2004). Crystal Fractionation is a mechanism involving the movement of crystals within a liquid resulting in one fraction containing little to no crystals and one fraction containing more crystals. Both mechanisms are common hypotheses used to explain compositional variation seen in granites (Becker, 1897, Bowen, 1949, Chappell, 1999, Chappell & Wyborn, 2004) but very few studies make an attempt to constrain thermodynamically whether the mineral assemblages that are proposed to be fractionated out of the magma are viable and whether the mineral proportions are realistic. This study attempts to do that by using phase equilibrium modelling software, Rcrust (Mayne et al., 2016) that has recently been developed at Stellenbosch University.

6.2.2 Fractionation model set up

6.2.2.1 Fractionation model design

The fractionation model was run at 3Kbars using 3.4wt. % H₂O for three heating paths at 700, 800 and 900°C (reasons for these P-T conditions and water content values are outlined in section 6.2.2.3). The model was designed to include a reactive subsystem, Bulk_Rs, (from here forth referred to as the reactive system) which consisted of crystals and melt which were both in thermodynamic equilibrium. Melt (Melt_Es) was then extracted from the Bulk_Rs in increments of 5wt. % to form the extract subsystem, Bulk_Es, (here forth referred to as the extract system) making this Bulk_Es no longer exist in thermodynamic equilibrium. The fractionation model was run using two different starting compositions; sample BG27, a granite from the middle unit and sample BG34, a granodiorite from the outer unit; described below in section 6.2.2.2. Fig.23 is an animation depicting the fractionation modelling. The reactive system undergoes sequential melt extraction events, the reactive system subsequently shrinks after each melt extraction event and this continues until there is no more melt left to extract. It is important to note that the crystal composition and proportions of minerals relative to one another remains the same with only melt leaving the system, however crystal proportions will increase relative to the shrinking

reactive system. Thermodynamic calculations were performed using Rcrust (Mayne et al., 2016): a P-T-X modelling tool that allows path dependence for phase stability calculations from a compiled form of Perple_X (Connolly, 2009). Calculations were based on the 2004 revised hp04ver.dat thermodynamic file and the internally consistent dataset of Holland & Powell (1998). Solution models were used as follows: Bio(TCC) for biotite (Tajcmanová et al., 2009), Cpx(HP) for clinopyroxene (Holland & Powell, 1996), feldspar for plagioclase and alkali-feldspars (Fuhrman & Lindsley, 1988; Holland & Powell, 2003), Gt(WPH) for garnet (White et al., 2007), Ilm(WPH) for ilmenite (White et al., 2000), magma(HP) for magma (Holland & Powell, 2001; White et al., 2001), Mt(W) for magnetite (Wood et al., 1991), Opx(HP) for orthopyroxene (Powell & Holland, 1999), Sp(HP) for spinel (Holland & Powell, 1998).

6.2.2.2 Starting compositions

Two compositions were investigated (BG27 and BG34) in the NCKFMASHT (Na₂O-CaO-K₂O-FeO-MgO-Al₂O₃-SiO₂-H₂O-TiO₂) chemical system. All iron was assumed to be FeO as all Fe was analysed as Fe₂O₃ in XRF analyses and was adjusted using a conversion factor of $FeO_t = FeO + 0.8998 * Fe_2O_3$. Calcium in apatite was corrected for by assuming all P₂O₅ occurs in the ideal apatite Ca₅(PO₄,CO₃)₃(F,O) thus $CaO_t = CaO - 1.316886 * P_2O_5$. This was corrected as the solution models used do not model P₂O₅, with all P₂O₅ occurring in apatite, Ca values had to subsequently be altered accordingly. Water was added to the normalised FeO and CaO corrected bulk compositions as 3.4 wt. % H₂O (Clemens & Watkins, 2001) then renormalized resulting in the starting compositions below (Refer to Appendix VI for complete calculations).

Table 12: Starting compositions used in fractionation modelling, BG27 and BG34 (all calculations can be found in Appendix VI).

Sample	SiO ₂	TiO ₂	Al ₂ O ₃	FeO	MnO	MgO	CaO	Na ₂ O	K ₂ O	H ₂ O
BG27	71	0.27	13.7	2.3	0.08	0.54	2.29	3.03	3.56	3.29
BG34	65	0.52	15.97	3.9	0.09	1.16	3.69	3.22	3.12	3.29

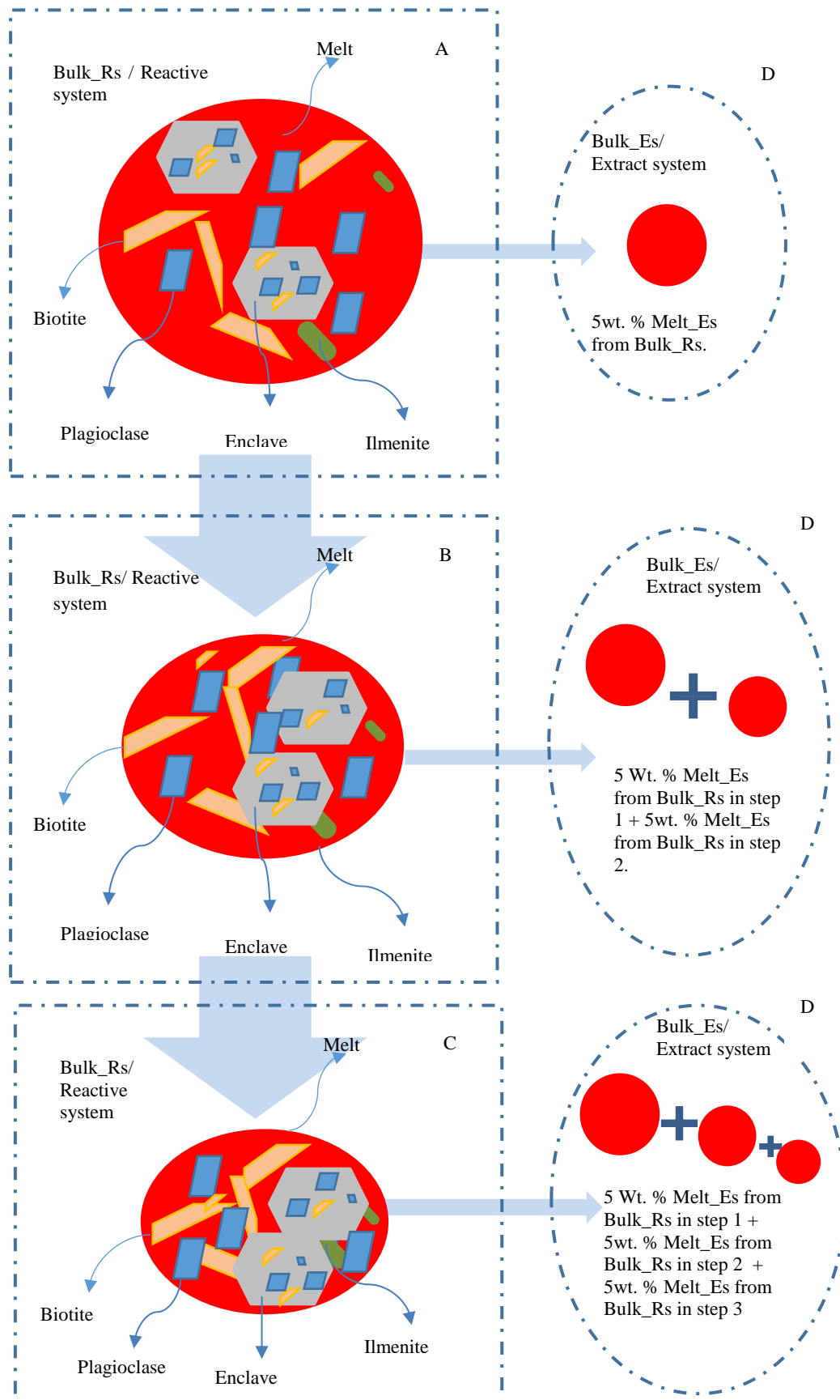


Figure 23: Animation representing fractionation model process, with A) as the starting bulk compositions of the reactive system, D) the melt extracted from the reactive system to form the extract system and B-C) representing the evolving compositions of the shrinking reactive system. Modelling was done at same pressure of 3kbar at various temperatures; 700°C, 800°C and 900°C run for two different starting compositions; BG27 (granite from the middle unit) and BG34 (granodiorite from the outer unit).

6.2.2.3 Parameters and Constrains of Fractionation modelling

The modelling was constrained at a pressure of 3kbs, although this pressure is poorly constrained, it was chosen because it represents a middle to upper crustal pressure. The assumption was made on the evidence of low metamorphic grades seen in the country rocks that the Buddusò pluton intruded. It is noteworthy to mention that adjusting the pressure by 1kb would not make a significant impact on the modelling.

A value of 3.4 wt. % H₂O content was used in the modelling this was based on the idea that granites that intrude the upper crust and achieve crustal differentiation do so by fluid absent partial melting. If a higher H₂O content was used, there would be free fluid present in the system and granites would intersect the solidus on ascent. If there was less than 3 wt. % H₂O in the system, it would be below the solidus (Clemens & Watkins, 2001).

Fig.27 shows the phase proportions for both models run at different temperatures; at higher temperatures, there is a higher proportion of melt to crystals. As mentioned before the composition and proportion of minerals do not change and if it does, it does so by a negligible amount, this is because it is being continuously buffered by the melt that is left in the system. The fractionation model does not work for higher temperatures as the melt to crystal fraction is considerably high. Vigneresse et al. (1996) refers to the Rigid Percolation Threshold (RPT) of a crystallising melt, this value is the minimum fraction of solids needed to form a three-dimensional framework, the RPT for most granite melts is 0.55/ 55% crystal proportion. Above this value, melt can be effectively squeezed from the system. At higher temperatures where melt viscosity is lowest, crystals would move as a function of buoyancy and either sink to the bottom or float to the top of the chamber. With the higher temperature modelling, dense crystals occur such as calcic plagioclase. Cox et al. (1979) estimated that a plagioclase with crystal radius 1mm would settle at a rate of approximately 20 meters per a year. This settling rate is drastically decreased or sometimes inhibited in melts with higher SiO₂ compositions because of their significantly higher field strengths (McBirney and Noyes, 1979). There were also no obvious cumulate structures noticeable in the Buddusò Pluton making the theory of crystal settling improbable.

6.2.3 Fractionation modelling results and interpretation

The modelling is done at various temperatures and the changing composition of the reactive system is plotted for the various heating paths (700, 800 and 900°C). The composition of the melt extracted (extract system) is also plotted on Fig.24&25, along with the corrected natural granite and enclave sample compositions. The blue dotted line on Fig.24&25 represent the reactive system's evolution at temperature 700°C which seems to fit the best, linearly, with respect to the natural samples major element chemistry. The model produces a mineral assemblage that closely resembles the natural samples: Quartz + Plagioclase + Biotite + Melt (Fig.27A&B).

6.2.3.1 Evaluating the enclaves

In Fig.24, the first model set up used BG34 (a granodiorite from the outer unit) as the starting composition. Melt was then extracted sequentially as explained in the model design, until no melt existed. This modelling was undertaken to investigate if the compositions of the crystal accumulation would approximately match that of the enclave compositions and to assess if the melt extracted would fit the granite and leucogranite compositions.

Fig.24 displays that high degrees of melt loss, produce crystal accumulations that approximately match with the high MgO, Al₂O₃, TiO₂ and low SiO₂ values of the enclaves (Fig.24 E, G&H). However with respect to other major elements, particularly the incompatible elements – the fit is poor and enclaves show a wider array of compositions (Fig.24A-D, F). This scatter is wider with respect to certain elements such as Na₂O and CaO (Fig.24A&F). This wide range in composition could reflect the enclaves that are produced by this fractionation process but then hybridised by addition of incompatible elements from the granite at lower temperatures. The wider composition space taken up by enclaves with respect to other elements (Fig.24B-D) can only be explained by compositional variation between the enclaves and the evolving reactive system. The granites also don't fit the melt extract system convincingly with granites and leucogranites showing a wide scatter in compositions relative to the trend at low temperature (700°C) in Fig.24A-C. Filter pressing at any of the three temperatures do not produce mafic enclaves which represent crystal accumulations from the granodioritic source or granites and leucogranites with compositions similar to melt extracted.

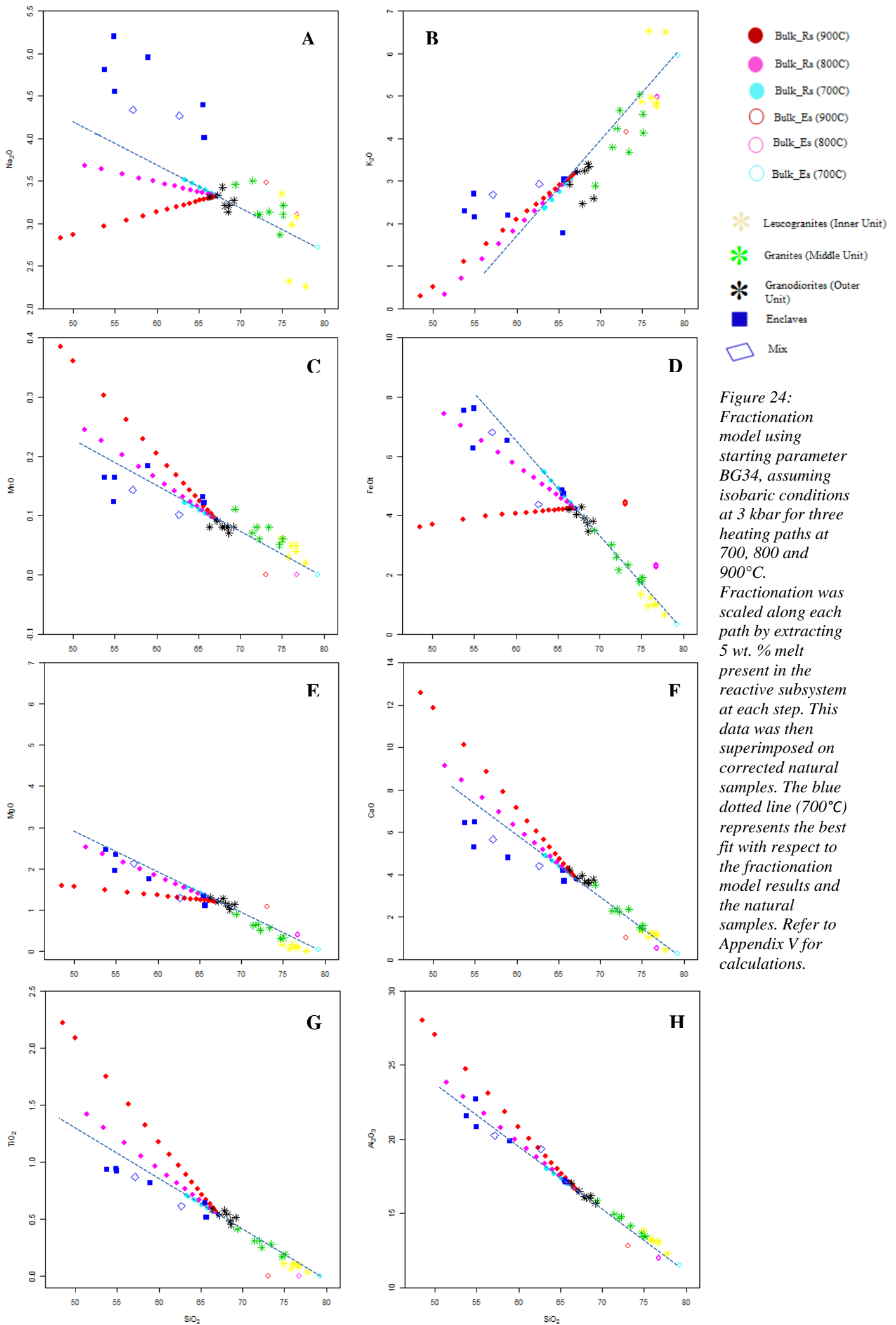


Figure 24: Fractionation model using starting parameter BG34, assuming isobaric conditions at 3 kbar for three heating paths at 700, 800 and 900°C. Fractionation was scaled along each path by extracting 5 wt. % melt present in the reactive subsystem at each step. This data was then superimposed on corrected natural samples. The blue dotted line (700°C) represents the best fit with respect to the fractionation model results and the natural samples. Refer to Appendix V for calculations.

6.2.3.2 Evaluating the granites

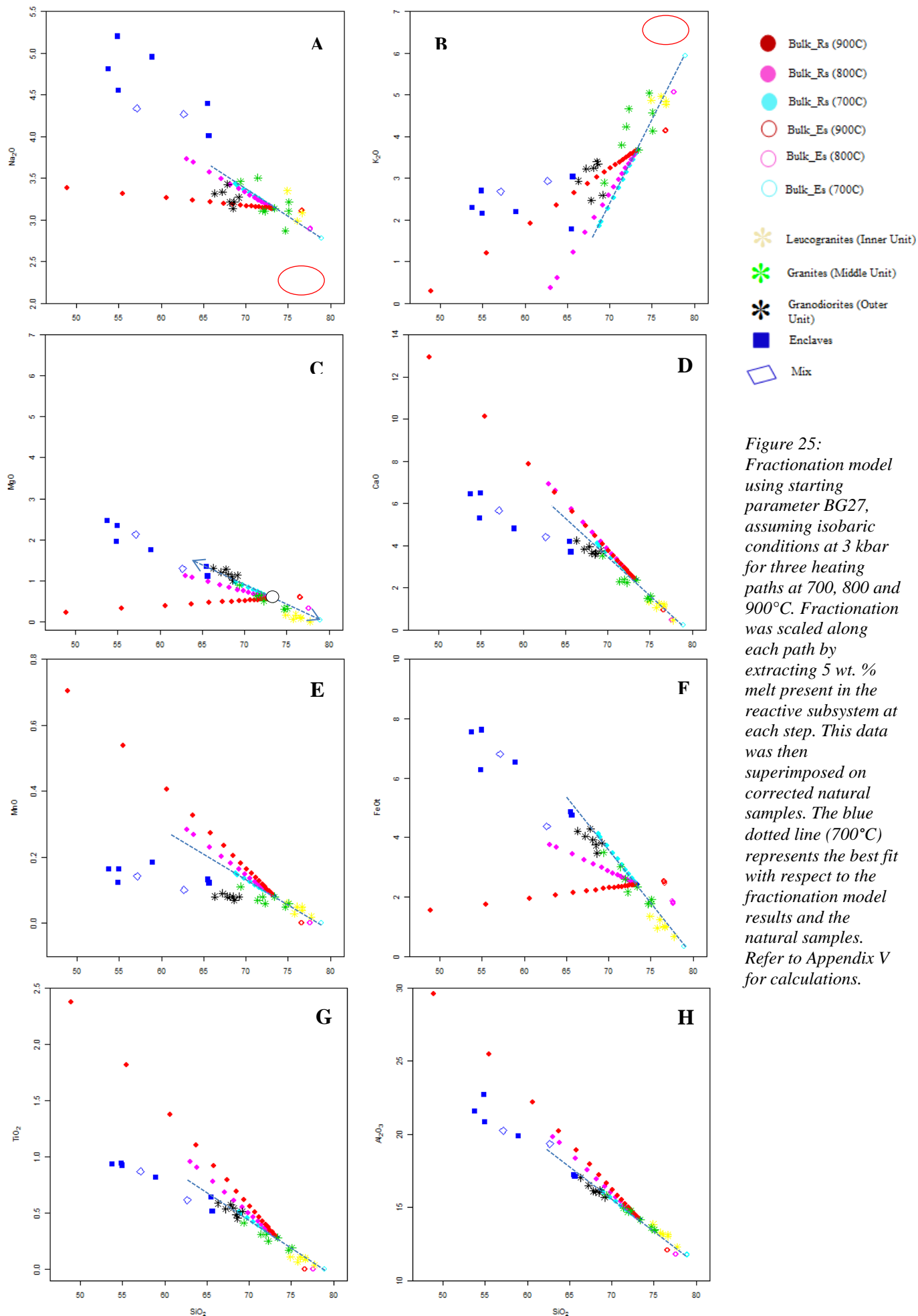
In Fig.25, the second model set up used BG27 (a granite from the middle unit) as the starting composition for the reactive system (Fig.23A). Melt was then extracted sequentially as explained in the model design, until no melt existed. This modelling was undertaken to investigate if the compositions of the crystal accumulation would approximately match that of the granodiorites' compositions and to assess if the magma extracted would fit the leucogranites' compositions.

With respect to Fig.25C-H, the granite suite fits the evolutionary reactive system and extract system trend portrayed by the blue dotted line on heating path 700°C. The granite suite fits linearly with respect to major element compositions; MgO, CaO, Na₂O, FeO, Al₂O₃ and TiO₂, on the fractionation model for low temperature 700°C (Fig.25C-H). The granite suite shows a wider scatter with respect to elements Na₂O and K₂O (Fig.25A&B). This could be because of the varying proportions of anorthite and K-feldspar in the granites; the two leucogranites circled in red on Fig.25 A&B show texturally larger amounts of interstitial microcline (Fig.4C). The enclaves show wide variety in composition and do not plot on the trend. The granodiorites follow the evolutionary compositional trend of the reactive system and the leucogranites follow the evolutionary compositional trend of the extract system, portrayed graphically by the arrows in Fig.25C. This modelling suggests in a thermodynamically constrained way, that the granodiorites are the consequence of low temperature (700°C to 750°C) filter pressing of a melt with compositions similar to that of the intermediate granites from the middle unit. The granodiorites represent the crystal accumulations and the leucogranites represent compositions similar to the melt being extracted.

Evidence that the $\mathcal{E}_{(176/177)\text{Hf}}$ range increases with increasing maficity in the granitic units provide further evidence for this filter processing process (Fig.21). Farina et al. (2014) suggests that transfer of Hf isotopic variation from detrital zircon crystals to magmatic zircon crystal is unavoidable in a felsic magma chamber. With the filter pressing process; when the melt is squeezed off the crystals to form the leucogranites, that melt flows, mixes and homogenizes consequently resulting in a smaller Hf isotopic compositional range.

The most major element and trace element chemistry fit for fractionating different minerals (as described in 4.4.1 &4.4.2) however an issue arises with respect to K₂O and TiO₂ (Fig.26). The strong TiO₂ vs. FeO+ MgO correlation suggests biotite accumulation. However biotite accumulation would show a positive trend for K₂O vs. FeO+ MgO. This could be explained be

explained by the large K-feldspar phenocrysts seen in some granodiorites with K-feldspar fractionation prompting K₂O depletion which would compensate for the offset caused by biotite



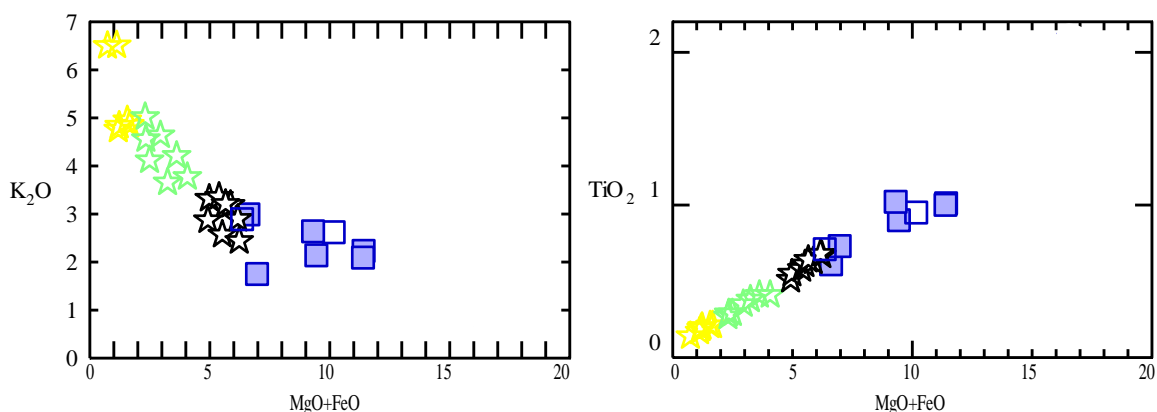


Figure 26: Major elements A) K_2O and B) TiO_2 plotted against $FeO + MgO$ for all granite and mafic enclave samples from the Buddusò Pluton.

accumulation. All the geochemical trends could be possible for a fractionating model based on the assumption that the magma is sufficiently crystallised and all the solid fraction is retained once the liquid fraction is squeezed off (refer to parameters section 6.2.2.3). Low temperature filter pressing explains the abundance of mafic enclaves in the outer unit as well as the different degrees of hybridisation portrayed by the enclaves.

6.2.4 Petrogenetic Model

The proposed model is presented in Fig.23 with the starting composition of the bulk reactive system similar to the composition of the intermediate granites from the middle unit (Fig.23A). This melt and crystal assemblage already contained some blobs of mafic enclave mush with melt and crystals. These blobs of mafic enclave magma and crystals interacted with the felsic granitic magma, on ascent, via dissolution and crystal capture consequently hybridising them. A deformation event took place most probably during the several magmatic events spanning between 340-280 Ma that resulted in the formation of the Corsica-Sardinia Batholith (Orsini, 1980; Beccaluva *et al.*, 1985; Paquette *et al.*, 2003) which disturbed the magma chamber. At this point the magma was mobilized into the lower pressure zones created by differential stress, thus forming the leucogranites (Fig.23D) without enclaves. The remaining magma consisted of a larger proportion of crystals and higher proportion of mafic enclaves in comparison to the lower magma fraction, namely the granodiorites (Fig.23C). With exploring this method as a process for the petrogenesis, the deformation had to have been localised and not seen throughout the chamber as some parts of the granitic body had to have been unaffected by filter pressing to maintain the intermediate composition with a lower proportion of enclaves (Fig.23A)

The fractionation model is built on the presence of the mafic enclave mush existing with the felsic granite magma. The model explains the distribution and chemical composition of the mafic enclaves however the question still exists; where does the mafic enclave magma come from and when was it introduced into the system to allow this model to be a viable process for the petrogenesis of the Buddusò Pluton?

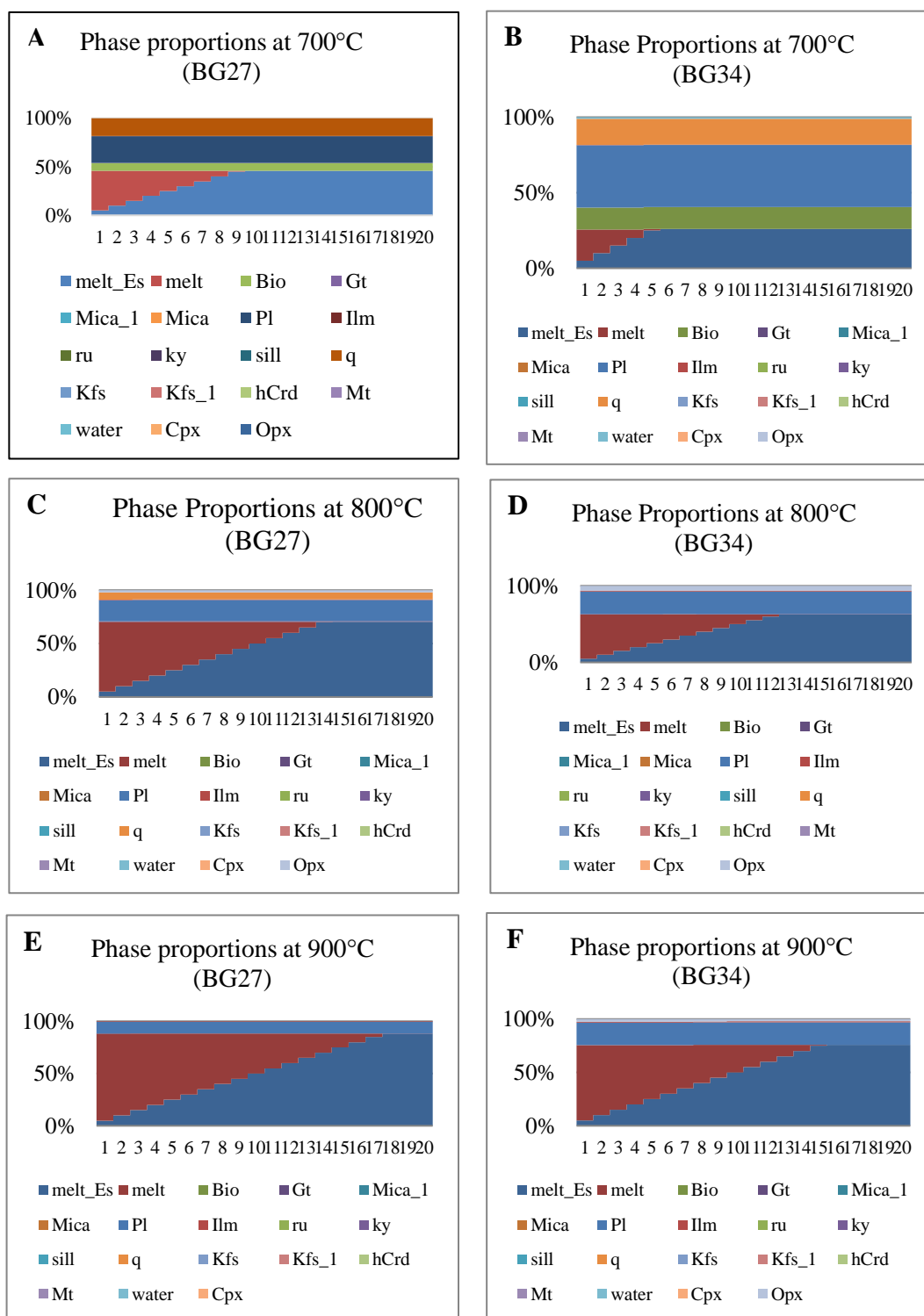


Figure 27: Graphs A-F showing the phase proportions and mineral assemblages of the two different fractionation models using starting parameters BG27 and BG34 at different temperatures. The proportion of each mineral phase and melt is plotted as a percentage against the steps of incremental melt loss. Each step indicates 5wt. % melt extraction. For full values and calculations refer to Appendix V.

Conclusions and Summaries

The mafic enclave magma and granite magma are crustally derived and comagmatic based on their similar range in compositions, similar magmatic age and Hf isotope signature. The magmas are proposed to be produced via partial melting of an andesitic source. The primary mechanism shaping the magmas is peritectic mineral entrainment and co-entrainment of accessory suite minerals when melting occurs. The magma is injected into the magma chamber in two pulses closely separated in time. The mafic enclave magma was injected first with a higher fraction of entrained ferromagnesian minerals and began to crystallise. The granitic magma was then injected with a lower fraction of entrained ferromagnesian minerals resulting in a composition close to that of the intermediate granites. The mafic enclave magma mush (crystals + magma) interacted with the granite magma via chemical exchange, diffusion and mechanical transfer during ascent prior to emplacement. The mafic enclave magma was consequently hybridised and the more viscous granite magma flowed over crystallised sheets of enclave magma consequently breaking it up into smaller pieces. The more mafic enclave magma and less mafic granite magma could have been injected at the same time, blobs of the mafic magma would begin to quench against the cooler less mafic granite magma and begin to crystallise. The enclaves are not considered as autoliths irrespective of their tight Ti:Fe+Mg correlation as no cumulate textures were identified in the enclave samples. Upon emplacement, the Buddusò Pluton saw a deformation event which took place most probably during the several magmatic events spanning between 340-280 Ma that resulted in the formation of the Corsica-Sardinia Batholith (Orsini, 1980; Beccaluva *et al.*, 1985; Paquette *et al.*, 2003), consequently disturbing the magma chamber. This deformation allowed for a low temperature filter pressing process to squeeze melt of the granite mush (enclave hybridised blobs of crystal and melt + less mafic granite magma (Fig.23A)) and mobilise it into the low-pressure zones created by the differential stress of the deformation. The crystal accumulation was representative of the granodiorites' compositions (Fig.23C) and the squeezed off magma representative of the leucogranites' compositions (Fig.23D). The entire pluton was not affected by the deformation resulting in some parts of the pluton keeping the granite mush composition. This would result in the three granitic units; granodiorites with abundant mafic enclaves; granites with fewer mafic enclaves and leucogranites with no mafic enclaves.

The study concludes that the mafic enclave magma and less mafic (felsic) granite magma are comagmatic and come from the same andesitic source. The proposed primary mechanism

controlling both magmas was peritectic mineral entrainment and co-entrainment of accessory suite minerals in varying proportions. The variation seen in the granites are not a result of a magma mixing process but rather a secondary filter pressing process at a low temperature during localised deformation of the Buddusò Pluton. The enclaves' chemistry was shaped by secondary hybridisation mechanism by the granite magma upon ascension to the pluton prior to emplacement.

Future Research

The study of enclaves allows for great insight into the different processes that worked on the magmatic body. The general consensus of magma mixing creating I-type granites with mafic enclaves needs to be re-evaluated. The presence of mafic enclaves in a granitic body shows a complex history and often is a result of more than one mechanism.

With respect to the Buddusò Pluton, zircon isotopic analyses are needed to establish more well documented U-Pb ages of each unit and its mafic enclaves. More Lu-Hf isotopic data is required to gain insight on source information. Up to date most authors have done extensive field, petrographical, geochemical, mineral chemical and Sr/Nd isotopic work. No scientist has investigated zircons from the pluton and isotopic analysis of zircon crystals was only partially investigated in this study working with a small zircon population. Detailed work on isotopic data from zircon grains from all three units and their enclaves is recommended for future research.

6.3 Peritectic assemblage entrainment (PAE)

Several authors have proposed the PAE model as the primary mechanism for I-type granite petrogenesis (Clemens & Stevens, 2012 & Clemens et al., 2011.). The model describes tiny crystals of peritectic minerals being entrained at varying amounts as escaping partial magma batches from the source rocks. These entrained minerals are defined by the stoichiometry of the partial melting reaction which produced them. The entrained minerals are resorbed on ascent and recycled into mafic minerals and plagioclase that crystallise from the magmas (Clemens et al., 2016b).

Fig.26 shows a tight TiO_2 vs. MgO positive correlation with a negative correlation of K_2O vs. MgO . Experimental magmas and inclusions modelled for both crustally derived and mantle derived magmas do not show a tight Ti vs. maficity trend (Stevens et al., 2007) but rather a scatter. The model disagrees with the fractionation of biotite as this would consequently show a positive correlation with respect to K_2O vs. $\text{FeO}+\text{MgO}$. If biotite were to fractionate, the fractionation of K-feldspar needed to compensate for the inducing depletion of K_2O in the magma would require a large amount of K-feldspar to be removed from the mineral assemblage (Farina et al., 2014). The PAE model suggests that the strong Ti:Fe+Mg correlation is the consequence of entrainment of the peritectic assemblage ($\text{Opx} + \text{Cpx} + \text{Pl} \pm \text{Grt} + \text{Il}$) and reflects the stoichiometry of the biotite-hornblende incongruent melting reaction (Clemens & Stevens, 2012).

Compatible major and trace elements in Fig.11-13 define tighter correlations in comparison to the wider scatter shown by incompatible major and trace elements. Villaros et al. (2009) ascribed the scattered trend seen in incompatible elements; (K_2O , Na_2O , Rb, Ba) to represent the co-entrainment of the accessory mineral suite as co-entrainment of accessory minerals controls the concentrations of the compatible elements that they are hosted in. This results in tighter correlations with respect to compatible elements and wider trends for incompatible elements (Clemens & Stevens., 2012).

6.3.1 The source of the Buddusò Pluton

This peritectic entrainment is proposed to occur at the source and is the primary mechanism which controls the chemistry of the granites. $\epsilon_{(176/177)\text{Hf}}$ isotopic ranges suggest that both the mafic enclave magma and the felsic granite magma are crustally derived magmas. The age of the source is

constrained by the youngest inherited zircon which, with respect to Fig.15, is close in age in comparison to the magmatic age of the Buddusò pluton. A source that is hornblende-bearing and the partial melting of it would result in the essential ingredients needed to form the range of compositions seen in the granites. Clemens et al. (2011) refers to an andesitic lava as a fitting suitable candidate for a source.

6.3.2 PAE Petrogenetic Model

The enclave and granites share the same magmatic U-Pb age of 294 ± 2 Ma (Fig.16) which suggests that they are either two coeval magmas or that they are comagmatic. The enclaves share a similar composition to that of the granites with respect to mineral assemblage and appear to have been hybridised by the granites to varying degrees bringing their compositions closer to that of the granitic suite (Fig.11-13). The wider scatter in major element and trace element chemistries of the mafic enclaves could possibly record an even more diverse starting composition. Some mafic enclaves lie on the Ti:Fe+MgO correlation which is suggestive of the enclaves being autolith. A petrogenetic model based on the PAE infers that both the enclave magma and the granite magma are from the same andesitic source. Both magmas show varying degrees of entrainment of the peritectic assemblage and co-entrainment of the accessory suite resulting from partial melting of the source. The mafic enclave magma was injected slightly earlier and began to crystallise upon successive injections of the less mafic granitic magma, with each successive injection of magma entraining lower proportions of ferromagnesian peritectic minerals. The granitic magma interacted with the enclave magma mush upon ascent which resulted in fragmentation and hybridisation of the enclave magma. However this model doesn't account for the small-scale isotope heterogeneity produced by the granites, if the magmas came from the same source, the Hf isotopic compositions should be the same. The small scale Hf isotopic heterogeneities could be explained by transfer of Hf variation from inherited zircons to magmatic zircons (Farina et al., 2014) during entrainment. However the decreasing $\epsilon_{\text{Hf}(t)}$ range from granodiorites through to leucogranites cannot be explained neither can the abundance of mafic enclaves decreasing in the same direction. This suggests that peritectic mineral entrainment was the primary mechanism for which the pluton achieved its chemical composition but secondary mechanisms had to occur. Low temperature filter pressing proposed in the fractionation modelling could dilute the $\epsilon_{\text{Hf}(t)}$ range towards the leucogranites as explained in section 6.2.3.2 and explain the abundance of mafic enclaves in the outer unit.

References

- Barbarin, B., 1999. A review of the relationships between granitoids types, their origins and their geodynamic environments. *Lithos*, **43(3)**, 605-626
- Barbarian, B., 2005. Mafic magmatic enclaves and mafic rocks associated with some granitoids of the central Sierra Nevada batholith, California: nature, origin and relations with the hosts, *Lithos*, **80**, 155-177.
- Baker, D.R., 1989. Trace versus trace element diffusion: diffusional decoupling of Sr concentration from Sr isotope composition. *Geochimica et Cosmochimica Acta*, **53**, 3015–3023.
- Barbey, B., Gasquet, D., Pin, C. & Bourgeix, A.L., 2008. Igneous banding, schlieren and mafic enclaves in calc-alkaline granites: The Buddusò pluton (Sardinia), *Lithos*, 147-163.
- Bartoli, O., Cesare, B., Poli, S., Bodnar, R.J., Acosta-Vigil, A., Frezzotti, M.I. & Meli, S., 2013. Recovering the composition of magma and the fluid regime at the onset of crustal anataxis and S-type granite formation. *Geology*, **41**, 115-118.
- Beccaluva, L., Civetta, L., Macciotta, G. & Ricci, C.A., 1985. Geochronology in Sardinia: results and problems. *Rendiconti Societa Italiana Mineralogia e Petrologia*, **40**, 57–72.
- Becker, G.F., 1897. Fractional crystallization of rocks. *American Journal of Science*, **4**, 257-261.
- Blichert-Toft, J. & Albarède, F., 1997. The Lu-Hf isotope geochemistry of chondrites and the evolution of the mantle-crust system. *Earth Planetary Science Letters*, **148**, 243-258.
- Bouvier, A., Vervoort, J.D., & Patchett, J.P., 2008. The Lu-Hf and Sm-Nd isotopic composition of CHUR: Constraints from unequilibrated chondrites and implications for the bulk composition of terrestrial planets. *Earth and Planetary science Letters*, **273**, 48-57.
- Bowen, N.L., 1949. The granite problem and the method of multiple prejudices. In: Giluly, J.(ed.) Origin of Granite. *Geology Society American memoirs*, **28**, 79-90.
- Bruneton, P. and Orsini, J.B., 1977. Le massif granitique de Buddusò (Sardaigne Nord-Orientale): une seule intrusion de type concentrique. *Comptes Rendus de l'Académie des Sciences*, **284**, 151
- Carminati E., Lustrino M., Cuffaro M., & Doglioni C., 2010. Tectonics, magmatism and geodynamics of Italy : what we know and what we imagine. *Journal of the Virtual Explorer*, **36(9)**.
- Clemens, J.D. & Watkins, J.M., 2001. The fluid regime of high-temperature metamorphism during granitoid magma genesis. *Contributions to Mineralogy and Petrology*, **140**, 600-606.

Clemens, J., 2003. S-type granite magmas-petrogenetic issues, models and evidence. *Earth Science Reviews*, **61(1-2)**, 1-18.

Clemens, J.D., Stevens, G. & Farina, F., 2011. The enigmatic sources of I-type granites and the clinopyroxene-ilmenite connexion. *Lithos* **126**, 174-181.

Clemens, J.D., Birch, W.D. & Dudley R.J., 2011. S-type ignimbrites with polybaric crystallisation histories: the Tolmie Igneous Complex, Central Victoria, Australia (and erratum). *Contributions to Mineralogy and Petrology*, **162(6)**, 1315-1337.

Clemens, J.D., Bryant C.J. & Wyborn D., 2012. Peraluminous I-type granites. *Lithos*, **153**, 142-153.

Clemens, J.D., & Stevens, G., 2012. What controls chemical variation in granitic magmas? *Lithos* **134 – 135**, 317-329.

Clemens, J.D., Stevens., G. & Elburg, M.A., 2016a. Petrogenetic processes in granitic magmas and their igneous microgranular enclaves from Central Victoria, Australia: match or mismatch? *Transactions of the Royal Society of South Africa*, DOI: 10.1080/0035919X.2016.1209702

Clemens, J.D., Regmi, K., Nicholls, I.A. & Maas, R., 2016b. The Tynong pluton, its mafic synplutonic sheets and igneous microgranular enclaves: the nature of the mantle connection in I-type granitic magmas. *Contribution to Mineralogy and Petrology*, **171**, 35.

Chappell, B.W., 1996, Magma Mixing and the Production of Compositional Variation within Granite Suites: Evidence from the Granites of Southeastern Australia. *Journal of Petrology*, **37(3)**, 449-470.

Chappell, B.W., 1999. Aluminium saturation in I- and S-type granites and the characterization of fractionated haplo-granites. *Lithos*, **46**, 535-551.

Chappell, B.W., White, A.J.R. & Wyborn, D., 1987. The importance of residual source material residue in granite petrogenesis, *Journal of Petrology*, **28**, 1111-1138.

Chappell, B.W. & White, A.J.R., 1992. I- and S-types granites in the Lachland Fold Belt. *Trans Royal Soc Edinb: Earth Sciences*, **83**, 1-26.

Chappell, B.W. & White, A.J.R., 2001. Two contrasting granite types: 25 years later. *Austrian Journal of Earth Sciences*, **48**, 489-499.

Chappell, B.W. & Wyborn, D., 2004. Cumulate and Cumulative Granites and Associated Rocks. *Resource Geology*, **54(3)**, 227-240.

Cocherie, A., 1984. Interaction manteaux-croûte : son rôle dans la genèse d'associations plutoniques calco-alcalines, contraintes géochimiques (éléments en traces et isotopes du strontium et de l'oxygène). *Thèse de doctorat, Université Rennes*, 245.

Cocherie, A., 1978. Géochimie des Terres Rares dans les granitoïdes. *Thèse 3-ème cycle, Institut de Géologie, Rennes*.

Cocirta, C., 1986. Les enclaves microgrenues sombres du massif de Bono (Sardaigne septentrionale). Signification pétrogénétique des plagioclases complexes et de leurs inclusions. *Comptes Rendus de l'Académie des Sciences*, **302(7)**, 441-446.

Cocirta, C. & Orsini, J.-B., 1986. Signification de la diversité de composition des enclaves microgrenues sombres en contexte plutonique. L'exemple des plutons calco-alcalins de Bono et Buddusò. *Comptes Rendus de l'Académie des Sciences*, **302**, 331-336.

Cocirta, C. & Michon, G., 1989. The mafic magmatic enclaves of some Northern Sardinian granitoids: the existence of two different acid-basic associations. *Rendiconti Della Società Italiana di Mineralogia e Petrologia*, **43-3**, 705-714.

Connolly, J. A. D., 2009. The geodynamic equation of state: what and how. *Geochemistry, Geophysics, Geosystems*, **10**.

Cox, G.C., Bell, J.D. & Pankhurst, R.J., 1979. The interpretation of Igneous Rocks, *Unwin Hyman*, 450.

Cüneyt, A. & Cahit, H., 1999. Mafic Microgranular Enclaves in the Kozak Granodiorite, Western Anatolia. *Turkish Journal of Earth Sciences*, **8**, 1-17.

Dahlquist, J.A., 2002. Mafic microgranular enclaves: early segregation from metaluminous magma (Sierra de Chepes), Pampean Ranges, NW Argentina, *Journal of South American Earth Sciences*, **15/6**, 643-655.

Del Moro, A., Dr Simplicio P., Ghezzi, C., Guasparri, G., Rita, F. & Sabatini, G., 1975. Radiometric data and intrusive sequence in the Sardinian Batholith. *Neues Jahrbuch für Mineralogie Abhandlungen*, **126**, 28-44.

Diedier, J., 1973. Granites and their enclaves: The bearing of enclaves on the origin of granites: Amsterdam, Netherlands, Elsevier. *Development in Petrology*, 393.

Diedier, J. & Barbarian, B., 1991. Enclaves and granite petrology, *Developments in Petrology*, 1-625.

Dodge, F.C.W. & Kistler, R.W., 1990. Some additional observations on inclusions in the granitic rocks of Sierra Nevada, *Journal of Geophysical Research*, **95**, 17841-17848.

Eichelberger, J.C., 1980. Vesiculation of mafic magma during replenishment of silicic magma reservoirs, *Nature*, **288**.446-450.

Farina, F., Stevens, G., Gerdes, A., & Frei, D., 2014. Small-scale Hf isotopic variability in the Peninsula pluton (South Africa): the processes that control inheritance of source $^{176}\text{Hf}/^{177}\text{Hf}$ diversity in S-type granites. *Contributions to Mineralogy and Petrology*, **168**, 1065.

- Flinders, J. & Clemens, J.D., 1996. Non-linear dynamics, chaos, complexity and enclaves in granitoid magmas. *Transactions of the Royal Society of Edinburgh. Earth Sciences*, **87**, 217–223.
- Fourcade, S. & Allegre, C.J., 1981. Trace-elements behaviour in granite genesis – a case-study the calc-alkaline plutonic association from the Querigut complex (Pyrenées, France). *Contributions to Mineralogy and Petrology*, **76(2)**, 177-195.
- Frei, D., & Gerdes, A., 2009. Precise and accurate in situ U–Pb dating of zircon with high sample throughput by automated LA–SF–ICP–MS. *Chemical Geology*, **261**, 261–270.
- Fuhrman, M. L. & Lindsley, D. H., 1988. Ternary-feldspar modeling and thermometry. *American Mineralogist*, **73**, 201-215.
- Gerdes, A., & Zeh, A., 2006. Combined U-Pb and Hf isotope LA-(MC-) ICP-MS analyses of detrital zircons: Comparison with SHRIMP and new constraints for the provenance and age of an Armorican metasediment in Central Germany. *Earth and Planetary Science Letters*, **249**, 47-61.
- Gerdes, A., & Zeh A., 2009. Zircon formation versus zircon alteration- new insights from combined U–Pb and Lu–Hf in situ LA–ICP–MS analyses and consequences for the interpretation of Archean zircons from the Central Zone of the Limpopo Belt. *Chemical Geology*, **261**, 230–243.
- Ghaffari, M. & Rashidnejad-Omran N., 2015. Magma mixing/mingling in Salmas granodiorite, NW Iran: evidence from mafic microgranular enclaves. *Arabian Journal of Geoscience*, **8**, 7141-7152.
- Hibbard, M.J., 1981. The magma mixing origin of mantled feldspars, *Contributions to Mineralogy and Petrology*, **76(2)**, 158-170.
- Hibbard, M.J., 1991. Textural anatomy of twelve magma-mixed granitoid systems. In: Didier J, Barbarin B (eds) Enclaves and granite petrology. *Elsevier*, 431–444.
- Holland, T. & Powell, R., 1998. An internally consistent thermodynamic data set for phases of petrological interest. *Journal of metamorphic Geology*, **16**, 309-343.
- Holland, T. & Powell, R., 1996. Thermodynamics of order-disorder in minerals: II. Symmetric formalism applied to solid solutions. *American Mineralogist*, **81**, 1425-1437.
- Holland, T. & Powell, R., 1998. An internally consistent thermodynamic data set for phases of petrological interest. *Journal of metamorphic Geology*, **16**, 309-343.
- Holland, T. & Powell, R., 2001. Calculation of phase relations involving haplogranitic magmas using an internally consistent thermodynamic dataset. *Journal of Petrology*, **42**, 673-683.
- Holland, T. & Powell, R., 2003. Activity–composition relations for phases in petrological calculations: an asymmetric multicomponent formulation. *Contributions to Mineralogy and Petrology*, **145**, 492-501.

Ilbeyli, N. & Pearce., 2005. Petrogenesis of Igneous Enclaves in Plutonic Rocks of the Central Anatolian Crystalline Complex, Turkey. *International Geology Review*, **47**, 1011-1034.

Irvine, T.N. & Baragar, W.R.A., 1971. A guide to the chemical classification of the common volcanic rocks. *Canadian Journal of Earth Sciences*, **8**, 523-548.

Johnston, A.D. & Wyllie, P.J., 1988. Interaction of granitic and basic magmas: experimental observations on contamination processes at 10 Kbar with H₂O. *Contributions to Mineralogy and Petrology*, **98**, 352-362.

Kocak, K., 2006. Hybridization of mafic microgranular enclaves: mineral and whole-rock chemistry from the Karamadazi Granitoid, Central Turkey. *International Journal of Earth Sciences*, **95**, 587-670.

Kokac, K., Zedef, V. & Kansun. G., 2011. Magma mixing/mingling in the Eocene Horoz (Nigde) granitoids, Central Southern Turkey: evidence from mafic microgranular enclaves, *Journal of Mineralogy and Petrology*, **103**, 149-167.

Kumar, S., Rino, V. & Pal, A.B., 2004. Field evidence of magma mixing from microgranular enclaves hosted in Palaeoproterozoic Malanjkhand granitoids, Central India. *Gondwana research*, **7(2)**, 539-548.

Leake, B.E., Woolley, A.R., Arps, C.E.S., Birch, W.D., Gilbert, M.C., Grice, J.D., Hawthorne, F.C., Kato, A., Kisch, H.J., Krivovichev, V.G., Linthout, K., Laird, J., Mandarino, J.A., Maresch, W.V., Nickel, E.H., Rock, N.M.S, Schumacher, J.C., Smith, D.C., Stephenson, N.C.N., Ungaretti, L., Whittaker, E.J.W., & Youzhi, G., 1997. Nomenclature of amphiboles: report of the subcommittee on amphiboles of the international mineralogical association, commission on new minerals and mineral names. *American Mineralogist*, **82**, 1019-1037.

Ludwig, K.R., 1990. Isoplot: a plotting and regression program for radiogenic isotope data. *US Geological Survey Open-File Report*, **version 2.03**, 88-57.

Matteini, M., Junges, S.L., Dantas, E.L., Pimentel, M.M. & Bühn, B., 2010. *In situ* zircon U-Pb and Lu-Hf isotope systematic on magmatic rocks: Insights on the crustal evolution of the Neoproterozoic Goiás Magmatic Arc, Brasília belt. *Gondwana Research*, **7**, 1-12.

Mayne, M.J., Moyen, J.F., Stevens, G. & Kaislaniemi, L., 2016. Rcrust: a tool for calculating path-dependent open system processes and application to magma loss. *Journal of metamorphic geology*, **34**, 663-682.

McBirney, A. & Noyes, R.M., 1979. Crystallization and Layering of the Skaergaard Intrusion. *Journal of Petrology*, **20(3)**, 487-554.

McDonough, W.F. & Sun, S., 1995. The composition of the Earth. *Chemical Geology*, **120**, 223-253.

Orsini, J.B., 1976. Les granitoïdes hercyniens corso-sardes : mise en évidence de deux associations magmatiques. *Bulletin de la Société Géologique de France*, **7**, 1203-1206.

Orsini, J.B., 1979. Contribution à la connaissance des granitoïdes tardiorogéniques du batholite corso-sarde. Les enclaves sombres de l'association plutonique calco-alkaline. *Bulletin de la Société Géologique de France*, **7**, 1203-1206.

Orsini, J.-B., Bruneton, P., Dupuy, C., Marmottans, M., 1977. Les enclaves microgrenues du massif de Buddusò (Sardaigne nord-orientale). *Trav. Sci. Lab. Pétrol., Université de Saint Jérôme*.

Orsini, J.-B. & Fernandez, A., 1987. Signification de la discordance structurale entre fluidalité magmatique et zonalité pétrographique dans les intrusions de granitoïdes: l'exemple de l'intrusion de Buddusò. *Comptes Rendus de l'Académie des Sciences*, **304**, 993–996.

Orsini, J.B., 1980. Le batholite corso-sarde: un exemple de batholite hercynien (structure, composition, organisation d'ensemble). Sa place dans la chaîne varisque de l'Europe moyenne. *Unpublished doctoral thesis, Université d'Aix-Marseille*, **III**, 370.

Paquette, J.L., Ménot, R.P., Pin, C. & Orsini, J.B., 2003. Episodic and short-lived granitic pulses in a post-collisional setting: evidence from precise U-Pb zircon dating through a crustal cross-section in Corsica. *Chemical Geology*, **198**, 1–20.

Perugini, D., Poli, G., Christofides, G. & Eleftheriads, G., 2003. Magma mixing in the Sithonia plutonic complex, Greece: Evidence from the mafic microgranular enclaves, *Journal of Mineralogy and Petrology*, **78**, 173-200.

Pietranik, A. & Koepcke, J., 2014. Plagioclase transfer from a host granodiorite to mafic microgranular enclaves: diverse records of magma mixing. *Mineralogy and Petrology*, **108**, 681-694.

Poli, G., Ghezzo, C. & Conticelli, S., 1989. Geochemistry of granitic rocks from the Hercynian Sardinia-Corsica batholith: Implication for magma genesis. *Lithos*, **23**, 247-266.

Powell, R. & Holland, T. J. B., 1999. Relating formulations of the thermodynamics of mineral solid solutions: activity modeling of pyroxenes, amphiboles, and micas. *American Mineralogist*, **84**, 1-14.

Roca, E., Sans, M., Cabrera, L. and Marzo M., 1999. Oligocene to Middle Miocene evolution of the Central Catalan margin (North-western Mediterranean). *Tectonophysics*, **315**, 209-229.

Rocco, I., Lustrino, M., Morra, V. & Melluso, L., 2012. Petrological, geochemical and isotopic characteristics of the lithospheric mantle beneath Sardinia (Italy) as indicated by ultramafic xenoliths enclosed in alkaline lavas. *International Journal of Earth Sciences*, **101**, 1111-1125.

Rossi, P., & Cocherie, A., 1991. Genesis of a Variscan batholith. Field, petrological and mineralogical evidence from the Corsica-Sardinia batholith. *The European Traverse, Part 7. Tectonophysics*, **195**, 319-346.

Scherer, E., Münker, C., & Mezger, K., 2001. Calibration of the lutetium-hafnium clock. *Science*, **293**, 683-687.

Stevens, G., Clemens, J.D. & Droop, G.T.R., 1997. Magma production during granulite-facies anatexis: experimental data from primitive metasedimentary protoliths. *Contributions to Mineralogy and Petrology*, **128**, 352-370.

Stevens, G., Villaros, A. & Moyen, J., 2007. Selective peritectic garnet entrainment as the origin of geochemical diversity in S-type granites. *Geology*, **35** (1), 9-12.

Stomer, J.C., 1972. Mineralogy and Petrology of the Raton-Clayton volcanic field, northeastern New Mexico. *Geological Society of America Bulletin*, **83**, 3299-3322.

Sun, S., & McDonough, W.F., 1989. Chemical isotopic systematics of oceanic basalts: implications for mantle composition and processes. In Saunders, A.D., Norry, M.J. (Eds.), *Magmatism in Ocean Basins. Geological Society special Publication*, 313-345.

Tajčmanová, L., Connolly, J. A. D. & Cesare, B., 2009. A thermodynamic model for titanium and ferric iron solution in biotite. *Journal of Metamorphic Geology*, **27**, 153-165.

Tischendorf, G., Gottesmann, B., Forster, H.J., & Trumbull, R.B., 1997. On Li-bearing micas: estimating Li from electron microprobe analyses and improved diagram for graphical representation. *Mineralogical Magazine*, **61**, 809-834.

White, R. W., Powell, R. & Holland, T. J. B., 2001. Calculation of partial melting equilibria in the system $\text{Na}_2\text{O}-\text{CaO}-\text{K}_2\text{O}-\text{FeO}-\text{MgO}-\text{Al}_2\text{O}_3-\text{SiO}_2-\text{H}_2\text{O}$ (NCKFMASH). *Journal of Metamorphic Geology*, **19**, 139-153.

White, R. W., Powell, R. & Holland, T. J. B., 2007. Progress relating to calculation of partial melting equilibria for metapelites. *Journal of Metamorphic Geology*, **25**, 511-527.

White, R. W., Powell, R., Holland, T. J. B. & Worley, B. A., 2000. The effect of TiO_2 and Fe_2O_3 on metapelitic assemblages at greenschist and amphibolite facies conditions: mineral equilibria calculations in the system $\text{K}_2\text{O}-\text{FeO}-\text{MgO}-\text{Al}_2\text{O}_3-\text{SiO}_2-\text{H}_2\text{O}-\text{TiO}_2-\text{Fe}_2\text{O}_3$. *Journal of Metamorphic Geology*, **18**, 497-512.

Wiebe, R.A., 1968. Plagioclase stratigraphy: a record of magmatic conditions and events in a granite stock. *American Journal of Science*, **266**, 690-703.

Wiebe, R. A., 1994. Silicic magma chambers as traps for basaltic magmas: the Cadillac Mountain Intrusive Complex, Mount Desert Island, Maine. *Journal of Geology*, **102**, 423-437.

Wood, B. J., Nell, J., & Woodland, A. B., 1991. Macroscopic and microscopic thermodynamic properties of oxides. In *Reviews in Mineralogy and Geochemistry*. **25**, 265-302.

- Vernon, R.H., 1983. Restite, xenoliths, and microgranitoid enclaves in granites, *Journal and Proceedings of the Royal Society of New South Wales*, **166**, 77-103.
- Vernon, R.H., 1984. Microgranitoid enclaves in granites – globules of hybrid magma quenched in a plutonic environment, *Nature*, **309**, 438-439.
- Vernon, R.H., 1990. Crystallization and hybridism in microgranitoid enclave magmas: microstructural evidence. *Journal of Geophysics Research*, **95**, 17849–17859.
- Vervoort, J.D., Patchett, P.J., Albarède, F., Blichert-Toft, J., Rudnick, R., & Downes, H., 2000. Hf–Nd isotopic evolution of the lower crust. *Earth Planet Science Letters*, **181**, 115–129
- Vignerresse, J.L., Barbey, P. & Cuney, M., 1996. Rheological transitions during partial melting and crystallization with application to felsic magma segregation and transfer. *Journal of Petrology*, **37**, 1579-1600
- Villaros, A., Stevens, G., & Buick, I. S., 2009. Tracking S-type granite from source to emplacement: clues from garnet in the Cape Granite Suite. *Lithos*, **112** (3) 217-235.
- Villaros, A., Buick, I.S., Stevens G., 2012. Isotopic variations in S-type granites: an inheritance from a heterogeneous source. *Contributions to Mineralogy and Petrology*, **163**, 243-257.
- Zorpi, M.J., Coulon, C., Orsini., J.B. & Cocirta., C., 1989. Magma mingling, zoning and emplacement in calc-alkaline granitoid plutons. *Tectonophysics*, **157**, 315-329.
- Zorpi, M.J., Coulon, C., Orsini., J.B. & Cocirta., C., 1991. Hybridization between felsic and mafic magmas in calc-alkaline granitoids; a case study in northern Sardinia, Italy. *Chemical Geology*, **92**, 45-86.

Appendices

Appendix I: Geological Setting and Past Work

Table 1: Partial chemical analyses of the granitic rocks and their mafic enclaves from the Harcourt Pluton, Central Victoria, Australia; adapted from Clemens et al., (2016b)

Sample No	FeO _T (wt%)	MgO (wt%)	FeO _T +MgO (wt%)	TiO ₂ (wt%)	Ba (ppm)	M (mol/100g)	Ti (mol/100g)	Ba (10 ⁴ mol/100g)
HAR1	3.34	1.42	4.76	0.52	687	0.082	0.0065	5
HAR15	3.45	1.47	4.92	0.53	671	0.085	0.0066	4.89
HAR16	3.14	1.3	4.45	0.47	689	0.076	0.0059	5.02
HAR17	3.34	1.22	4.56	0.5	672	0.077	0.0062	4.9
HAR18	1.78	0.7	2.48	0.26	529	0.042	0.0033	3.85
HAR19	3	1.24	4.23	0.46	583	0.072	0.0057	4.25
HC1	3.41	1.31	4.72	0.5	672	0.08	0.0063	4.89
HC2	3.7	1.72	5.43	0.58	744	0.094	0.0073	5.42
HC3	2.98	1.38	4.36	0.46	688	0.076	0.0058	5.01
HC4	3.42	1.56	4.98	0.54	791	0.086	0.0067	5.76
HC5	3.44	1.56	5.01	0.54	729	0.087	0.0068	5.31
HC6	3.11	1.37	4.49	0.48	675	0.077	0.006	4.92
HC7	3.34	1.5	4.84	0.52	716	0.084	0.0066	5.21
G8-04	2.88	1.34	4.22	0.41		0.073	0.0052	0
G8-58	3.34	1.57	4.92	0.52		0.086	0.0065	
G8-60	3.36	1.64	5.01	0.52		0.088	0.0065	
BR1	1.27	0.83	2.11	0.29		0.038	0.0037	
TR1	1.28	0.3	1.58	0.08		0.025	0.001	
MR1	3.43	1.36	4.79	0.49		0.082	0.0061	
ML1(HK)	3.29	1.57	4.86	0.54		0.085	0.0067	
99	3.38	1.3	4.68	0.52	720	0.079	0.0065	5.24
100	3.63	1.65	5.28	0.55	788	0.091	0.0069	5.74
101	3.6	1.72	5.32	0.56	939	0.093	0.007	6.84
102	3.59	1.63	5.22	0.57	850	0.09	0.0071	6.19
103	2.75	1.22	3.97	0.4	728	0.069	0.005	5.3
104	3.18	1.43	4.6	0.45	594	0.08	0.0056	4.33
LGT 1771	2.37	1.2	3.56	0.37	575	0.063	0.0046	4.19
LFB1602	1.83	0.75	2.58	0.3	460	0.044	0.0038	3.35
WV35	3.25	1.43	4.68	0.52	680	0.081	0.0065	4.95
WV36	3.5	1.54	5.04	0.57	730	0.087	0.0071	5.32
WV37	3.22	1.42	4.64	0.52	665	0.08	0.0065	4.84
WV38	3.34	1.3	4.64	0.52	650	0.079	0.0065	4.73
WV39	1.99	0.57	2.55	0.28	555	0.042	0.0036	4.04
WV92	2.86	1.25	4.11	0.44		0.071	0.0055	4.04
WV111	3.19	1.44	4.64	0.51	660	0.08	0.0064	4.81
WV182	2.97	1.36	4.33	0.48	675	0.075	0.006	4.92
HAR2	4.87	2.13	7	0.78	310	0.121	0.0098	2.26
HAR3	5.49	3.1	8.59	0.91	384	0.153	0.0114	2.8
HAR4	4.83	3.42	8.25	0.69	432	0.152	0.0087	3.15
HAR 5	6.28	2.7	8.98	0.85	220	0.154	0.0106	1.6
HAR8	7.97	3.48	11.45	1.17	1099	0.197	0.0146	8.01
HAR9	6.16	2.7	8.86	0.98	452	0.153	0.0123	3.29
HAR10	5.92	2.76	8.68	0.98	668	0.151	0.0122	4.87
HAR12	4.09	1.75	5.84	0.63	450	0.1	0.0079	3.28
HAR13	6.43	2.75	9.18	1.21	637	0.158	0.0152	4.64

Appendix II: Whole-rock Geochemistry

Major element chemistry

Table 1: Table showing major element chemistry of samples a (KC) = Kcode (used in Igpet06 software), b(BD) = Beyond detection, c(Bet.08) = Barbey et al., 2008, d(Leuco-med) = leucogranite medium,

Sample	KC ^a	Unit	Barbey	Locality	SiO ₂	TiO ₂	Al ₂ O ₃	Cr ₂ O ₃	Fe ₂ O ₃	MnO	MgO	CaO	Na ₂ O	K ₂ O	P ₂ O ₅	sum
BG1	11	leuco	inner	G	74.72	0.11	13.82	BD ^b	1.51	0.06	0.16	1.38	3.34	4.86	0.03	100.00
BG10	11	leuco	inner	F	75.90	0.11	13.14	BD	1.38	0.05	0.17	1.29	2.98	4.95	0.03	100.00
BG18	11	leuco	inner	M	76.49	0.09	13.11	BD	1.11	0.04	0.08	1.22	3.08	4.76	0.02	100.00
BG19	11	leuco	inner	M	76.51	0.10	13.00	BD	1.14	0.05	0.09	1.17	3.08	4.84	0.02	100.00
Sa14	7	monzogranite	inner	Bet.08 ^c	74.93	0.10	13.72	BD	1.33	0.00	0.18	1.69	2.78	5.20	0.07	100.00
Sa25	7	monzogranite	inner	Bet.08	76.33	0.08	13.17	BD	1.17	0.04	0.21	1.52	3.17	4.25	0.06	100.00
BG25	11	leuco	inner	D	75.61	0.07	13.25	BD	1.06	0.03	0.06	1.07	2.32	6.51	0.02	100.00
BG32	11	leuco	inner	N	77.67	0.04	12.29	BD	0.74	0.02	0.00	0.47	2.26	6.50	0.01	100.00
BG2	29	leuco-med ^d	middle	I	70.94	0.31	14.88	BD	3.45	0.07	0.62	2.39	3.48	3.77	0.09	100.00
BG23	29	leuco-med	middle	D	71.92	0.25	14.72	BD	2.45	0.06	0.50	2.30	3.09	4.64	0.06	100.00
BG24	29	leuco-med	middle	D	71.52	0.31	14.62	BD	2.97	0.08	0.64	2.48	3.09	4.21	0.08	100.00
BG27	29	leuco-med	middle	D	72.99	0.28	14.09	BD	2.67	0.08	0.56	2.46	3.12	3.66	0.08	100.00
BG3	29	med ^e	middle	I	74.39	0.17	13.59	BD	2.00	0.05	0.31	1.55	2.86	5.02	0.05	100.00
BG30	29	med	middle	N	74.78	0.19	13.41	BD	2.01	0.06	0.33	1.51	3.09	4.56	0.05	100.00
BG31	29	med	middle	N	74.79	0.19	13.42	BD	2.16	0.06	0.33	1.67	3.20	4.12	0.05	100.00
Sa19b	8	enclave	middle	Bet.08	64.95	0.48	17.34	BD	5.37	0.12	1.26	3.31	5.10	1.86	0.21	100.00
Sa24	7	ND ^f	middle	Bet.08	70.84	0.31	14.90	BD	3.54	0.07	0.75	2.71	3.43	3.35	0.10	100.00
Sa17c	7	monzogranite	middle	Bet.08	75.30	0.08	13.40	BD	1.52	0.00	0.19	1.34	2.92	5.18	0.07	100.00
Sa22c	7	ND	middle	Bet.08	75.22	0.09	13.50	BD	1.42	0.04	0.24	1.52	3.08	4.82	0.07	100.00
Sa17s	7	schlieren	middle	Bet.08	70.13	0.33	14.98	BD	4.20	0.12	0.83	2.54	3.82	2.93	0.12	100.00
Sa22s	7	schlieren	middle	Bet.08	61.04	0.88	15.63	BD	10.13	0.27	2.16	2.66	3.33	3.65	0.25	100.00
BG21	4	enclave	middle	D	64.78	0.51	16.89	BD	5.52	0.12	1.09	3.93	3.95	2.99	0.22	100.00
BG22	4	enclave	middle	D	64.54	0.63	16.98	BD	5.65	0.13	1.32	4.43	4.33	1.75	0.24	100.00
BG29	4	enclave	middle	D	57.71	0.80	19.46	BD	7.73	0.18	1.71	5.11	4.85	2.14	0.32	100.00
BG8	4	enclave	middle	F	51.04	1.95	17.45	0.01	10.95	0.19	5.56	7.53	3.88	0.90	0.54	100.00
BG9	4	enclave	middle	F	50.41	1.96	17.50	0.01	10.94	0.18	5.78	7.81	3.64	1.26	0.53	100.00
Sa21	8	enclave	middle	Bet.08	66.63	0.51	16.12	BD	5.32	0.10	1.36	3.74	4.28	1.75	0.18	100.00
Sa18	8	enclave	middle	Bet.08	68.41	0.38	16.03	BD	4.31	0.08	0.97	3.51	4.69	1.44	0.17	100.00
BG13	12	Hbl-bearing	outer	C	68.04	0.45	16.06	BD	3.98	0.07	1.00	3.77	3.19	3.32	0.12	100.00
BG14	12	Hbl-bearing	outer	C	67.85	0.48	15.87	BD	4.31	0.08	1.08	3.72	3.11	3.36	0.13	100.00
BG26	12	med	outer	D	68.79	0.41	15.74	BD	4.02	0.11	0.89	3.63	3.43	2.87	0.10	100.00
BG33	12	Hbl-bearing	outer	H	68.50	0.51	15.54	BD	4.40	0.08	1.12	3.90	3.24	2.57	0.13	100.00
BG34	12	Hbl-bearing	outer	H	66.57	0.53	16.35	BD	4.67	0.09	1.19	3.96	3.30	3.19	0.14	100.00
BG35	12	Hbl-bearing	outer	H	67.07	0.57	15.95	BD	4.97	0.08	1.26	4.11	3.39	2.44	0.15	100.00
BG36	12	Hbl-bearing	outer	H	67.48	0.54	15.92	BD	4.52	0.08	1.14	3.78	3.18	3.21	0.13	100.00
BG48	12	Hbl-bearing	outer	B	65.58	0.58	16.86	BD	4.88	0.08	1.29	4.39	3.28	2.90	0.16	100.00
Sa05b	7	granodiorite	outer	Bet.08	67.33	0.50	15.88	BD	5.00	0.07	1.23	4.09	3.79	1.93	0.17	100.00
Sa15	7	granodiorite	outer	Bet.08	69.15	0.40	15.37	BD	3.83	0.05	0.93	3.36	3.02	3.74	0.15	100.00
Sa04	7	ND	outer	Bet.08	69.91	0.31	16.14	BD	2.99	0.04	0.64	4.02	4.06	1.76	0.12	100.00
Sa10	7	granodiorite	outer	Bet.08	71.14	0.31	14.64	BD	3.23	0.04	0.68	2.69	3.08	4.07	0.12	100.00
Sa13b	7	ND	outer	Bet.08	72.00	0.31	14.50	BD	2.69	0.05	0.71	2.32	3.31	3.99	0.10	100.00
Sa07	7	monzogranite	outer	Bet.08	75.42	0.11	13.32	BD	1.41	0.00	0.26	1.72	2.52	5.17	0.07	100.00
Sa08	7	ND	outer	Bet.08	55.72	1.29	17.13	BD	11.84	0.19	2.75	2.93	3.10	4.77	0.27	100.00
Sa09	7	bt-rich layer	outer	Bet.08	59.27	0.92	17.33	BD	8.82	0.14	2.08	3.71	3.51	3.96	0.26	100.00
Sa13a	8	enclave	outer	Bet.08	68.81	0.38	15.81	BD	3.43	0.05	0.89	2.56	3.54	4.36	0.16	100.00
Sa05a	8	enclave	outer	Bet.08	54.84	0.85	17.46	BD	10.65	0.23	3.50	6.08	3.91	2.26	0.22	100.00
BG38	4	enclave	outer	H	52.35	0.91	21.01	BD	9.02	0.16	2.40	6.82	4.68	2.23	0.43	100.00
BG15	3	mix	outer	C	61.85	0.61	19.11	BD	5.07	0.10	1.28	4.64	4.21	2.89	0.22	100.00
BG15	4	enclave	outer	C	53.54	0.90	20.29	BD	9.11	0.16	2.28	6.81	4.43	2.09	0.39	100.00
BG16	3	mix	outer	C	55.88	0.85	19.81	BD	8.08	0.14	2.08	5.97	4.24	2.62	0.34	100.00
BG16	4	enclave	outer	C	53.70	0.92	22.22	BD	7.41	0.12	1.91	5.63	5.09	2.64	0.35	100.00

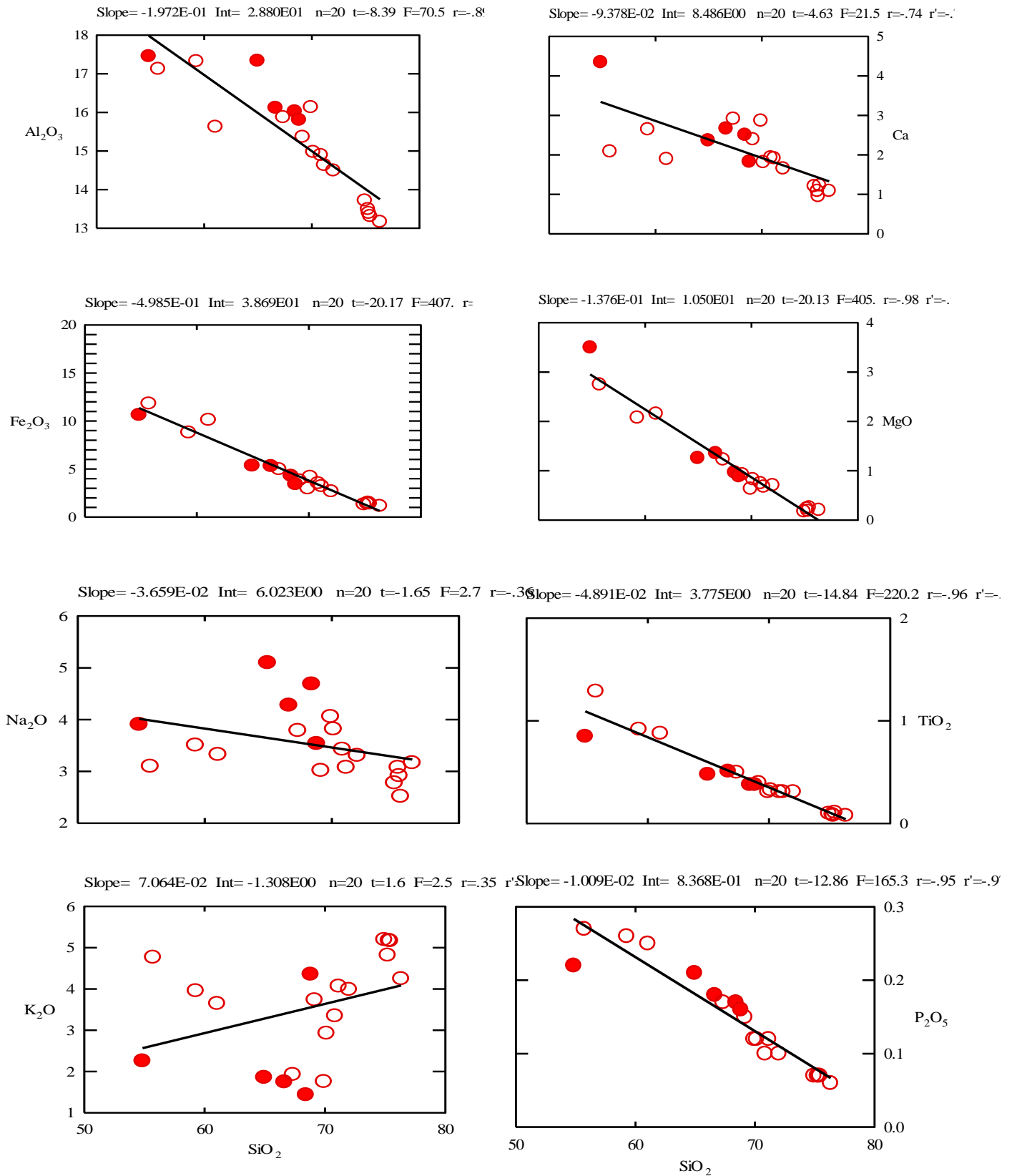


Figure 1: Harker plots of granite and enclave samples from Barbey, (2010) study showing major elements vs SiO_2 . Regression line ($y=mx+c$) showing regression parameters; Slope(m)= slope gradient, Int(y)=slope intercept, n = number of samples, r =Pearson's coefficient and r' = Spearman's rank correlation coefficient. ($\text{E-}01=10^{-1}$).

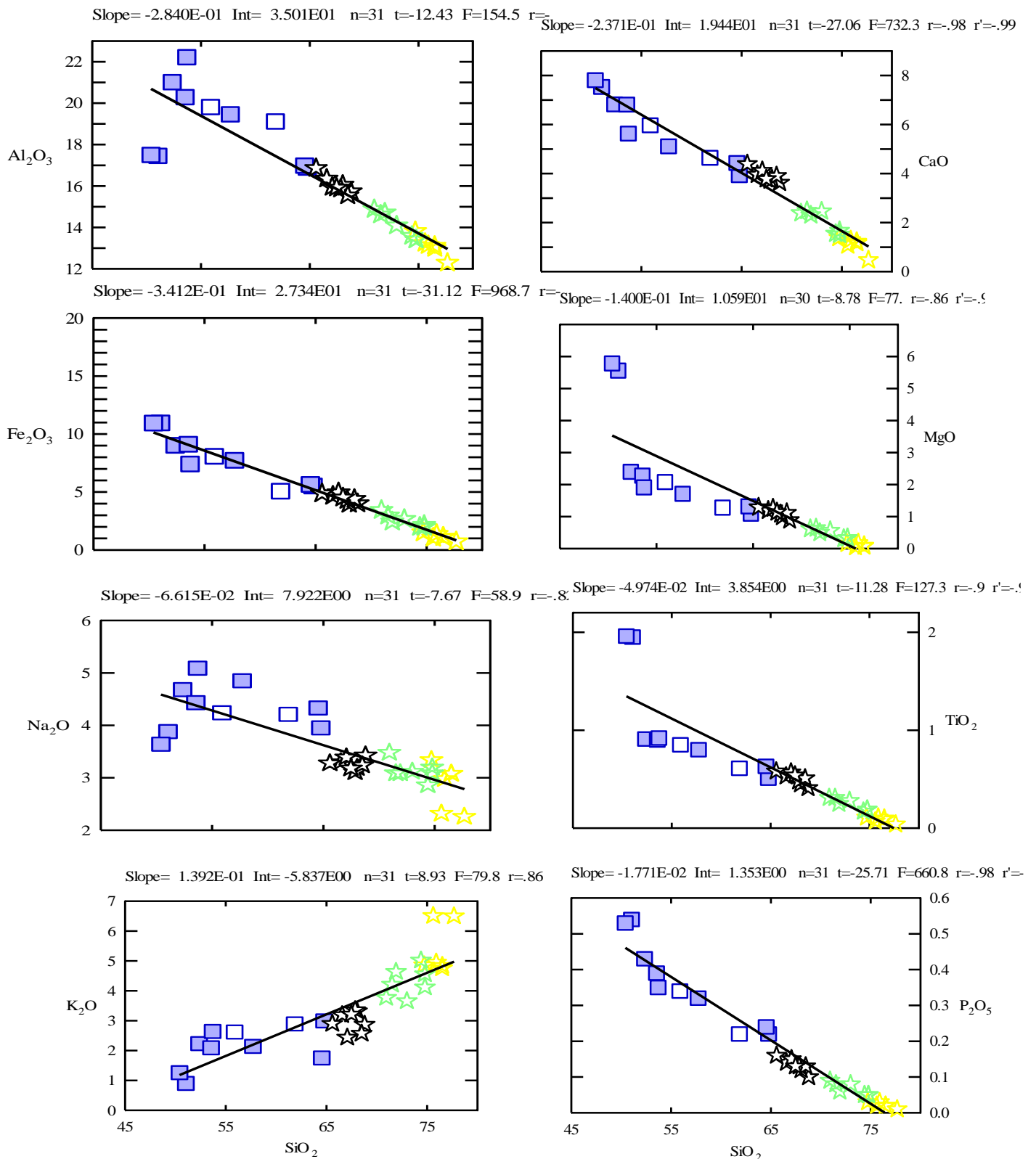


Figure 2: Harker plots of granite and enclave samples from this study showing major elements vs SiO_2 . Regression line ($y=mx+c$) showing regression parameters; Slope(m)= slope gradient, Int(y)=slope intercept, n= number of samples, r=Pearson's coefficient and r'= Spearman's rank correlation coefficient. ($\text{E-}01=10^{-1}$).

Trace element chemistry

Table 2a: Table showing trace element chemistry of samples

Sample	Unit	Barbey	Locality	Sc	V	Cr	Co	Ni	Cu	Zn	Rb	Sr	Y	Zr	Nb
BG1	leuco	inner	G	7.72	13.50	10.53	157.56	7.14	4.19	31.67	158.25	52.96	9.44	75.96	10.22
BG10	leuco	inner	F	6.85	14.20	10.96	165.22	6.20	3.89	52.17	146.21	58.69	13.75	93.37	6.96
BG18	leuco	inner	M	5.74	9.76	11.02	163.15	7.79	3.77	31.25	158.93	47.93	14.26	76.98	8.26
BG19	leuco	inner	M	6.30	12.12	14.82	169.39	8.53	3.54	31.13	164.60	42.68	13.03	74.74	7.66
BG25	leuco	Inner	D	4.42	20.69	11.43	143.89	6.49	2.89	22.76	180.58	126.67	11.70	99.20	3.30
BG32	leuco	inner	N	3.79	14.21	10.28	132.73	6.40	2.80	16.04	177.30	68.94	17.75	65.08	3.35
Sa14	monzogranite	inner	Bet.08	BD	7.00	BD	1.00	BD	BD	25.00	141.00	72.00	13.00	89.00	4.00
Sa25	monzogranite	inner	Bet.08	BD	10.00	BD	1.00	BD	BD	25.00	143.00	77.00	15.00	79.00	5.00
Sa17c	monzogranite	middle	Bet.08	BD	8.00	BD	1.00	BD	BD	23.00	136.00	67.00	14.00	91.00	6.00
Sa22c	ND	middle	Bet.08	BD	6.00	BD	1.00	BD	BD	25.00	123.00	70.00	11.00	93.00	6.00
BG2	med	middle	I	11.23	34.29	17.27	161.94	8.07	16.85	72.50	125.06	128.15	16.89	169.22	13.88
BG23	leuco-med	middle	D	8.08	35.20	14.11	141.01	7.86	7.30	38.48	147.77	173.19	13.30	152.75	9.43
BG24	leuco-med	middle	D	9.01	41.49	13.32	131.09	8.38	9.75	63.21	156.82	181.92	15.29	181.39	11.62
BG27	med	middle	D	8.11	35.39	10.95	135.07	7.43	6.58	44.22	145.94	130.75	9.22	121.41	10.30
BG3	med	middle	I	7.99	22.07	12.62	147.95	7.76	5.46	45.58	124.08	99.52	11.78	114.35	7.85
BG30	med	middle	N	10.38	19.30	15.74	151.58	5.69	4.36	44.05	139.06	96.14	20.85	142.02	11.95
BG31	med	middle	N	8.20	23.00	11.95	195.03	6.69	8.00	52.62	137.27	102.08	19.74	138.59	11.82
Sa24	ND	middle	Bet.08	BD	36.00	BD	3.00	BD	BD	62.00	118.00	108.00	12.00	164.00	11.00
Sa17s	schlieren	middle	Bet.08	BD	20.00	BD	4.00	BD	BD	80.00	137.00	93.00	24.00	165.00	22.00
Sa22s	schlieren	middle	Bet.08	BD	64.00	6.00	9.00	BD	BD	169.00	234.00	85.00	48.00	488.00	38.00
Sa19b	enclave	middle	Bet.08	BD	28.00	BD	5.00	BD	BD	94.00	119.00	80.00	25.00	153.00	17.00
BG21	enclave	middle	D	16.44	57.13	9.45	88.84	8.19	7.01	63.35	124.22	205.34	41.49	268.99	13.88
BG22	enclave	middle	D	14.14	60.74	10.43	90.21	9.75	19.43	93.37	126.43	200.49	27.40	306.19	15.56
BG29	enclave	middle	D	21.41	47.90	9.90	55.15	5.17	9.25	86.86	153.37	197.74	50.72	556.54	19.79
BG8	enclave	enclave	F	33.61	224.53	109.31	52.73	48.20	32.17	84.29	20.14	461.32	48.97	324.38	18.21
BG9	enclave	enclave	F	35.82	237.41	113.14	74.51	50.10	49.25	101.51	29.85	509.44	47.64	327.15	18.28
Sa21	enclave	middle	Bet.08	BD	56.00	BD	6.00	BD	BD	98.00	108.00	90.00	17.00	201.00	12.00
Sa18	enclave	middle	Bet.08	BD	23.00	BD	4.00	BD	BD	80.00	106.00	89.00	18.00	305.00	15.00
BG13	Hbl-bearing	outer	C	13.50	55.21	12.77	110.25	7.82	6.29	48.56	90.75	214.45	19.60	210.33	10.79
BG14	Hbl-bearing	outer	C	15.09	60.34	12.76	136.55	5.94	13.39	49.01	92.39	204.79	19.85	197.88	10.32
BG26	Hbl-bearing	outer	D	16.00	58.32	14.02	117.13	9.06	8.12	58.75	129.28	199.14	26.71	218.61	13.49
BG33	Hbl-bearing	outer	H	15.54	66.32	13.77	124.61	9.96	12.10	51.68	96.26	230.31	24.83	245.00	12.80
BG34	Hbl-bearing	outer	H	16.40	69.52	18.17	108.17	8.40	2.79	63.18	109.14	243.14	28.65	266.31	14.86
BG35	Hbl-bearing	outer	H	15.15	74.55	14.96	109.28	8.33	6.49	64.14	101.92	229.24	27.30	276.70	15.08
BG36	Hbl-bearing	outer	H	15.88	67.70	19.31	118.80	7.43	13.25	56.43	110.03	239.35	27.29	257.09	14.73
BG48	Hbl-bearing	outer	B	15.41	74.37	15.29	113.25	6.72	11.48	58.04	95.58	268.96	23.70	283.98	11.88
Sa05b	granodiorite	outer	Bet.08	BD	57.00	7.00	6.00	BD	BD	81.00	99.00	176.00	16.00	250.00	13.00
Sa15	granodiorite	outer	Bet.08	BD	43.00	10.00	5.00	BD	BD	57.00	108.00	195.00	17.00	177.00	9.00
Sa04	ND	outer	Bet.08	BD	29.00	BD	4.00	BD	BD	50.00	66.00	182.00	11.00	195.00	7.00
Sa10	granodiorite	outer	Bet.08	BD	39.00	BD	3.00	BD	BD	53.00	110.00	140.00	17.00	161.00	9.00
Sa13b	ND	outer	Bet.08	BD	29.00	BD	3.00	BD	BD	43.00	99.00	160.00	14.00	175.00	8.00
Sa13a	MME	outer	Bet.08	BD	38.00	BD	4.00	BD	BD	55.00	117.00	180.00	18.00	233.00	10.00
Sa07	monzogranite	outer	Bet.08	BD	12.00	BD	1.00	BD	BD	23.00	111.00	131.00	7.00	103.00	4.00
Sa08	ND	outer	Bet.08	BD	116.00	9.00	14.00	BD	BD	175.00	254.00	119.00	44.00	539.00	30.00
Sa09	bt-rich layer	outer	Bet.08	BD	91.00	10.00	11.00	BD	BD	141.00	182.00	150.00	36.00	381.00	23.00
Sa05a	enclave	outer	Bet.08	BD	162.00	45.00	16.00	17.00	BD	173.00	138.00	135.00	53.00	100.00	11.00
BG38	enclave	outer	H	49.29	119.96	11.82	55.08	8.15	9.16	102.03	116.32	266.21	84.62	509.45	23.77
BG15	enclave	outer	C	43.98	106.38	10.78	64.28	5.67	8.80	99.98	109.65	274.80	65.52	479.07	20.80
BG16	enclave	outer	C	12.84	104.51	12.46	58.71	8.51	2.55	100.29	160.14	273.83	54.48	1052.51	20.76
BG15	mix	outer	C	13.31	73.43	11.38	72.95	6.29	4.13	68.72	123.63	255.05	36.17	741.96	14.52
BG16	mix	outer	C	35.30	97.23	13.14	66.44	7.59	7.90	96.23	118.97	259.37	54.93	479.98	18.62

Table 2b: Table showing trace element chemistry of samples

Sample	Unit	Barbey	locality	Mo	Sn	Cs	Ba	La	Ce	Pr	Nd	Sm	Eu	Gd	Tb
BG1	leuco	inner	G	1.04	1.52	1.61	259.24	14.56	35.31	3.78	14.57	3.07	0.37	2.41	0.31
BG10	leuco	inner	F	0.87	2.57	1.95	316.35	15.71	35.38	3.99	14.57	3.22	0.50	2.47	0.33
BG18	leuco	inner	M	0.81	3.44	1.62	227.49	12.23	26.35	2.98	11.87	2.86	0.43	2.60	0.42
BG19	leuco	inner	M	0.99	3.22	1.90	201.62	10.85	23.98	2.65	10.73	2.66	0.37	2.15	0.35
BG25	leuco	Inner	D	0.83	1.57	1.98	950.99	20.43	45.76	4.94	18.14	3.41	0.68	2.32	0.33
BG32	leuco	inner	N	1.07	1.64	1.63	521.91	13.59	30.83	3.51	13.08	2.78	0.45	2.43	0.41
Sa14	monzogranite	inner	Bet.08	BD	BD	2.00	294.00	11.90	24.50	3.09	10.70	2.55	0.69	2.05	0.35
Sa25	monzogranite	inner	Bet.08	BD	BD	2.00	301.00	8.10	16.50	2.11	7.88	2.12	0.57	2.21	0.40
Sa17c	monzogranite	middle	Bet.08	BD	BD	2.00	305.00	15.10	31.40	3.83	13.80	3.13	0.51	2.46	0.35
Sa22c	ND	middle	Bet.08	BD	BD	2.00	285.00	17.60	37.50	4.51	15.90	3.09	0.49	2.28	0.32
BG2	med	middle	I	0.92	2.96	2.28	769.83	35.42	67.89	7.46	27.02	5.04	0.81	4.29	0.57
BG23	leuco-med	middle	D	1.02	3.52	1.65	1147.75	46.14	87.35	9.70	36.10	6.15	1.05	4.33	0.50
BG24	leuco-med	middle	D	1.04	3.61	1.83	1151.99	50.62	98.08	10.80	39.23	6.17	1.08	4.95	0.59
BG27	med	middle	D	0.85	3.39	2.42	723.47	28.21	62.42	6.26	22.23	3.89	0.74	2.82	0.36
BG3	med	middle	I	0.91	1.83	1.81	719.78	29.37	60.99	6.66	24.26	3.97	0.67	2.80	0.39
BG30	med	middle	N	0.70	2.95	1.64	583.11	42.40	82.98	9.51	36.36	6.54	0.66	5.15	0.61
BG31	med	middle	N	0.88	2.87	2.04	477.05	30.00	61.05	6.90	26.53	4.97	0.79	3.91	0.51
Sa24	ND	middle	Bet.08	BD	BD	1.00	335.00	35.30	69.50	8.17	29.20	5.43	0.76	3.84	0.52
Sa17s	schlieren	middle	Bet.08	BD	BD	4.00	327.00	45.60	90.90	10.34	37.00	6.56	0.69	4.91	0.78
Sa22s	schlieren	middle	Bet.08	BD	BD	6.00	313.00	128.00	265.00	31.60	112.00	20.60	0.79	12.80	1.85
Sa19b	enclave	middle	Bet.08	BD	BD	2.00	80.00	36.20	69.00	8.96	33.50	6.99	0.63	5.54	0.76
BG21	enclave	middle	D	0.86	4.29	1.27	665.20	56.07	105.64	11.94	46.34	9.74	1.30	9.09	1.31
BG22	enclave	middle	D	0.97	3.63	1.64	261.85	58.59	108.29	11.51	41.79	7.84	1.16	6.78	1.01
BG29	enclave	middle	D	1.01	4.78	2.52	289.51	49.57	96.63	11.45	47.49	10.88	1.25	10.86	1.56
BG8	enclave	enclave	F	1.35	2.92	0.53	464.15	36.30	78.66	10.28	44.73	9.89	2.48	9.33	1.38
BG9	enclave	enclave	F	1.95	3.24	1.18	488.76	36.80	82.12	10.39	47.24	10.57	2.72	9.61	1.42
Sa21	enclave	middle	Bet.08	BD	BD	1.00	148.00	33.70	66.80	7.76	27.80	5.42	0.70	4.29	0.59
Sa18	enclave	middle	Bet.08	BD	BD	1.00	78.00	37.40	72.40	8.00	28.70	5.51	0.64	4.48	0.67
BG13	Hbl-bearing	outer	C	0.93	2.45	1.58	1281.62	42.16	79.46	8.58	31.97	5.87	1.31	4.38	0.64
BG14	Hbl-bearing	outer	C	1.01	2.20	1.68	1222.49	50.51	96.25	10.15	37.81	6.02	1.22	4.92	0.62
BG26	Hbl-bearing	outer	D	0.99	3.33	1.54	650.71	33.85	66.29	7.21	28.73	5.79	1.16	5.88	0.84
BG33	Hbl-bearing	outer	H	1.12	3.40	1.35	840.83	54.10	100.13	10.90	42.84	8.05	1.37	5.99	0.75
BG34	Hbl-bearing	outer	H	1.22	3.17	1.73	1235.99	59.10	109.88	12.13	46.97	8.83	1.41	6.67	0.88
BG35	Hbl-bearing	outer	H	0.90	3.70	1.45	674.89	66.26	123.00	13.45	51.58	8.83	1.43	6.65	0.93
BG36	Hbl-bearing	outer	H	1.00	3.36	1.40	1234.41	65.66	118.88	13.27	47.92	7.89	1.45	6.51	0.84
BG48	Hbl-bearing	outer	B	0.78	4.04	1.86	1319.49	67.70	122.15	13.26	49.33	7.83	1.65	6.14	0.78
Sa05b	granodiorite	outer	Bet.08	BD	BD	3.00	408.00	40.00	76.50	8.53	28.80	4.92	1.20	3.71	0.56
Sa15	granodiorite	outer	Bet.08	BD	BD	4.00	1197.00	49.90	95.20	10.56	36.80	6.06	1.23	3.88	0.60
Sa04	ND	outer	Bet.08	BD	BD	2.00	399.00	19.70	37.30	4.10	14.60	2.78	1.08	2.32	0.34
Sa10	granodiorite	outer	Bet.08	BD	BD	2.00	867.00	41.30	78.90	8.96	31.70	5.18	1.15	3.92	0.58
Sa13b	ND	outer	Bet.08	BD	BD	2.00	921.00	37.80	65.00	27.20	7.93	4.69	1.08	3.38	0.49
Sa13a	MME	outer	Bet.08	BD	BD	2.00	1077.00	49.70	93.20	35.30	10.11	5.76	1.22	4.44	0.62
Sa07	monzogranite	outer	Bet.08	BD	BD	1.00	940.00	16.30	32.40	3.67	13.50	2.28	0.97	1.70	0.24
Sa08	ND	outer	Bet.08	BD	BD	5.00	683.00	214.00	381.00	141.00	41.80	21.50	1.34	14.30	1.80
Sa09	bt-rich layer	outer	Bet.08	BD	BD	3.00	640.00	122.00	240.00	26.39	93.00	14.70	1.40	9.48	1.39
Sa05a	enclave	outer	Bet.08	BD	BD	4.00	185.00	9.31	30.20	5.54	29.20	9.31	1.35	9.80	1.58
BG38	enclave	outer	H	0.87	5.07	1.96	392.82	11.51	30.18	5.56	33.71	13.62	2.17	15.66	2.51
BG15	enclave	outer	C	0.87	10.73	1.81	470.48	20.24	51.16	8.06	43.09	13.35	2.18	12.51	2.04
BG16	enclave	outer	C	1.04	6.66	6.41	330.36	143.39	258.00	27.60	101.25	15.48	1.91	11.62	1.59
BG15	mix	outer	C	0.89	4.82	4.00	797.20	113.62	211.33	22.67	82.22	12.85	1.63	9.20	1.22
BG16	mix	outer	C	0.77	10.40	1.93	741.13	48.53	95.03	11.76	51.58	12.34	1.93	11.24	1.76

Table 2c: Table showing trace element chemistry of samples

Sample	KC	Unit	Barbey	locality	Dy	Ho	Er	Tm	Yb	Lu	Hf	Ta	W	Pb	Th	U	LREE	HREE
BG1	11	leuco	inner	G	1.73	0.33	1.05	0.18	1.19	0.20	2.52	0.42	962.19	38.04	9.64	2.46	74.07	4.98
BG10	11	leuco	inner	F	2.06	0.44	1.49	0.24	2.07	0.34	3.20	0.59	1069.10	35.66	10.27	2.91	75.84	6.97
BG18	11	leuco	inner	M	2.84	0.55	1.37	0.23	1.50	0.27	2.69	0.79	1007.09	32.66	17.50	2.64	59.32	7.17
BG19	11	leuco	inner	M	2.28	0.44	1.15	0.17	1.20	0.19	2.52	0.70	1028.28	37.71	14.44	2.77	53.39	5.79
BG25	11	leuco	Inner	D	2.07	0.43	1.29	0.20	1.48	0.23	3.14	0.37	888.65	35.47	11.03	2.79	95.67	6.02
BG32	11	leuco	inner	N	2.76	0.59	2.01	0.36	2.55	0.41	2.76	0.40	842.18	40.73	18.74	3.83	66.66	9.09
Sa14	7	monzogranite	inner	Bet.08	2.16	0.40	1.19	0.16	1.09	0.20	3.00	BD	BD	BD	9.00	3.00	55.48	5.55
Sa25	7	monzogranite	inner	Bet.08	2.36	0.51	1.41	0.23	1.52	0.23	3.00	BD	BD	BD	9.00	3.00	39.49	6.66
Sa17c	7	monzogranite	middle	Bet.08	1.95	0.41	1.33	0.18	1.42	0.26	3.00	BD	BD	BD	9.00	2.00	70.23	5.90
Sa22c	7	ND	middle	Bet.08	1.74	0.34	0.97	0.14	0.95	0.18	3.00	BD	BD	BD	11.00	2.00	81.37	4.64
BG2	29	med	middle	I	3.10	0.60	1.67	0.26	1.51	0.23	4.46	0.71	985.76	19.88	11.58	1.61	147.92	7.95
BG23	29	leuco-med	middle	D	2.84	0.54	1.29	0.16	1.20	0.13	4.26	0.53	854.60	23.24	17.49	1.61	190.81	6.66
BG24	29	leuco-med	middle	D	3.57	0.64	1.41	0.20	1.35	0.18	5.01	0.60	828.70	24.81	19.56	1.56	210.93	7.94
BG27	29	med	middle	D	1.94	0.36	0.87	0.12	0.75	0.11	3.26	0.51	876.73	25.99	11.45	2.19	126.56	4.52
BG3	29	med	middle	I	2.11	0.42	1.12	0.18	1.24	0.18	3.25	0.47	923.74	24.63	12.34	1.70	128.73	5.64
BG30	29	med	middle	N	3.72	0.67	2.26	0.37	2.26	0.34	4.27	0.75	928.59	26.42	18.72	1.85	183.60	10.24
BG31	29	med	middle	N	3.44	0.68	2.18	0.36	2.29	0.34	4.20	0.79	1229.16	24.82	14.64	2.24	134.15	9.81
Sa24	7	ND	middle	Bet.08	2.44	0.40	1.17	0.15	0.94	0.18	5.00	BD	BD	BD	13.00	2.00	152.20	5.80
Sa17s	7	schlieren	middle	Bet.08	4.11	0.78	2.23	0.29	2.00	0.39	5.00	BD	BD	BD	16.00	3.00	196.00	10.58
Sa22s	7	schlieren	middle	Bet.08	9.43	1.64	4.40	0.59	3.72	0.67	16.00	BD	BD	BD	52.00	5.00	570.79	22.30
Sa19b	7	enclave	middle	Bet.08	4.10	0.81	2.22	0.30	1.88	0.28	4.00	BD	BD	BD	11.00	1.00	160.82	10.35
BG21	4	enclave	middle	D	8.29	1.50	4.32	0.57	3.45	0.47	6.65	0.78	511.38	16.36	16.78	3.19	240.12	19.90
BG22	4	enclave	middle	D	5.67	1.08	2.75	0.33	2.08	0.28	6.61	0.58	514.00	13.32	14.25	0.81	235.96	13.20
BG29	4	enclave	middle	D	9.71	2.00	4.92	0.64	4.00	0.56	11.60	0.85	268.04	14.83	15.28	0.92	228.13	23.39
BG8	4	enclave	enclave	F	9.06	1.76	5.10	0.72	4.77	0.68	6.81	0.92	104.84	8.27	4.41	0.75	191.66	23.48
BG9	4	enclave	enclave	F	9.15	1.84	5.29	0.72	4.70	0.77	6.92	0.99	218.09	6.92	4.50	1.14	199.45	23.87
Sa21	8	enclave	middle	Bet.08	2.98	0.53	1.49	0.22	1.28	0.24	5.00	BD	BD	BD	10.00	1.00	146.47	7.33
Sa18	8	enclave	middle	Bet.08	3.53	0.64	1.61	0.23	1.56	0.26	8.00	BD	BD	BD	10.00	2.00	157.13	8.50
BG13	12	Hbl-bearing	outer	C	3.98	0.75	2.22	0.33	2.20	0.30	5.45	0.61	667.27	13.40	10.77	1.94	173.72	10.42
BG14	12	Hbl-bearing	outer	C	3.44	0.74	1.98	0.29	1.84	0.29	5.01	0.52	802.03	10.93	11.94	2.16	206.89	9.20
BG26	12	Hbl-bearing	outer	D	5.27	1.03	2.83	0.41	2.44	0.36	5.34	0.75	710.41	17.17	11.66	2.32	148.91	13.19
BG33	12	Hbl-bearing	outer	H	4.96	0.96	2.61	0.38	2.64	0.35	6.33	0.63	715.91	12.11	14.03	1.72	223.38	12.65
BG34	12	Hbl-bearing	outer	H	5.90	1.09	3.00	0.41	2.78	0.38	6.53	0.65	618.23	13.88	15.24	1.53	244.98	14.44
BG35	12	Hbl-bearing	outer	H	5.31	1.08	2.83	0.39	2.57	0.35	6.78	0.72	649.63	11.95	16.48	1.75	271.21	13.45
BG36	12	Hbl-bearing	outer	H	5.08	0.98	2.88	0.36	2.56	0.36	6.35	0.71	674.43	13.86	15.20	1.51	261.58	13.07
BG48	12	Hbl-bearing	outer	B	4.70	0.91	2.50	0.33	2.30	0.36	6.93	0.54	693.45	12.39	14.14	1.86	268.05	11.88
Sa05b	7	granodiorite	outer	Bet.08	2.98	0.56	1.55	0.24	1.46	0.24	6.00	BD	BD	BD	9.00	1.00	163.66	7.59
Sa15	7	granodiorite	outer	Bet.08	3.12	0.59	1.62	0.21	1.51	0.24	4.00	BD	BD	BD	15.00	2.00	203.63	7.89
Sa04	7	ND	outer	Bet.08	1.92	0.37	1.08	0.17	1.06	0.19	5.00	BD	BD	BD	6.00	7.00	81.88	5.13
Sa10	7	granodiorite	outer	Bet.08	3.07	0.55	1.59	0.24	1.63	0.27	4.00	BD	BD	BD	13.00	2.00	171.11	7.93
Sa13b	7	ND	outer	Bet.08	2.59	0.48	1.35	0.21	1.45	0.24	5.00	BD	BD	BD	9.00	2.00	147.08	6.81
Sa13a	8	MME	outer	Bet.08	3.40	0.64	1.71	0.26	1.91	0.30	6.00	BD	BD	BD	12.00	2.00	199.73	8.84
Sa07	7	monzogranite	outer	Bet.08	1.27	0.25	0.71	0.11	0.82	0.12	3.00	BD	BD	BD	7.00	1.00	70.82	3.52
Sa08	7	ND	outer	Bet.08	8.79	1.55	4.04	0.58	3.82	0.61	14.00	BD	BD	BD	53.00	3.00	814.94	21.19
Sa09	7	bt-rich layer	outer	Bet.08	7.19	1.23	3.39	0.45	2.80	0.47	10.00	BD	BD	BD	37.00	3.00	506.97	16.92
Sa05a	8	enclave	outer	Bet.08	10.10	1.81	4.95	0.73	4.40	0.62	3.00	BD	BD	BD	2.00	1.00	94.71	24.19
BG38	4	enclave	outer	H	16.39	3.24	8.75	1.22	7.28	0.96	11.01	0.72	222.23	11.80	2.24	0.74	112.41	40.36
BG15	4	enclave	outer	C	13.19	2.54	6.78	0.94	5.86	0.81	10.32	0.63	292.08	10.34	3.78	1.10	150.61	32.16
BG16	4	enclave	outer	C	9.83	1.98	5.87	0.80	6.10	1.03	25.24	1.22	257.24	13.72	36.79	2.58	559.25	27.20
BG15	3	mix	outer	C	7.16	1.39	3.97	0.60	4.15	0.62	18.55	0.87	416.01	14.94	30.91	2.94	453.52	19.11
BG16	3	mix	outer	C	11.02	2.11	5.69	0.77	4.98	0.70	10.72	0.64	310.88	12.08	10.60	1.14	232.42	27.03

Appendix III: Mineral Chemistry

Plagioclase

Table 1: Representative plagioclase analyses from enclaves For all tables in this section: $An\% = Ca/(Ca+Na+K)*100$. An(%) content was only calculated for accurate plagioclase compositions.

Type	Enclave																			
Sample	BG12D					BG15A					BG29					BG44				
Spot No.	1	2	4	5	9	11	8	10	14	15	1	2	3	4	5	1	2	3	4	5
SiO ₂	59.58	59.43	59.47	60.08	59.35	63.08	59.90	60.15	58.16	59.69	58.03	57.54	60.35	60.44	60.86	60.19	59.31	59.46	60.03	59.96
TiO ₂	0.00	0.00	0.00	0.00	0.00	0.00	0.00	0.00	0.00	0.00	0.00	0.00	0.00	0.00	0.00	0.00	0.00	0.00	0.00	0.00
Al ₂ O ₃	25.65	25.13	25.71	25.59	25.99	23.06	25.46	24.93	26.27	25.40	26.08	27.05	25.01	24.67	24.61	25.09	25.31	25.42	25.10	24.90
FeO	0.15	0.15	0.00	0.00	0.00	0.00	0.00	0.00	0.00	0.18	0.16	0.00	0.00	0.00	0.00	0.00	0.00	0.16	0.14	0.00
MnO	0.00	0.00	0.00	0.00	0.00	0.00	0.00	0.00	0.00	0.00	0.00	0.00	0.00	0.00	0.00	0.00	0.00	0.00	0.00	0.00
MgO	0.00	0.00	0.00	0.00	0.00	0.00	0.00	0.00	0.00	0.00	0.00	0.00	0.00	0.00	0.00	0.00	0.00	0.00	0.00	0.00
CaO	7.70	7.39	7.65	7.49	8.18	2.79	7.48	7.07	8.60	7.43	8.47	9.18	6.91	6.77	6.68	7.11	7.67	7.49	7.22	7.15
BaO	0.00	0.00	0.00	0.00	0.00	0.00	0.00	0.00	0.00	0.00	0.00	0.00	0.00	0.00	0.00	0.00	0.00	0.00	0.00	0.00
Na ₂ O	7.44	7.59	7.42	7.60	7.19	9.19	7.49	7.71	6.87	7.38	6.95	6.79	7.95	8.07	8.07	7.76	7.33	7.60	7.65	7.60
K ₂ O	0.18	0.10	0.18	0.12	0.15	0.71	0.14	0.17	0.08	0.30	0.24	0.00	0.20	0.13	0.11	0.12	0.00	0.08	0.16	0.14
Total	100.71	99.79	100.45	100.89	100.87	98.82	100.46	100.03	99.99	100.38	99.93	100.56	100.42	100.07	100.33	100.27	99.62	100.21	100.30	99.76
Si	2.64	2.65	2.64	2.65	2.63	2.82	2.66	2.68	2.60	2.65	2.60	2.56	2.67	2.68	2.70	2.67	2.66	2.64	2.67	2.68
Ti	0.00	0.00	0.00	0.00	0.00	0.00	0.00	0.00	0.00	0.00	0.00	0.00	0.00	0.00	0.00	0.00	0.00	0.00	0.00	0.00
Al	1.34	1.32	1.35	1.33	1.36	1.21	1.33	1.31	1.39	1.33	1.38	1.42	1.31	1.29	1.29	1.31	1.34	1.33	1.31	1.31
Fe ²⁺	0.01	0.01	0.00	0.00	0.00	0.00	0.00	0.00	0.00	0.01	0.01	0.00	0.00	0.00	0.00	0.00	0.00	0.01	0.01	0.00
Mn	0.00	0.00	0.00	0.00	0.00	0.00	0.00	0.00	0.00	0.00	0.00	0.00	0.00	0.00	0.00	0.00	0.00	0.00	0.00	0.00
Mg	0.00	0.00	0.00	0.00	0.00	0.00	0.00	0.00	0.00	0.00	0.00	0.00	0.00	0.00	0.00	0.00	0.00	0.00	0.00	0.00
Ca	0.37	0.35	0.36	0.35	0.39	0.13	0.36	0.34	0.41	0.35	0.41	0.44	0.33	0.32	0.32	0.34	0.37	0.36	0.34	0.34
Ba	0.00	0.00	0.00	0.00	0.00	0.00	0.00	0.00	0.00	0.00	0.00	0.00	0.00	0.00	0.00	0.00	0.00	0.00	0.00	0.00
Na	0.64	0.66	0.64	0.65	0.62	0.80	0.64	0.67	0.60	0.64	0.60	0.59	0.68	0.69	0.69	0.67	0.64	0.66	0.66	0.66
K	0.01	0.01	0.01	0.01	0.01	0.04	0.01	0.01	0.00	0.02	0.01	0.00	0.01	0.01	0.01	0.01	0.00	0.00	0.01	0.01
Tot.cat.	5.00	5.00	5.00	5.00	5.00	5.00	5.00	5.00	5.00	5.00	5.00	5.00	5.00	5.00	5.00	5.00	5.00	5.00	5.00	5.00
An	36.01	34.77	35.92	35.01	38.26	13.76	35.29	33.31	40.69	35.12	39.71	42.76	32.09	31.46	31.18	33.37	36.64	35.13	33.98	33.95
Ab	62.97	64.66	63.06	64.30	60.89	82.09	63.93	65.76	58.84	63.18	0.59	0.57	0.67	0.68	0.68	65.96	63.36	64.44	65.14	65.24
Or	1.02	0.57	1.02	0.69	0.85	4.15	0.77	0.93	0.47	1.70	0.01	0.00	0.01	0.01	0.01	0.67	0.00	0.43	0.88	0.81

Table 2: Representative analyses of plagioclase from granites

Type	Granite																							
Sample	BG10						BG12C2						BG12D						BG13A					
Spot																								
No.	6	7	8	9	10	11	5	4	6	7	8	9	6	4	8	9	10	8	9	10	12	13		
SiO ₂	62.74	68.08	68.50	63.45	65.25	62.78	60.36	57.94	59.47	59.52	58.71	59.24	60.38	58.36	60.77	60.20	59.65	57.83	60.47	59.45	60.04	59.42		
TiO ₂	0.00	0.00	0.00	0.00	0.00	0.00	0.00	0.00	0.00	0.00	0.00	0.00	0.00	0.00	0.00	0.00	0.00	0.00	0.00	0.00	0.00	0.00		
Al ₂ O ₃	22.50	19.34	19.52	22.82	21.33	22.82	24.94	25.97	25.29	25.14	25.31	25.08	25.37	26.22	25.14	24.84	25.24	26.39	24.27	24.65	24.80	24.85		
FeO	0.00	0.00	0.00	0.00	0.00	0.00	0.21	0.00	0.00	0.00	0.00	0.00	0.00	0.15	0.00	0.00	0.00	0.00	0.00	0.00	0.00	0.15		
MnO	0.00	0.00	0.00	0.00	0.00	0.00	0.00	0.00	0.00	0.00	0.00	0.00	0.00	0.00	0.00	0.00	0.00	0.00	0.00	0.00	0.00	0.00		
MgO	0.00	0.00	0.00	0.00	0.00	0.00	0.00	0.00	0.00	0.00	0.00	0.00	0.00	0.00	0.00	0.00	0.00	0.00	0.00	0.00	0.00	0.00		
CaO	4.40	0.57	0.31	4.39	2.75	4.67	7.10	8.07	7.37	7.24	7.59	7.27	7.12	8.42	7.00	7.04	7.63	8.79	6.55	6.75	6.96	7.13		
BaO	0.00	0.00	0.00	0.00	0.00	0.00	0.00	0.00	0.00	0.00	0.00	0.00	0.00	0.00	0.00	0.00	0.00	0.00	0.00	0.00	0.00	0.00		
Na ₂ O	8.94	11.50	11.66	9.32	10.26	8.98	7.72	7.09	7.50	7.46	7.46	7.53	7.76	6.94	7.79	7.62	7.55	6.68	7.87	7.49	7.60	7.54		
K ₂ O	0.26	0.00	0.00	0.20	0.07	0.13	0.16	0.20	0.13	0.10	0.15	0.11	0.13	0.14	0.20	0.14	0.10	0.11	0.16	0.21	0.25	0.14		
Total	98.83	99.49	99.99	100.16	99.68	99.38	100.49	99.28	99.77	99.46	99.21	99.23	100.76	100.22	100.90	99.84	100.18	99.79	99.31	98.56	99.78	99.23		
Si	2.81	2.99	2.99	2.80	2.88	2.80	2.68	2.61	2.66	2.67	2.64	2.66	2.67	2.60	2.68	2.69	2.65	2.59	2.71	2.69	2.68	2.67		
Ti	0.00	0.00	0.00	0.00	0.00	0.00	0.00	0.00	0.00	0.00	0.00	0.00	0.00	0.00	0.00	0.00	0.00	0.00	0.00	0.00	0.00	0.00		
Al	1.19	1.00	1.01	1.19	1.11	1.20	1.30	1.38	1.33	1.33	1.34	1.33	1.32	1.38	1.31	1.31	1.32	1.40	1.28	1.31	1.31	1.32		
Fe ²⁺	0.00	0.00	0.00	0.00	0.00	0.00	0.01	0.00	0.00	0.00	0.00	0.00	0.00	0.01	0.00	0.00	0.00	0.00	0.00	0.00	0.00	0.01		
Mn	0.00	0.00	0.00	0.00	0.00	0.00	0.00	0.00	0.00	0.00	0.00	0.00	0.00	0.00	0.00	0.00	0.00	0.00	0.00	0.00	0.00	0.00		
Mg	0.00	0.00	0.00	0.00	0.00	0.00	0.00	0.00	0.00	0.00	0.00	0.00	0.00	0.00	0.00	0.00	0.00	0.00	0.00	0.00	0.00	0.00		
Ca	0.21	0.03	0.01	0.21	0.13	0.22	0.34	0.39	0.35	0.35	0.37	0.35	0.34	0.40	0.33	0.34	0.36	0.42	0.31	0.33	0.33	0.34		
Ba	0.00	0.00	0.00	0.00	0.00	0.00	0.00	0.00	0.00	0.00	0.00	0.00	0.00	0.00	0.00	0.00	0.00	0.00	0.00	0.00	0.00	0.00		
Na	0.78	0.98	0.99	0.80	0.88	0.78	0.66	0.62	0.65	0.65	0.65	0.66	0.66	0.60	0.67	0.66	0.65	0.58	0.68	0.66	0.66	0.66		
K	0.01	0.00	0.00	0.01	0.00	0.01	0.01	0.01	0.01	0.01	0.01	0.01	0.01	0.01	0.01	0.01	0.01	0.01	0.01	0.01	0.01	0.01		
Tot.cat.	500	5.00	5.00	5.00	5.00	5.00	5.00	5.00	5.00	5.00	5.00	5.00	5.00	5.00	5.00	5.00	5.00	5.00	5.00	5.00	5.00	5.00		
An	21.06	2.65	1.43	20.42	12.86	22.14	33.40	38.16	34.94	34.71	35.69	34.56	33.42	39.84	32.82	33.54	35.62	41.85	31.23	32.87	33.14	34.05		
Ab	77.47	97.35	98.57	78.50	86.73	77.12	65.72	60.70	64.33	64.73	63.48	64.80	65.85	59.37	66.06	65.64	63.81	57.54	67.87	65.94	65.47	65.15		
Or	1.48	0.00	0.00	1.08	0.41	0.74	0.88	1.14	0.74	0.56	0.84	0.65	0.72	0.78	1.12	0.82	0.57	0.62	0.91	1.19	1.39	0.80		

Table 2 (continued): Plagioclase in granites

Type	Granite																		
Sample	BG15B					BG26				BG44					BG46A				
Spot																			
No.	5	6	11	12	13	3	7	10	12	1	2	3	8	9	4	5	6	7	8
SiO ₂	59.99	59.42	60.50	58.53	58.68	60.81	59.43	61.03	60.15	60.37	60.05	59.31	60.72	58.86	59.48	59.11	59.23	59.19	59.59
TiO ₂	0.00	0.00	0.24	0.00	0.00	0.00	0.00	0.00	0.00	0.00	0.00	0.00	0.00	0.00	0.00	0.00	0.00	0.00	0.00
Al ₂ O ₃	24.37	25.02	23.58	25.48	25.26	24.06	24.94	23.69	24.27	25.00	25.11	25.20	24.88	26.05	25.35	25.73	25.75	24.79	24.97
FeO	0.18	0.00	0.16	0.00	0.00	0.16	0.19	0.00	0.00	0.15	0.00	0.00	0.00	0.15	0.00	0.00	0.00	0.17	0.00
MnO	0.00	0.00	0.00	0.00	0.00	0.00	0.00	0.00	0.00	0.00	0.00	0.00	0.00	0.00	0.00	0.00	0.00	0.00	0.00
MgO	0.00	0.00	0.00	0.00	0.00	0.00	0.00	0.00	0.00	0.00	0.00	0.00	0.00	0.00	0.00	0.00	0.00	0.00	0.00
CaO	6.94	7.34	5.85	7.87	7.54	6.18	7.11	5.75	6.84	7.09	7.17	7.65	7.11	8.20	7.22	7.77	7.80	7.30	7.22
BaO	0.00	0.00	0.00	0.00	0.00	0.00	0.00	0.00	0.00	0.00	0.00	0.00	0.00	0.00	0.00	0.00	0.00	0.00	0.00
Na ₂ O	7.87	7.35	8.10	7.08	7.21	8.08	7.59	8.37	7.98	7.63	7.68	7.52	7.90	7.18	7.70	7.27	7.13	7.46	7.69
K ₂ O	0.00	0.17	0.22	0.09	0.14	0.27	0.18	0.13	0.14	0.23	0.13	0.15	0.00	0.09	0.12	0.13	0.14	0.16	0.16
Total	99.35	99.30	98.67	99.04	98.82	99.55	99.44	98.96	99.37	100.48	100.14	99.83	100.72	100.52	99.88	100.01	100.05	99.08	99.62
Si	2.69	2.67	2.73	2.64	2.65	2.72	2.66	2.74	2.69	2.68	2.67	2.65	2.69	2.62	2.65	2.64	2.65	2.67	2.66
Ti	0.00	0.00	0.01	0.00	0.00	0.00	0.00	0.00	0.00	0.00	0.00	0.00	0.00	0.00	0.00	0.00	0.00	0.00	0.00
Al	1.29	1.33	1.25	1.35	1.34	1.27	1.32	1.25	1.28	1.31	1.32	1.33	1.30	1.36	1.33	1.35	1.36	1.32	1.32
Fe ²⁺	0.01	0.00	0.01	0.00	0.00	0.01	0.01	0.00	0.00	0.01	0.00	0.00	0.00	0.01	0.00	0.00	0.00	0.01	0.00
Mn	0.00	0.00	0.00	0.00	0.00	0.00	0.00	0.00	0.00	0.00	0.00	0.00	0.00	0.00	0.00	0.00	0.00	0.00	0.00
Mg	0.00	0.00	0.00	0.00	0.00	0.00	0.00	0.00	0.00	0.00	0.00	0.00	0.00	0.00	0.00	0.00	0.00	0.00	0.00
Ca	0.33	0.35	0.28	0.38	0.36	0.30	0.34	0.28	0.33	0.34	0.34	0.37	0.34	0.39	0.34	0.37	0.37	0.35	0.35
Ba	0.00	0.00	0.00	0.00	0.00	0.00	0.00	0.00	0.00	0.00	0.00	0.00	0.00	0.00	0.00	0.00	0.00	0.00	0.00
Na	0.68	0.64	0.71	0.62	0.63	0.70	0.66	0.73	0.69	0.66	0.66	0.65	0.68	0.62	0.67	0.63	0.62	0.65	0.67
K	0.00	0.01	0.01	0.01	0.01	0.02	0.01	0.01	0.01	0.01	0.01	0.01	0.00	0.01	0.01	0.01	0.01	0.01	0.01
Tot.cat.	5.00	5.00	5.00	5.00	5.00	5.00	5.00	5.00	5.00	5.00	5.00	5.00	5.00	5.00	5.00	5.00	5.00	5.00	5.00
An	32.77	35.22	28.16	37.86	36.33	29.26	33.76	27.33	31.89	33.49	33.81	35.68	33.21	38.51	33.91	36.86	37.36	34.76	33.88
Ab	67.23	63.79	70.57	61.64	62.86	69.21	65.23	71.96	67.36	65.20	65.47	63.48	66.79	60.99	65.41	62.40	61.84	64.34	65.25
Or	0.00	0.99	1.28	0.50	0.82	1.53	1.00	0.71	0.75	1.32	0.72	0.85	0.00	0.50	0.67	0.74	0.80	0.90	0.87

All FeO is calculated as Fe²⁺.

Table 3: Scanning electron microscope probe analysis along a traverse of a plagioclase crystal from sample BG44 displayed in Fig.8.

Spot No.	1	2	3	4	5	6	7	8	9	10	11	12	13	14	15
SiO ₃	63.58	60.00	61.03	59.05	59.09	59.90	58.35	56.21	57.94	59.05	60.42	60.47	60.54	61.62	62.85
TiO ₂	0.40	0.00	0.00	0.00	0.00	0.00	0.00	0.00	0.00	0.00	0.00	0.00	0.00	0.00	0.00
Al ₂ O ₃	19.95	25.89	24.51	26.54	26.45	25.87	26.77	28.22	27.26	26.56	25.77	25.31	25.27	24.80	25.67
Cr ₂ O ₃	0.00	0.00	0.00	0.00	0.00	0.00	0.00	0.00	0.00	0.00	0.00	0.00	0.00	0.00	0.00
FeO	0.00	0.00	0.00	0.00	0.00	0.00	0.00	0.00	0.00	0.00	0.00	0.00	0.00	0.00	0.00
MnO	0.00	0.00	0.00	0.00	0.00	0.00	0.00	0.00	0.00	0.00	0.00	0.00	0.00	0.00	0.00
MgO	0.61	0.00	0.00	0.00	0.00	0.00	0.00	0.00	0.00	0.00	0.00	0.00	0.00	0.00	0.00
CaO	4.92	7.51	6.34	8.04	8.20	7.61	8.63	10.13	8.98	8.18	7.14	7.01	6.88	6.42	6.44
Na ₂ O	6.18	7.59	8.11	7.24	7.35	7.66	6.82	5.90	6.57	7.24	7.91	7.96	7.92	8.37	8.77
K ₂ O	0.99	0.08	0.19	0.10	0.11	0.13	0.08	0.00	0.00	0.10	0.09	0.17	0.16	0.17	0.16
Total	96.62	101.08	100.19	100.98	101.20	101.18	100.65	100.47	100.75	101.12	101.33	100.92	100.76	101.38	103.89
Si	2.89	2.65	2.71	2.61	2.61	2.64	2.59	2.51	2.57	2.61	2.66	2.67	2.68	2.71	2.69
Ti	0.01	0.00	0.00	0.00	0.00	0.00	0.00	0.00	0.00	0.00	0.00	0.00	0.00	0.00	0.00
Al	1.07	1.35	1.28	1.38	1.38	1.35	1.40	1.49	1.43	1.38	1.34	1.32	1.32	1.28	1.30
Cr	0.00	0.00	0.00	0.00	0.00	0.00	0.00	0.00	0.00	0.00	0.00	0.00	0.00	0.00	0.00
Fe ²⁺	0.00	0.00	0.00	0.00	0.00	0.00	0.00	0.00	0.00	0.00	0.00	0.00	0.00	0.00	0.00
Mn	0.00	0.00	0.00	0.00	0.00	0.00	0.00	0.00	0.00	0.00	0.00	0.00	0.00	0.00	0.00
Mg	0.04	0.00	0.00	0.00	0.00	0.00	0.00	0.00	0.00	0.00	0.00	0.00	0.00	0.00	0.00
Ca	0.24	0.36	0.30	0.38	0.39	0.36	0.41	0.49	0.43	0.39	0.34	0.33	0.33	0.30	0.30
Na	0.55	0.65	0.70	0.62	0.63	0.66	0.59	0.51	0.57	0.62	0.67	0.68	0.68	0.71	0.73
K	0.06	0.00	0.01	0.01	0.01	0.01	0.00	0.00	0.00	0.01	0.01	0.01	0.01	0.01	0.01
An(%)			29.84	37.82			40.94	48.68	43.03			32.43	32.14		
Distance (mm)	0.00	0.02	0.04	0.06	0.08	0.10	0.12	0.14	0.16	0.18	0.20	0.22	0.24	0.26	0.28
Tot.cat.	4.86	5.01	5.00	5.01	5.02	5.01	5.00	5.00	5.00	5.01	5.01	5.01	5.01	5.01	5.03

Table 3 (cont.): Scanning electron microscope probe analysis along a traverse of a plagioclase crystal from sample BG44 displayed in Fig.8.

Spot No.	16	17	18	19	20	21	22	23	24	25	26	27	28	29	30
SiO ₂	61.57	61.33	60.64	60.27	59.73	58.32	59.57	59.60	60.66	60.52	60.57	60.75	61.22	61.39	65.27
TiO ₂	0.00	0.00	0.00	0.00	0.00	0.00	0.00	0.00	0.00	0.00	0.00	0.00	0.00	0.00	0.00
Al ₂ O ₃	24.85	24.72	25.54	25.55	25.95	26.75	25.95	25.99	25.47	25.45	25.26	25.48	25.25	25.10	23.60
FeO	0.00	0.00	0.00	0.00	0.00	0.00	0.00	0.00	0.00	0.00	0.00	0.00	0.00	0.00	0.00
MnO	0.00	0.00	0.00	0.00	0.00	0.00	0.00	0.00	0.00	0.00	0.00	0.00	0.00	0.00	0.00
MgO	0.00	0.00	0.00	0.00	0.00	0.00	0.00	0.00	0.00	0.00	0.00	0.00	0.00	0.00	0.00
CaO	6.31	6.53	6.92	6.78	7.67	8.69	7.83	7.63	7.12	7.07	7.06	6.99	6.65	6.41	4.66
Na ₂ O	8.41	8.37	8.02	7.92	7.44	6.89	7.40	7.47	7.86	7.88	7.81	7.79	8.19	8.14	9.60
K ₂ O	0.20	0.21	0.19	0.15	0.12	0.19	0.14	0.18	0.11	0.17	0.20	0.17	0.19	0.23	0.16
Total	101.3	101.1	101.3	100.6	100.9	100.8	100.8	100.8	101.2	101.0	100.9	101.1	101.5	101.2	103.2
	3	6	2	8	0	2	9	8	2	8	1	8	1	8	8
Si	2.70	2.70	2.67	2.67	2.64	2.59	2.64	2.64	2.67	2.67	2.68	2.68	2.69	2.70	2.80
Ti	0.00	0.00	0.00	0.00	0.00	0.00	0.00	0.00	0.00	0.00	0.00	0.00	0.00	0.00	0.00
Al	1.29	1.28	1.32	1.33	1.35	1.40	1.35	1.36	1.32	1.32	1.32	1.32	1.31	1.30	1.19
Fe ²⁺	0.00	0.00	0.00	0.00	0.00	0.00	0.00	0.00	0.00	0.00	0.00	0.00	0.00	0.00	0.00
Mn	0.00	0.00	0.00	0.00	0.00	0.00	0.00	0.00	0.00	0.00	0.00	0.00	0.00	0.00	0.00
Mg	0.00	0.00	0.00	0.00	0.00	0.00	0.00	0.00	0.00	0.00	0.00	0.00	0.00	0.00	0.00
Ca	0.30	0.31	0.33	0.32	0.36	0.41	0.37	0.36	0.34	0.33	0.33	0.33	0.31	0.30	0.21
Na	0.72	0.72	0.68	0.68	0.64	0.59	0.64	0.64	0.67	0.67	0.67	0.67	0.70	0.69	0.80
K	0.01	0.01	0.01	0.01	0.01	0.01	0.01	0.01	0.01	0.01	0.01	0.01	0.01	0.01	0.01
An(%)				31.83	36.05	40.63	36.62	35.71				32.92			
Distance (mm)	0.30	0.32	0.34	0.36	0.38	0.40	0.42	0.44	0.46	0.48	0.50	0.52	0.54	0.58	0.60
Tot.cat.	5.02	5.02	5.02	5.01	5.00	5.01	5.01	5.01	5.01	5.01	5.01	5.00	5.01	5.01	5.01

Table 4: Scanning electron microscope probe analysis along a traverse of a plagioclase crystal from sample BG12C2 displayed in Fig.9A&B.

Spectrum	1	2	3	4	5	6	7	8	9	10	11	12	13	14	15	16	17
SiO ₂	58.54	60.83	59.85	59.61	60.49	59.92	47.54	47.99	59.19	62.48	59.62	57.28	58.57	58.33	64.90	59.13	57.06
TiO ₂	0.23	0.00	0.00	0.00	0.00	0.00	0.00	0.00	0.16	0.00	0.00	0.00	0.00	0.00	0.27	0.00	0.00
Al ₂ O ₃	23.83	22.68	24.53	24.52	24.03	24.66	32.83	33.16	21.16	25.44	25.04	25.84	26.12	25.96	17.66	25.50	24.88
FeO	1.63	1.30	0.00	0.00	0.00	0.00	1.00	1.06	0.22	0.00	0.00	0.00	0.17	0.00	0.00	0.00	0.17
MnO	0.00	0.00	0.00	0.00	0.00	0.00	0.00	0.00	0.00	0.00	0.00	0.00	0.00	0.00	0.00	0.00	0.00
MgO	0.32	0.39	0.00	0.00	0.00	0.00	0.79	0.91	0.32	0.00	0.00	0.00	0.00	0.00	0.00	0.00	0.00
CaO	7.27	5.15	7.45	7.40	6.66	7.35	0.00	0.00	0.74	6.08	7.68	8.77	8.67	8.66	0.16	8.37	8.58
Na ₂ O	7.17	8.03	7.30	7.08	7.35	7.28	0.19	0.15	2.28	8.20	7.16	6.39	6.64	6.48	0.32	6.68	6.92
K ₂ O	0.27	0.63	0.10	0.16	0.46	0.10	11.05	11.03	11.97	0.66	0.08	0.00	0.09	0.09	16.00	0.13	0.13
Tot	99.26	98.99	99.23	98.76	98.98	99.32	93.41	94.31	96.04	102.87	99.58	98.29	100.25	99.52	99.31	99.82	97.75
Si	0.97	1.01	1.00	0.99	1.01	1.00	0.79	0.80	0.99	1.04	0.99	0.95	0.97	0.97	1.08	0.98	0.95
Al	0.23	0.22	0.24	0.24	0.24	0.24	0.32	0.33	0.21	0.25	0.25	0.25	0.26	0.25	0.17	0.25	0.24
Ti	0.00	0.00	0.00	0.00	0.00	0.00	0.00	0.00	0.00	0.00	0.00	0.00	0.00	0.00	0.00	0.00	0.00
Fe ²⁺	0.02	0.02	0.00	0.00	0.00	0.00	0.01	0.01	0.00	0.00	0.00	0.00	0.00	0.00	0.00	0.00	0.00
Mg	0.01	0.01	0.00	0.00	0.00	0.00	0.02	0.02	0.01	0.00	0.00	0.00	0.00	0.00	0.00	0.00	0.00
Mn	0.00	0.00	0.00	0.00	0.00	0.00	0.00	0.00	0.00	0.00	0.00	0.00	0.00	0.00	0.00	0.00	0.00
Ca	0.13	0.09	0.13	0.13	0.12	0.13	0.00	0.00	0.01	0.11	0.14	0.16	0.15	0.15	0.00	0.15	0.15
Na	0.12	0.13	0.12	0.11	0.12	0.12	0.00	0.00	0.04	0.13	0.12	0.10	0.11	0.10	0.01	0.11	0.11
K	0.00	0.01	0.00	0.00	0.00	0.00	0.12	0.12	0.13	0.01	0.00	0.00	0.00	0.00	0.17	0.00	0.00
Si	2.55	2.63	2.58	2.59	2.61	2.58	2.24	2.24	2.67	2.59	2.57	2.52	2.52	2.53	2.84	2.55	2.52
Al	1.22	1.15	1.25	1.25	1.22	1.25	1.83	1.83	1.13	1.24	1.27	1.34	1.33	1.33	0.91	1.30	1.30
Ti	0.01	0.00	0.00	0.00	0.00	0.00	0.00	0.00	0.01	0.00	0.00	0.00	0.00	0.00	0.01	0.00	0.00
Fe	0.06	0.05	0.00	0.00	0.00	0.00	0.04	0.04	0.01	0.00	0.00	0.00	0.01	0.00	0.00	0.00	0.01
Mg	0.02	0.02	0.00	0.00	0.00	0.00	0.06	0.06	0.02	0.00	0.00	0.00	0.00	0.00	0.00	0.00	0.00
Mn	0.00	0.00	0.00	0.00	0.00	0.00	0.00	0.00	0.00	0.00	0.00	0.00	0.00	0.00	0.00	0.00	0.00
Ca	0.34	0.24	0.34	0.34	0.31	0.34	0.00	0.00	0.04	0.27	0.35	0.41	0.40	0.40	0.01	0.39	0.41
Na	0.61	0.67	0.61	0.60	0.61	0.61	0.02	0.01	0.20	0.66	0.60	0.54	0.55	0.54	0.03	0.56	0.59
K	0.02	0.03	0.01	0.01	0.03	0.01	0.66	0.66	0.69	0.04	0.00	0.00	0.00	0.01	0.89	0.01	0.01
Si/(3-Ca)	0.96	0.95	0.97	0.97	0.97	0.97	0.75	0.75	0.90	0.95	0.97	0.97	0.97	0.97	0.95	0.98	0.97
An%	52.24	40.26	52.79	53.24	49.04	52.53					54.07		58.85	59.41	1.57	57.76	
Distance	0.00	0.08	0.16	0.24	0.32	0.40	0.48	0.56	0.64	0.72	0.80	0.88	0.96	1.04	1.12	1.20	1.28
Tot.cat.	4.83	4.80	4.79	4.79	4.78	4.79	4.84	4.84	4.76	4.79	4.80	4.81	4.81	4.81	4.69	4.80	4.83

Table 4(cont.): Scanning electron microscope probe analysis along a traverse of a plagioclase crystal from sample BG12C2 displayed in Fig.9A&B.

Spectrum	18	19	20	21	22	23	24	25	26	27	28	29	30	31	32	33	34
SiO ₂	61.32	58.93	60.27	60.06	60.49	60.04	60.48	60.39	66.04	1.81	26.78	27.14	28.47	25.86	26.44	24.71	60.74
TiO ₂	0.00	0.00	0.00	0.00	0.00	0.00	0.00	0.00	0.00	0.00	0.00	0.00	18.06	0.00	0.00	0.00	0.00
Al ₂ O ₃	24.34	25.84	24.93	24.84	24.97	24.91	24.99	24.81	20.87	0.84	18.24	17.42	8.91	18.91	18.45	16.91	24.86
FeO	0.15	0.17	0.00	0.00	0.19	0.15	0.00	0.18	0.00	1.60	31.83	31.19	13.88	31.60	31.98	31.06	0.22
MnO	0.00	0.00	0.00	0.00	0.00	0.00	0.00	0.00	0.00	0.00	0.63	0.50	0.19	0.63	0.66	0.48	0.00
MgO	0.00	0.00	0.00	0.00	0.00	0.00	0.00	0.00	0.00	0.55	11.91	12.42	4.09	11.60	11.52	10.38	0.00
CaO	6.22	8.45	7.20	7.24	7.33	7.52	7.57	7.54	2.69	48.72	0.00	0.00	16.39	0.00	0.00	0.00	7.34
Na ₂ O	7.78	6.62	7.21	6.31	7.19	7.31	7.34	7.35	8.45	0.00	0.00	0.00	0.00	0.00	0.00	0.00	7.40
K ₂ O	0.20	0.13	0.21	0.95	0.28	0.20	0.22	0.25	2.49	0.00	0.00	0.00	0.00	0.09	0.00	0.00	0.21
Tot	100.00	100.14	99.83	99.40	100.45	100.13	100.60	100.52	100.53	53.53	89.39	88.68	89.98	88.68	89.06	83.53	100.78
Si	1.02	0.98	1.00	1.00	1.01	1.00	1.01	1.01	1.10	0.03	0.45	0.45	0.47	0.43	0.44	0.41	1.01
Al	0.24	0.25	0.24	0.24	0.24	0.24	0.25	0.24	0.20	0.01	0.18	0.17	0.09	0.19	0.18	0.17	0.24
Ti	0.00	0.00	0.00	0.00	0.00	0.00	0.00	0.00	0.00	0.00	0.00	0.00	0.23	0.00	0.00	0.00	0.00
Fe	0.00	0.00	0.00	0.00	0.00	0.00	0.00	0.00	0.00	0.02	0.44	0.43	0.19	0.44	0.45	0.43	0.00
Mg	0.00	0.00	0.00	0.00	0.00	0.00	0.00	0.00	0.00	0.01	0.30	0.31	0.10	0.29	0.29	0.26	0.00
Mn	0.00	0.00	0.00	0.00	0.00	0.00	0.00	0.00	0.00	0.00	0.01	0.01	0.00	0.01	0.01	0.01	0.00
Ca	0.11	0.15	0.13	0.13	0.13	0.13	0.14	0.13	0.05	0.87	0.00	0.00	0.29	0.00	0.00	0.00	0.13
Na	0.13	0.11	0.12	0.10	0.12	0.12	0.12	0.12	0.14	0.00	0.00	0.00	0.00	0.00	0.00	0.00	0.12
K	0.00	0.00	0.00	0.01	0.00	0.00	0.00	0.00	0.03	0.00	0.00	0.00	0.00	0.00	0.00	0.00	0.00
Si	2.61	2.54	2.58	2.59	2.58	2.57	2.58	2.58	2.76	0.24	1.64	1.67	1.68	1.60	1.63	1.63	2.58
Al	1.22	1.31	1.26	1.26	1.26	1.26	1.25	1.25	1.03	0.13	1.32	1.26	0.62	1.38	1.34	1.32	1.25
Ti	0.00	0.00	0.00	0.00	0.00	0.00	0.00	0.00	0.00	0.00	0.00	0.00	0.80	0.00	0.00	0.00	0.00
Fe ²⁺	0.01	0.01	0.00	0.00	0.01	0.01	0.00	0.01	0.00	0.18	1.63	1.60	0.69	1.63	1.65	1.72	0.01
Mg	0.00	0.00	0.00	0.00	0.00	0.00	0.00	0.00	0.00	0.11	1.09	1.14	0.36	1.07	1.06	1.02	0.00
Mn	0.00	0.00	0.00	0.00	0.00	0.00	0.00	0.00	0.00	0.00	0.03	0.02	0.01	0.03	0.03	0.02	0.00
Ca	0.28	0.39	0.33	0.33	0.34	0.34	0.35	0.34	0.12	7.02	0.00	0.00	1.04	0.00	0.00	0.00	0.33
Na	0.64	0.55	0.60	0.53	0.59	0.61	0.61	0.61	0.68	0.00	0.00	0.00	0.00	0.00	0.00	0.00	0.61
K	0.01	0.01	0.01	0.05	0.02	0.01	0.01	0.01	0.13	0.00	0.00	0.00	0.00	0.01	0.00	0.00	0.01
Si/(3-Ca)	0.96	0.97	0.97	0.97	0.97	0.97	0.97	0.97	0.96	-0.06	0.55	0.56	0.86	0.53	0.54	0.54	0.97
An%	46.52	58.23	51.98	53.55	52.36	52.74	52.78	52.58	22.75								51.83
Distance	1.36	1.44	1.52	1.60	1.68	1.76	1.84	1.92	2.00	2.08	2.16	2.24	2.32	2.40	2.48	2.56	2.64
Tot.cat.	4.78	4.81	4.79	4.77	4.79	4.80	4.80	4.80	4.73	7.69	5.70	5.70	5.20	5.71	5.70	5.71	4.79

Table 4(cont.): Scanning electron microscope probe analysis along a traverse of a plagioclase crystal from sample BG12C2 displayed in Fig.9A&B.

Spectrum	35	37	38	39	40	41	42	43	44	45	46	47	48	49	50
SiO ₂	60.69	59.98	61.05	60.81	60.24	61.63	60.04	59.80	58.44	59.02	52.76	48.37	50.97	60.23	59.98
TiO ₂	0.00	0.00	0.00	0.00	0.00	0.00	0.00	0.00	0.00	0.00	0.00	0.15	0.00	0.00	0.00
Al ₂ O ₃	25.34	25.29	25.20	24.38	25.12	24.10	25.31	25.21	26.11	25.63	31.39	28.88	34.34	24.77	25.36
FeO	0.24	0.00	0.00	0.17	0.19	0.00	0.00	0.00	0.00	0.00	0.20	4.09	0.65	0.00	0.20
MnO	0.00	0.00	0.00	0.00	0.00	0.00	0.00	0.00	0.00	0.00	0.00	0.00	0.00	0.00	0.00
MgO	0.00	0.00	0.00	0.00	0.00	0.00	0.00	0.00	0.00	0.00	0.00	1.77	1.53	0.00	0.00
CaO	7.63	7.77	7.39	6.69	7.57	6.27	7.94	7.84	8.95	8.24	1.21	0.24	0.17	7.41	7.80
Na ₂ O	7.23	7.13	7.46	7.57	7.13	8.01	7.13	7.03	6.56	6.67	3.34	0.31	0.22	7.12	7.09
K ₂ O	0.14	0.14	0.14	0.11	0.14	0.11	0.12	0.16	0.00	0.00	7.83	10.89	11.40	0.16	0.08
Tot	101.26	100.30	101.25	99.74	100.39	100.12	100.54	100.03	100.07	99.56	96.72	94.68	99.28	99.68	100.52
Si	1.01	1.00	1.02	1.01	1.00	1.03	1.00	1.00	0.97	0.98	0.88	0.81	0.85	1.00	1.00
Al	0.25	0.25	0.25	0.24	0.25	0.24	0.25	0.25	0.26	0.25	0.31	0.28	0.34	0.24	0.25
Ti	0.00	0.00	0.00	0.00	0.00	0.00	0.00	0.00	0.00	0.00	0.00	0.00	0.00	0.00	0.00
Fe	0.00	0.00	0.00	0.00	0.00	0.00	0.00	0.00	0.00	0.00	0.00	0.06	0.01	0.00	0.00
Mg	0.00	0.00	0.00	0.00	0.00	0.00	0.00	0.00	0.00	0.00	0.00	0.04	0.04	0.00	0.00
Mn	0.00	0.00	0.00	0.00	0.00	0.00	0.00	0.00	0.00	0.00	0.00	0.00	0.00	0.00	0.00
Ca	0.14	0.14	0.13	0.12	0.13	0.11	0.14	0.14	0.16	0.15	0.02	0.00	0.00	0.13	0.14
Na	0.12	0.12	0.12	0.12	0.12	0.13	0.12	0.11	0.11	0.11	0.05	0.00	0.00	0.11	0.11
K	0.00	0.00	0.00	0.00	0.00	0.00	0.00	0.00	0.00	0.00	0.08	0.12	0.12	0.00	0.00
Si	2.57	2.57	2.58	2.60	2.58	2.62	2.56	2.57	2.52	2.55	2.36	2.29	2.26	2.59	2.56
Al	1.27	1.28	1.26	1.23	1.27	1.21	1.27	1.28	1.33	1.31	1.65	1.61	1.79	1.25	1.28
Ti	0.00	0.00	0.00	0.00	0.00	0.00	0.00	0.00	0.00	0.00	0.00	0.01	0.00	0.00	0.00
Fe ²⁺	0.01	0.00	0.00	0.01	0.01	0.00	0.00	0.00	0.00	0.00	0.01	0.16	0.02	0.00	0.01
Mg	0.00	0.00	0.00	0.00	0.00	0.00	0.00	0.00	0.00	0.00	0.00	0.12	0.10	0.00	0.00
Mn	0.00	0.00	0.00	0.00	0.00	0.00	0.00	0.00	0.00	0.00	0.00	0.00	0.00	0.00	0.00
Ca	0.35	0.36	0.33	0.31	0.35	0.29	0.36	0.36	0.41	0.38	0.06	0.01	0.01	0.34	0.36
Na	0.59	0.59	0.61	0.63	0.59	0.66	0.59	0.58	0.55	0.56	0.29	0.03	0.02	0.59	0.59
K	0.01	0.01	0.01	0.01	0.01	0.01	0.01	0.01	0.00	0.00	0.45	0.66	0.64	0.01	0.00
Si/(3-Ca)	0.97	0.97	0.97	0.97	0.97	0.96	0.97	0.97	0.98	0.97			0.75	0.97	0.97
An%		54.31		49.16	53.66	46.18	54.89	54.84	60.11	57.73	13.57	3.37	2.42	53.12	54.68
Distance	2.72	2.88	2.96	3.04	3.12	3.20	3.28	3.36	3.44	3.52	3.60	3.68	3.77	3.85	3.93
Tot.cat.	4.79	4.80	4.79	4.78	4.79	4.78	4.80	4.80	4.81	4.80	4.81	4.90	4.85	4.79	4.80

Table 5: Scanning electron microscope probe analysis along a traverse of a plagioclase crystal from sample BG12C2 displayed in Fig.9C&D.

Spot No.	1	2	3	4	5	6	7	8	9	10	11	12	13	14	15	16	17	18	19	20
SiO ₂	59.63	59.72	58.19	39.75	42.70	59.05	59.40	58.91	58.57	56.82	58.19	59.51	59.09	56.66	58.18	56.79	53.80	59.57	59.64	56.93
TiO ₂	0.00	0.00	0.00	0.00	0.00	0.00	0.00	0.00	0.00	0.00	0.00	0.00	0.00	0.00	0.00	0.00	0.00	0.00	0.00	0.00
Al ₂ O ₃	24.32	24.82	24.90	30.44	29.38	25.60	24.81	24.59	25.50	24.77	25.60	24.97	24.68	26.71	25.83	25.41	27.86	25.03	24.75	22.55
FeO	0.13	0.00	0.00	1.66	2.69	0.15	0.00	0.55	0.00	1.01	0.00	0.13	0.00	0.00	0.00	0.15	0.27	0.00	0.00	0.00
MnO	0.00	0.00	0.00	0.00	0.00	0.00	0.00	0.00	0.00	0.00	0.00	0.00	0.00	0.00	0.00	0.00	0.00	0.00	0.00	0.00
MgO	0.00	0.00	0.00	0.00	0.00	0.00	0.00	0.00	0.00	0.00	0.00	0.00	0.00	0.00	0.00	0.00	0.12	0.00	0.00	0.00
CaO	7.68	7.77	8.58	24.77	23.29	1.86	8.06	8.73	8.69	6.97	9.03	8.12	7.89	10.02	9.11	9.00	0.53	7.86	7.85	6.97
Na ₂ O	7.29	7.46	6.84	0.00	1.00	6.94	7.16	6.96	6.87	6.66	6.71	7.09	7.23	6.08	6.52	6.29	1.95	7.18	7.29	6.62
K ₂ O	0.13	0.00	0.12	0.15	0.00	3.52	0.07	0.00	0.07	0.99	0.00	0.00	0.00	0.09	0.00	0.14	9.27	0.12	0.17	0.00
Total	99.18	99.76	98.63	96.78	99.07	97.12	99.50	99.75	99.70	97.22	99.52	99.82	98.89	99.55	99.64	97.78	93.80	99.76	99.70	93.07
Si	0.99	0.99	0.97	0.66	0.71	0.98	0.99	0.98	0.97	0.95	0.97	0.99	0.98	0.94	0.97	0.95	0.90	0.99	0.99	0.95
Al	0.24	0.24	0.24	0.30	0.29	0.25	0.24	0.24	0.25	0.24	0.25	0.24	0.24	0.26	0.25	0.25	0.27	0.25	0.24	0.22
Ti	0.00	0.00	0.00	0.00	0.00	0.00	0.00	0.00	0.00	0.00	0.00	0.00	0.00	0.00	0.00	0.00	0.00	0.00	0.00	0.00
Fe ²⁺	0.00	0.00	0.00	0.02	0.04	0.00	0.00	0.01	0.00	0.01	0.00	0.00	0.00	0.00	0.00	0.00	0.00	0.00	0.00	0.00
Mg	0.00	0.00	0.00	0.00	0.00	0.00	0.00	0.00	0.00	0.00	0.00	0.00	0.00	0.00	0.00	0.00	0.00	0.00	0.00	0.00
Mn	0.00	0.00	0.00	0.00	0.00	0.00	0.00	0.00	0.00	0.00	0.00	0.00	0.00	0.00	0.00	0.00	0.00	0.00	0.00	0.00
Ca	0.14	0.14	0.15	0.44	0.42	0.03	0.14	0.16	0.15	0.12	0.16	0.14	0.14	0.18	0.16	0.16	0.01	0.14	0.14	0.12
Na	0.12	0.12	0.11	0.00	0.02	0.11	0.12	0.11	0.11	0.11	0.11	0.11	0.12	0.10	0.11	0.10	0.03	0.12	0.12	0.11
K	0.00	0.00	0.00	0.00	0.00	0.04	0.00	0.00	0.00	0.01	0.00	0.00	0.00	0.00	0.00	0.00	0.10	0.00	0.00	0.00
Si	2.58	2.57	2.54	1.97	2.05	2.58	2.57	2.55	2.53	2.53	2.53	2.56	2.57	2.47	2.52	2.52	2.48	2.56	2.57	2.62
Al	1.24	1.26	1.28	1.78	1.66	1.32	1.26	1.26	1.30	1.30	1.31	1.27	1.26	1.37	1.32	1.33	1.51	1.27	1.26	1.22
Ti	0.00	0.00	0.00	0.00	0.00	0.00	0.00	0.00	0.00	0.00	0.00	0.00	0.00	0.00	0.00	0.00	0.00	0.00	0.00	0.00
Fe	0.00	0.00	0.00	0.07	0.11	0.01	0.00	0.02	0.00	0.04	0.00	0.00	0.00	0.00	0.00	0.01	0.01	0.00	0.00	0.00
Mg	0.00	0.00	0.00	0.00	0.00	0.00	0.00	0.00	0.00	0.00	0.00	0.00	0.00	0.00	0.00	0.00	0.01	0.00	0.00	0.00
Mn	0.00	0.00	0.00	0.00	0.00	0.00	0.00	0.00	0.00	0.00	0.00	0.00	0.00	0.00	0.00	0.00	0.00	0.00	0.00	0.00
Ca	0.36	0.36	0.40	1.32	1.20	0.09	0.37	0.41	0.40	0.33	0.42	0.37	0.37	0.47	0.42	0.43	0.03	0.36	0.36	0.34
Na	0.61	0.62	0.58	0.00	0.09	0.59	0.60	0.58	0.58	0.57	0.56	0.59	0.61	0.51	0.55	0.54	0.17	0.60	0.61	0.59
K	0.01	0.00	0.01	0.01	0.00	0.20	0.00	0.00	0.00	0.06	0.00	0.00	0.00	0.01	0.00	0.01	0.55	0.01	0.01	0.00
Si/(3-Ca)	0.98	0.97	0.98	1.17	1.14	0.88	0.98	0.96	0.98	0.95	0.98	0.98	0.97	0.98	0.98	0.98	0.83	0.97	0.97	0.99
An	53.53	53.52	57.82				55.28	58.10	58.13	51.30	59.81	55.84	54.68	64.35	60.69	60.90			53.94	
Distance	0.00	0.11	0.22	0.33	0.44	0.54	0.65	0.76	0.87	0.98	1.09	1.20	1.31	1.41	1.52	1.63	1.74	0.18	1.96	2.07
Tot.cat.	4.80	4.80	4.81	5.14	5.12	4.77	4.80	4.82	4.82	4.82	4.82	4.80	4.80	4.84	4.82	4.82	4.76	4.80	4.80	4.77

Potassium Feldspar*Table 6: Potassium Feldspar in enclaves*

Type	Enclave														
Sample	BG12D			BG15A			BG29			BG44					
Spot No.	8	10	12	3	6	12	7	8	9	10	12	6	7	9	11
SiO ₂	62.72	63.62	62.96	65.46	65.07	65.33	64.81	65.28	65.04	65.06	64.96	65.67	65.41	65.44	64.97
TiO ₂	0.00	0.00	0.00	0.00	0.00	0.00	0.00	0.00	0.00	0.00	0.00	0.00	0.00	0.00	0.00
Al ₂ O ₃	20.28	20.04	19.57	17.93	18.06	17.84	17.92	18.10	18.24	18.14	17.93	18.22	17.98	18.07	18.57
FeO	0.18	0.00	0.00	0.00	0.00	0.14	0.17	0.16	0.16	0.34	0.00	0.00	0.00	0.00	0.00
MnO	0.00	0.00	0.00	0.00	0.00	0.00	0.00	0.00	0.00	0.00	0.00	0.00	0.00	0.00	0.00
MgO	0.00	0.00	0.00	0.00	0.00	0.00	0.00	0.00	0.00	0.00	0.00	0.00	0.00	0.00	0.00
CaO	0.71	0.17	0.20	0.12	0.00	0.12	0.18	0.00	0.00	0.12	0.00	0.18	0.14	0.15	0.65
BaO	1.66	0.00	0.46	0.00	0.00	0.00	0.32	0.31	0.39	0.33	0.26	0.43	0.31	0.30	0.28
Na ₂ O	0.49	0.51	0.19	0.34	0.48	0.39	0.90	0.58	0.38	0.56	0.76	0.53	0.38	0.33	1.14
K ₂ O	14.59	15.45	15.75	16.47	16.28	16.35	15.46	16.35	16.07	16.20	15.87	15.95	16.41	16.47	14.84
Total	100.64	99.79	99.13	100.32	99.89	100.18	99.77	100.79	100.27	100.75	99.77	100.99	100.62	100.77	100.46
Si	2.91	2.94	2.95	3.02	3.01	3.02	3.00	3.00	3.01	2.99	3.01	3.02	3.01	3.01	2.99
Ti	0.00	0.00	0.00	0.00	0.00	0.00	0.00	0.00	0.00	0.00	0.00	0.00	0.00	0.00	0.00
Al	1.11	1.09	1.08	0.97	0.99	0.97	0.98	0.98	0.99	0.98	0.98	0.99	0.98	0.98	1.01
Fe ²⁺	0.01	0.00	0.00	0.00	0.00	0.01	0.01	0.01	0.01	0.01	0.00	0.00	0.00	0.00	0.00
Mn	0.00	0.00	0.00	0.00	0.00	0.00	0.00	0.00	0.00	0.00	0.00	0.00	0.00	0.00	0.00
Mg	0.00	0.00	0.00	0.00	0.00	0.00	0.00	0.00	0.00	0.00	0.00	0.00	0.00	0.00	0.00
Ca	0.04	0.01	0.01	0.01	0.00	0.01	0.01	0.00	0.00	0.01	0.00	0.01	0.01	0.01	0.03
Ba	0.03	0.00	0.01	0.00	0.00	0.00	0.01	0.01	0.01	0.01	0.00	0.01	0.01	0.01	0.01
Na	0.04	0.05	0.02	0.03	0.04	0.04	0.08	0.05	0.03	0.05	0.07	0.05	0.03	0.03	0.10
K	0.86	0.91	0.94	0.97	0.96	0.96	0.91	0.96	0.95	0.95	0.94	0.93	0.96	0.97	0.87
Tot. cat	5.00	5.00	5.00	5.00	5.00	5.00	5.00	5.00	5.00	5.00	5.00	5.00	5.00	5.00	5.00
An	3.76	0.85	1.04	0.61	0.00	0.57	0.87	0.00	0.00	0.61	0.00	0.90	0.69	0.75	3.19
Ab	4.71	4.73	1.77	3.03	4.29	3.51	0.08	0.05	0.03	0.05	0.07	4.78	3.38	2.97	10.15
Or	91.53	94.41	97.19	96.37	95.71	95.92	0.91	0.95	0.97	0.94	0.93	94.32	95.93	96.28	86.66

Table7: Potassium feldspar in granites

Type	Granite														
Sample	BG10					BG12D					BG13A				
Spot															
No.	1	2	3	4	5	2	3	5	7	12	3	4	5	6	7
SiO ₂	65.01	65.18	64.98	64.45	64.86	65.51	65.21	65.62	65.38	64.65	64.28	65.35	65.10	64.88	65.56
TiO ₂	0.00	0.00	0.00	0.00	0.00	0.00	0.00	0.00	0.00	0.00	0.00	0.00	0.00	0.00	0.00
Al ₂ O ₃	17.77	17.99	17.89	17.94	17.94	18.32	18.07	18.28	18.22	18.18	17.99	18.01	18.26	18.27	18.20
FeO	0.00	0.00	0.00	0.00	0.00	0.00	0.00	0.00	0.00	0.00	0.00	0.00	0.00	0.00	0.00
MnO	0.00	0.00	0.00	0.00	0.00	0.00	0.00	0.00	0.00	0.00	0.00	0.00	0.00	0.00	0.00
MgO	0.00	0.00	0.00	0.00	0.00	0.00	0.00	0.00	0.00	0.00	0.00	0.00	0.00	0.00	0.00
CaO	0.00	0.00	0.00	0.00	0.00	0.00	0.00	0.00	0.00	0.00	0.12	0.00	0.14	0.12	0.00
BaO	0.00	0.00	0.00	0.00	0.00	0.51	0.34	0.37	0.54	0.62	0.67	0.39	0.93	0.93	0.37
Na ₂ O	0.28	0.38	0.45	0.46	0.43	0.50	0.48	0.44	0.58	0.58	0.79	0.55	0.86	0.93	0.81
K ₂ O	16.57	16.28	16.51	16.28	16.27	16.14	16.17	16.23	15.97	15.86	15.28	15.92	15.46	15.52	15.68
Total	99.63	99.83	99.82	99.13	99.50	100.98	100.27	100.94	100.69	99.89	99.13	100.23	100.75	100.65	100.61
Si	3.02	3.02	3.01	4.40	3.01	3.01	3.01	3.01	3.01	3.00	3.01	3.02	3.00	2.99	3.02
Ti	0.00	0.00	0.00	0.00	0.00	0.00	0.00	0.00	0.00	0.00	0.00	0.00	0.00	0.00	0.00
Al	0.97	0.98	0.98	8.94	0.98	0.99	0.98	0.99	0.99	0.99	0.99	0.98	0.99	0.99	0.99
Fe ²⁺	0.00	0.00	0.00	0.00	0.00	0.00	0.00	0.00	0.00	0.00	0.00	0.00	0.00	0.00	0.00
Mn	0.00	0.00	0.00	6.00	0.00	0.00	0.00	0.00	0.00	0.00	0.00	0.00	0.00	0.00	0.00
Mg	0.00	0.00	0.00	0.00	0.00	0.00	0.00	0.00	0.00	0.00	0.00	0.00	0.00	0.00	0.00
Ca	0.00	0.00	0.00	62.74	0.00	0.00	0.00	0.00	0.00	0.00	0.01	0.00	0.01	0.01	0.00
Ba	0.00	0.00	0.00	0.00	0.00	0.01	0.01	0.01	0.01	0.01	0.01	0.01	0.02	0.02	0.01
Na	0.03	0.03	0.04	22.50	0.04	0.04	0.04	0.04	0.05	0.05	0.07	0.05	0.08	0.08	0.07
K	0.98	0.96	0.97	0.00	0.96	0.95	0.95	0.95	0.94	0.94	0.91	0.94	0.91	0.91	0.92
Tot.															
cat.	5.00	5.00	5.00	0.00	5.00	5.00	5.00	5.00	5.00	5.00	5.00	5.00	5.00	5.00	5.00
An	0.00	0.00	0.00	0.00	0.00	0.00	0.00	0.00	0.00	0.00	0.60	0.00	0.69	0.60	0.00
Ab	2.49	3.38	3.96	4.16	3.82	4.46	4.32	3.97	5.22	5.25	7.20	5.00	7.77	8.26	7.26
Or	97.51	96.62	96.04	95.84	96.18	95.54	95.68	96.03	94.78	94.75	92.20	95.00	91.54	91.14	92.74

Table 7 (cont.): Potassium feldspar in granites

Type	Granite																		
Sample	BG15B				BG26					BG44					BG46A				
Spot No.	3	4	7	8	4	5	6	8	9	11	5	6	7	10	9	10	11	12	13
SiO ₂	64.63	64.46	64.88	64.17	64.84	64.30	65.22	64.06	64.94	64.71	65.05	65.43	65.12	65.15	64.83	64.96	65.00	65.74	65.30
TiO ₂	0.00	0.00	0.00	0.00	0.00	0.00	0.00	0.00	0.00	0.00	0.00	0.00	0.00	0.00	0.00	0.00	0.00	0.00	0.00
Al ₂ O ₃	18.06	18.10	17.77	17.90	17.83	18.26	17.92	17.88	18.00	17.82	18.27	18.05	17.98	18.37	18.13	18.32	18.01	17.97	18.37
FeO	0.00	0.00	0.00	0.00	0.00	0.00	0.00	0.00	0.00	0.00	0.00	0.00	0.00	0.00	0.00	0.00	0.00	0.23	0.00
MnO	0.00	0.00	0.00	0.00	0.00	0.00	0.00	0.00	0.00	0.00	0.00	0.00	0.00	0.00	0.00	0.00	0.00	0.00	0.00
MgO	0.00	0.00	0.00	0.00	0.00	0.00	0.00	0.00	0.00	0.00	0.00	0.00	0.00	0.00	0.00	0.00	0.00	0.00	0.00
CaO	0.00	0.00	0.00	0.00	0.00	0.13	0.00	0.19	0.00	0.00	0.00	0.00	0.12	0.00	0.00	0.00	0.00	0.00	0.15
BaO	0.00	0.00	0.00	0.72	0.50	0.87	0.34	0.78	0.00	0.00	0.77	0.46	0.55	0.54	0.44	0.79	0.42	0.43	0.49
Na ₂ O	0.55	0.55	0.52	0.59	0.91	0.81	0.56	0.74	0.37	0.49	0.67	0.49	0.35	0.76	0.59	0.71	0.68	0.64	0.61
K ₂ O	15.99	16.20	16.24	15.68	15.48	15.48	15.94	15.45	16.35	16.18	16.07	16.11	16.52	15.52	15.69	15.67	15.75	15.78	16.01
Total	99.23	99.31	99.42	99.06	99.56	99.85	99.98	99.10	99.66	99.18	100.83	100.55	100.65	100.35	99.68	100.46	99.86	100.79	100.94
Si	3.01	3.00	3.02	3.01	3.01	2.99	3.02	3.00	3.01	3.02	2.99	3.02	3.00	3.01	3.01	3.00	3.01	3.03	3.00
Ti	0.00	0.00	0.00	0.00	0.00	0.00	0.00	0.00	0.00	0.00	0.00	0.00	0.00	0.00	0.00	0.00	0.00	0.00	0.00
Al	0.99	0.99	0.97	0.99	0.98	1.00	0.98	0.99	0.98	0.98	0.99	0.98	0.98	1.00	0.99	1.00	0.98	0.97	0.99
Fe ²	0.00	0.00	0.00	0.00	0.00	0.00	0.00	0.00	0.00	0.00	0.00	0.00	0.00	0.00	0.00	0.00	0.00	0.01	0.00
Mn	0.00	0.00	0.00	0.00	0.00	0.00	0.00	0.00	0.00	0.00	0.00	0.00	0.00	0.00	0.00	0.00	0.00	0.00	0.00
Mg	0.00	0.00	0.00	0.00	0.00	0.00	0.00	0.00	0.00	0.00	0.00	0.00	0.00	0.00	0.00	0.00	0.00	0.00	0.00
Ca	0.00	0.00	0.00	0.00	0.00	0.01	0.00	0.01	0.00	0.00	0.00	0.00	0.01	0.00	0.00	0.00	0.00	0.00	0.01
Ba	0.00	0.00	0.00	0.01	0.01	0.02	0.01	0.01	0.00	0.00	0.01	0.01	0.01	0.01	0.01	0.01	0.01	0.01	0.01
Na	0.05	0.05	0.05	0.05	0.08	0.07	0.05	0.07	0.03	0.04	0.06	0.04	0.03	0.07	0.05	0.06	0.06	0.06	0.05
K	0.95	0.96	0.96	0.94	0.92	0.92	0.94	0.92	0.97	0.96	0.94	0.95	0.97	0.91	0.93	0.92	0.93	0.93	0.94
Tot. cat.	5.00	5.00	5.00	5.00	5.00	5.00	5.00	5.00	5.00	5.00	5.00	5.00	5.00	5.00	5.00	5.00	5.00	5.00	5.00
An	0.00	0.00	0.00	0.00	0.00	0.66	0.00	0.96	0.00	0.00	0.00	0.00	0.61	0.00	0.00	0.00	0.00	0.00	0.74
Ab	5.01	4.91	4.64	5.39	8.19	7.34	5.09	6.76	3.30	4.37	5.95	4.40	3.11	6.95	5.37	6.46	6.13	5.79	5.45
Or	94.99	95.09	95.36	94.61	91.81	91.99	94.91	92.27	96.70	95.63	94.05	95.60	96.28	93.05	94.63	93.54	93.87	94.21	93.81

BiotiteTable 8: Biotite in enclaves. $a=BD^a = \text{Below Detection}$, $b=Xmg^b = Mg/(Fe^{2+}+Mg)$, $c=Xmg(div)^c = \text{Divalent} = Mg/(Fe^{2+}+Mn+Mg+Ca)$

Type	Enclave														
Sample No	BG12D					BG15A					BG44				
Spot No.	2	3	4	5	6	2	3	4	5	6	3	4	5	6	7
SiO ₂	36.20	36.18	36.50	36.39	36.44	36.03	35.76	35.77	35.15	35.68	35.65	35.38	35.58	35.70	35.58
TiO ₂	2.63	2.25	2.27	2.59	3.31	3.18	3.38	3.60	3.23	3.47	3.29	1.86	3.63	3.62	2.62
Al ₂ O ₃	15.46	15.38	15.55	15.86	15.07	15.20	15.23	15.03	14.98	15.17	14.81	15.50	15.00	14.96	15.33
FeO	24.57	24.39	24.18	23.42	24.37	24.47	23.87	24.48	24.35	23.75	24.52	22.97	24.56	23.98	23.41
MnO	0.70	0.67	0.67	0.68	0.79	0.62	0.80	0.88	0.97	0.80	0.77	0.83	0.68	0.77	0.58
MgO	8.16	8.05	8.16	8.06	7.58	7.47	7.36	7.29	7.12	7.40	7.51	8.50	7.25	7.32	8.23
CaO	0.00	0.00	0.00	0.00	0.00	0.11	0.00	0.00	0.00	0.00	0.00	0.00	0.00	0.14	0.17
BaO	0.00	0.00	0.00	0.00	0.00	BD ^a	BD	BD	BD	BD	BD	BD	BD	BD	BD
Na ₂ O	0.00	0.00	0.00	0.00	0.00	0.00	0.19	0.00	0.20	0.16	0.00	0.00	0.00	0.17	0.00
K ₂ O	9.35	9.43	9.44	9.51	9.28	9.12	9.27	9.21	9.10	9.45	9.52	9.02	9.21	9.25	8.87
Total	97.06	96.36	96.77	96.50	96.85	96.21	95.85	96.26	95.10	96.03	96.07	94.05	95.92	95.91	94.80
Si	2.79	2.80	2.81	2.80	2.81	2.80	2.79	2.78	2.77	2.78	2.78	2.79	2.78	2.78	2.79
Al	1.21	1.20	1.19	1.20	1.19	1.20	1.21	1.22	1.23	1.22	1.22	1.21	1.22	1.22	1.21
∑ Z	4.00	4.00	4.00	4.00	4.00	4.00	4.00	4.00	4.00	4.00	4.00	4.00	4.00	4.00	4.00
Al	0.19	0.21	0.22	0.24	0.18	0.19	0.18	0.16	0.17	0.17	0.15	0.24	0.16	0.16	0.20
Ti	0.15	0.13	0.13	0.15	0.19	0.19	0.20	0.21	0.19	0.20	0.19	0.11	0.21	0.21	0.15
Fe ²⁺	1.58	1.58	1.56	1.51	1.57	1.59	1.55	1.59	1.61	1.55	1.60	1.52	1.60	1.56	1.53
Mn	0.05	0.04	0.04	0.04	0.05	0.04	0.05	0.06	0.06	0.05	0.05	0.06	0.05	0.05	0.04
Mg	0.94	0.93	0.94	0.92	0.87	0.86	0.85	0.85	0.84	0.86	0.87	1.00	0.84	0.85	0.96
∑ X	2.90	2.90	2.89	2.86	2.86	2.86	2.84	2.86	2.87	2.83	2.87	2.92	2.86	2.83	2.89
Ca	0.00	0.00	0.00	0.00	0.00	0.01	0.00	0.00	0.00	0.00	0.00	0.00	0.00	0.01	0.01
Na	0.00	0.00	0.00	0.00	0.00	0.00	0.03	0.00	0.03	0.02	0.00	0.00	0.00	0.03	0.00
K	0.92	0.93	0.93	0.93	0.91	0.90	0.92	0.91	0.92	0.94	0.95	0.91	0.92	0.92	0.89
∑ Y	0.92	0.93	0.93	0.93	0.91	0.91	0.95	0.91	0.95	0.96	0.95	0.91	0.92	0.96	0.90
Tot.cat.	7.82	7.83	7.82	7.80	7.77	7.78	7.79	7.78	7.81	7.80	7.82	7.83	7.78	7.79	7.79
Xmg ^b	0.37	0.37	0.38	0.38	0.36	0.35	0.35	0.35	0.34	0.36	0.35	0.40	0.34	0.35	0.39
Xmg(div) ^c	0.37	0.36	0.37	0.37	0.35	0.35	0.35	0.34	0.33	0.35	0.35	0.39	0.34	0.34	0.38

Table 9: Biotite in granites

Type	Granite																													
Sample Spot No.	BG10						BG12D						BG13A						BG15B						BG26					
	1	3	4	5	6	7	2	3	4	5	6	1	2	3	4	5	5	6	7	8	9	10	1	2	3	4				
SiO ₂	35.48	35.46	35.85	35.58	35.83	35.89	36.31	36.46	36.29	36.24	36.30	36.09	35.56	35.63	35.71	35.51	35.48	35.65	35.64	35.69	35.82	35.21	35.75	35.61	35.67	36.44				
TiO ₂	3.10	3.44	2.74	2.87	2.95	3.21	2.75	3.21	3.11	2.71	3.15	2.94	2.69	3.20	3.65	3.22	2.50	2.82	3.21	2.55	3.07	3.67	3.14	3.35	3.38	3.25				
Al ₂ O ₃	15.50	14.85	15.15	14.69	14.77	15.84	16.08	15.64	15.43	15.48	14.99	15.10	14.65	14.77	14.12	14.31	15.19	15.02	14.82	15.25	15.11	14.82	14.89	14.46	14.46	14.77				
FeO	25.40	25.10	26.06	26.64	26.37	24.96	23.94	24.14	24.70	24.21	24.43	23.84	24.37	24.48	24.63	24.52	24.77	23.82	24.68	24.07	24.14	23.75	24.20	24.43	24.39	24.26				
MnO	1.65	1.69	1.68	1.58	1.80	1.46	0.94	0.65	0.70	0.71	0.72	0.44	0.45	0.29	0.38	0.45	0.59	0.75	0.80	0.64	0.67	0.78	1.18	1.15	1.02	1.20				
MgO	6.06	6.17	6.40	5.99	6.15	5.76	7.84	7.53	7.43	7.76	7.67	7.58	7.73	7.34	7.34	7.45	6.95	7.61	7.54	7.76	7.45	6.94	7.65	7.05	7.28	7.48				
CaO	0.00	0.15	0.13	0.00	0.00	0.12	0.00	0.00	0.00	0.00	0.00	0.00	0.00	0.00	0.00	0.00	0.00	0.00	0.12	0.00	0.00	0.00	0.00	0.13	0.00	0.00				
BaO	BD	BD	BD	BD	BD	BD	0.32	0.00	0.00	0.00	0.00	BD	BD	BD	BD	BD	BD	BD	BD	BD	BD	BD	BD	BD	BD	BD				
Na ₂ O	0.00	0.00	0.21	0.00	0.00	0.00	0.00	0.17	0.00	0.00	0.00	0.00	0.00	0.00	0.00	0.00	0.00	0.00	0.00	0.00	0.17	0.00	0.18	0.28	0.21	0.00				
K ₂ O	9.12	9.19	9.28	9.27	9.25	9.17	9.29	9.43	9.42	9.35	9.52	9.59	9.35	9.66	9.53	9.52	9.06	9.31	9.32	9.25	9.30	9.36	9.24	9.19	9.10	9.38				
Total	96.30	96.04	97.49	96.62	97.13	96.40	97.48	97.22	97.10	96.46	96.77	95.58	94.81	95.37	95.34	94.97	94.53	94.99	96.13	95.20	95.73	94.52	96.22	95.65	95.51	96.76				
Si	2.78	2.79	2.78	2.80	2.80	2.79	2.78	2.79	2.79	2.80	2.80	2.82	2.81	2.80	2.81	2.81	2.81	2.80	2.78	2.80	2.80	2.79	2.78	2.80	2.80	2.82				
Al	1.22	1.21	1.22	1.20	1.20	1.21	1.22	1.21	1.21	1.20	1.20	1.18	1.19	1.20	1.19	1.19	1.19	1.20	1.22	1.20	1.20	1.21	1.22	1.20	1.20	1.18				
∑ Z	4.00	4.00	4.00	4.00	4.00	4.00	4.00	4.00	4.00	4.00	4.00	4.00	4.00	4.00	4.00	4.00	4.00	4.00	4.00	4.00	4.00	4.00	4.00	4.00	4.00	4.00				
Al	0.21	0.16	0.17	0.16	0.16	0.25	0.23	0.21	0.19	0.21	0.17	0.20	0.17	0.17	0.12	0.14	0.23	0.19	0.14	0.21	0.19	0.17	0.15	0.14	0.14	0.16				
Ti	0.18	0.20	0.16	0.17	0.17	0.19	0.16	0.19	0.18	0.16	0.18	0.17	0.16	0.19	0.22	0.19	0.15	0.17	0.19	0.15	0.18	0.22	0.18	0.20	0.20	0.19				
Fe ²⁺	1.66	1.65	1.69	1.75	1.72	1.62	1.53	1.55	1.59	1.57	1.58	1.56	1.61	1.61	1.62	1.62	1.64	1.57	1.61	1.58	1.58	1.57	1.58	1.61	1.60	1.57				
Mn	0.11	0.11	0.11	0.11	0.12	0.10	0.06	0.04	0.05	0.05	0.05	0.03	0.03	0.02	0.03	0.03	0.04	0.05	0.05	0.04	0.04	0.05	0.08	0.08	0.07	0.08				
Mg	0.71	0.72	0.74	0.70	0.72	0.67	0.90	0.86	0.85	0.89	0.88	0.88	0.91	0.86	0.86	0.88	0.82	0.89	0.88	0.91	0.87	0.82	0.89	0.83	0.85	0.86				
∑ X	2.87	2.85	2.88	2.89	2.89	2.83	2.88	2.84	2.86	2.87	2.86	2.84	2.88	2.84	2.84	2.86	2.88	2.87	2.87	2.88	2.85	2.83	2.88	2.84	2.86	2.86				
Ca	0.00	0.01	0.01	0.00	0.00	0.01	0.00	0.00	0.00	0.00	0.00	0.00	0.00	0.00	0.00	0.00	0.00	0.00	0.01	0.00	0.00	0.00	0.01	0.00	0.00	0.00				
Na	0.00	0.00	0.03	0.00	0.00	0.00	0.00	0.02	0.00	0.00	0.00	0.00	0.00	0.00	0.00	0.00	0.00	0.00	0.00	0.00	0.03	0.00	0.03	0.04	0.03	0.00				
K	0.91	0.92	0.92	0.93	0.92	0.91	0.91	0.92	0.93	0.92	0.94	0.95	0.94	0.97	0.96	0.96	0.92	0.93	0.93	0.93	0.93	0.94	0.92	0.92	0.91	0.93				
∑ Y	0.91	0.93	0.96	0.93	0.92	0.92	0.91	0.95	0.93	0.92	0.94	0.95	0.94	0.97	0.96	0.96	0.92	0.93	0.94	0.93	0.95	0.94	0.94	0.97	0.94	0.93				
Tot.cat.	7.78	7.78	7.84	7.82	7.81	7.75	7.79	7.79	7.79	7.80	7.80	7.80	7.82	7.81	7.80	7.82	7.79	7.80	7.81	7.81	7.80	7.78	7.82	7.82	7.80	7.78				
X _{Mg} ^a	0.30	0.30	0.30	0.29	0.29	0.29	0.37	0.36	0.35	0.36	0.36	0.36	0.36	0.35	0.35	0.35	0.33	0.36	0.35	0.36	0.35	0.34	0.36	0.34	0.35	0.35				
X _{Mg} ^b	0.29	0.29	0.29	0.27	0.28	0.28	0.36	0.35	0.34	0.36	0.35	0.36	0.36	0.35	0.34	0.35	0.33	0.36	0.34	0.36	0.35	0.34	0.35	0.33	0.34	0.34				

Table 9(cont.): Biotite in granites

Type	Granites																										
Sample Spot No.	BG26 (cont.)					BG29					BG44					BG46A											
	5	6	7	8	9	10	11	12	1	3	4	6	7	8	10	1	2	3	4	5	6	2	4	5	6	9	
SiO ₂	35.64	37.58	24.78	35.72	35.86	36.10	36.00	35.89	35.62	36.01	36.00	35.86	35.84	35.53	35.71	35.94	35.77	35.96	35.85	35.79	35.69	35.88	36.25	35.69	35.90	35.57	
TiO ₂	3.47	0.00	0.00	2.92	3.51	3.09	3.35	3.46	3.58	3.51	3.72	3.63	3.46	3.36	3.70	2.73	2.12	3.13	2.91	3.24	3.08	3.13	3.16	3.20	2.00	3.21	
Al ₂ O ₃	14.54	22.15	19.65	14.93	14.44	14.74	14.62	14.68	14.47	14.61	13.96	14.63	14.70	14.47	14.75	15.18	15.35	15.04	15.38	15.41	14.80	15.25	15.23	15.25	15.76	15.08	
FeO	24.22	13.49	31.49	24.20	24.19	24.10	24.02	24.61	24.45	24.39	24.67	24.35	24.33	24.74	25.04	24.83	23.83	24.33	23.96	24.00	24.23	24.63	23.84	24.58	24.43	24.66	
MnO	1.23	0.35	1.92	0.96	1.28	1.03	1.14	1.06	0.87	0.94	1.09	1.11	0.99	1.05	1.13	0.64	0.77	0.75	0.73	0.71	0.72	0.77	0.76	0.59	0.63	0.82	
MgO	7.27	0.00	10.27	7.36	7.53	7.53	7.42	6.99	7.30	7.26	7.22	7.30	7.06	7.13	6.97	7.90	7.87	7.49	7.39	7.39	7.62	7.53	7.66	7.51	7.85	7.13	
CaO	0.13	22.47	0.09	0.00	0.00	0.00	0.00	0.00	0.11	0.00	0.00	0.00	0.15	0.13	0.00	0.13	0.00	0.00	0.11	0.00	0.00	0.00	0.00	0.00	0.00	0.00	
BaO	BD	BD	BD	BD	BD	BD	BD	BD	BD	BD	BD	BD	BD	BD	BD	BD	BD	BD	BD	BD	BD	BD	BD	BD	BD	BD	BD
Na ₂ O	0.26	0.00	0.00	0.23	0.20	0.18	0.21	0.00	0.17	0.19	0.00	0.00	0.00	0.21	0.00	0.00	0.00	0.00	0.00	0.00	0.00	0.00	0.00	0.00	0.00	0.00	
K ₂ O	9.15	0.00	0.00	9.14	9.19	9.25	9.26	9.01	9.31	9.38	9.22	9.26	9.27	9.21	9.21	9.21	9.38	9.34	9.33	9.23	9.28	9.31	9.51	9.26	9.48	9.23	
Total	95.92	96.04	88.21	95.47	96.19	96.04	96.01	95.71	95.89	96.28	95.87	96.14	95.79	95.83	96.51	96.55	95.10	96.04	95.67	95.78	95.41	96.49	96.40	96.08	96.05	95.69	
Si	2.79	2.76	2.14	2.80	2.80	2.81	2.81	2.81	2.79	2.80	2.82	2.79	2.80	2.79	2.78	2.79	2.81	2.80	2.80	2.79	2.80	2.78	2.80	2.78	2.79	2.79	
Al	1.21	1.24	1.86	1.20	1.20	1.19	1.19	1.19	1.21	1.20	1.18	1.21	1.20	1.21	1.22	1.21	1.19	1.20	1.20	1.21	1.20	1.22	1.20	1.22	1.21	1.21	
∑ Z	4.00	4.00	4.00	4.00	4.00	4.00	4.00	4.00	4.00	4.00	4.00	4.00	4.00	4.00	4.00	4.00	4.00	4.00	4.00	4.00	4.00	4.00	4.00	4.00	4.00	4.00	
Al	0.13	0.67	0.13	0.18	0.12	0.16	0.15	0.16	0.12	0.14	0.11	0.14	0.16	0.13	0.14	0.17	0.23	0.18	0.21	0.20	0.17	0.18	0.19	0.18	0.24	0.18	
Ti	0.20	0.00	0.00	0.17	0.21	0.18	0.20	0.20	0.21	0.21	0.22	0.21	0.20	0.20	0.22	0.16	0.13	0.18	0.17	0.19	0.18	0.18	0.18	0.19	0.12	0.19	
Fe ²⁺	1.58	0.83	2.27	1.59	1.58	1.57	1.57	1.61	1.60	1.59	1.62	1.59	1.59	1.62	1.63	1.61	1.56	1.58	1.56	1.56	1.59	1.60	1.54	1.60	1.59	1.61	
Mn	0.08	0.02	0.14	0.06	0.08	0.07	0.07	0.07	0.06	0.06	0.07	0.07	0.07	0.07	0.07	0.04	0.05	0.05	0.05	0.05	0.05	0.05	0.05	0.04	0.04	0.05	
Mg	0.85	0.00	1.32	0.86	0.88	0.87	0.86	0.82	0.85	0.84	0.84	0.85	0.82	0.83	0.81	0.91	0.92	0.87	0.86	0.86	0.89	0.87	0.88	0.87	0.91	0.83	
∑ X	2.85	1.52	3.86	2.86	2.86	2.86	2.85	2.86	1.99	2.00	2.01	2.01	2.02	2.02	2.06	2.90	2.89	2.86	2.85	2.86	2.87	2.88	2.85	2.87	2.90	2.87	
Ca	0.01	1.77	0.01	0.00	0.00	0.00	0.00	0.00	0.01	0.00	0.00	0.00	0.01	0.01	0.00	0.01	0.00	0.00	0.01	0.00	0.00	0.00	0.00	0.00	0.00	0.00	
Na	0.04	0.00	0.00	0.04	0.03	0.03	0.03	0.00	0.03	0.03	0.00	0.00	0.00	0.03	0.00	0.00	0.00	0.00	0.00	0.00	0.00	0.00	0.00	0.00	0.00	0.00	
K	0.91	0.00	0.00	0.91	0.91	0.92	0.92	0.90	0.93	0.93	0.92	0.92	0.92	0.92	0.92	0.91	0.94	0.93	0.93	0.92	0.93	0.92	0.94	0.92	0.94	0.92	
∑ Y	0.96	1.77	0.01	0.95	0.94	0.95	0.95	0.90	0.96	0.96	0.92	0.92	0.94	0.97	0.92	0.92	0.94	0.93	0.94	0.92	0.93	0.92	0.94	0.92	0.94	0.92	
Tot.cat.	7.81	7.29	7.87	7.81	7.81	7.80	7.80	7.76	7.81	7.80	7.78	7.78	7.78	7.82	7.78	7.82	7.83	7.79	7.79	7.77	7.80	7.80	7.79	7.79	7.84	7.79	
Xmg ^a	0.35	0.00	0.37	0.35	0.36	0.36	0.36	0.34	0.35	0.35	0.34	0.35	0.34	0.34	0.33	0.36	0.37	0.35	0.35	0.35	0.36	0.35	0.36	0.35	0.36	0.34	
Xmg ^b	0.34	0.00	0.35	0.34	0.35	0.35	0.34	0.33	0.34	0.34	0.33	0.34	0.33	0.33	0.32	0.35	0.36	0.35	0.35	0.35	0.35	0.35	0.36	0.35	0.36	0.33	

Hornblende*Table 10: Hornblende in enclaves*

Type	Enclave																					
Sample Spot No.	BG12D					BG15A					BG29					BG44						
	5	6	7	8	9	1	2	3	4	5	6	2	3	4	5	6	7	1	2	3	4	5
SiO ₂	42.49	42.71	42.61	42.03	42.21	41.99	41.84	42.02	42.18	42.50	43.33	42.88	43.11	42.78	42.99	43.17	42.70	42.54	42.80	42.46	40.31	41.45
TiO ₂	1.07	0.97	1.11	0.96	1.19	1.32	1.21	1.15	1.20	1.41	1.12	0.99	1.12	1.12	0.94	1.07	1.03	0.96	1.12	1.03	0.79	1.20
Al ₂ O ₃	9.87	10.07	9.75	10.09	10.25	10.06	9.85	10.37	10.17	10.00	9.32	9.62	9.59	9.74	9.49	9.68	9.89	9.46	8.95	9.38	11.79	10.28
FeO	22.54	22.79	22.11	22.70	22.74	23.08	22.98	23.11	23.14	23.31	23.03	23.98	24.00	23.77	24.12	24.12	23.83	23.61	23.27	23.23	24.70	23.73
MnO	0.52	0.61	0.54	0.64	0.69	0.75	0.59	0.65	0.73	0.69	0.61	1.00	0.96	0.87	0.83	1.01	0.84	0.66	0.61	0.65	0.53	0.66
MgO	7.04	6.75	6.84	6.70	6.67	6.61	6.53	6.66	6.67	6.50	6.95	6.57	6.41	6.23	6.19	6.23	6.28	6.96	7.20	6.95	5.91	6.35
CaO	11.89	11.90	11.85	11.81	12.11	11.73	11.87	11.99	12.14	11.78	11.94	11.33	11.30	11.30	11.27	11.28	11.38	12.00	11.69	11.77	11.92	11.80
Na ₂ O	1.13	1.13	1.20	1.09	0.97	1.39	1.15	1.28	1.28	1.24	1.11	1.41	1.50	1.48	1.35	1.48	1.51	1.07	1.10	1.17	1.24	1.16
K ₂ O	1.11	1.14	1.11	1.12	1.21	1.23	1.19	1.27	1.26	1.16	1.09	1.12	1.03	1.11	1.19	1.11	1.12	1.03	1.05	1.04	1.21	1.24
Total	97.68	98.07	97.13	97.13	98.04	98.17	97.20	98.51	98.76	98.58	98.50	98.89	99.00	98.40	98.36	99.15	98.58	98.30	97.79	97.69	98.40	97.87
Si	6.59	6.60	6.63	6.56	6.53	6.51	6.55	6.49	6.51	6.56	6.67	6.61	6.63	6.62	6.66	6.64	6.60	6.59	6.65	6.61	6.29	6.47
Al	1.41	1.40	1.37	1.44	1.47	1.49	1.45	1.51	1.49	1.44	1.33	1.39	1.37	1.38	1.34	1.36	1.40	1.41	1.35	1.39	1.71	1.53
Al	0.39	0.43	0.42	0.42	0.40	0.35	0.37	0.38	0.36	0.37	0.35	0.36	0.37	0.40	0.39	0.39	0.40	0.32	0.29	0.33	0.46	0.36
Ti	0.13	0.11	0.13	0.11	0.14	0.15	0.14	0.13	0.14	0.16	0.13	0.11	0.13	0.13	0.11	0.12	0.12	0.11	0.13	0.12	0.09	0.14
Fe ²⁺	2.92	2.94	2.88	2.96	2.94	2.99	3.01	2.99	2.99	3.01	2.96	3.09	3.09	3.08	3.13	3.10	3.08	3.06	3.02	3.02	3.23	3.10
Mn	0.07	0.08	0.07	0.09	0.09	0.10	0.08	0.09	0.10	0.09	0.08	0.13	0.12	0.11	0.11	0.13	0.11	0.09	0.08	0.09	0.07	0.09
Mg	1.63	1.55	1.59	1.56	1.54	1.53	1.52	1.53	1.53	1.49	1.59	1.51	1.47	1.44	1.43	1.43	1.45	1.61	1.67	1.61	1.38	1.48
Ca	1.97	1.97	1.98	1.98	2.01	1.95	1.99	1.99	2.01	1.95	1.97	1.87	1.86	1.87	1.87	1.86	1.89	1.99	1.95	1.96	1.99	1.97
Na	0.34	0.34	0.36	0.33	0.29	0.42	0.35	0.38	0.38	0.37	0.33	0.42	0.45	0.44	0.41	0.44	0.45	0.32	0.33	0.35	0.37	0.35
K	0.22	0.23	0.22	0.22	0.24	0.24	0.24	0.25	0.25	0.23	0.21	0.22	0.20	0.22	0.23	0.22	0.22	0.20	0.21	0.21	0.24	0.25
Tot.cat.	15.67	15.65	15.64	15.67	15.66	15.74	15.69	15.74	15.74	15.67	15.63	15.72	15.69	15.69	15.68	15.69	15.72	15.70	15.67	15.69	15.84	15.74
Xmg	0.36	0.35	0.36	0.34	0.34	0.34	0.34	0.34	0.34	0.33	0.35	0.33	0.32	0.32	0.31	0.32	0.32	0.34	0.36	0.35	0.30	0.32

Table 11: Hornblende in granites

Type	Granite																							
Sample	BG12C2					BG12D					BG15B					BG44				BG46A				
Spot No.	1	2	5	6	7	2	3	5	4	6	3	4	5	6	7	2	3	4	5	8	1	2	6	7
SiO ₂	40.75	42.30	42.09	41.43	42.38	41.74	41.83	40.54	41.62	41.70	41.49	42.14	40.99	41.27	40.34	41.35	41.54	42.22	41.70	41.63	41.30	42.87	41.99	42.95
TiO ₂	2.16	1.17	1.20	1.67	1.21	0.95	0.95	0.89	1.13	0.97	1.15	1.10	0.95	1.09	0.96	1.11	1.30	1.14	1.26	1.65	2.17	1.17	1.67	1.21
Al ₂ O ₃	10.46	10.24	10.49	10.46	10.37	10.36	10.62	12.18	10.50	10.65	9.37	9.29	10.04	9.31	11.01	10.02	9.95	9.54	10.04	9.94	10.23	10.03	10.23	10.15
FeO	23.57	23.77	23.52	23.95	23.72	22.90	22.62	24.11	21.97	22.63	23.78	24.01	24.33	23.92	24.33	23.63	23.53	23.76	24.12	23.69	22.40	22.60	22.77	22.55
MnO	0.56	0.55	0.44	0.61	0.51	0.52	0.58	0.65	0.64	0.65	0.69	0.79	0.63	0.69	0.63	0.56	0.58	0.72	0.74	0.52	0.65	0.64	0.70	0.59
MgO	6.46	6.65	6.83	6.69	6.82	6.38	6.34	7.37	6.66	6.49	6.71	6.69	6.17	6.62	5.87	6.31	6.66	6.59	6.54	6.50	6.24	6.43	6.47	6.59
CaO	11.35	11.45	11.48	11.54	11.39	12.00	11.93	9.87	11.97	11.89	11.49	11.78	11.85	11.44	11.95	11.74	11.70	11.69	11.57	11.75	11.81	11.92	12.02	11.86
Na ₂ O	1.53	1.29	1.11	1.34	1.34	1.03	1.15	1.08	1.30	1.21	1.25	1.15	1.22	1.16	1.24	1.18	1.21	1.18	1.23	1.29	1.52	1.28	1.33	1.33
K ₂ O	0.99	1.24	1.08	1.23	1.23	1.17	1.24	0.98	1.23	1.19	1.14	1.01	1.22	1.12	1.17	1.22	1.16	1.17	1.19	1.11	0.99	1.24	1.23	1.23
Total	97.81	98.66	98.24	98.93	98.97	97.07	97.26	97.66	97.02	97.37	97.06	97.96	97.40	96.62	97.50	97.12	97.64	98.01	98.39	98.08	97.31	98.17	98.42	98.46
Si	6.36	6.53	6.50	6.40	6.51	6.53	6.53	6.30	6.50	6.50	6.54	6.57	6.46	6.54	6.36	6.50	6.49	6.57	6.48	6.48	6.45	6.62	6.49	6.60
Al	1.64	1.47	1.50	1.60	1.49	1.47	1.47	1.70	1.50	1.50	1.46	1.43	1.54	1.46	1.64	1.50	1.51	1.43	1.52	1.52	1.55	1.38	1.51	1.40
Al	0.29	0.39	0.42	0.31	0.39	0.44	0.48	0.54	0.44	0.46	0.28	0.28	0.33	0.28	0.40	0.36	0.32	0.32	0.32	0.30	0.33	0.44	0.35	0.44
Ti	0.25	0.14	0.14	0.19	0.14	0.11	0.11	0.10	0.13	0.11	0.14	0.13	0.11	0.13	0.11	0.13	0.15	0.13	0.15	0.19	0.25	0.14	0.19	0.14
Fe ²⁺	3.08	3.07	3.04	3.10	3.05	3.00	2.95	3.14	2.87	2.95	3.13	3.13	3.21	3.17	3.21	3.11	3.07	3.09	3.14	3.08	2.93	2.92	2.94	2.90
Mn	0.07	0.07	0.06	0.08	0.07	0.07	0.08	0.09	0.08	0.09	0.09	0.10	0.08	0.09	0.08	0.07	0.08	0.09	0.10	0.07	0.09	0.08	0.09	0.08
Mg	1.50	1.53	1.57	1.54	1.56	1.49	1.48	1.71	1.55	1.51	1.58	1.56	1.45	1.56	1.38	1.48	1.55	1.53	1.52	1.51	1.45	1.48	1.49	1.51
Ca	1.90	1.89	1.90	1.91	1.88	2.01	1.99	1.64	2.00	1.99	1.94	1.97	2.00	1.94	2.02	1.98	1.96	1.95	1.93	1.96	1.98	1.97	1.99	1.95
Na	0.46	0.39	0.33	0.40	0.40	0.31	0.35	0.32	0.39	0.37	0.38	0.35	0.37	0.36	0.38	0.36	0.37	0.36	0.37	0.39	0.46	0.38	0.40	0.40
K	0.20	0.24	0.21	0.24	0.24	0.23	0.25	0.19	0.24	0.24	0.23	0.20	0.24	0.23	0.24	0.24	0.23	0.23	0.24	0.22	0.20	0.24	0.24	0.24
Tot.cat.	15.75	15.72	15.67	15.77	15.73	15.67	15.68	15.73	15.72	15.71	15.76	15.72	15.80	15.75	15.81	15.74	15.74	15.71	15.75	15.72	15.68	15.65	15.70	15.66
Xmg	0.33	0.33	0.34	0.33	0.34	0.33	0.33	0.35	0.35	0.34	0.33	0.33	0.31	0.33	0.30	0.32	0.34	0.33	0.33	0.33	0.33	0.34	0.34	0.34

Appendix IV: Zircon

Only values within the +/-2s error margin of 15 and below for concordance (Conc%) were plotted.

Table1: Table showing data from Lu-Hf-Yb and U-Pb isotope analysis used to generate Fig.15-19 from zircon grains within sample BG15 and BG26s. **Highlight** = inherited zircon crystal. **Highlight**= concordant samples; **red text**= inherited concordant zircon grains. $^{207}\text{Pb}/^{235}\text{U}$ and $^{207}\text{Pb}/^{206}\text{Pb}$ values in ppm.

Sample	SPOT_NAME	$^{207}\text{Pb}/^{235}\text{U}$	$\pm 2s$	$^{206}\text{Pb}/^{238}\text{U}$	$\pm 2s$	$^{207}\text{Pb}/^{206}\text{Pb}$	$\pm 2s$	Conc %	AGE	$\pm 2s$	(176/177) Hf_{Lu}	$\text{eHf}_{\text{Lu-T}}$	+/- 2s	TDM	AGE
BG15	zircon 07	292	13	291	8	296	38	98	291	8	0.282414	-6.6	0.9	1.30	293
BG15	zircon 09	303	12	299	10	335	27	89	335	27	0.282446	-5.5	0.8	1.24	293
BG15	zircon 11	293	11	290	9	309	26	94	309	26	0.282451	-5.3	0.6	1.23	293
BG15	zircon 12	294	12	293	10	304	25	96	293	10	0.282438	-5.8	1.0	1.26	293
BG15	zircon 13	302	12	297	8	340	32	87	340	32	0.282463	-4.9	1.0	1.21	293
BG15	zircon 14	295	13	293	11	307	28	95	293	11	0.282402	-7.0	1.2	1.33	293
BG15	zircon 15	329	14	328	10	340	34	96	328	10	0.282472	-3.8	1.1	1.17	328
BG15	zircon 16	298	11	297	10	302	20	98	297	10					
BG15	zircon 20	291	13	289	8	306	37	95	289	8	0.282430	-6.1	0.9	1.27	293
BG15	zircon 21	825	45	538	15	1707	43	32	1707	43	0.282362	23.6	1.2	0.78	1707
BG15	zircon 22	303	10	304	9	297	20	102	304	9	0.282475	-4.5	1.0	1.18	293
BG15	zircon 23	293	22	293	14	293	66	100	293	14	0.282461	-5.0	0.9	1.21	293
BG15	zircon 25	294	18	295	9	290	62	101	295	9	0.282477	-4.4	1.0	1.18	293
BG15	zircon 26	293	12	294	9	288	31	102	294	9	0.282446	-5.5	1.0	1.24	293
BG15	zircon 27	292	9	290	8	302	19	96	290	8	0.282496	-3.7	1.1	1.14	293
BG15	zircon 28	297	13	296	8	300	38	99	296	8	0.282472	-4.5	1.2	1.19	293
BG15	zircon 33	348	46	346	13	363	144	95	346	13	0.282447	-4.2	1.0	1.22	346
BG15	zircon 35	294	12	293	10	304	28	96	293	10	0.282441	-5.7	0.9	1.25	293
BG15	zircon 37	323	25	319	11	355	79	90	355	79	0.282474	-3.1	0.9	1.16	355
BG15	zircon 38	297	10	296	8	303	23	98	296	8					
BG15	zircon 39	292	13	291	9	302	37	96	291	9					
BG35	Zircon_111	278	15	277	8	291	54	95	277	8	0.282484	-4.1	0.9	1.20	293
BG35	Zircon_119	288	12	287	10	298	27	96	287	10	0.282467	-4.7	0.8	1.16	293
BG35	Zircon_120	293	14	294	9	283	42	104	294	9	0.282489	-3.9	0.8	1.25	293
BG35	Zircon_126	293	13	288	7	328	43	88	328	43	0.282441	-5.7	1.3	0.56	293
BG35	Zircon_127	833	55	515	16	1812	53	28	1812	53	0.282443	28.9	5.4	1.27	1812
BG35	Zircon_128	284	11	281	7	302	31	93	302	31	0.282432	-6.0	0.7	1.18	293
BG35	Zircon_129	335	14	331	12	358	22	92	358	22	0.282462	-3.5	0.8	1.23	358
BG35	Zircon_130	459	15	457	11	471	26	97	457	11	0.282419	-2.8	1.1	1.20	457
BG35	Zircon_131	331	15	328	8	354	46	93	354	46	0.282456	-3.8	1.0	1.19	354
BG35	Zircon_132	316	13	313	9	333	33	94	333	33	0.282464	-3.9	0.7	1.19	333
BG35	Zircon_133	296	13	297	8	293	38	101	297	8	0.282471	-4.6	4.7	1.19	293
BG35	Zircon_133	296	13	297	8	293	38	101	297	8	0.282533	-2.4	1.7	1.07	293

Table1(cont.): Table showing data from Lu-Hf–Yb and U-Pb isotope analysis used to generate Fig.15-19 from zircon grains within sample BG25. **Highlight** = inherited zircon crystal. **Highlight** = concordant samples; **red text** = inherited concordant zircon grains.

Sample	SPOT_NAME	²⁰⁷ Pb/ ²³⁵ U	±2s	²⁰⁶ Pb/ ²³⁸ U	±2s	²⁰⁷ Pb/ ²⁰⁶ Pb	±2s	Conc %	AGE	±2s	(176/177)Hf _{Lu}	eHf _{Lu-T}	+/- 2s	TDM	AGE
BG26	zircon 46	296	18	294	12	310	51	95	294	12	0.282467	-4.7	1.0	1.20	293
BG26	zircon 47	292	13	291	12	299	26	97	291	12	0.282469	-4.7	0.7	1.20	293
BG26	zircon 48	294	13	295	9	290	34	102	295	9	0.282446	-5.5	1.0	1.24	293
BG26	zircon 49	299	12	298	8	300	34	100	298	8	0.282474	-4.5	0.9	1.19	293
BG26	zircon 50	293	13	293	10	293	31	100	293	10	0.282463	-4.9	0.7	1.21	293
BG26	zircon 51	348	23	347	12	352	66	99	347	12	0.282373	-6.9	1.0	1.36	347
BG26	zircon 53	286	12	284	9	302	31	94	302	31	0.282438	-5.8	1.0	1.26	293
BG26	zircon 54	295	16	294	9	300	54	98	294	9	0.282485	-4.1	0.7	1.17	293
BG26	zircon 55	297	12	294	10	317	29	93	317	29	0.282472	-4.6	0.5	1.19	293
BG26	zircon 59	285	15	285	11	288	40	99	285	11	0.282459	-5.0	0.8	1.21	293
BG26	zircon 60	292	11	292	9	293	25	100	292	9	0.282441	-5.6	0.8	1.25	293
BG26	zircon 61	278	11	277	8	288	32	96	277	8	0.282443	-5.6	1.0	1.25	293
BG26	zircon 64	291	16	291	11	292	47	100	291	11	0.282460	-5.0	1.0	1.21	293
BG26	zircon 65	288	11	287	9	297	25	96	287	9	0.282420	-6.4	0.9	1.29	293
BG26	zircon 67	288	10	287	7	296	25	97	287	7	0.282418	-6.5	0.8	1.30	293
BG26	zircon 68	297	44	291	12	350	159	83	350	159	0.282364	-7.1	1.0	1.38	350
BG26	zircon 72	291	15	292	10	280	47	104	292	10	0.282432	-6.0	0.8	1.27	293
BG26	zircon 75	291	16	289	13	314	34	92	314	34	0.282374	-8.0	1.0	1.38	293
BG26	zircon 76	293	11	292	8	303	31	96	292	8	0.282444	-5.5	1.0	1.24	293
BG26	zircon 77	295	18	293	11	308	57	95	293	11	0.282377	-7.9	0.8	1.37	293
BG26	zircon 79	289	16	288	13	295	39	97	288	13	0.282446	-5.5	0.8	1.24	293
BG26	zircon 80	292	17	292	13	291	41	100	292	13	0.282476	-4.4	1.0	1.18	293
BG26	zircon 85	292	17	291	12	300	44	97	291	12	0.282441	-5.7	0.7	1.25	293
BG26	zircon 86	319	14	319	11	324	28	99	319	11	0.282455	-5.1	1.0	1.22	293
BG26	zircon 87	290	15	289	11	294	38	98	289	11	0.282442	-5.6	0.9	1.25	293
BG26	zircon 88	294	12	293	9	302	32	97	293	9	0.282414	-6.6	0.9	1.30	293
BG26	zircon 89	283	13	276	9	338	33	82	338	33	0.282397	-7.2	1.0	1.33	293
BG26	zircon 90	297	11	296	8	307	31	96	296	8	0.282384	-7.7	1.0	1.36	293
BG26	zircon 91	294	15	294	13	292	32	101	294	13					
BG26	zircon 92	293	14	293	9	298	40	98	293	9	0.282416	-6.5	1.0	1.30	293
BG26	zircon 93	2271	78	2151	60	2380	17	90	2380	17	0.281196	-2.2	0.8	2.77	2380
BG26	zircon 93	2271	78	2151	60	2380	17	90	2380	17	0.281244	-0.5	0.8	2.68	2380
BG26	zircon 94	333	48	334	13	326	159	102	334	13	0.282358	-7.7	1.0	1.39	334
BG26	zircon 98	287	24	288	14	285	76	101	288	14	0.282323	-9.8	1.0	1.48	293
BG26	zircon 99	289	14	289	11	290	35	100	289	11					
BG26	zircon 100	285	19	284	13	286	55	100	284	13	0.282418	-6.4	1.2	1.29	293
BG26	zircon 101	291	18	290	15	295	43	98	290	15					
BG26	zircon 102	295	15	294	8	302	50	97	294	8	0.282425	-6.2	0.9	1.32	293
BG26	zircon 103	294	20	293	15	307	51	95	293	15	0.282407	-6.9	1.1	1.38	293
BG26	zircon 104	282	42	283	12	279	161	101	283	12	0.282374	-8.0	1.1	1.25	293
BG26	zircon 105	289	20	289	9	296	71	98	289	9	0.282439	-5.7	0.9	1.28	293
BG26	zircon 106	295	16	294	14	301	35	98	294	14	0.282425	-6.2	0.7	1.29	293
BG26	zircon 107	294	15	294	11	295	42	100	294	11	0.282422	-6.3	1.1	1.17	293

Table 2: Table showing more Lu-Hf-Yb isotopic analysis of granite samples. (Note only Lu-Hf_YB isotope analyses were done on BG19, BG2, BG3 & BG 48.) TDM calculated based on assumed magmatic age of 293 Ma.

Granite														
Inner					Middle									
BG19					BG2					BG3				
Spot Name	(176/177)HfLu	eHfLu-T	+/- 2s	TDM	Spot Name	(176/177)HfLu	eHfLu-T	+/- 2s	TDM	Spot Name	(176/177)HfLu	eHfLu-T	+/- 2s	TDM
BG19_118	0.28246	-4.82795	0.49642	1.20447	BG2_143	0.28243	-5.94763	0.53503	1.26591	BG3_7	0.28244	-5.75228	0.57727	1.25520
BG19_119	0.28244	-5.75191	0.45081	1.25518	BG2_144	0.28245	-5.48146	0.49700	1.24034	BG3_8	0.28245	-5.33684	0.73201	1.23240
BG19_120	0.28244	-5.79893	0.74546	1.25776	BG2_145	0.28242	-6.56003	0.53491	1.29949	BG3_9	0.28244	-5.85451	0.69891	1.26081
BG19_126	0.28242	-6.24182	0.69457	1.28205	BG2_146	0.28243	-5.90165	0.51735	1.26339	BG3_10	0.28242	-6.40322	0.54332	1.29090
BG19_129	0.28247	-4.78098	0.55588	1.20189	BG2_150	0.28245	-5.39105	1.00624	1.23538	BG3_11	0.28245	-5.20071	0.98904	1.22493
BG19_130	0.28164	-33.85019	0.61102	2.77489	BG2_151	0.28242	-6.34190	0.97595	1.28754	BG3_12	0.28238	-7.67149	0.66769	1.36038
BG19_133	0.28245	-5.34529	0.62359	1.23287	BG2_152	0.28244	-5.62019	0.66897	1.24795	BG3_13	0.28244	-5.56648	0.41847	1.24501
BG19_137	0.28229	-10.92949	1.04796	1.53847	BG2_153	0.28244	-5.68828	0.57522	1.25169	BG3_14	0.28244	-5.51459	0.60695	1.24216
BG19_139	0.28245	-5.40057	0.62075	1.23590	BG2_154	0.28241	-6.57427	0.52402	1.30027	BG3_15	0.28239	-7.57931	0.57171	1.35534
BG19_141	0.28248	-4.33288	0.73969	1.17727	BG2_155	0.28246	-5.05343	0.96343	1.21685	BG3_16	0.28245	-5.45058	0.58158	1.23864
BG19_142	0.28247	-4.76932	0.66839	1.20125	BG2_156	0.28244	-5.63128	0.71093	1.24856	BG3_20	0.28242	-6.30132	0.53522	1.28531
					BG2_157	0.28244	-5.74233	0.84281	1.25465	BG3_21	0.28244	-5.59086	0.54770	1.24634
					BG2_158	0.28243	-5.94452	0.87843	1.26574	BG3_22	0.28245	-5.41777	0.55353	1.23684
					BG2_159	0.28243	-6.03331	0.87763	1.27061	BG3_23	0.28239	-7.59380	1.23506	1.35613
										BG3_24	0.28243	-6.05855	0.60181	1.27200
										BG3_25	0.28244	-5.66577	0.71032	1.25045
										BG3_26	0.28243	-5.96645	0.68955	1.26695
										BG3_27	0.28243	-6.02743	0.45926	1.27029
										BG3_28	0.28245	-5.24074	0.55252	1.22713
										BG3_29	0.28244	-5.83143	0.66902	1.25954
										BG3_33	0.28239	-7.40602	0.71902	1.34585
										BG3_34	0.28243	-6.18731	0.57594	1.27906
										BG3_35	0.28245	-5.47460	1.04768	1.23996
										BG3_36	0.28243	-6.20089	0.62245	1.27980
										BG3_37	0.28244	-5.69404	0.64235	1.25200
										BG3_38	0.28242	-6.22489	0.59558	1.28112

Table 2(cont.): Table showing more Lu-Hf-Yb isotopic analysis of granite samples. (Note only Lu-Hf_YB isotope analyses were done on BG19, BG2, BG3 & BG 48.) TDM calculated based on assumed magmatic age of 293 Ma.

Granite																			
Outer																			
BG13					BG26					BG26				BG26					
Spot Name	(176/177)HfLu	eHfLu-T	+/- 2s	TDM	Spot Name	(176/177)HfLu	eHfLu-T	+/- 2s	TDM	Spot Name	(176/177)HfLu	eHfLu-T	+/- 2s	TDM	Spot Name	(176/177)HfLu	eHfLu-T	+/- 2s	TDM
BG13_86	0.28247	-4.75252	0.46450	1.20032	BG26_7	0.28244	-5.82309	0.45613	1.25908	BG26_20	0.28244	-5.75072	0.58347	1.25511	BG26_76	0.28244	-5.54709	0.97480	1.24394
BG13_88	0.28247	-4.45662	0.59959	1.18407	BG26_7b	0.28245	-5.18769	0.46750	1.22422	BG26_36	0.28244	-5.69942	0.66788	1.25230	BG26_77	0.28238	-7.93046	0.82357	1.37456
BG13_89	0.28245	-5.25756	0.66691	1.22805	BG26_8	0.28245	-5.27168	0.48746	1.22883	BG26_37	0.28243	-5.88137	0.62187	1.26228	BG26_79	0.28245	-5.46817	0.82818	1.23961
BG13_90	0.28247	-4.73313	0.57589	1.19926	BG26_9	0.28244	-5.72590	0.48870	1.25375	BG26_38	0.28244	-5.66511	0.76677	1.25042	BG26_80	0.28248	-4.42011	1.02429	1.18207
BG13_91	0.28247	-4.78864	0.58573	1.20231	BG26_9b	0.28245	-5.25686	0.39713	1.22801	BG26_39	0.28242	-6.21852	0.62646	1.28077	BG26_85	0.28244	-5.65337	0.66065	1.24977
BG13_93	0.28217	-15.30702	0.61280	1.77683	BG26_10	0.28103	-55.4849	0.60619	3.91633	BG26_46	0.28247	-4.72344	0.96399	1.19873	BG26_86	0.28246	-5.14558	0.96770	1.22190
BG13_94	0.28247	-4.54676	1.07631	1.18902	BG26_11	0.28243	-6.00074	0.56577	1.26883	BG26_47	0.28247	-4.66848	0.71241	1.19571	BG26_87	0.28244	-5.60998	0.86333	1.24739
BG13_98	0.28246	-4.92967	0.44555	1.21005	BG26_12	0.28245	-5.41424	0.44886	1.23665	BG26_48	0.28245	-5.47303	0.96035	1.23988	BG26_88	0.28241	-6.61192	0.94892	1.30234
BG13_99	0.28247	-4.75067	0.63460	1.20022	BG26_21	0.28242	-6.56746	0.56951	1.29990	BG26_49	0.28247	-4.48307	0.94211	1.18552	BG26_89	0.28240	-7.20451	0.97724	1.33481
BG13_100	0.28246	-5.07123	0.52314	1.21782	BG26_23	0.28245	-5.28322	0.84617	1.22946	BG26_50	0.28246	-4.86382	0.74096	1.20644	BG26_90	0.28238	-7.65723	1.01605	1.35960
BG13_101	0.28245	-5.41460	0.67606	1.23667	BG26_24	0.28244	-5.70464	0.56921	1.25259	BG26_51	0.28237	-6.85753	0.96122	1.36031	BG26_92	0.28242	-6.53468	0.96686	1.29810
BG13_103	0.28244	-5.64893	0.61697	1.24953	BG26_25	0.28243	-5.94155	0.69524	1.26558	BG26_53	0.28244	-5.76960	0.98577	1.25615	BG26_93	0.28120	-2.23263	0.77755	2.77325
BG13_104	0.28245	-5.17688	0.59630	1.22362	BG26_26	0.28241	-6.58846	0.61336	1.30105	BG26_54	0.28248	-4.11104	0.68135	1.16508	BG26_94	0.28124	-0.52380	0.78261	2.67887
BG13_105	0.28245	-5.18524	0.58290	1.22408	BG26_27	0.28245	-5.33973	0.50586	1.23256	BG26_55	0.28247	-4.56744	0.53393	1.19016	BG26_95	0.28236	-7.67006	0.98209	1.39411
BG13_106	0.28244	-5.60748	0.84858	1.24725	BG26_28	0.28245	-5.49414	0.65154	1.24104	BG26_59	0.28246	-4.99781	0.84219	1.21379	BG26_98	0.28232	-9.83959	1.02134	1.47896
BG13_107	0.28249	-3.94035	0.45684	1.15570	BG26_29	0.28244	-5.65937	0.58341	1.25010	BG26_60	0.28244	-5.64604	0.84795	1.24937	BG26_100	0.28242	-6.44749	1.16710	1.29332
BG13_111	0.28225	-12.29435	0.60682	1.61290	BG26_33	0.28244	-5.76997	0.58428	1.25617	BG26_61	0.28244	-5.57621	0.98398	1.24554	BG26_102	0.28243	-6.19964	0.94239	1.31631
BG13_113	0.28247	-4.58141	0.81033	1.19093	BG26_34	0.28244	-5.56077	0.49452	1.24469	BG26_64	0.28246	-4.98140	0.96712	1.21289	BG26_103	0.28241	-6.86680	1.12527	1.38010
BG13_114	0.28245	-5.17822	0.58099	1.22370	BG26_35	0.28241	-6.60189	0.56701	1.30179	BG26_65	0.28242	-6.40217	0.89719	1.29084	BG26_104	0.28237	-8.03172	1.09907	1.25256
					BG26_13	0.28242	-6.29038	0.64695	1.28471	BG26_67	0.28242	-6.47981	0.77169	1.29510	BG26_105	0.28244	-5.70409	0.85879	1.28144
					BG26_14	0.28245	-5.28061	0.54866	1.22932	BG26_68	0.28236	-7.09485	0.95180	1.37579	BG26_106	0.28242	-6.23074	0.68197	1.28728
					BG26_15	0.28244	-5.75876	0.58668	1.25555	BG26_72	0.28243	-5.97561	0.82481	1.26745	BG26_107	0.28242	-6.33722	1.05644	1.16617
					BG26_16	0.28242	-6.44758	0.59812	1.29333	BG26_75	0.28237	-8.03735	0.99622	1.38041					

Table 2 (cont.): Table showing more Lu-Hf-Yb isotopic analyses of granite samples. (Note only Lu-Hf_YB isotope analyses were done on BG19, BG2, BG3 & BG 48.) TDM calculated based on assumed magmatic age of 293 Ma.

Granite														
Outer														
BG35					BG35					BG48				
Spot Name	(176/177)HfLu	eHfLu-T	+/- 2s	TDM	Spot Name	(176/177)HfLu	eHfLu-T	+/- 2s	TDM	Spot Name	(176/177)HfLu	eHfLu-T	+/- 2s	TDM
BG35_59	0.28244	-5.54483	0.50250	1.24382	BG35_111	0.28248	-4.13083	0.89592	1.19923	BG48_7	0.28246	-4.96139	0.50570	1.21179
BG35_60	0.28247	-4.75816	0.66948	1.20063	BG35_119	0.28247	-4.73262	0.75002	1.15619	BG48_8	0.28245	-5.38013	0.49530	1.23478
BG35_61	0.28246	-4.86384	0.49503	1.20644	BG35_120	0.28249	-3.94917	0.75989	1.25039	BG48_11	0.28245	-5.29518	0.51553	1.23012
BG35_62	0.28245	-5.16763	0.53481	1.22312	BG35_126	0.28244	-5.66469	1.32554	0.56329	BG48_12	0.28245	-5.29714	0.79672	1.23022
BG35_64	0.28246	-4.86582	0.85942	1.20655	BG35_127	0.28244	28.91474	5.35877	1.26643	BG48_13	0.28246	-4.97235	0.46523	1.21239
BG35_65	0.28246	-4.90085	0.74580	1.20847	BG35_128	0.28243	-5.95697	0.67439	1.18236	BG48_14	0.28243	-5.89261	0.46745	1.26290
BG35_66	0.28245	-5.43198	0.77623	1.23762	BG35_129	0.28246	-3.45088	0.79551	1.22594	BG48_15	0.28246	-4.94830	0.63482	1.21107
BG35_66	0.28245	-5.34081	0.83566	1.23262	BG35_130	0.28242	-2.76057	1.05646	1.19579	BG48_16	0.28244	-5.79501	0.95204	1.25754
BG35_67	0.28246	-4.96079	0.76101	1.21176	BG35_131	0.28246	-3.75503	1.03418	1.18912	BG48_22	0.28246	-5.03936	0.61848	1.21607
BG35_68	0.28246	-5.00050	0.57768	1.21394	BG35_132	0.28246	-3.94854	0.68900	1.19169	BG48_23	0.28245	-5.34902	0.66630	1.23307
BG35_72	0.28243	-5.99321	0.68174	1.26842	BG35_133	0.28247	-4.59527	4.68888	1.19169	BG48_24	0.28245	-5.44089	0.79595	1.23811
BG35_73	0.28245	-5.42012	0.67386	1.23697	BG35_133	0.28253	-2.40833	1.66614	1.07143	BG48_26	0.28245	-5.22002	0.55289	1.22599
BG35_74	0.28245	-5.21774	0.64293	1.22587	BG35_47	0.28244	-5.53495	0.70828	1.24327	BG48_27	0.28247	-4.72396	0.51355	1.19876
BG35_75	0.28246	-5.04576	0.80067	1.21642	BG35_40	0.28247	-4.78228	0.54988	1.20196	BG48_29	0.28246	-4.84450	0.50495	1.20537
					BG35_49	0.28245	-5.49439	0.68085	1.24105	BG48_33	0.28247	-4.66641	0.94077	1.19559
					BG35_50	0.28244	-5.65505	0.54580	1.24986	BG48_34	0.28240	-7.09897	0.86420	1.32903
					BG35_50b	0.28245	-5.26469	0.53763	1.22844	BG48_35	0.28244	-5.68738	0.62278	1.25164
					BG35_51	0.28246	-4.89614	0.67328	1.20821	BG48_36	0.28246	-4.92704	0.53338	1.20991
					BG35_51b	0.28247	-4.48009	0.57447	1.18536	BG48_37	0.28246	-4.99807	0.80829	1.21381
					BG35_52	0.28245	-5.23059	0.59836	1.22657	BG48_38	0.28228	-11.20005	0.93528	1.55323
					BG35_53	0.28245	-5.25863	0.58017	1.22811	BG48_39	0.28246	-4.90927	0.92573	1.20893
					BG35_54	0.28247	-4.76688	0.67915	1.20111	BG48_40	0.28245	-5.42719	0.81992	1.23736
					BG35_55	0.28247	-4.74323	0.63941	1.19981					

Crystal Fractionation

Fractionation modelling- starting parameters

Table 1a: Starting parameters after applied corrections for sample BG27, one of the two samples used to model the crystal fractionation.

	SiO ₂	TiO ₂	Al ₂ O ₃	FeO	MnO	MgO	CaO	Na ₂ O	K ₂ O	H ₂ O	Total	P ₂ O ₅	Fe ₂ O ₃
BG27 - Starting	72.99	0.28	14.09		0.08	0.56	2.46	3.12	3.66		97.24		2.67
BG27 - Starting normalised	75.06	0.29	14.49	0.00	0.08	0.58	2.53	3.21	3.76	0.00	100.00		
BG27 - Fe corrected	75.06	0.29	14.49	2.40	0.08	0.58	2.53	3.21	3.76	0.00	102.40		
BG27 - Fe normalised	73.30	0.28	14.15	2.35	0.08	0.56	2.47	3.13	3.68	0.00	100.00	0.08	
BG27 - CaO corrected	73.30	0.28	14.15	2.35	0.08	0.56	2.37	3.13	3.68	0.00	99.89		
BG27 - CaO normalised	73.38	0.28	14.16	2.35	0.08	0.56	2.37	3.14	3.68	0.00	100.00		
BG27 - H ₂ O add	73.38	0.28	14.16	2.35	0.08	0.56	2.37	3.14	3.68	3.40	103.40		
BG27 - H ₂ O normalised	70.97	0.27	13.70	2.27	0.08	0.54	2.29	3.03	3.56	3.29	100.00		
Starting parameters after corrections	70.97	0.27	13.70	2.27	0.08	0.54	2.29	3.03	3.56	3.29	100.00		

Table 1b: Starting parameters after applied corrections for sample BG34, one of the two samples used to model the crystal fractionation.

	SiO ₂	TiO ₂	Al ₂ O ₃	FeO	MnO	MgO	CaO	Na ₂ O	K ₂ O	H ₂ O	Total	P ₂ O ₅	Fe ₂ O ₃
BG34 - Starting	66.57	0.53	16.35		0.09	1.19	3.96	3.30	3.19		95.18		4.67
BG34 - starting normalised	69.94	0.56	17.18	0.00	0.09	1.25	4.16	3.47	3.35	0.00	100.00		
BG34 - Fe corrected	69.94	0.56	17.18	4.20	0.09	1.25	4.16	3.47	3.35	0.00	104.20		
BG34 - Fe normalised	67.12	0.53	16.49	4.03	0.09	1.20	3.99	3.33	3.22	0.00	100.00	0.14	
BG34 - CaO corrected	67.12	0.53	16.49	4.03	0.09	1.20	3.81	3.33	3.22	0.00	99.82		
BG34 - CaO normalised	67.24	0.54	16.52	4.04	0.09	1.20	3.82	3.33	3.22	0.00	100.00		
BG34 - H ₂ O add	67.24	0.54	16.52	4.04	0.09	1.20	3.82	3.33	3.22	3.40	103.40		
BG34 - normalised	65.03	0.52	15.97	3.91	0.09	1.16	3.69	3.22	3.12	3.29	100.00		
Starting parameters after corrections	65.03	0.52	15.97	3.91	0.09	1.16	3.69	3.22	3.12	3.29	100.00		

Calculations explained:

Starting normalised: Take each starting oxide and divide it by the starting total and multiply by 100:

E.g. SiO₂ starting concentration = 72.99

Starting Total =97.24

$(72.99/97.24)*100=75.016$

Fe corrected: All Fe is treated as FeO. Starting Fe₂O₃ value (2.67) multiplied by conversion factor (0.8998) = 2.40 which is the corrected Fe value. All oxides are resumed to include the new FeO total.

Fe normalised: Take each oxide and divide it by the new Total (includes new FeO amount) and multiply by100.

CaO Corrected: It was assumed that all P₂O₅ occurs in the ideal apatite Ca₅(PO₄,CO₃)₃(F,O) thus CaO_t=CaO - 1.316886*P₂O₅.

CaO Normalised: Take each oxide and divide it by the new Total (includes new CaO amount) and multiply by100.

H₂O add: Add in 3.40 wt. % H₂O, this is the amount of water used when modelling. Re-sum the Total.

H₂O Normalised: Take each oxide and divide it by the new Total (includes H₂O) and multiply by100.

Fractionation modelling – Outputs

Table 2: Fractionation modelling outputs for plots shown in Fig.24 & 25.

Sample	Step	Press. ^a	Temp. ^b	TiO ₂	Al ₂ O ₃	FeO	MnO	MgO	CaO	Na ₂ O	K ₂ O	SiO ₂	sum
bg27_Bulk_rs_700_3_1	1	3	700	0.29	14.28	2.45	0.09	0.58	2.48	3.15	3.56	73.11	100
bg27_Bulk_rs_700_3_2	2	3	700	0.31	14.42	2.56	0.09	0.61	2.60	3.17	3.43	72.81	100
bg27_Bulk_rs_700_3_3	3	3	700	0.33	14.56	2.69	0.10	0.65	2.73	3.20	3.28	72.47	100
bg27_Bulk_rs_700_3_4	4	3	700	0.35	14.73	2.83	0.10	0.68	2.88	3.23	3.12	72.09	100
bg27_Bulk_rs_700_3_5	5	3	700	0.37	14.91	2.99	0.11	0.72	3.05	3.26	2.93	71.67	100
bg27_Bulk_rs_700_3_6	6	3	700	0.39	15.12	3.17	0.12	0.77	3.24	3.29	2.72	71.18	100
bg27_Bulk_rs_700_3_7	7	3	700	0.42	15.36	3.38	0.12	0.82	3.45	3.33	2.48	70.63	100
bg27_Bulk_rs_700_3_8	8	3	700	0.45	15.64	3.62	0.13	0.88	3.71	3.38	2.19	69.98	100
bg27_Bulk_rs_700_3_9	9	3	700	0.49	15.97	3.90	0.15	0.95	4.00	3.43	1.87	69.23	100
bg27_Bulk_rs_700_3_10	10	3	700	0.50	16.03	3.95	0.15	0.97	4.05	3.44	1.81	69.10	100
bg27_Bulk_rs_700_3_11	11	3	700	0.50	16.03	3.95	0.15	0.97	4.05	3.44	1.81	69.10	100
bg27_Bulk_rs_700_3_12	12	3	700	0.50	16.03	3.95	0.15	0.97	4.05	3.44	1.81	69.10	100
bg27_Bulk_rs_700_3_13	13	3	700	0.50	16.03	3.95	0.15	0.97	4.05	3.44	1.81	69.10	100
bg27_Bulk_rs_700_3_14	14	3	700	0.50	16.03	3.95	0.15	0.97	4.05	3.44	1.81	69.10	100
bg27_Bulk_rs_700_3_15	15	3	700	0.50	16.03	3.95	0.15	0.97	4.05	3.44	1.81	69.10	100
bg27_Bulk_rs_700_3_16	16	3	700	0.50	16.03	3.95	0.15	0.97	4.05	3.44	1.81	69.10	100
bg27_Bulk_rs_700_3_17	17	3	700	0.50	16.03	3.95	0.15	0.97	4.05	3.44	1.81	69.10	100
bg27_Bulk_rs_700_3_18	18	3	700	0.50	16.03	3.95	0.15	0.97	4.05	3.44	1.81	69.10	100
bg27_Bulk_rs_700_3_19	19	3	700	0.50	16.03	3.95	0.15	0.97	4.05	3.44	1.81	69.10	100
bg27_Bulk_rs_700_3_20	20	3	700	0.50	16.03	3.95	0.15	0.97	4.05	3.44	1.81	69.10	100
bg27_Bulk_rs_800_3_1	1	3	800	0.29	14.28	2.38	0.09	0.57	2.47	3.15	3.61	73.17	100
bg27_Bulk_rs_800_3_2	2	3	800	0.31	14.42	2.42	0.09	0.58	2.58	3.16	3.52	72.93	100
bg27_Bulk_rs_800_3_3	3	3	800	0.33	14.56	2.46	0.10	0.60	2.70	3.18	3.43	72.66	100
bg27_Bulk_rs_800_3_4	4	3	800	0.35	14.73	2.50	0.10	0.61	2.84	3.19	3.32	72.36	100
bg27_Bulk_rs_800_3_5	5	3	800	0.37	14.92	2.54	0.11	0.63	2.99	3.22	3.20	72.02	100
bg27_Bulk_rs_800_3_6	6	3	800	0.40	15.13	2.59	0.12	0.66	3.17	3.24	3.07	71.64	100
bg27_Bulk_rs_800_3_7	7	3	800	0.43	15.37	2.64	0.13	0.68	3.37	3.27	2.91	71.20	100
bg27_Bulk_rs_800_3_8	8	3	800	0.46	15.66	2.71	0.14	0.71	3.61	3.30	2.73	70.68	100
bg27_Bulk_rs_800_3_9	9	3	800	0.50	16.00	2.79	0.15	0.74	3.89	3.34	2.51	70.08	100
bg27_Bulk_rs_800_3_10	10	3	800	0.55	16.40	2.88	0.16	0.78	4.22	3.39	2.26	69.36	100
bg27_Bulk_rs_800_3_11	11	3	800	0.61	16.88	2.99	0.18	0.83	4.62	3.45	1.95	68.48	100
bg27_Bulk_rs_800_3_12	12	3	800	0.68	17.49	3.13	0.20	0.89	5.13	3.52	1.56	67.39	100
bg27_Bulk_rs_800_3_13	13	3	800	0.78	18.26	3.33	0.23	0.97	5.77	3.60	1.07	65.99	100
bg27_Bulk_rs_800_3_14	14	3	800	0.90	19.27	3.60	0.27	1.07	6.61	3.71	0.43	64.15	100
bg27_Bulk_rs_800_3_15	15	3	800	0.91	19.35	3.61	0.27	1.08	6.67	3.72	0.38	64.01	100
bg27_Bulk_rs_800_3_16	16	3	800	0.91	19.35	3.61	0.27	1.08	6.67	3.72	0.38	64.01	100
bg27_Bulk_rs_800_3_17	17	3	800	0.91	19.35	3.61	0.27	1.08	6.67	3.72	0.38	64.01	100
bg27_Bulk_rs_800_3_18	18	3	800	0.91	19.35	3.61	0.27	1.08	6.67	3.72	0.38	64.01	100
bg27_Bulk_rs_800_3_19	19	3	800	0.91	19.35	3.61	0.27	1.08	6.67	3.72	0.38	64.01	100
bg27_Bulk_rs_800_3_20	20	3	800	0.91	19.35	3.61	0.27	1.08	6.67	3.72	0.38	64.01	100
bg27_Bulk_rs_900_3_1	1	3	900	0.29	14.28	2.34	0.09	0.56	2.44	3.14	3.66	73.21	100
bg27_Bulk_rs_900_3_2	2	3	900	0.31	14.40	2.33	0.09	0.55	2.53	3.14	3.63	73.01	100
bg27_Bulk_rs_900_3_3	3	3	900	0.33	14.54	2.33	0.10	0.55	2.62	3.14	3.60	72.80	100
bg27_Bulk_rs_900_3_4	4	3	900	0.35	14.69	2.32	0.10	0.55	2.72	3.15	3.56	72.56	100
bg27_Bulk_rs_900_3_5	5	3	900	0.37	14.87	2.31	0.11	0.54	2.84	3.15	3.53	72.28	100
bg27_Bulk_rs_900_3_6	6	3	900	0.40	15.07	2.30	0.12	0.54	2.98	3.16	3.48	71.97	100
bg27_Bulk_rs_900_3_7	7	3	900	0.43	15.30	2.28	0.13	0.53	3.13	3.16	3.43	71.61	100
bg27_Bulk_rs_900_3_8	8	3	900	0.46	15.56	2.27	0.14	0.53	3.31	3.17	3.37	71.18	100
bg27_Bulk_rs_900_3_9	9	3	900	0.51	15.88	2.25	0.15	0.52	3.53	3.18	3.30	70.69	100
bg27_Bulk_rs_900_3_10	10	3	900	0.56	16.26	2.23	0.16	0.51	3.78	3.19	3.22	70.09	100
bg27_Bulk_rs_900_3_11	11	3	900	0.62	16.72	2.20	0.18	0.50	4.10	3.20	3.12	69.36	100
bg27_Bulk_rs_900_3_12	12	3	900	0.69	17.30	2.17	0.21	0.49	4.49	3.22	2.99	68.46	100
bg27_Bulk_rs_900_3_13	13	3	900	0.79	18.04	2.12	0.23	0.47	4.99	3.24	2.83	67.29	100
bg27_Bulk_rs_900_3_14	14	3	900	0.92	19.02	2.07	0.27	0.45	5.65	3.26	2.61	65.75	100
bg27_Bulk_rs_900_3_15	15	3	900	1.10	20.39	1.99	0.33	0.42	6.57	3.30	2.31	63.60	100
bg27_Bulk_rs_900_3_16	16	3	900	1.37	22.42	1.87	0.41	0.37	7.95	3.35	1.86	60.39	100
bg27_Bulk_rs_900_3_17	17	3	900	1.81	25.78	1.68	0.54	0.30	10.22	3.44	1.12	55.11	100
bg27_Bulk_rs_900_3_18	18	3	900	2.30	29.43	1.48	0.68	0.21	12.68	3.54	0.32	49.36	100
bg27_Bulk_rs_900_3_19	19	3	900	2.30	29.43	1.48	0.68	0.21	12.68	3.54	0.32	49.36	100
bg27_Bulk_rs_900_3_20	20	3	900	2.30	29.43	1.48	0.68	0.21	12.68	3.54	0.32	49.36	100

Table 2(cont.): Fractionation modelling outputs for plots shown in Fig.24 & 25.

Sample	Step	Press.	Temp.	TiO2	Al2O3	FeO	MnO	MgO	CaO	Na2O	K2O	SiO2	sum
bg34_Bulk_rs_700_3_1	1	3	700	0.56	16.77	4.23	0.10	1.26	4.00	3.36	3.09	66.64	100
bg34_Bulk_rs_700_3_2	2	3	700	0.59	17.05	4.44	0.10	1.32	4.19	3.40	2.94	65.97	100
bg34_Bulk_rs_700_3_3	3	3	700	0.63	17.36	4.67	0.11	1.39	4.41	3.43	2.77	65.22	100
bg34_Bulk_rs_700_3_4	4	3	700	0.67	17.71	4.93	0.12	1.48	4.66	3.48	2.58	64.39	100
bg34_Bulk_rs_700_3_5	5	3	700	0.71	18.11	5.22	0.12	1.57	4.94	3.52	2.36	63.45	100
bg34_Bulk_rs_700_3_6	6	3	700	0.72	18.18	5.28	0.12	1.58	5.00	3.53	2.32	63.26	100
bg34_Bulk_rs_700_3_7	7	3	700	0.72	18.18	5.28	0.12	1.58	5.00	3.53	2.32	63.26	100
bg34_Bulk_rs_700_3_8	8	3	700	0.72	18.18	5.28	0.12	1.58	5.00	3.53	2.32	63.26	100
bg34_Bulk_rs_700_3_9	9	3	700	0.72	18.18	5.28	0.12	1.58	5.00	3.53	2.32	63.26	100
bg34_Bulk_rs_700_3_10	10	3	700	0.72	18.18	5.28	0.12	1.58	5.00	3.53	2.32	63.26	100
bg34_Bulk_rs_700_3_11	11	3	700	0.72	18.18	5.28	0.12	1.58	5.00	3.53	2.32	63.26	100
bg34_Bulk_rs_700_3_12	12	3	700	0.72	18.18	5.28	0.12	1.58	5.00	3.53	2.32	63.26	100
bg34_Bulk_rs_700_3_13	13	3	700	0.72	18.18	5.28	0.12	1.58	5.00	3.53	2.32	63.26	100
bg34_Bulk_rs_700_3_14	14	3	700	0.72	18.18	5.28	0.12	1.58	5.00	3.53	2.32	63.26	100
bg34_Bulk_rs_700_3_15	15	3	700	0.72	18.18	5.28	0.12	1.58	5.00	3.53	2.32	63.26	100
bg34_Bulk_rs_700_3_16	16	3	700	0.72	18.18	5.28	0.12	1.58	5.00	3.53	2.32	63.26	100
bg34_Bulk_rs_700_3_17	17	3	700	0.72	18.18	5.28	0.12	1.58	5.00	3.53	2.32	63.26	100
bg34_Bulk_rs_700_3_18	18	3	700	0.72	18.18	5.28	0.12	1.58	5.00	3.53	2.32	63.26	100
bg34_Bulk_rs_700_3_19	19	3	700	0.72	18.18	5.28	0.12	1.58	5.00	3.53	2.32	63.26	100
bg34_Bulk_rs_700_3_20	20	3	700	0.72	18.18	5.28	0.12	1.58	5.00	3.53	2.32	63.26	100
bg34_Bulk_rs_800_3_1	1	3	800	0.57	16.75	4.14	0.10	1.24	3.99	3.35	3.13	66.74	100
bg34_Bulk_rs_800_3_2	2	3	800	0.60	17.01	4.25	0.10	1.29	4.17	3.36	3.03	66.18	100
bg34_Bulk_rs_800_3_3	3	3	800	0.63	17.31	4.38	0.11	1.34	4.38	3.38	2.91	65.56	100
bg34_Bulk_rs_800_3_4	4	3	800	0.67	17.64	4.52	0.12	1.40	4.62	3.40	2.78	64.86	100
bg34_Bulk_rs_800_3_5	5	3	800	0.71	18.01	4.67	0.12	1.47	4.88	3.43	2.64	64.07	100
bg34_Bulk_rs_800_3_6	6	3	800	0.76	18.43	4.85	0.13	1.55	5.19	3.46	2.47	63.17	100
bg34_Bulk_rs_800_3_7	7	3	800	0.82	18.91	5.06	0.14	1.63	5.54	3.49	2.28	62.14	100
bg34_Bulk_rs_800_3_8	8	3	800	0.88	19.48	5.30	0.15	1.74	5.94	3.52	2.06	60.94	100
bg34_Bulk_rs_800_3_9	9	3	800	0.96	20.14	5.58	0.17	1.86	6.42	3.56	1.80	59.53	100
bg34_Bulk_rs_800_3_10	10	3	800	1.05	20.93	5.91	0.18	2.00	6.98	3.61	1.49	57.84	100
bg34_Bulk_rs_800_3_11	11	3	800	1.17	21.88	6.32	0.20	2.18	7.67	3.67	1.11	55.81	100
bg34_Bulk_rs_800_3_12	12	3	800	1.30	23.06	6.82	0.23	2.40	8.52	3.74	0.65	53.28	100
bg34_Bulk_rs_800_3_13	13	3	800	1.39	23.82	7.14	0.24	2.54	9.06	3.79	0.35	51.66	100
bg34_Bulk_rs_800_3_14	14	3	800	1.39	23.82	7.14	0.24	2.54	9.06	3.79	0.35	51.66	100
bg34_Bulk_rs_800_3_15	15	3	800	1.39	23.82	7.14	0.24	2.54	9.06	3.79	0.35	51.66	100
bg34_Bulk_rs_800_3_16	16	3	800	1.39	23.82	7.14	0.24	2.54	9.06	3.79	0.35	51.66	100
bg34_Bulk_rs_800_3_17	17	3	800	1.39	23.82	7.14	0.24	2.54	9.06	3.79	0.35	51.66	100
bg34_Bulk_rs_800_3_18	18	3	800	1.39	23.82	7.14	0.24	2.54	9.06	3.79	0.35	51.66	100
bg34_Bulk_rs_800_3_19	19	3	800	1.39	23.82	7.14	0.24	2.54	9.06	3.79	0.35	51.66	100
bg34_Bulk_rs_800_3_20	20	3	800	1.39	23.82	7.14	0.24	2.54	9.06	3.79	0.35	51.66	100
bg34_Bulk_rs_900_3_1	1	3	900	0.57	16.70	4.05	0.10	1.21	3.96	3.32	3.17	66.92	100
bg34_Bulk_rs_900_3_2	2	3	900	0.60	16.92	4.05	0.10	1.22	4.13	3.31	3.12	66.55	100
bg34_Bulk_rs_900_3_3	3	3	900	0.63	17.15	4.05	0.11	1.24	4.31	3.30	3.05	66.15	100
bg34_Bulk_rs_900_3_4	4	3	900	0.67	17.42	4.06	0.12	1.25	4.51	3.29	2.98	65.70	100
bg34_Bulk_rs_900_3_5	5	3	900	0.71	17.72	4.06	0.12	1.27	4.74	3.28	2.90	65.18	100
bg34_Bulk_rs_900_3_6	6	3	900	0.76	18.07	4.07	0.13	1.29	5.01	3.27	2.80	64.60	100
bg34_Bulk_rs_900_3_7	7	3	900	0.82	18.46	4.08	0.14	1.32	5.31	3.25	2.70	63.93	100
bg34_Bulk_rs_900_3_8	8	3	900	0.89	18.92	4.08	0.15	1.35	5.66	3.23	2.57	63.14	100
bg34_Bulk_rs_900_3_9	9	3	900	0.97	19.47	4.06	0.17	1.37	6.08	3.21	2.42	62.24	100
bg34_Bulk_rs_900_3_10	10	3	900	1.06	20.13	4.04	0.18	1.41	6.58	3.19	2.25	61.16	100
bg34_Bulk_rs_900_3_11	11	3	900	1.18	20.93	4.01	0.20	1.45	7.19	3.16	2.04	59.84	100
bg34_Bulk_rs_900_3_12	12	3	900	1.32	21.93	3.97	0.23	1.50	7.94	3.12	1.78	58.21	100
bg34_Bulk_rs_900_3_13	13	3	900	1.51	23.20	3.92	0.26	1.56	8.90	3.08	1.44	56.12	100
bg34_Bulk_rs_900_3_14	14	3	900	1.75	24.88	3.85	0.30	1.64	10.18	3.02	1.00	53.37	100
bg34_Bulk_rs_900_3_15	15	3	900	2.08	27.22	3.74	0.36	1.75	11.94	2.94	0.40	49.58	100
bg34_Bulk_rs_900_3_16	16	3	900	2.15	27.66	3.71	0.37	1.77	12.28	2.93	0.28	48.85	100
bg34_Bulk_rs_900_3_17	17	3	900	2.15	27.66	3.71	0.37	1.77	12.28	2.93	0.28	48.85	100
bg34_Bulk_rs_900_3_18	18	3	900	2.15	27.66	3.71	0.37	1.77	12.28	2.93	0.28	48.85	100
bg34_Bulk_rs_900_3_19	19	3	900	2.15	27.66	3.71	0.37	1.77	12.28	2.93	0.28	48.85	100
bg34_Bulk_rs_900_3_20	20	3	900	2.15	27.66	3.71	0.37	1.77	12.28	2.93	0.28	48.85	100

